University of Liverpool, Department of Engineering

Novel, Induced-Flow, Centrifugal Water Pumping System for Off-Grid Application

Thesis submitted in accordance with the requirements of the University of Liverpool for the degree of Doctor in Philosophy

By

Neale Davies

August 2015

Dedication

Dedicated to my family and friends

Most importantly, to Lucy

Abstract

Water provision in rural areas represents a significant challenge, especially within the context of resource and sanitation in developing countries. High set-up costs, lack of installation expertise and reliability issues, arising from fluctuating operational conditions, have prevented many people from receiving the full benefit of automated pumping systems. The specific aim of this thesis is to assess the feasibility of using a tunable, induced flow subsystem as a means of optimising the power utilization and performance of a centrifugal pump over a wider range of operating conditions than typically expected. More generally, the research presented is undertaken to reduce the high implementation costs and localised limitations of rural water pumps by developing the theory towards a ''one-size-fits-all'' pumping system.

The theoretical analysis of an induced flow centrifugal pumping system is presented, coupled with the analogous electrical system. The results of simulations performed using both systems are compared to experimental results, obtained using an induced flow subsystem (IFS) test rig constructed at the University of Liverpool. All sets of results demonstrate consistent IFS characteristics, identifying its capability to maintain maximum power point (MPP) operation of the centrifugal pump irrespective of load. Further, the experimental results reveal a boost in output pressure which enables the pump to achieve an improved hydraulic power and increased operating range over the same system without an IFS.

It is concluded that, through the addition of an IFS, the performance of a centrifugal pump may be decoupled from its operating head, expanding its range of

serviceable conditions and demonstrating potential to develop a ''one-size-fits-all'' system. Ultimately, this could offer a cheaper and more reliable supply of a resource which is vital to life in any rural location: *clean water.*

Acknowledgements

First and foremost, my thanks go to Drs. Tim Short and Mark Johnson for their supervision throughout this PhD. In particular, I would like to express my gratitude to Dr. Tim Short, for his guidance, encouragement and eternal optimism throughout my research. A mention also goes to Dr. Aram Hassan for his work with Dr. Short. My thanks also go to the sustainable research team for their encouragement and (overoptimistic) belief in my research. In particular, a mention must go to Ms. Ruth Sutton for her continual provision of interesting discussions and debates over new ideas and research projects.

I gratefully acknowledge the EPSRC and University of Liverpool for providing my main source of funding throughout my studies. Additional thanks go to the University for its Facilities and excellent academic support staff, in particular Ms. Denise Stewart and Mr. Jack Carter-Hallam.

My express thanks go to all my family and friends for all their support and many adventures. Thanks to my Granddad for humouring me with talks about fantastical valve operation mechanics and enlightening me on several areas of electrical engineering. Particular mentions go to Dave, Ed and Helen for sticking around from the beginning; Carl, Phil and Nicki for providing excellent musical distractions from work; Alison, Vera and Mark for their belief in me; Alastair and Patrick for their understanding; and Mark Croft for his wisdom. Of course, none of my endeavours to date have been possible without the encouragement of my parents.

Finally, to Lucy; thank you for your belief in me, exceptional patience and most of all love.

Publications

1. Davies N, Short T.D, Hassan A, *Optimizing photovoltaic water pumping systems for developing countries through the addition of a novel induced flow subsystem*, Renewable Energy in the Service of Mankind Vol II 1,47, Springer International Publishing, Switzerland (*Due for publication, 2016*)

Presentations at Conferences

1. World Renewable Energy Congress WREC XIII, 3rd -8th August 2014, Kingston University London, Paper and presentation titled, '*Optimizing photovoltaic water pumping systems for developing countries through the addition of a novel induced flow subsystem'*

Contents

Nomenclature

Symbol	Definition	Units
A	*Internal Pipe Cross Sectional Area*	m^2
C	*Electrical Capacitance*	H
D	*Duty*	-
E	*Modulus of Elasticity*	N/m^2
F	*Force*	N
H	*Head*	m
I	*Current*	A
K	*Hydraulic Softness/Compressibility*	Pa/m^3
L	*Inductance*	kg/m^4
L_E	*Electrical Inductance*	F
M	*Mass*	kg
P	*Pressure*	Pa
ΔP	*Pressure Difference*	Pa
Q	*Flow Rate*	m^3/s
ΔQ	*Change in Flow Rate*	m^3/s
T	*Time Period*	s
V	*Voltage*	V
a	*Acceleration*	m^2/s
c	*Wave Celerity*	m/s
d	*Diameter*	m
e	*Pipe Thickness*	m

f	*Frequency*	Hz
g	*Acceleration Due To Gravity*	m^2/s
k	*Mechanical Stiffness*	N/m
l	*Length*	m
m	*Dimensionless ratio of Inductance* $= L_2/L_1$	-
$\dot{m}$	*Mass Flow Rate*	kg/s
r	*Dimensionless Frequency Ratio* $= \omega/\omega_n$	-
p	*Power*	W
Δs	*Change in Length*	m
t	*Time*	s
u	*Velocity*	m/s
v	*Volume*	m^3
Λ	*Constant of Flow* $= Q_{BEP}.\left(1 + \mathbb{R}\left(\frac{1+D}{1-D}\right)\right)$	m^3/s
Ψ	*Constant of Flow* $= \frac{2.Q_{BEP}.\mathbb{R}}{(1-D)}$	m^3/s
ε	*Bulk Elasticity Modulus*	N/m^3
η	*Pump Efficiency*	-
ρ	*Fluid Density*	kg/m^3
ω	*Angular frequency*	rad/s
ω_n	*System Natural Frequency*	rad/s
$\mathbb{R}$	*Flow Ripple*	-

Subscripts

Av	*relating to the average value*
BEP	*relating to the best efficiency point*

D	*relating to the discharge pipe*
E	*denotes electrical term*
ECV	*relating to the electronic control valve*
H	*denotes hydraulic term*
K	*relating to the capacitance chamber*
$L1$	*relating to the inductance pipe*
MAX	*denotes maximum value*
MIN	*denotes minimum value*
OFF	*Relating to ECV inactive period*
ON	*Relating to ECV active period*
OWV	*relating to the one-way valve*
$Pump$	*relating to the centrifugal pump*
c	*relating to closed period*
i	*denotes internal diameter*
o	*relating to open period*
p	*relating to a pipe*

Abbreviations

AC – *Alternating Current*

BEP – *Best Efficiency Point*

ECV– *Electronic Control Valve*

DC – *Direct Current*

IFS – *Induced Flow Subsystem*

MDG – *Millennium Development Goals*

MPP – *Maximum Power Point*

NTIofV – *Nonlinear transfer function component (Current to Voltage)*

OWV – *One-Way Valve*

PV(P) – *Photo Voltaic (Pump)*

SELF – *Solar Electric Light Fund*

UoL – *University of Liverpool*

WHO – *World Health Organisation*

Chapter 1

Introduction

1.1 Access to Water in Remote Areas

Water supply and sanitation in rural areas (particularly in developing countries) represents an issue affecting almost a third of the global population. Pumping systems utilising off-grid power sources can be one way of providing access to water where connection to a grid power supply would otherwise be impossible or too expensive. Such systems include the use of diesel generators, or more suitably, sustainable power systems.

Despite advances in water pumping systems for off-grid locations, high set-up costs and reliability issues due to fluctuations in operating conditions have prevented many people from seeing their benefits. Further, limitations to system performance and reliability, coupled with capita cost per unit have restricted the use of pumping systems in some areas for agricultural or domestic needs. The focus of this research is to reduce the high implementation costs and stability issues associated with centrifugal pumping systems by developing the theory towards a self-regulating, 'one-size-fits-all'

pumping system for providing a supply of a resource which is vital to any community or persons living/working in a rural area: *clean water*.

1.2 The Thesis

Clean water is a resource which is vital for both domestic and industrial applications. Sustainable water pumps such as those involving photovoltaic (PV) or wind power sources can be one way of providing a clean, sustainable water source for drinking, sanitation, irrigation and agriculture [1] - but they are not without their flaws. Targets set nearly 3 decades ago to implement 10 million PV pumps [2] saw only 0.6% of this figure realized by the end of the 20th century [3], many of which had been shown to be non-operational by 2001 [4]. Reasons for failing to reach this target could be through various problems with pump design, component reliability or the implementation cost per unit. One way of combating these problems would be to introduce a means for an existing pumping system to self-regulate – compensating for any fluctuations in operating conditions and thereby improving the reliability of discharge flow from the pump by optimising the use of power to the system. Such a system would also lend itself to an auto-setup capability, eliminating the need for site specific assessment which in turn would lower the cost of installing a single unit; a factor which is deemed extremely important in the provision of access to water in rural areas [5, 6]. In essence, a system capable of both auto-setup and self-regulations would effectively be a one-size-fits-all pump.

1.2.1 The Research Hypothesis

While the concept of using induced flow sub-systems (IFS's) in conjunction with positive displacement pumps has been the subject of many studies for almost four

decades now [7-11], the principles of this concept have never been applied to pump regimes focused around a centrifugal pump. As has been demonstrated previously, by Burton and Short, the addition of such a system to the more recent PV pumping regimes can be beneficial to their operation [6, 12-15]. Given similarities to the hydraulic ram [16], the same could hold true for centrifugal pumps, for which the operation and uses have been well known and researched for many years. This is further reinforced by the similarities between the centrifugal pump characteristic curve and that of PV panels (I-V Curve) [17, 18] , the latter of which can be modified/controlled through the use of a 'Maximum Power Point Tracker' (MPPT). Using an electric-hydraulic analogy, a modified centrifugal pumping circuit based on a DC switch-mode 'Boost Converter' could be a way to enable optimum operation of the pump; this would essentially provide a mechanical means of tracking the MPP of the centrifugal pump curve. Such a system would be based around the use of a tuned hydraulic, induced flow, subsystem to an existing centrifugal pump array, such as the ones found in existing induced flow reciprocating pumping systems. This would allow the pump to constantly operate at its 'Best Efficiency Point' BEP operating conditions, independent of any variable conditions, hence enabling the pump to make use of available energy across a wider range of heads than typically expected from a pump of its type. In addition, it is expected that such a pump would provide a higher rate of discharge flow as well as improving the pumps lifespan and reliability, making it especially suitable for off-grid needs. These theories are expanded upon later in the thesis and more on the subject of induced flow systems with reciprocating pumps will be included in **Chapter 3**.

Given this information, it is possible to state that the research hypothesis is therefore:

> *''The use of an IFS can ensure that the centrifugal pump is itself operating at its MPP (BEP) thereby decoupling its operation from the conditions around it.''*

1.2.2 Research Impact

Although this research project is primarily focused on the furthering of sustainable pumping systems and developing the theory towards a novel centrifugal pumping system, the research will potentially have an impact on a wider range of areas within the academic community. Some of these areas include:

- Utilization of a novel induced flow subsystem; expanding the application of centrifugal pumps for sustainable borehole pumping, benefiting not only PVP's but also Diesel, wind and hybrid energy powered, off-grid, pumping systems.
- Development in the field of fluid dynamic theory of systems involving centrifugal pumps; beneficial to both the fluid dynamics and hydraulic engineering communities.
- Furtherance of research into the need for sustainable water pumping methods within a global context; beneficial to sanitation and resource academics.
- Continued research into the novel area of PV pumping systems and their uses in both developing countries and rural areas in need of reliable water supply.
- Advances in off-grid, agricultural and domestic water pumping.

Furthermore, the development of a new form of PV pumping system could hold potential benefits for 'real world' use outside of academia, where:

- The implementation cost of sustainable borehole pumping units will be lowered due to the removal of site-specific assessments.
- The use of a tuned hydraulic system will expand the application of centrifugal pumps within the context of sustainable borehole pumping, allowing for pump performance across a wider range of conditions – equating to a more stable supply of water in rural areas.
- This research marks a step towards an "auto-setup", "one-size fits all", sustainable pumping system.

1.3 Research Aim

The aim of this research is to assess the feasibility of using a tuned hydraulic sub-system in conjunction with a centrifugal pump as a means of optimizing its power utilisation and discharge performance over a greater range of operating conditions than would be typical for a pump of its type. Such a system would be capable of maintaining BEP operation of the pump, independent of the operating conditions, thereby eliminating the need for site specific assessment and providing a "one-size fits all" style design capable of ''self-regulation'' – features identified as being of high importance when addressing the issues of developing new low head solar pumps [19]. Ultimately this will help lower the cost of implementation and make this form of sustainable pumping technology more widely available.

1.4 Project Objectives

The following objectives were identified as a means of ensuring that the project realizes the specific aim outlined previously:

- Develop an analytical theory, considering in detail the validity of the assumptions made in the project proposal.
- Use the analytical theory to produce a numerical study into the pumping systems operation under varying hydraulic conditions.
- Compare any analytical theory to existing electrical theory on the use of boost-converters in order to validate the electric-hydraulic analogy for this research.
- Design and manufacture a centrifugal pump test bed as a means of assessing the accuracy of the computational model and hence analytical theory.
- Use the centrifugal pump test bed with the addition of the tuned hydraulic system to obtain performance data for the modified system.
- Compare all set of data from analytical to experimental as a means of providing evidence of any performance improvements with the tuned hydraulic system.

1.5 Thesis Structure

The thesis itself is broken down into 9 Chapters. Each chapter attempts to take a logical progression through the individual stages of the research project and finally arrive at a concluding chapter which discusses some of the findings of the research and poses future research questions. The project was divided into 4 main stages, reflected in the chapter choices. These stages are as follows:

1. Literature review and research planning (**Chapters 1-3**).

2. Theoretical analysis and design of the pumping system (**Chapters 4** and **5**).
3. Numerical and electrical analysis of the pumping system (**Chapters 6** and **7**).
4. Experimental testing and analysis (**Chapter 8**).

The chapters are arranged in such a way so as to provide the clearest narrative and to introduce new themes and ideas as they become relevant. It is also noted that the research was intended primarily to be a feasibility study into the broader aspects of the novel pumping system designed.

1.6 Summary

The introduction presented in this chapter has briefly touched upon some of the broader ideas that will be further discussed in this thesis. These include the idea that a tuned hydraulic system may be introduced to a centrifugal pump, based on ideas previously seen in other induced flow systems. It has also been stated that through an electric-hydraulic analogy, the centrifugal IFS pump could borrow from boost-converter design from DC power electronic theory. The aim, objectives and research hypothesis has been presented, along with a brief overview of thesis structure. Ultimately this research offers an investigatory study into the potential for an auto-setup pumping system based around the use of a simple, single stage, centrifugal pump.

Chapter 2

Off-Grid Water Pumping

This chapter covers a broad range of literature surrounding water pumping in rural areas. This stretches from the background surrounding the research, such as the need for reliable water supplies in off-grid locations, to the types of pump currently available and the benefits and drawbacks of each (highlighting the relevance of this research). Although the developed novel pumping system is able to operate with any of the range of power systems available for off-grid use, the wealth of literature concerning sustainable systems (such as those based on the use of PV, wind or hybrid energy) has led much of the research presented to be focused on these systems (in particular PVP's).

2.1 Introduction to off-grid Water Pumping

Over one third of the global population (mostly in developing countries) live in rural or remote areas with poor access to mains power supplies or water utilities. In some parts of the world, including sub-Saharan Africa, access to reliable mains electricity in rural areas is as low as 12%. Overall, this translates to over a third of people in rural areas worldwide [20]. This lack of access is usually due to either the

expense of connection to a grid-supply or simply through impracticality. The World Bank predicts a global population growth of 2.5 billion within the next 35 years and the global share in population for developing countries to rise from 85% to 88% [21], further expanding this issue. In these areas, water demands are met by employing pumping systems which rely on power sources that are suitable for off-grid use. The pumping systems can range from simple manual hand pumps, to automated electrical pumps [2, 22]. Of the electrical systems, sustainable power sources such as PV panels and wind turbines have been the focus of much study in recent past due to their effectiveness and suitability of operation in remote locations. This is coupled with their lower lifetime costs in comparison to a standard fuel based pumping system, which require regular access to fuel and continued maintenance.

As the majority of this body of work will be considering the performance of a novel pumping system and its relevance in relation to existing pumping systems (in particular sustainable ones), it is first necessary to consider the reasons behind the need for sustainable pumping systems and indeed, the need for clean water itself.

2.2 Sanitation and Water Resource in Developing Communities

Access to clean water is among one of the most basic human needs that exists in the world today, yet is a need that is still not fully met in many developing countries. Of the 884 million people worldwide without access to safe drinking water [23], more than 5 million people in developing countries die each year as a direct result of diseases caused by unsafe drinking water or lack of clean water for sanitation [24]. Clean water is required, not only for drinking to sustain the human body, but also for sanitation and hygiene purposes – the cleaning of eating and cooking utensils, washing of the hands

and face, and keeping the body and clothes in contact with the body free of dirt, bacteria and other parasites. The average adult requires around 3 litres of drinking water per day for hydration, which is relatively minimal when compared to the additional 17 litres of water needed to cover the most basic needs of a single person; as suggested by the World Health Organization (WHO) [25]. Furthermore, the spread of disease due to unclean water supply does not stop at its consumption or use for sanitation. Water-related disease and transfer may be split into several categories [24], more commonly referred to as ingested, washed, sourced and aerosol diseases:

- Waterborne disease – The classification for disease spread through the ingestion of contaminated water. Most commonly this includes diarrheal diseases, but also includes parasitic infection that causes serious illness.
- Water-washed disease - Diseases spread through lack of clean water for personal hygiene, usually contagious or diarrheal diseases that are easily spread from person to person. Simply having contact with dirty water supplies whilst washing clothing or the body is enough for infection.
- Water-based diseases – Arising from disease carrying organisms which require water as part of their life cycle, often transferring these diseases to human hosts when the water is used for washing.
- Water-related insect diseases - This related to the spread of disease by insects that breed or live around contaminated water supplies. Such diseases include malaria and several varieties of fever. Although not directly linked to a lack of clean water, such diseases can still be avoided through a reliable supply of clean water in a developing community.

In the year 2000, the United Nations introduced a series of millennium development goals (MDG's) to address access to clean water for drinking and sanitation purposes in an effort to reduce the global mortality rates from water related diseases [26]. In 2015, the UN released a report which stated that the number of people without access to clean and sustainable water sources had been halved (as part of target 7C of the MDG's [27]). There is, however, still a reported 2.4 billion without this facility. It was previously estimated that if no measure was taken to address this basic unmet need that as many as 135 million people would have died from disease caused by a lack of clean water within the first two decades of the 21st century [24] – largely contributed to by deaths due to diarrheal based diseases alone. The same study concluded that even if many of the goals set at the turn of the millennium are reached, the total mortality figure will still stand to be as many as 76 million. Despite this well documented problem, and even given that it has been a cause for concern for quite some time, it would seem surprising that it wasn't until as late as 2010 that the United Nations recognized the access to clean water as a fundamental human right [23].

2.2.1 Water Resource and Social Development

Much of the time, water contamination of local sources such as springs or streams is due to their overuse for more than basic consumption needs. As communities require nearby supplies for the cleaning of clothes and disposal of wastes, including human excreta, people must travel further afield for cleaner water sources for drinking. Failure to do so only increases the risk of disease from contaminated water supplies. Often, the solution requires sending women and children within a community to fetch water from these further afield sources- expending valuable time that could be used more constructively within a community, such as time spent in education or

creating stronger social links. Such activities are vital for any community. Even the United Nations general assembly paper calling for the right to clean water noted as a matter of severity that more than 443 million school days a year are lost as a result of water and sanitation related diseases [23]. Although not directly linked to the diseases themselves, the time spent gathering clean water can stunt the development of a community.

With such a great need for clean water existing in developing communities and the grave threat of disease from contaminated local water supplies, it seems needless that some people must do without clean water or have to travel great distances to slightly improve the quality of the water they have access to. This is especially true when, for the vast majority of cases, there will be an abundant supply of clean water below the ground. This is where borehole pumps can be considered very beneficial. Studies in to the impact of the installation of a basic borehole pump within a community have shown a drastic improvement in health and sanitation in the area, with a 50% reduction in illness due to a clean water source [28]. While the installation of a manual borehole well is indeed greatly beneficial to a community, it may still be observed that there is room for improvement. A manual pump, for example, will require a person to operate the pump for water to be drawn – a simple task if only a small amount of water is needed for personal consumption, but an altogether larger task if a water supply is needed for agricultural use or supplying livestock. Couple this with the greater amount of water required on a daily basis for personal hygiene and sanitation [25] and the task of using a manual pump to provide clean water for a growing community becomes a continuous one.

It is seen that, while access to a simple mechanical borehole pump can make a drastic difference to the health of a developing community [28], it would be more beneficial still to introduce an automated pump. As discussed in **Chapter 1**, the introduction of borehole pumps to a developing community provides a reliable source of clean water for drinking and sanitation, without having to travel great distances. Mechanical pumps, however, also require manual operation for an output flow to occur, which can be time consuming where larger quantities of water are concerned. Automated borehole pumps provide a continuous flow output throughout the day, allowing for time to be spent in more constructive way – which is beneficial not only monetarily for families within a community, but also for the development of a community as a whole. Evidence of such benefits can be observed in projects such as the 'Programme Regionale Solaire' (PRS) [29] which saw 626 PV pumps installed in the Sahel region of Africa. Consider also the additional benefit of powering an automated system with a sustainable power source. The use of solar or wind energy in rural/off-grid areas could help to translate a potentially already abundant and 'free' source of energy into an all more valuable commodity: water.

2.3 The Pumping System

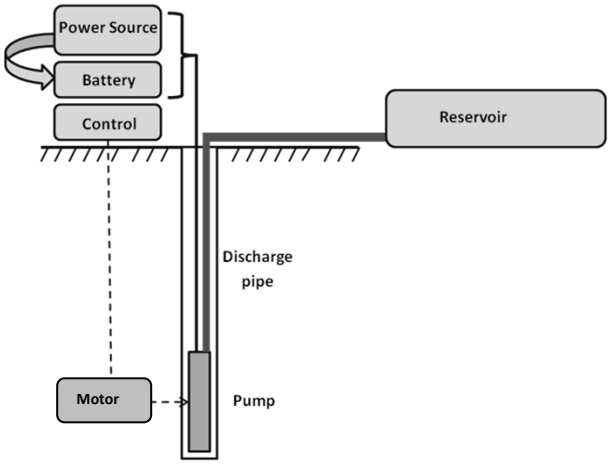

Fig. 2-1. General arrangement of an automated pumping system

The general arrangement of any automated pumping system may be illustrated by considering **Figure 2-1**. It describes a simple system comprising a power source, controller, a pump and motor, and a means of storing the pumping systems output; this is in the form of a battery for storing the energy needed for pumping, or water reservoir. The style illustrated in **Figure 2-1** is of a submersible borehole pumping arrangement, meaning that the pump itself is situated beneath the water level within the borehole itself to pump water to the surface, as opposed to ground level 'suction' or 'floating' style pumps which are not situated in a borehole and instead 'draw' water from the well. Benefits of submersion include capability to self-prime, increased versatility and ability to yield discharge flow at greater pumping heads (surface or floating centrifugal pumps are used for pumping heads below 7m,[2] due to their inherent suction limitations). The main components of a pumping system are best

considered individually, highlighting the broad range of installation configurations currently available.

2.3.1 The Controller

A controller is employed as a buffer between the power source and the pump motor, providing a broad range of control mechanics. This ranges from conversion of AC to DC for specific motor use, provision of an AC signal for AC motors through an inverter, optimization of the power usage of the pump, or improved pump start-up characteristics (the link between reliability of a system and the inverter is discussed along with AC motors in **Section 2.3.3**). The power output from the controller is relayed to the pump motor which in turn drives the pump. In the case of PVP systems, controllers include the use of MPP trackers. These allow power to be drawn from the PV panel so as to provide optimum power for the motor.

2.3.2 The Battery/Reservoir

In various pumping systems the need for a battery is obviated with the addition of a water reservoir, which in many cases is preferable for its simplicity, cost effectiveness, maintainability and lifespan [12-14]. Barlow *et al.* suggest that, at a minimum, some form of water storage is essential for village level use. In this case supply for up to 5 days is considered good and water storage tanks should be designed to have a low impact on static head of the pumping system [2]. It is further argued that to reduce overall costs, several pumps feeding individual storage systems should be considered over a single larger pumping system with piped distribution.

The use of a battery carries with it a level of environmental consideration, due to disposal of the battery at the end of its operating life, usually in the form of lead or

acid waste. This is especially true for rural areas using an off-grid pumping system as it becomes increasingly difficult to dispose of an obsolete battery efficiently. This, along with the demand for regular maintenance and intermittent replacement of such pumping systems, may be difficult for potential consumers [12]. Short does, however, continue to discuss that in some cases the use of a battery can be beneficial. Battery storage not only provides additional power for auxiliary facilities, such as lighting and low power devices, but also allows for the operation of pumping systems outside of usual hours (daylight hours in the case of PV) or adverse environmental conditions. Batteries can also be used directly between a PV array and pump motor as a 'substitute' MPPT (as the charging of an electric battery is close to constant voltage), making use of their charging curve.

2.3.3 The Pump Motor

Dependent on the power source, the electrical output can be in either DC or AC format. A wide variety of sustainable borehole pumps currently available make use of DC motors; the GRUNDFOS SQ Flex series of pumps and the LORENTZ PS pumps provide a couple of examples. The experimental tests presented in **Chapter 8** of this thesis also use a DC motor/pump combination, albeit a small scale one. Aside from making use of different types of current operation there are a series of other factors which can affect a motors performance and selection for use with a pump. Motor type characteristics are now considered:

- **AC Motors –** The output from many wind powered and diesel generators is in an AC format, making this motor type well suited to these power supplies. In

the case of PV power, as the output from PV panels is generally DC, there is the additional requirement of an inverter/additional electronic control equipment.

The inverter is often labeled the component most likely to cause issues in rural pumping systems [4, 12]; these have been identified as the most sensitive component in the system. In a case study evaluated by Posorski the inverter accounted for 70% of the 22 hardware failures observed in rural PVP systems; despite the overall downtime of the pumps being low (around 1.5% of cumulative pump lifespan) [30-32]. Posorski further identifies that the problem may be that not all inverters are equipped for MPP tracking and that further technical refinement is needed to avoid sub-optimal pump operating conditions and losses due to mismatching. This lends to the idea that a DC system without the need for such controls may be more appropriate for off-grid application. This is echoed in a number of studies, including those by Hahn [33, 34] which identify room for improvement in some components of a PVP system. This time, the inverter failed in almost 20% of cases. Similar inverter issues were recorded by Barlow *et al. [35]* and Metwally and Anis [36], who identify the complexity of some inverter based systems having an overall detrimental effect on reliability, and again by Anderson when considering PVP systems in Botswana [37]. Additionally, AC motors have been shown to be generally less efficient than their DC counterpart, despite a greater range of opportunities for improvements. Furthermore, the additional and sometimes complex electronics required for AC motors increase the initial cost of a pumping system.

AC motors do, however, have their advantages. The motor housing itself can be filled with water, so there is no need for reliable seals, save to prevent dirt contamination. AC motors have very little wear associated with their long term use and so are highly reliable and require little maintenance, making them especially suited to rural water pumping. Also, there already exists a wide variety of AC motors, at low cost, available for use with off-grid systems [38]. Thus, there is indeed the agreement for offsetting the cost and reliability issues of an inverter with the increased reliability and reduced cost of an AC motor. In PV systems the argument for offsetting increases as the systems size increases [39] due to the start up losses in the inverter being relatively lower for larger systems.

- **DC Motors –** DC motors are available in several different formats: Brushed, Brushless, Separately excited and switched reluctance. The latter two are not discussed in detail here save to identify the fact that both have need for complex electrical control systems [40, 41].

  Brushed motors rely on carbon blocks called brushes which are used through contact to create a turning field for the motor to function. As contact is involved, the brushes wear down with time and so require maintenance; this is a feature which is emphasized as being detrimental to the performance of pumps in remote locations [12, 39, 42]. Although maintenance and replacement of these brushes is relatively simple, it does require additional training for any person/s involved in addition to pump downtime, both of which can result in increased running costs and reduced reliability [2, 43]. In addition

to this, the motor housing must be air filled and sealed to prevent short circuit occurring and disrupting the motors operation. This requires high quality seals around the motor. What's more, if the motor chamber becomes flooded with water, the motor itself is often irreparably damaged. The primary advantage with this type of motor is that for PV pumps, no converter is required and overall they have a very high efficiency – up to 100% more efficient than a similar sized AC motor. Further to this, brushed motors are viable as part of a directly coupled pumping system (the benefits of this are discussed later in **Section 2.4.4)**.

Brushless motors do not suffer the same mechanical wear and maintenance drawbacks as their brushed counterparts as they do not rely on contact to create a turning field. Additionally, there is no need for reliable seals around the motor housing, as the motor chambers are often filled with water anyway. This makes brushless motors more reliable and less maintenance intensive, as well as able to deliver high efficiencies. It is for this reason that many modern PV pumps use DC brushless motors.

2.4 Off-Grid Power Supply

In many rural areas without access to grid-power sources there are several methods for generating the power to pump water. These range from the more traditional methods of pumping water by hand, through the use of animals or mechanical wind systems, to the more modern alternatives of diesel*, wind-electric, PV or hybrid systems. For the purposes of this research it is the automated energy generation systems which are of the most interest, specifically those using sustainable energy (particularly solar). Such systems have been favoured in a wealth of literature for their particular suitability to rural areas. Diesel pumps are, however, included in the interest of completeness.

2.4.1 Diesel Powered Pumps

Diesel pumps are often selected as the primary energy generation source for many rural area applications (especially those with higher energy demands, [44]) due to their availability, relatively modest start-up costs and ease of installation. Furthermore, they provide a well understood line of technology with parts readily available for servicing and only basic levels of technical understanding needed for operation and maintenance. They do, however suffer from a wide range of drawbacks. Despite their low initial costs, regular reliance on a fuel source can lead them to become more expensive over the course of a systems lifetime (discussed further in **Section 2.5)**. In addition to this, fuel is sometimes unavailable in rural areas, leading to downtime in the

* - Where diesel pumps are mentioned, the same may be applied to petrol fuelled pumps as an alternative. However, it is often considered the more expensive fuel type; hence the preference of diesel powered pumps

operation of water pumps. Diesel generators also suffer from high levels of maintenance and reliability issues due to high speed moving parts which can again lead to pumping downtime and continued observation [30]. As a result, sustainable energy generation systems have been championed by various studies [11, 45, 46].

2.4.2 Solar Pumps

There exists an almost overwhelming amount of literature concerning PV's and their uses, efficiency and theory. With regards to water pumping in rural locations there need only be considered a few key areas, these being:

- Reliability of PVP's.
- Suitability to rural/remote locations.
- Cost

PVP's have been the subject of much interest and research for well over 3 decades now with a wide variety of pumping system sizes studied ranging from the larger (>1kW) systems to smaller, sub 1kW, sizes which are far more useful in the context of water provision for rural areas (be they community based, agricultural or individual demands) [11, 47]. Such pumping systems have proven to be very reliable, with most of the issues arising from complex inverter or control systems, as discussed previously, and not with the solar system itself. In the particular case of photovoltaic (PV) pumps, the use of sustainable energy is justified further with the high solar irradiation associated with many developing countries [48, 49]. Furthermore, the need for water is often highest around the times when irradiation is also at its highest i.e. the summer period or 'dry seasons', further strengthening the argument for PVP's.

Short and Oldach [1] suggest, and are echoed by others [45, 48], that despite the high initial capital required for PV panels, their reliability in rural application should outweigh this factor and place PV power systems as the chief energy source. This is in addition to the suitability of such systems which are able to utilize an abundance of readily available solar energy. Production of energy from a solar source has itself added environmental benefits. Unlike diesel generators, solar or wind power systems do not generate any pollutants as by-products of their operation and are effectively 'clean' to run after offsetting their embodied energy costs from manufacturing. This is doubly true if used in conjunction with a pumping system which does not rely on the use of a separate battery system. Furthermore, the use of PV's lessens the dependency on diesel or petroleum based fuels which can be difficult and expensive to obtain in addition to being environmentally damaging due to spills and pollutants [50].

2.4.3 PV Optimisation

The output power of a solar array is dependent upon the intensity of solar radiation instant on a PV panel at any given time. As such, this value fluctuates throughout the course of the day as the level of insolation rises and then falls. It is possible to employ a maximum power point tracker (MPPT) to control where the power is drawn from the I/V curve as demonstrated in **Figure 2-2**. By making use of the electrical resistance equation, an MPPT can use the dynamic characteristic resistance of an I/V curve across varying degrees of irradiation to maintain a maximum power draw from the panels across varying levels of insolation and provide the pump motor with sufficient power. This is done through the use of a tracking algorithm based usually on the manufacturers' data for MPP [51]. Varying forms of DC-DC converters have been employed as an electrical 'buffer' controlled by the tracking algorithm to decouple the

current operational conditions from the panels power provision. Both buck and boost-converters are used [52-54]. More on boost converters and their relevance to this research is presented in **Chapter 3.**

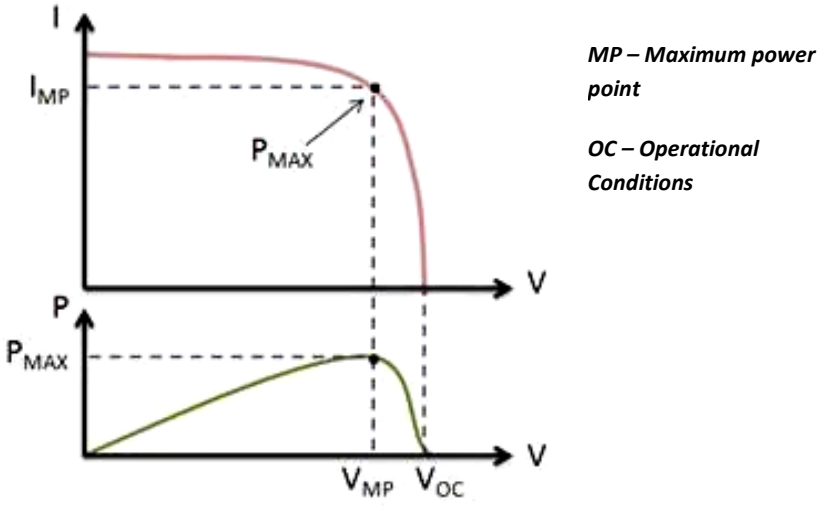

Fig. 2-2. Illustration of maximum power point across I-V curve

As a further means of optimising the amount of power available to the pumping system, mechanical or manual solar tracking may also be implemented. Mechanical tracking involves a simple solar tracking circuit attached to a motorized rack capable of physically rotating/re-aligning the PV panels of a system. The control circuit uses the motor and rack system to physically tilt the PV panels in the correct direction to receive maximum solar irradiation. Such tracking systems can yield an increase in solar energy of between 20-50%. In the case of work by Kolhe *et al.* increases in power generation of 20% were seen by simply readjusting the PV array manually 3 times a day in addition to increased discharge flows [18]. More recently, Canton found similar results for manual alignments (17%) and even improvements of up to 8% for monthly or seasonal

adjustments [55]. Limits of such tracking systems include cloud coverage and diffusion of light in a region.

2.4.4 Direct Coupling

The disadvantages of the complexity of electronic control needed for many pumping systems have been discussed. One possible solution highlighted by Short *et al.* in several articles is to completely remove the electronic control altogether and employ direct coupling of the motor to the pump. Direct coupling involves the power source (most likely PV) directly driving the pump motor with no additional control subsystems [56]. This is only possible for motors which require a DC current and so is not possible for AC motors or pumping systems exclusive to AC power supply. Additionally, such a system requires good matching of pump motor and array components, but overall has been shown to be simple and reliable [57-59].

Directly coupled pumping systems are argued to be the more reliable option for off-grid pumping solutions when compared to those involving some form of electronic control [58, 60]. They also benefit from lower cost than systems utilizing electronic control. It has further been suggested that the most appropriate technology for rural application would be one utilizing a centrifugal pump in conjunction with a directly coupled brushed DC PM motor [61] (benefits of centrifugal pumps discussed in **Section 2.6.3**). Further, in the specific case of PVP's, a DC motor driving a centrifugal pump has been shown to give a well-matched load to the power array, with the system making use of the majority of power available [62].

Unfortunately, for directly coupled systems, several problems still exist. Firstly, such systems still rely on site specific assessment and sizing; adding potentially

unnecessary expense and complication. Also, in directly coupled systems, the operating point is found to deviate quite substantially from the PVs MPP [63] and the power utilization is poor across variations in environmental conditions [1, 51].

2.4.5 Wind Turbine Pumps

Wind powered pumping systems benefit from most of the same characteristics of PV systems, such as low environmental impact and minimal running costs after initial installation, and are included here to complete the range of sustainable systems available. Wind powered pumping systems may be separated into two main categories: those which use direct mechanical translation of power (such as those used with positive displacement pumps) and those which convert mechanical wind power into electric energy for use with all pump types. It is the latter which is of more relevance to this thesis, as mechanical turbines are seldom used in conjunction with centrifugal pumps [64]. Wind electric systems are typically the lesser used of the sustainable systems, including wind-mechanical, due to better resource matching from solar-electric power [46] (particularly in smaller systems). Despite this, hybrid systems, making use of both wind turbine and PV systems, have shown promise in delivering improved discharge flows than either individually powered system [46].

2.5 Cost

Pumps which make use of a sustainable energy source such as PV or wind-electric pumps have the inherent benefit of, after the initial cost of installation and pumping unit itself, being much cheaper to run than other fuel based operational systems – typically diesel generator pumps. There have been several site-specific studies into the monetary comparison between diesel and PV pumps over the

operational time of the pump [1, 45, 65], giving the general conclusion that, while PV and wind-electric systems have a much higher initial implementation cost, the operational costs per year are considerably lower (assuming an average solar pump lifespan of 20 years). A significant portion of the initial cost of sustainable pumps comes from the installation, where a higher level of expertise is required for correct set up and pump/power/motor system specification. This often equates to an installation cost of up to 500% more than an equivalently sized diesel generator [45] and overall initial capital costs of 300% more [1]. In the particular case of directly coupled PVP's, much of the additional component costs for battery and control systems are negated [66] and the performance of such a system can be optimized through the addition of more PV panels. **Tables 2-1** and **2-2** illustrate the data simulated as part of a study carried out by the 'Solar Electric Light Fund' (SELF)[65], comparing the long-term costs of diesel and PV water pumps. As part of the comparison, the pumps considered were a 4kW diesel generator and a 2kW solar array with a pump of roughly 1 horsepower, capable of delivering 5000 gallons per day at a depth of 100m – an amount which is great enough to supply a community of around 200 people, according to the WHO's suggested daily water allowances [25].

Table 2-1 - "Worst case" for solar: Fuel cost: $1.20 per liter. Consumption rate: 0.3 liters per kilowatt [65]

	Initial Capital	Operating Cost/ Year	Total Net Present Cost	$ per kilowatt
PVP Option	$12,300	$335	$16,472	$0.66
Diesel Option	$2,000	$4,854	$62,494	$2.48

Table 2-2 - "Best case" for solar: Fuel cost: $1.70 per liter. Consumption rate: 0.7 liters per kilowatt [65]

	Initial Capital	Operating Cost/ Year	Total Net Present Cost	$ per kilowatt
PVP Option	$12,300	$335	$16,472	$0.66
DS Option	$2,000	$12,525	$158,094	$6.27

Similar studies have also shown the overall life-cycle costs of PV and sustainable pumps to be lower than that of same size diesel pumps [45]. Furthermore, the cost of fuel is increasing, meaning that data gathered during previous studies will no longer be as valid in a decade or more and the gap between operational costs of diesel and PV based pumping systems may widen. This contributes to the suitability of not only PV systems, but also wind and hybrid.

2.6 Types of Pump

The pump is driven by the motor to convert the mechanical power of the system into a useable hydraulic power where hydraulic power, p_H, is described as the product of discharge flow, Q_D, and pumping head, $H = P/\rho g$ [67]. The types of pump most commonly used in submersible borehole pumps may be split into two main varieties – positive displacement and centrifugal. Each variety of pumps can be further split into individual styles of pump, each with its own merits and disadvantages to specific operating conditions [2]. Although it is centrifugal pump that provides the main focus for this research it is worth examining the operation and features of other varieties of pump, in particular the reciprocating (piston) pump, introducing the idea of

induced flow pumping systems and their use in expanding a pumps operating range and suitability for off-grid pumping.

2.6.1 Reciprocating Pumps

The reciprocating (or piston) pump is the first of the positive displacement style pumps discussed here. The reciprocating pump relies on the conversion of rotational motion to linear motion to allow a diaphragm to draw water into the pump, then force it out of the pump with the return stroke [2, 68]. One basic layout for a reciprocating pump is shown in **Figure 2-3.** The figure illustrates the use of a reciprocating piston which, through the use of one-way valves, can introduce and evacuate fluid from the pump chamber. In the case of submersible pumps, the motor and piston are arranged in the most practical format to save on space.

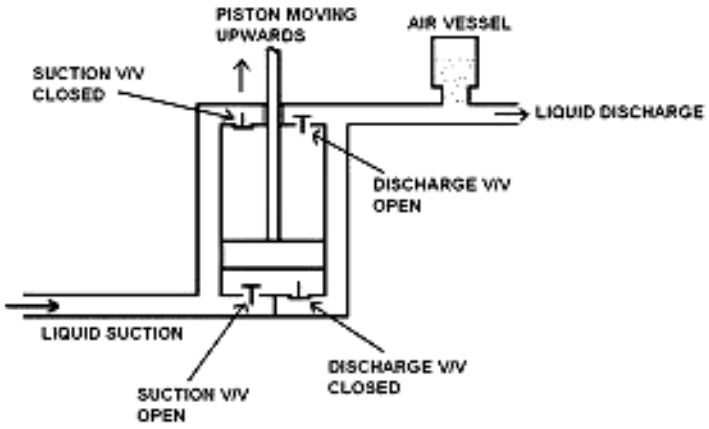

Fig. 2-3 - General layout of a positive displacement pump, in this example with a double acting piston **[69]**

As there is a necessary transfer of motion from rotational to linear, positive displacement pumps have the inherent disadvantage of more moving parts and a more complex drive system than other pump types, making them more difficult to maintain

than the simpler centrifugal pump. They tend to be less reliable than single-stage centrifugal pumps but more reliable than multistage versions (dependant on the complexity) [70]. Reciprocating pumps, along with all varieties of positive displacement pumps, have the advantage of being able to produce an output flow whenever the motor is rotating, provided the motor can overcome the initial torque required to start the pump; which can be up to three times that of the torque required during standard operation [64]. This reason makes such pumps well suited to low power pumping applications such as small scale sustainable pumps, so long as the start-up torque can be overcome using some form of electronic control or boost system [11]. This, however, may be undesirable in many cases due to the increased complexity of the pumping system and possible maintenance issues. Further, as the discharge flow from a positive displacement pump is proportional to the rotational speed of the motor, these types of pumps are relatively decoupled from their operating head. This makes them the more suitable choice for higher head pumping applications [2].

Additionally, positive displacement pumps tend to have higher pumping efficiencies than centrifugal pumps (typically up to 70% compared to the centrifugals 30%) [11], especially at higher heads, where the additional frictional forces associated with piston pumps are smaller in relation to the hydrostatic forces. At lower heads, the frictional losses in piston pumps make them the less efficient choice, however, and centrifugal pumps dominate.

2.6.2 Helical Pumps

The helical (or progressive cavity) pump is another style of positive displacement pump. A rotating shaft supports a screw in a sealed vessel which, when

turned through the action of the pump motor, forces the water linearly through the pumping chamber and to the exit out of the pump. As the pitch of the thread varies from that of the stator housing, a single helical cavity is formed which delivers 'packets' of water at the pump outlet. These are relatively simple pumps and are commonly used within modern submersible borehole systems as they are easily adapted to pumping in confined geometries. A brief outline of the layout of such a pump is described in **Figure 2-4**.

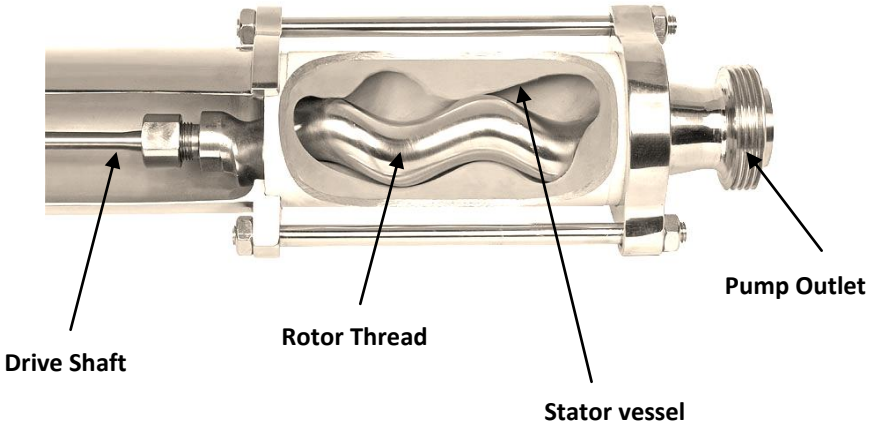

***Fig. 2-4 - General layout of a helical pump (image sourced* [71])**

Helical pumps have seen much development over the last decade, taking them from a relatively unknown pump type [2] to a common variety offered by many pump manufacturers; the LORENTZ™ PS-HR range and Mono™ pumps, for example. Helical pumps, like their piston pump counterparts, are able to deliver discharge flow under low power levels as long as the pump motor is operating. They are particularly suited to medium/high pumping heads and provide good levels of discharge flow (although not as high as centrifugal pumps at low heads). Helical pumps additionally benefit from the same high efficiencies as piston pumps but with electrical load characteristics more

similar to centrifugal pumps, making them suitable for a broad range of applications. Their main drawback, however, is the complexity in manufacturing of the rotor/stator housing. Due to high tolerances, the process is more costly than other styles of pump leading to increased capital investment per unit. Furthermore, the stator housing is particularly susceptible to wear over time, especially in pumping locations with high degrees of sediment, silt or iron oxide in the water.

2.6.3 Centrifugal Pumps

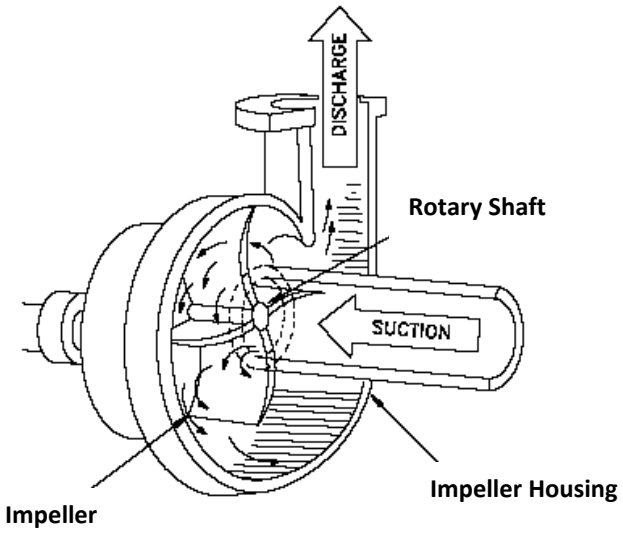

Fig. 2-5 - General layout of a centrifugal pump

Centrifugal pumps are based on the principle that water can be drawn from a source given the application of a centrifugal force to the end of a pipe (providing the pump is first primed). In its simplest form, the centrifugal pump may be described by considering a T- junction with the single arm submerged in water. If the T- junction is rotated about a centre point which is along the same axis as the submerged pipe section, water will be forced out of the open ends of the T-section pipes and create suction upwards (providing the rotational speed is great enough to overcome the

gravitational force of the liquid). More typically, the T-junction is replaced by a more finely tuned impeller in nearly all modern centrifugal pumps. As such the centrifugal pump is split into two main sections: the impeller, which rotates about an axis which is coupled to the drive shaft of a motor, and the pump housing. This creates a seal around the impeller, so that its rotation creates a pressure difference capable of drawing fluid through the pump. The basic layout of the centrifugal pump is illustrated in **Figure 2-5**. This example, using a single impeller is considered to be a single-state centrifugal pump.

Centrifugal pumps are often the preferred choice for pumping applications due to their reliability and well known performance across a range of operating conditions, but especially when pumping at low heads and high discharge volumes [2, 11, 68]. Due to this reliability, and coupled with the fact that they require little maintenance with parts easily available for a low cost, centrifugal pumps may be considered a good option with regards to an appropriate technology for rural locations. For low heads, single stage-pumps are capable of high levels of discharge flow and are commonly suited to water provision for irrigation and domestic use. For higher heads, multiple impellers may be stacked to produce a multistage centrifugal pump, capable of operating under much higher loads. Consequently, for pumping situations requiring high flow rates of water beyond low heads (typically those above 15m or so), multistage centrifugal pumps are the preferred option [2]. The drawback of increasing the number of 'levels' to a pump is the increase in reliability issues and added expense.

One of the key disadvantages of centrifugal pumps is that their efficiency and pumping performance drop rapidly upon any deviation in operating conditions from the

pumps best efficiency point (BEP). Further, the ability to make use of available energy is reduced resulting in, particularly for sustainable power systems, lost pumping potential unless the system is coupled with a battery (enabling the system to utilize stored energy at a later time). This is best illustrated by the general pumps trend in **Figure 2-6**.

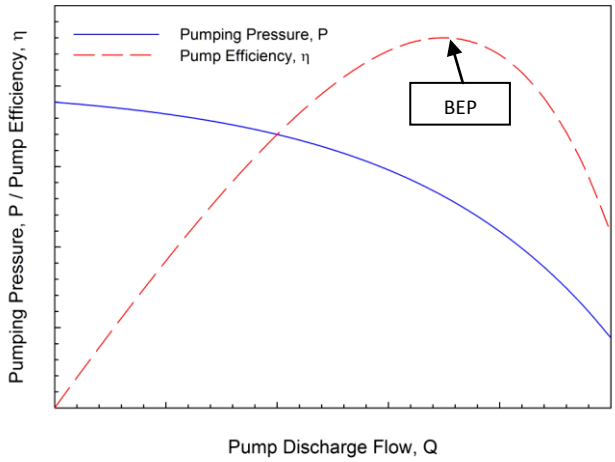

Figure 2-6. Identification of BEP with regards to pump flow rate (General illustration)

Any deviation from the pumps preferred operating conditions is thusly cause for concern and is chiefly combated through the appropriate site assessments and system calibration. This helps to avoid a shortened lifespan and maintenance issues. Unfortunately, the additional time taken in assessing a systems suitability for a given site and expertise in system installation comes with an increase in cost. This potentially makes some systems less affordable.

Centrifugal pumps benefit from having a lower start up torque than running torque, enabling operation under low levels of power (low insolation levels in the case of PVP's). Unlike with positive displacement pumps however, a centrifugal pump is unable to provide a discharge flow until the impeller has generated sufficient pressure

to overcome the operating load; this often leads to the implementation of control systems to provide sufficient power for operation. This varies for different models and manufacturers and also with the number of modules used in a system [2]. Pressure generation aside, the operational torque characteristics of centrifugal pumps make them ideal candidates for directly coupled systems, the benefits of which have already been discussed in **Section 2.4.4**. Of particular interest is the cost benefits of such a system for low pumping heads for irrigation purposes [72].

2.7 Limitations to Current Technology

2.7.1 Operating Conditions

The conditions under which a sustainable pump must operate are not expected to be constant and any environmental changes, such as increased or decreased rainfall in the wet and dry seasons, can impact upon a pumps performance. In the case of PV pumps, the reasons for this are twofold. Firstly, changes in the weather conditions can mean the difference in a relatively low or high borehole water level. Such a fluctuation in the pumping head can result in a decrease in performance for a standard centrifugal pump as well as any other type of pump. Ordinarily, it is not possible to compensate entirely for changes in environmental conditions such as rainfall, save implementing a pump with a good range of pumping heads. Secondly, for PV pumps, any changes in the intensity of solar irradiation in an area due to, for example, cloud cover or changes in daylight hours can impact upon the amount of power available to power the pump. Three ways of countering this effect are to employ a maximum power point tracking (MPPT) controller to the system, sufficient reserve water storage and/or battery storage. However as already mentioned in the argument for PVP's, insolation levels are

often in-line with the power demand for highest water supply during periods of most demand. In the case of wind-electric and wind-PV hybrid systems, environmental changes in wind speed also have an impact on potential pumping capabilities of pumps.

2.7.2 Borehole Dynamics

In addition to changes in pumping head due to environmental effects, there also exists the issue of 'dynamic drawdown' [67]. During pumping, the water level in any borehole will drop as water is displaced as discharge flow. Water from the surrounding area must then balance the displaced water until equilibrium is achieved. Depending on several factors the degree to which the water level is 'drawn down' will vary. These include the discharge rate, soil permeability and area of the borehole. Naarvarte *et al.* provide a comprehensive summary of typical values of the static and dynamic levels of water in locations around Angola and Morocco, in addition to an informative guide on the phenomenon. These fluctuations in water level must be taken into account, especially in the case of centrifugal pumps, when specifying the pumping system for a particular location. Much as with any other site specific assessments, this adds to the installation cost and also adds another degree of complexity to the operation of a pumping system.

2.7.3 Installation Losses

When installing any pumping system, there is almost always a degree of human error involved in aligning and fitting all of the components as well as securing the pump in place in addition to component matching [12]. These errors can contribute to the pump operating outside of its BEP conditions due to an increased head from additional friction or losses through components. Further to this, and regardless of correct

installation or not, there lies a friction head within the system which, over time, will increase due to wear on the parts and internal corrosion of the pipes. Such losses can never be entirely avoided, but they can be lessened by introducing filters before the pump and ensuring all components are well protected. Poor component matching and improper installation have been previously shown to have a significant impact on a pumping systems operation, with entire systems failing [73]. This leads to the demand for either suitable technical expertise in selection and installation of equipment or the ability of a pumping system to self-calibrate and negate lack of expertise.

2.7.4 Power Utilization

Irrespective of the power source and degree to which power is freely available, a centrifugal pump is only able to utilize a finite amount of energy at any one time, dependant on current operating conditions. As previously established, the likelihood of a pump being able to continuously draw from its MPP is low, particularly in the use of direct coupled systems [12, 63]. Even in the case of optimization through an MPPT it would still be beneficial to utilize the optimum power available in the form of improved discharge flow, especially in pump/power systems where there is a surplus energy already available (this particularly relates to solar at high levels of insolation).

Additional generated energy may be stored in a battery system for later use, but ideally a simpler system would forgo the added complexity and expense of a battery for the storage of additional water in a reservoir. Thus, it would be more desirable for a pumping system to be able to utilize any and preferably all energy available to it at a given time, storing any surplus water for times of higher demand or lower pumping capacity.

2.7.5 Appropriate Technology?

"*Appropriate technology and village level operation are two design ideologies that, when considered together, can contribute towards the sustainability of (solar powered) water pumps." – T. D. Short 2003*

In spite of being able to deliver a reliable supply of clean water to a developing community, there is still the challenge of deciding whether or not a particular type of technology is appropriate [68]. This begs the question: are centrifugal pumps, in the context of sustainable pumping, an appropriate technology? To consider an answer to this, the term appropriate technology must be defined. Dunn [74] summarises the term by considering the aims of an appropriate technology to:

- Improve the quality of life of people.
- Maximise the use of renewable resources.
- Create work places where people live.

In addition to these aims, there are also a set of criteria that a technology must adhere to. As such, a technology must be able to:

- Employ local skills.
- Employ local material resources.
- Operate within local financial constraints.
- Be compatible with local culture and practices.
- Satisfy local wishes and needs.

While automated pumps may fulfill the aims of an appropriate technology, it is clear to see that, for a pumping solution to be entirely suitable, the pump selected must be

easily maintained at a level within the capability of a developing community or independent rural location.

2.9 An Ideal Pumping System?

With regards to water pumping in rural areas, it would seem that the most ideal system would be one which was capable of reliable operation for a low cost. Of course it would also seem apparent that the broad range of options available in this area makes it hard to settle on a single set system. Whitfield *et al.* [75] propose that PV systems offer the ideal solution for remote areas, particularly in developing countries; but there does, however, still exist the need to reduce their cost. The methods suggested for realizing this are by either increasing the efficiency (and hence reducing the number of PV panels required) or by lowering the cost per panel. Although this could provide a means of increasing the availability of off-grid pumping systems, it would seem odd that the efficiency and unit cost of the pumps themselves were not fully considered. Some of these issues have been addressed again by Whitfield [19, 76] who suggests pump and motor improvements including the use of brushless motors and direct drive; both to remove losses. Within the context of PVP's, an ideal system may similarly be described as being a combination of several key factors [77]:

- Efficiency.
- Low initial and operational costs.
- Robustness and durability.
- Load Matching

Twidell [78, 79] argues, however, that efficiency and the saving of sustainable energy is not that important for its part, as there is an abundance of energy available at no cost.

Twidell further reasons that the primary motive for improving efficiency would be to reduce the size, and hence cost, of a device. Thus, with the falling cost of sustainable power systems (in particular PV panels) creating an overall reduction in system costs, the logical conclusion is that the effectiveness of the non-power portion of a system should be improved (i.e. the pump and its subsystems). This has been highlighted in much of Short's work, which suggests that both a reduction in cost and increase in ability to deliver appropriate levels of water output for a given power input are the highest priorities. Further, the issue of site specific assessment still exists. As argued by Short and Burton the fluctuating operating conditions faced by borehole pumps has proven to be a challenge which is most usually overcome through incurrence of cost. Consequently, there exists a need for:

> ''…a pump…. applicable to any site conditions, including variation in head – without modification'' (Short and Burton 2003) [11]

Such a pump would be able to perform across a range of heads for a low power input, combining the characteristics of both centrifugal and positive displacement pumps as discussed previously. This leads towards the idea of a pump with 'auto-setup' capability [5, 64, 80]. This form of pumping system would indeed go some way to reducing implementation costs and making water pumps more readily available.

2.10 Summary

This chapter has presented a broad literature review into the various pump types, power systems and requirements of off-grid water pumps, highlighting many of the benefits and problems associated with each. Furthermore, the need for clean water

supply for both domestic and agricultural means has been addressed; the need for a one-size-fits-all pump has been identified as a possible solution to meet these demands.

From investigating the suitability of various off-grid power systems, it has been concluded that the use of renewable energy systems in conjunction with centrifugal pumps could provide the lowest cost and most sustainable solution. Similarities between the operating curves of both the centrifugal pump and PV panel have been identified. As the operation of a PV panel may be modified through the use of an electrical 'buffer' (MPPT) to decouple its performance from operating conditions, it would be possible to suggest a similar buffer to be introduced to the operation of a centrifugal pump. This could allow a single stage centrifugal pump to draw from its BEP across a wider range of heads than previously possible and eliminate the need for multi-staging and site specific assessments; hence reducing the associated costs. This presents an interesting and novel avenue of research into the furtherance of centrifugal pumping technology. The means of providing a BEP tracking system is discussed further in **Chapter 4**.

Chapter 3

Induced Flow Pumping

Following on from some of the ideas introduced in **Chapter 2,** this chapter covers the basic principles of induced flow pumping with reciprocating pumps. It aims to further highlight its benefits and how, by comparison to similar induced flow systems (such as the hydraulic ram), it is possible to suggest a modified version for use with centrifugal pumps. Taking into account the electric-hydraulic analogy, the theory from both hydraulic rams and boost-converters from DC-DC power electronics is used to provide a starting point in defining a novel pumping system.

3.1 Induced Flow in Reciprocating Pumps

Pumps employing the principles of induced or inertial flow have been well understood and studied for many years with many simple examples outlined by Ewbank [81] and discussed as part of other studies by Burton and Short [7]. Early examples rely upon the fact that flowing water has inertia and once accelerated by an external force will continue to flow until all energy is dissipated. The simplest example of this is the 'joggle-tube'; a single rigid pipe with a valve located at one end which moves water through this inertial principle; illustrated by **Figure 3-1**. As water is accelerated up

through the tube it gains kinetic energy which, upon ending the upward motion of the tube, allows flow from the tube outlet. In this way the tube itself is acting as a 'fluid inductance' much in the same way as an electrical inductor. The principles of this simple idea have been expanded upon with the development of the induced flow reciprocating pump, first modeled by Lobo-Guerrero [82] and developed by others thereafter [8, 83, 84].

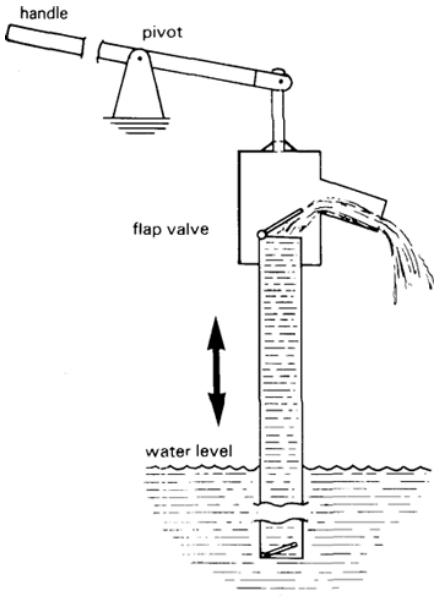

Fig. 3-1 – A simple hand pump version of the joggle tube **[85]**

The induced flow reciprocating pump makes use of a fluid inductance and capacitance in order to increase its water discharge rate over a standard reciprocating pump of a given size and speed. Further, it expands the operational range of the pump; this allows for greater power utilization at lower heads than typically expected of a reciprocating pump. In **Chapter 2** the idea of an 'ideal' pumping system was introduced as a means of expanding the operating range of traditional pump types, building toward

a ''one-size-fits-all'' pump. In some ways, the induced flow reciprocating pump goes towards providing a viable option [6, 12, 64].

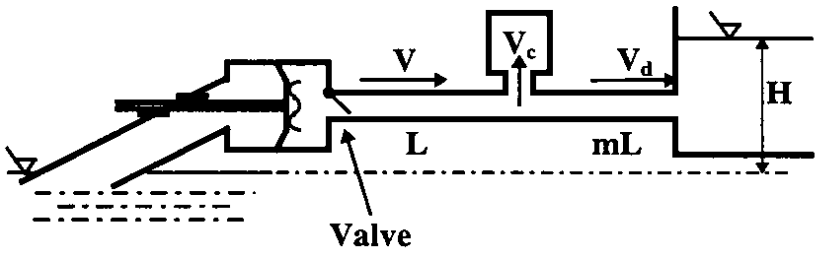

Fig. 3-2 – Over-resonant induced flow reciprocating pump (from Burton and Short [8]) where: L- Inductance Pipe, V – Flow velocity in the inductance pipe, V_c – Flow velocity in the capacitance chamber, V_d- Velocity in the discharge pipe, mL- Discharge inductance and H – System head or load.

The standard configuration of an induced flow reciprocating pump includes both a hydraulic capacitance and inductance, in addition to a non-return valve to eliminate backflow. The action of the capacitance and inductance introduces to the system a natural frequency, $\omega_n = \sqrt{K/L}$ [8](where K is the hydraulic 'softness' and L the inductance, discussed more in **Chapter 4**). This inductance-capacitance system enables the pump to deliver a discharge flow during the 'return' stroke of the piston arm; this makes use of the fluid inertia in the inductance pipe and 'suction' effect of the capacitance chamber. Earlier sub-resonant versions arranged the capacitance directly after the piston chamber, which was then followed by the inductance pipe (leading on to the discharge pipe) [7, 64] and have been shown to operate at volumetric efficiencies of up to 250% [84]. However, stability problems have been identified with this arrangement at operating frequencies close to resonant [86] in addition to the difficulty of de-coupling the inductance pipe from the discharge pipe (the additional discharge

pipe length in effect adds to the already present inductance length) [8]. This decoupling issue was partially resolved with the creation of the twin cylinder version of the pump, however reordering the inductor-capacitance system eliminates the problem [87] and allows for the suitability of submersible borehole pumping. The resulting over-resonant system is described by **Figure 3-2** and is fully analysed by Burton and Short [8, 64] who observed a doubling of discharge flow at low heads compared to existing PV or wind systems.

3.2 The Hydraulic Ram

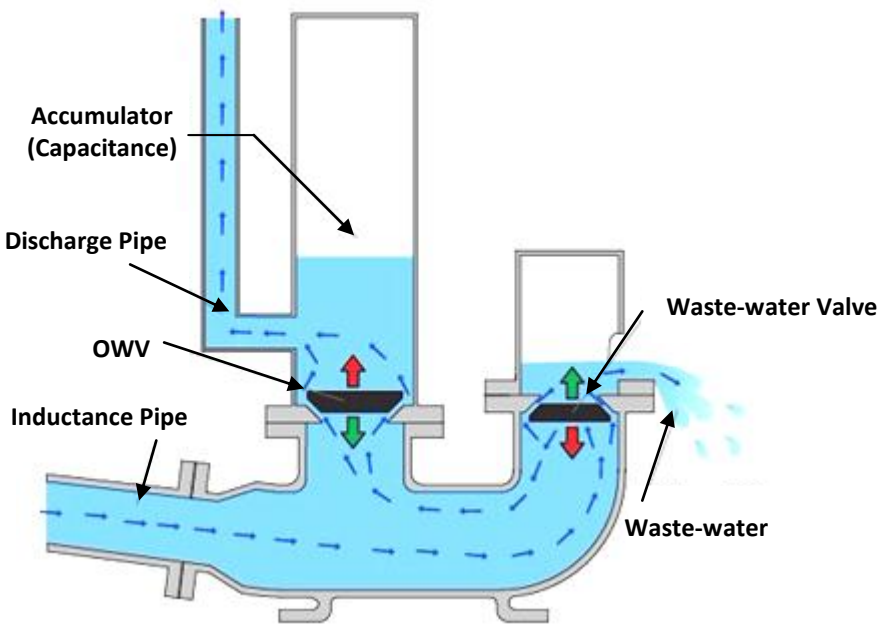

Fig. 3-2 - Basic hydraulic ram layout

The hydraulic (or water) ram has been used as a means of elevating water for an age, with some early accounts of force pumps using an air cavity dating as far back as 300 B.C by the Greeks [88]. Even the first recorded design of a hydraulic ram was

coined by Whitehurst in 1775 [89] with the more modern automated version following shortly after with Montgolfier's pump [90]. Since then, the more widely accepted version of the pumps design has been implemented and its operation studied and improved [88, 91-93], with the pump being used throughout the 20th century mainly to supply farmland or to power water features on large estates. More recently, the hydraulic ram is being seen as a good option for rural water pumping for its simplicity, low cost and sustainability [16, 94, 95]. The hydraulic ram, much like the induced flow pumps mentioned previously, relies on the inertia of a fluid in motion for its components to function together. Its operation is now examined.

Figure 3-3 illustrates the basic layout of a modern hydraulic ram. It identifies the main components as being similar to those found in **Figure 3-2**: the over resonant induced flow pump from Burton and Short [8]. The sequence of operation begins with the acceleration of water through the inductance pipe; this is most commonly due to gravity. The accelerated fluid then passes through the main cavity of the pump where it flows out to atmosphere via the waste-water valve. Once the kinetic force of the fluid is strong enough to close the waste-valve, the fluid is left with no other option but to be forced back through the pump cavity through a process called *'water hammer'.* The effect of this is to raise the pressure within the pump cavity and open the OWV into the accumulator chamber, causing a small amount of water to flow through. With the drop in pressure within the cavity from the shock wave travelling back through the pump, the waste-water valve is 'drawn' open again, allowing the process to repeat. As this sequence of events continues, the pressure in the accumulation chamber builds and forces water up through the discharge pipe until it reaches the pump outlet. As with

Burton and Short's induced flow pump the positioning of the inductance and capacitance allows for the decoupling of pumping head and input flow.

Due to the nature of their operation being fully reliant on a readily available water source, which may be used to provide a continuous flow through the inductance pipe, hydraulic rams have limitations to their use. Not least is the limitation to mainly hilly areas with all year round water supplies, making them unsuitable for many rural areas [16]. Further, as a large amount of the water used to provide the lift through the pump is lost from the waste-water valve, the scale of pumping is limited.

3.3 Electric-Hydraulic Analogy

The electric-hydraulic analogy (or sometimes hydraulic analogy) may be used to relate equations defining the transport of fluid through a system to the flow of current through a DC electrical circuit. In this way, there may be several comparisons drawn between the operating characteristics of both systems, namely: Voltage-Pressure, Flow-Current and ground reservoir-earth relationships [96]. This analogy has previously been used by Short in his definition of the induced flow reciprocating pump [64]. In the following sections, the boost-converter from DC power electronics is compared to the hydraulic ram and a simple equivalent design produced for a centrifugal pumping system.

3.3.1 The DC-DC Boost-Converter

Boost converters are used to convert DC power at one voltage to DC power of a greater output voltage (converse to buck-converters). They are commonly used in applications with design limitations on space, hence the requirement to provide higher voltages through other means than with a standard stacked series of power cells. A

primary example of this is electric or hybrid car batteries. **Figure 3-3** provides an illustration for a simple boost-converter:

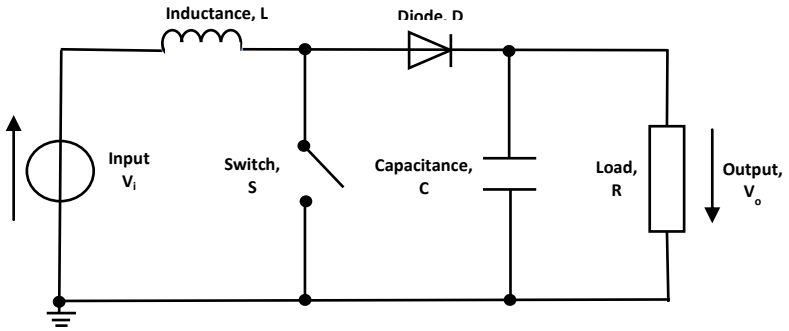

Fig. 3-3 - DC-DC boost converter circuit

This design may be seen to be analogous to the hydraulic ram system illustrated by **Figure 3-2**. Both make use of an inductance, capacitance, one-way valve to regulate flow 'upstream' to the system output, and a release valve to ensure an increase in flow through the inductance periodically between system discharges. The only main difference between the two systems is that with the boost-converter, the switch, or 'waste-valve', is electronically controlled and based on a system duty (dependent on the operating conditions and resonant parameters of the circuit).

3.3.2 Centrifugal Water Pump with Pressure Boost

Making use of the electric-hydraulic analogy and recalling that an MPPT may be used to decouple a PV panels output from its operating conditions, it is possible to replace the electrical components in the boost-converter circuit with hydraulic components to form a pressure-boost circuit. In this case, the input voltage is replaced by a constant system pressure (created by a centrifugal pump), much like the constant flow source in a hydraulic ram. In the same way an MPPT applies the correct resistance

or load to the electrical PV circuit (ensuring maximum power is drawn from the panel), the equivalent hydraulic circuit would correct the load on the pump to ensure maximum hydraulic power. More detail on the design of such a system is presented in **Chapter 4.** The basic layout is presented in **Figure 3-4**.

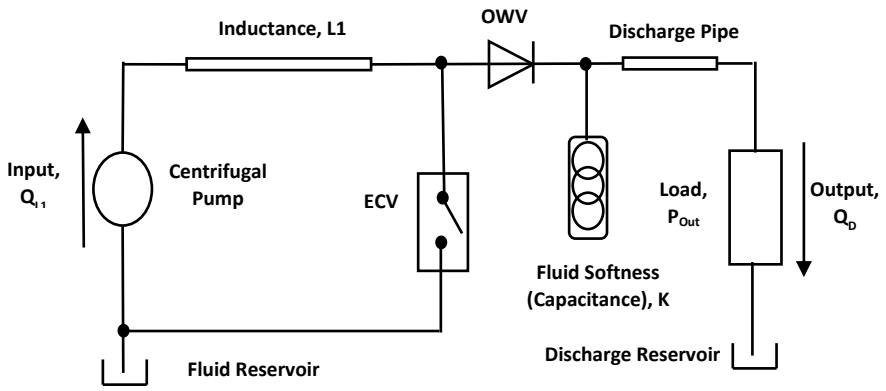

Fig. 3-4 – Hydraulic equivalent 'boost-converter' circuit

Similar hydraulic circuits have been suggested as a means of pressure boosting in mechatronics and fluid power control systems [97-101]. Although such articles highlight the benefits of high speed valves as a means of hydraulic pressure-boost and suitability of the application of such circuits for use with centrifugal pumps, the theory has not yet been applied to water pumping systems with the main focus being discharge flow and maintenance of BEP conditions for the centrifugal pump.

3.4 Summary and Conclusions

The principles and advantages of an induced flow system in reciprocating pumps have been identified, illustrating how the operational range of a pump may be expanded to make such pumps more applicable to lower heads. Further, from the

comparison of this system to a traditional hydraulic ram, similarities have been drawn to boost-converters as a means of pressure boosting in hydraulic circuits.

Chapter 2 discussed the idea that an auto-setup capability for any pumping system would provide a means of eliminating the need for costly site specific assessments and also ensure that a pumping system could operate across a wide range of fluctuating conditions. By applying the concept of a boost converter to a pumping system, based around the use of a centrifugal pump, it should be possible to decouple the pump from the operational head. This would negate any disadvantageous effects of fluctuations in borehole water levels and ensure that the pump could deliver a discharge flow across a wider range of conditions; expanding the use of single-stage centrifugal pumps from low head applications to much higher ones. In this way, a centrifugal pump could behave more like a hybrid between positive displacement pump and centrifugal, much like the induced flow system suggested and developed by Burton and Short. Further, by eliminating the need for site specific assessments, and through using the cheaper single-stage centrifugal pump, the cost of such a system would be reduced, making the pumping technology more widely available. The design of this novel system is discussed in **Chapter 4**.

Chapter 4

The Pumping System

Following on from the brief pumping system description in **Chapter 3**, this chapter aims to provide a more detailed analysis of how the over-resonant induced flow style pumping system can be modified to work in conjunction with a centrifugal pump.

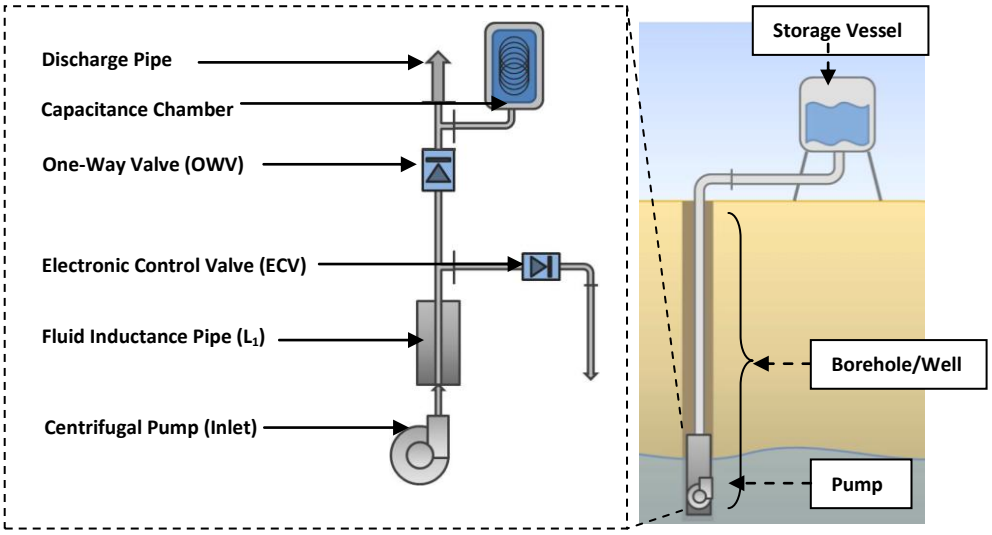

Fig. 4-1 - Brief overview of the tuned hydraulic subsystem components within the full pumping array

Figure 4-1 is essentially an expanded version of **Figure 3-5** showing the various sub-systems needed for an induced flow arrangement, with the addition of the ECV sub-system needed to set up flow oscillations with a centrifugal pump. It has been

arranged to give a more clear idea of how such a system would look when implemented in a borehole pumping system. The pumping system is primarily a centrifugal borehole pump with an outflow pipe leading to a water storage vessel at ground level. Between the pump outlet and storage tank, there are the additional sub-systems required for induced flow and pump optimization: being the fluid inductance pipe, capacitance chamber and ECV sections. These sections are defined in more detail later in this chapter, but first it is necessary to consider how they may be defined mathematically.

4.1 Mathematical Model

When selecting which methods should be used in the analysis of flow and pressure through the pumping system, it was clear that only dynamic models could be used as both of the characteristics to be quantified across the system are time-dependent. Further, it was seen as necessary to incorporate the effects of inertia within the system due to the rapid changes in flow characteristics as a result of the ECV.

For the linear analysis presented in **Chapter 5**, it was decided that the equations used were to be based on a lumped parameter model. Where the distributed parameter model accounts for the transients in the fluid flow, the lumped parameter model does not and instead treats the fluid in the system as a rigid body. Although this model may appear to be inferior, it does allow for equations to be developed through a linear analysis of the system without the need for complex computational flow dynamics (CFD). It also allows for the use of the steady flow energy equation for a low speed, incompressible fluid [102]. This was not only beneficial in the completion of the theoretical model for the numerical simulations in this thesis (and as a time saving

device so as experimental testing could be carried out), but also provided a very simple model of the pumping system, which could be used to predict performance.

Previous work by Short [64] has used the lumped parameter model for analysis based on the fact that the resulting equations from analyzing the components through the pumping system are:

''*firstly simple second order differential equations…….and…….secondly, identical to the describing equations of an electrical circuit*''.

The validity of using the lumped parameter model may also be assessed through the use of Chaudry's criterion, **Eqn. 4-1**, [103] or more conservatively by the criterion set by Wylie and Streeter, **Eqn. 4-2**, [104] where it may be seen that the lumped parameter model is more suited to use across smaller sections of pipe work, such as those in the pumping system up to the capacitance chamber.

$$\frac{\omega l}{c} \ll 1 \qquad \textbf{Eqn. 4-1}$$

$$\frac{\omega l}{c} < \frac{\pi}{12} \qquad \textbf{Eqn. 4-2}$$

4.2 System Analysis

4.2.1 The Inductance Pipe

The fluid inductance pipe is essentially a short length of pipe joining the outlet of the pump to the junction before the E-OWV. The flow through the inductance pipe may be described by considering the forces across its length. Assuming the pipe to be frictionless, the force across the pipe may be represented by **Eqn. 4-3**, where the

acceleration term in the equation may be expressed in terms of its change in velocity with relation to time.

$$\sum F = Ma = M\frac{du}{dt} \qquad \textbf{Eqn. 4-3}$$

Considering that $P = F/A$ and also that the mass of fluid flowing through the pipe may be expressed using the mass-density equation, $M = \rho V$, then **Eqn. 4-3** may be replaced with **Eqn. 4-4**.

$$\Delta P = \frac{\rho l}{A}\frac{dQ}{dt} \qquad \textbf{Eqn. 4-4}$$

Within this equation the inductance of the pipe, L, has in previous works [64] been shown in the form outlined by **Eqn. 4-5**. By substituting into **Eqn. 4-4** and rearranging, a secondary formula for the inductance in the pipe can be achieved:

$$L = \frac{\rho l}{A} \qquad \textbf{Eqn. 4-5}$$

$$\Delta P = L\frac{dQ}{dt} \qquad \textbf{Eqn. 4-6}$$

This is analogous to the electrical equation for inductance in a circuit, again defined and highlighted by Short [64] and given by **Eqn. 4-7**:

$$V = L\frac{dI}{dt} \qquad \textbf{Eqn. 4-7}$$

Such a relationship is useful when determining the appropriate length to use in the inductance pipe as it allows the inductance value to be fixed for specific values of valve opening times, which are discussed in more detail later in this section.

Alternatively **Eqn. 4-6** may be defined and proven by using Euler's equation, assuming that the flow through the pipe is frictionless and one-dimensional [105].

$$\frac{1}{\rho}\frac{dP}{ds} = \frac{du}{dt} + g\frac{dz}{ds} \qquad \textbf{Eqn. 4-8}$$

As is defined in **Section 4.3** of this chapter, the change in height (dz) across the ECV and induced flow components of the piping system may be neglected. As such, **Eqn. 4-9** is produced, which may be rearranged and written in the form described by **Eqn. 4-10.**

$$\frac{1}{\rho}\frac{dP}{ds} = \frac{du}{dt} \qquad \textbf{Eqn. 4-9}$$

$$\frac{1}{\rho}\frac{dP}{ds} = \frac{1}{A}.\frac{dQ}{dt} \qquad \textbf{Eqn. 4-10}$$

where:

$$Q = u.A$$

From inspection of **Eqn. 4-10** it is clear that by taking the ds term in the equation to represent the pipe length traversed by the fluid over time, dt, the equation may be rearranged to produce the same form as **Eqn. 4-6.** By using the same inductance formula as before, **Eqn. 4-4** is again obtained. This equation will become more useful in defining the relationship between the flows across different points in the linear analysis performed in **Chapter 5**.

4.2.2 The Capacitance Chamber

The capacitance chamber is a component which houses a means of providing a fluid softness, K, or degree of compressibility. This could take the form of an

arrangement of compressible material housed within the chamber, a compressible fluid cavity or even a mechanical compressibility. In the case of the experimental rig described in **Chapter 8**, a set of compressible rubber ovoids within a rigid chamber was selected. Regardless of the means, this 'accumulator' acts as a fluid capacitance which allows pumping energy to be stored within the system, much in the same way as an electrical capacitor stores energy within an electrical circuit. Using this electrical analogy it is possible to relate the capacitance of the fluid system to the inductance through the natural frequency of the system:

$$\omega_n = \sqrt{\frac{1}{LC}} = \sqrt{\frac{K}{L}} \qquad \textbf{Eqn. 4-11}$$

where the inductance value, L, is as described in **Eqn. 4-5** and the capacitance, C, can be described as the inverse of hydraulic stiffness, or 'softness', of the fluid accumulator, K.

Further equations to describe the relationship between pressure and flow in the capacitance chamber have been previously developed and used by Short [64]. These equations make use of **Eqn. 4-12**, where it is assumed that if the capacitance chamber is always completely flooded with water such that $n = -1$ and a linear relationship may be used to describe how the volume of the chamber changes with respect pressure (*NB the change in volume is proportional to the change in pressure, due to the fact that as the pressure in the capacitance chamber increases, the 'fluid softness' in the chamber will be compressed and hence the volume of water in the chamber will increase also. For this reason, the index value, $n = -1$, is used to ensure that the hydraulic stiffness, K, remains a constant).*

$$Pv^n = K$$ **Eqn. 4-12**

The volume of water in the chamber may be shown to be equal to the integral over time of the flow into the chamber [64], such that:

$$Q = \frac{dv}{dt} = \frac{1}{K}\frac{dP}{dt}$$ **Eqn. 4-13**

Further, it may be shown that this equation is equivalent to **Eqn. 4-14** through rearrangement.

$$P = K \int Q\, dt$$ **Eqn. 4-14**

Thus, the pressure in the capacitance chamber is equal to the integral of the flow through the chamber, with respect to time, multiplied by the hydraulic stiffness of the material or mechanisms used within the chamber. Much like the relationship demonstrated previously in **Eqn. 4-6**, **Eqn. 4-14** is of much use in relating the pressure and flow between various points through the system, after the OWV section. This is covered in the linear analysis presented in **Chapter 5**.

4.1.3 The Electronic Control Valve (ECV)

The ECV is an electronically operated one-way valve which is capable of high frequency operation. It is used to create oscillations in the flow through the pumping system so as to make use of the induced flow subsystems and control the effective static pressure head acting on the centrifugal pump – allowing it to continuously operate near to its BEP (analogous to the operating of the waste-water valve from the hydraulic ram pumps discussed in **Chapter 3**, or the electronic switch in a boost-converter). The valve is operated by a control circuit and feeds directly back into the borehole water source at times when the valve is open, acting to 'short circuit' the flow

and hence briefly reduce the effective pressure head acting on the pump. At periods when the valve is closed, the water is allowed to pass freely through the rest of the system to the discharge pipe and pump outlet. Through varying the duty and frequency ratio at which this valve operates, it should be theoretically possible to sustain an effective operating head of the centrifugal pump close to its the BEP.

4.3 Best Efficiency Point Tracking

As described in **Chapter 2**, centrifugal pumps have specific operating conditions under which their efficiency is optimum; their so called 'Best Efficiency Point'. Through the addition of the sub-systems outlined in **Figure 4-1** and through introduction of a control system for the ECV, the effective load pressure to the pump may be manipulated so as to allow the centrifugal pump to operate at or near to its BEP continuously. This effect is achieved through constant monitoring of the difference between static pressure head and best efficiency point pressure and altering the operational characteristics of the ECV. This is best understood by analyzing the process through which the operation of the valve is controlled.

Consider the highlighted region of the pumping system illustrated in **Figure 4-2**. It represents the junction arrangement following directly after the inductance section, to **node 2** (where node placement corresponds to those used in **Figures 5-1** in the equation definitions chapter, **Chapter 5**). Flow from the centrifugal pump flows directly through the inductance pipe, carrying a flow rate of Q_{L1}, which branches at **node 2**. Flow from here either passes through the ECV, or carries on if able, toward the OWV and system outlet. The flow from **node 2** to the OWV is defined by the flow rate Q_{OWV}, while the flow across the ECV is defined by Q_{ECV}. The flow across both of these

sections is controlled via the ECV such that when the valve is open, all flow is diverted back to the borehole water source (submergence pressure), effectively creating a 'short circuit'.

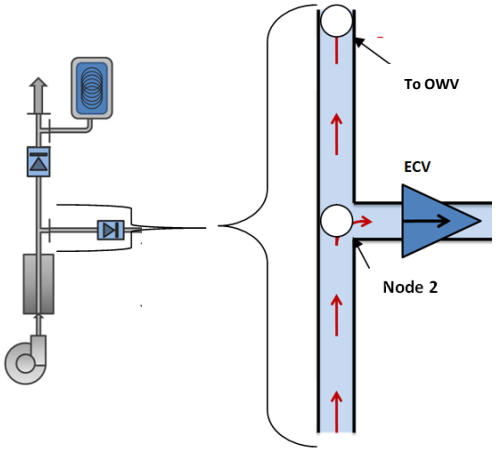

Fig. 4-2 - Pumping system junction at ECV

At all other times the flow is directed through the OWV, leading to the system outlet pipe or fluid capacitance. By controlling the timing of the ECV according to the operational conditions of the pump, the periodic opening of the valve will create oscillations in the flow through the system. These oscillations moderate the effective pressure head on the system to match the BEP of the centrifugal pump, allowing the pump to operate more efficiently across a greater range of heads than would otherwise be expected.

In order to derive a basic series of equations to define the systems dimensions and behavior, and to proceed with the linear analysis using lumped parameter methods, the following is initially assumed about the system:

1. Electronic valve switching occurs perfectly, resulting in fluid flow through either the ECV or OWV, but not both or neither.

2. The flow rate through the ECV increases linearly from minimum to maximum and flow through the OWV is transferred instantaneously upon switching.
3. The system is considered frictionless.
4. The pump operation is considered to be continuous and at BEP flow and pressure.
5. There are no external forces acting on the system.
6. Changes in height between the pump outlet and discharge pipe (i.e. subsystem height) are neglected.
7. Energy must be conserved at all times.

4.3.1 Valve Opening Period

Although the duty cycle is used to determine the operational characteristics of the ECV, it is the time period of the valve that is directly affected by the pumping system parameters. As such, the duty cycle value must be used in conjunction with other known values within the system to determine the correct opening period of the valve to achieve BEP operation. Firstly, the time period of the valve may be represented as the time it takes for the valve to complete a full cycle of opening and closing:

$$T = t_o + t_c \qquad \textbf{Eqn. 4-15}$$

Here, t_o and t_c are the opening and closing periods of the valve respectively. In order to begin to construct a more detailed definition of the opening period, the time period, T, must first be expressed in terms of the known values within the system. The starting point is the basic relationship:

$$T = \frac{1}{f}$$ **Eqn. 4-16**

Then, taking the angular frequency equation:

$$\omega = 2\pi f$$ **Eqn. 4-17**

and combining with equation **Eqn. 4-16**:

$$T = \frac{2\pi}{\omega}$$ **Eqn. 4-18**

The frequency ratio then defines the relationship between the operating frequency of the system and the natural frequency created by the interaction between the inductance and capacitance, such that:

$$r = \frac{\omega}{\omega_n}$$ **Eqn. 4-19**

This in turn allows for a more useful variation of **Eqn. 4-16**, describing the time period in terms of the natural frequency of the pumping system as follows:

$$T = \frac{\pi}{r\omega_n}$$ **Eqn. 4-20**

Expanding the equation for natural frequency completely:

$$\omega_n = \sqrt{\frac{KA}{\rho l}}$$ **Eqn. 4-21**

In this equation all values, aside from the density of the water flowing through the pump, may be defined manually using reasonable values, where the capacitance is altered through the variation in 'fluid softness' (i.e. the addition or removal of compressible rubber balls from the capacitance chamber) and the inductance is varied

by changing the length of the inductance pipe situated at the pump outlet. As such, the time period for the system may be defined as:

$$T = \frac{\pi}{r.\sqrt{\frac{KA}{\rho l}}} \quad \textbf{Eqn. 4-22}$$

Finally, the operation of the ECV is set by determining its opening period based on the time period and duty cycle of the system as follows:

$$t_o = TD \quad \textbf{Eqn. 4-23}$$

In this way, the BEP operation of the pump is decoupled from the operating conditions of the system as described in **Chapter 3**.

4.3.2 The Duty Cycle

By considering the flow from the centrifugal pump outlet is diverted through either the ECV or OWV, it is possible to define the overall flow at the exit of the inductance pipe as follows:

$$Q_{L1} = Q_{OWV} + Q_{ECV} \quad \textbf{Eqn. 4-24}$$

As the flow may be through only one component at a time due to perfect switching, the duty cycle may be used to define each flow rate in terms of a single flow rate, hence:

$$Q_{L1} = (1 - D)Q_{L1} + DQ_{L1} \quad \textbf{Eqn. 4-25}$$

where:

$$Q_{OWV} = (1 - D)Q_{L1} \quad \textbf{Eqn. 4-26}$$

and:

$$Q_{ECV} = DQ_{L1}$$ **Eqn. 4-27**

Next, the energy flow in the system must be considered, so as to introduce the pressure terms needed for the definition of the duty cycle. As it is assumed that there are no external forces acting on the system and that all pipe work sections between the nodes are frictionless, the steady flow energy equation may be reduced to:

$$\sum \rho Q \left(\frac{P}{\rho} + \frac{u^2}{2} \right) = 0$$ **Eqn. 4-27**

Through a series of expanding the energy equation and combining with the flow rate values from **Eqn. 4-25**, a detailed account of which may be found in **Appendix A**, the following equation may be derived to describe the flow through the ECV section of the IFS circuit:

$$\frac{P_{L1}}{\rho} + \frac{{Q_{L1}}^2}{2A^2} = (1 - D)\left(\frac{P_{OWV}}{\rho} + \frac{(1-D)^2 {Q_{L1}}^2}{2A^2} \right) + D\left(\frac{P_{ECV}}{\rho} + \frac{D^2 {Q_{L1}}^2}{2A^2} \right)$$ **Eqn. 4-28**

Continuing to rearrange and simplify, again demonstrated in **Appendix A**, the above equation may be manipulated in order to find an equation defining the static pressure head in terms of the duty cycle as:

$$P_{OWV} = \frac{P_{L1} - DP_{OWV}}{(1-D)} + \frac{3\rho D {Q_{L1}}^2}{2A^2}$$ **Eqn. 4-29**

At this point, it is also possible to begin replacing terms in the equation with more useful equivalents (addressed in **Appendix A**) to demonstrate their relevance to the system. As such, after further simplification, **Eqn. 4-29** may be represented as:

$$P_{Out} = \frac{P_{BEP}}{(1-D)} + \frac{3\rho D {Q_{BEP}}^2}{2A^2}$$ **Eqn. 4-30**

Here, P_{Out} represents the static pressure head of the system under any given operating conditions and P_{BEP} the BEP operating pressure of the pump (required to remain constant in order to achieve optimum power utilization and hydraulic power output from the pump). As the static pressure head will be a variable in this equation, any control system within the pumping unit would have to adjust the opening period of the ECV so as to match the required BEP pressure. By rearranging **Eqn. 4-30** into quadratic form in terms of D, the duty cycle at each pumping head may be calculated. This gives rise to the quadratic equation:

$$\epsilon D^2 - (P_{Out} + \epsilon)D + \Delta P = 0 \qquad \textbf{Eqn. 4-31}$$

where:

$$\epsilon = \frac{3\rho {Q_{BEP}}^2}{2A^2} \qquad \textbf{Eqn. 4-32}$$

and:

$$\Delta P = P_{Out} - P_{BEP} \qquad \textbf{Eqn. 4-33}$$

Consider a system which consists of a submersible, centrifugal pump, the GRUNDFOS SQ Flex 5A-3, with $Q_{BEP} = 5 \times 10^{-4} m^3 s^{-1}$, pipe diameter $d = 0.0254m$ and an inductance pipe length, $l = 0.4m$. By using **Eqn. 4-31**, as the operating conditions deviate from the BEP of the centrifugal pump due to either environmental or degradation reasons, the duty cycle of the ECV can be altered so as both P_{BEP} and Q_{BEP} remain constant at the pump outlet. This is illustrated by **Figure 4-3**, which shows the variation in duty cycle across a range of pressure differences due to increasing static pressure head. Furthermore, as the increase in duty cycle is shown to be exponentially

decaying with an increase in pressure head, there is theoretically no maximum limit to the pressure difference the pump can operate at.

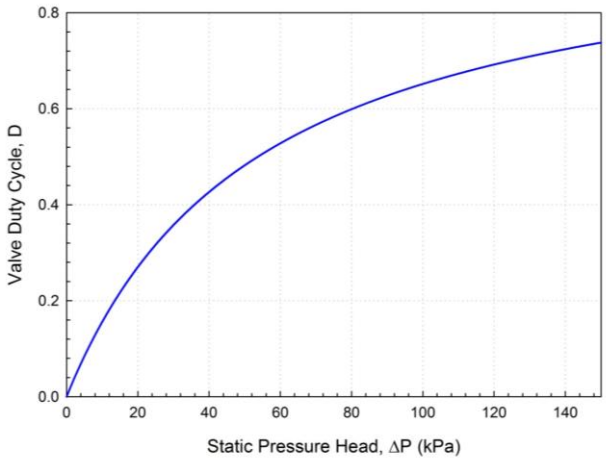

Fig. 4-3 - Example of duty cycle required to maintain BEP

Additionally, recalling **Eqn. 4-23** now that the duty cycle may be defined, the opening period of the valve, for the same example pump, evolves as shown in **Figure 4-4.** This illustrates how the valve is required to be open for increasingly larger periods of time as the pressure head increases, so as to reduce the effective head value to match that of the BEP pressure.

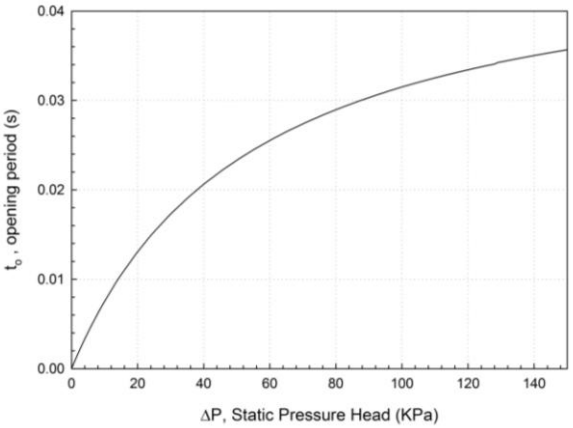

Figure 4-4 – Example of opening period required to maintain BEP

Following this theory it is possible to suggest that with no theoretical limit on how fast the ECV could operate, there would equally be no limit on the maximum head achievable by an IFS centrifugal pump.

4.3.3 Best Efficiency Vs Output Flow

Although the IFS would enable a centrifugal pump to operate at its BEP under a variety of conditions, the addition of the ECV and subsequent opening period would reduce the total discharge flow if used at heads below those of the pumps natural MPP. This would be due to the compensation in the defining equations for the ECV, which hold the pump output at it BEP, effectively increasing the operational load on the pump. As such, in a practical system, it would be beneficial to introduce a lower end limiting constraint to the ECV's operation. This constraint would inhibit the opening of the valve at times in the pumps operation where a significantly improved flow rate could be achieved without putting excess loading on the pump (i.e. times where the pressure head is lower than the BEP pressure).

4.4 Summary

This chapter has presented the initial design of a hydraulic system which is equivalent to a boost-converter and uses similar subsystems to those found in induced flow reciprocating pumps and hydraulic rams. An analysis of each component has been presented using a lumped parameter model, providing the basis for full linear analysis of the pumping system in **Chapter 5.** In particular, the operation of the ECV was discussed, concluding that for a pump operating in continuous mode, there would be no theoretical limit on the pumping head that the IFS centrifugal pump could deliver a discharge flow (based on flow reduction due to MPP and hydraulic power output

consistency). Furthermore, through the use of the ECV and OWV, the centrifugal pump should be completely decoupled from any variation in operating conditions above BEP.

Chapter 5

Characteristic Equations

This chapter looks at how the principles of over-resonant, induced flow pumping affect the output flow of the pumping system described in **Chapter 4** and discusses the approach used to produce a series of equations for defining this flow. These equations are then used in **Chapter 6** as part of the numerical analysis of the pumping system.

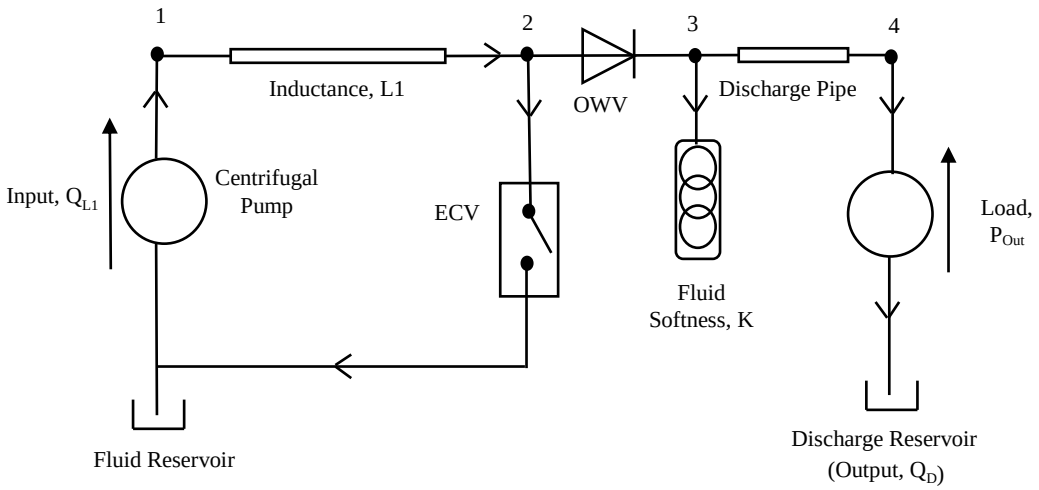

Fig. 5-1. *Hydraulic circuit with IFS*

5.1 Defining flow

Considering **Fig. 5.1,** the flow through each component is defined by considering the flows through the nodes between the components on the hydraulic circuit. As the flow into and out of each node must be balanced, the components may be defined in relation to one another during different stages of the time period.

Starting with the flow through **node 1**, from continuity:

$$Q_{Pump}\,(t) = Q_{L1} \qquad \textbf{Eqn. 5-1}$$

This initial definition is straightforward. As there is no possible divergence in flow, all flow that leaves the centrifugal pump at the start of the hydraulic circuit must travel through the inductance pipe. Moving on to the second node:

$$Q_{L1}\,(t) = Q_{ECV} + Q_{OWV} \qquad \textbf{Eqn. 5-2}$$

Differentiating provides another useful statement:

$$\frac{dQ_{L1}}{dt}\,(t) = \frac{dQ_{ECV}}{dt} + \frac{dQ_{OWV}}{dt} \qquad \textbf{Eqn. 5-3}$$

Following in the same manner, the flow through **node 3** is also considered:

$$Q_{OWV} = Q_K + Q_D\,(t) \qquad \textbf{Eqn. 5-4}$$

$$\frac{dQ_{OWV}}{dt} = \frac{dQ_K}{dt} + \frac{dQ_D}{dt}\,(t) \qquad \textbf{Eqn. 5-6}$$

Finally, there is no need to provide a formal definition of flow at **node 4** as it is solely equal to the discharge flow from the discharge pipe. This set of equations provides the basic definition for the flow through the hydraulic circuit at any point in a single time

period. They will be the starting point for deriving an expression for the output, or discharge, flow from the system.

5.2 Defining Inductance Flow

It is understood that, in reality, there will be a period of time in the operation of the ECV where the valve is neither open nor shut completely and is instead in a state of transition. Additionally, depending on whether the valves resting state is 'normally open' or 'normally closed', the delay time between activation and completion of both open and closed actions will differ (usually as a result of the return spring of a valve having a shorter delay time). However, for the purposes of defining the equations of operation, the switching between operating states of the ECV is taken to be instantaneous and perfect, as defined in **Chapter 4**. As such, there will be only two distinct time conditions under which the system operates:

1. ECV is ON (Open); $Q_{L1}\,(t) = Q_{L1}\,(t)_{ON}$
2. ECV is OFF (Closed); $Q_{L1}\,(t) = Q_{L1}\,(t)_{OFF}$

This is best illustrated in **Figure 5-2** which shows the evolution of flow through the inductance pipe across one time period. By definition of Duty within the system the average flow through the inductance pipe, irrespective of pumping head, will be equal to the BEP flow for the pump, Q_{BEP}. As defined in **Chapter 4,** this is due to the duty cycles dependency on the output head at which the ECV operates. It is clear to see from **Figure 5-2** that for this to be true the change in the flow associated with each time condition must be equal and opposite, such that:

$$Q_{L1}\,(nT)_{ON} = Q_{L1}\,(nT)_{OFF} \qquad \textbf{Eqn. 5-7}$$

$$Q_{L1}\,(\,nT + nt_o)_{ON} = Q_{L1}\,(nT + nt_o)_{OFF} \qquad \textbf{Eqn. 5-8}$$

This ensures that the flow through the inductance pipe, L_1, is continuously fluctuating about the average flow rate, Q_{BEP}. This fluctuation is called the flow 'ripple'. The relationship between the flow $Q_{L1}\,(\,t)_{ON}$ and $Q_{L1}\,(\,t)_{OFF}$ is also used as the starting point for defining the boundary conditions of discharge flow later in this chapter.

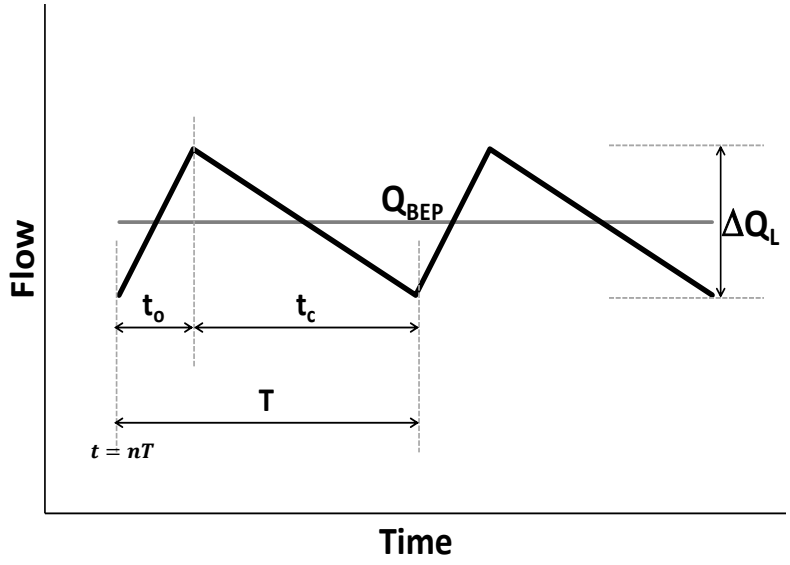

Fig. 5-2. Evolution of flow through inductance pipe, L1

Taking the 'ripple' in inductance flow to be exactly half of $\Delta Q_{L1}\,(t)_{\,ON}$ the equation describing the amplitude of 'ripple' as a proportion of Q_{BEP} is given as follows:

$$\mathbb{R} = \frac{\Delta Q_{L1}\,(t)}{2Q_{BEP}} \qquad \textbf{Eqn. 5-9}$$

The addition of the term Q_{BEP} is to convert the 'ripple' into a flow which may be used in defining $Q_{L1}\,(\,t)_{ON}$ and $Q_{L1}\,(\,t)_{OFF}$ at a given time. Furthermore it is now possible to describe Q_{MAX} and Q_{MIN}.

$$Q_{L1\,(MAX)} = (1 + \mathbb{R})Q_{BEP} \qquad \textbf{Eqn. 5-10}$$

$$Q_{L1\,(MIN)} = (1 - \mathbb{R})Q_{BEP} \qquad \textbf{Eqn. 5-11}$$

The maximum and minimum flows, Q_{MAX} and Q_{MIN}, vary according to the duty cycle and hence the 'ripple' in flow increases in amplitude as the pumping head increases. This may be demonstrated by defining the difference between Q_{MAX} and Q_{MIN} using the same theory to define the change in current across a DC boost converter, as discussed in **Chapter 4**. In such a way $\Delta Q_{L1}\,(t)$ may be described by both **Eqn. 5-12** and **5-13.**

$$\Delta Q_{L1}\,(t)_{\,ON} = \frac{DTP_{BEP}}{L_1} \qquad \textbf{Eqn. 5-12}$$

$$\Delta Q_{L1}\,(t)_{\,OFF} = \frac{(P_{BEP} - P_{Out})(1-D)T}{L_1} \qquad \textbf{Eqn. 5-13}$$

Moving on to define the evolution of $Q_{L1}\,(t)$ across the full time period, it can be seen from **Figure 5-2** that the flow increases or decreases linearly between Q_{MAX} and Q_{MIN} across the two conditions that make up a single time period. In the case of the $Q_{L1}\,(t)_{ON}$ condition, it is clear that by using **Eqn. 5-12** in conjunction with **Eqn. 5-11** the evolution of flow may be described as so:

$$Q_{L1}\,(t)_{\,ON} = (1 - \mathbb{R})Q_{BEP} + \left(\frac{t}{t_o}\right)\frac{DTP_{BEP}}{L_1} \qquad \textbf{Eqn. 5-14}$$

Likewise, by assuming the flow to be a linear progression from Q_{MAX} to Q_{MIN} across the valve closed condition, then the equation to describe the evolution of flow for $Q_{L1}\,(t)_{OFF}$ may be described by **Eqn. 5-15**.

$$Q_{L1}\,(t)_{\,OFF} = (1 + \mathbb{R})Q_{BEP} - \left(\frac{t - t_o}{t_c}\right)\frac{DTP_{BEP}}{L_1} \qquad \textbf{Eqn. 5-15}$$

where:

$$t_c = T(1 - D) \qquad \textbf{Eqn. 5-16}$$

Of course, by inspection of **Eqns. 5-14** and **5-15,** the time factor used as a multiplier in the second half of each equation will only hold true for a single time period (that being the initial time period) after which the numerator becomes larger than the denominator.

5.2.1 Additional Definition of Duty

Recalling that the total change in flow from a certain time nT to $nT + TD$ must be equal and opposite to the change in flow from $nT + TD$ to $(n + 1)T$ (where $'n'$ denotes the number of the period over which the flow wave is operating, from $0 \rightarrow \infty$), then:

$$\Delta Q_{L1}\,(t)_{\,ON} \;+\; \Delta Q_{L1}\,(t)_{\,OFF} = 0 \qquad \textbf{Eqn. 5-17}$$

Substituting in **Eqn's. 5-12** and **5-13**:

$$\frac{DTP_{BEP}}{L_1} + \frac{(P_{BEP} - P_{Out})(1-D)T}{L_1} = 0 \qquad \textbf{Eqn. 5-18}$$

Eqn. 5-18 may then be rearranged to provide an additional definition for the duty cycle based on the pumping head requirement of the system and the BEP operating pressure of the pump entering the inductance pipe. This equation is analogous to a boost-converter (or step-up converter) operating in continuous mode, where the output pressure is always higher than the input pressure (P_{BEP}), such that:

$$D = 1 - \frac{P_{BEP}}{P_{Out}} \qquad \textbf{Eqn. 5-19}$$

where:

$$P_{Out} = \rho g H_{Out} \qquad \textbf{Eqn. 5-20}$$

This definition of duty is directly comparable to the definition previously derived in **Chapter 4** from the steady-state energy equation and represented by **Eqn. 4-26**. A plot of the two duties is shown in **Figure 5-3**. It is seen from the figure that the two duty curves are indistinguishable; indicating that taking the boost converter definition of duty is a suitable substitute and additional definition for pumping system duty. Thus, the simpler definition presented in **Eqn. 5-19** is used in subsequent manipulations.

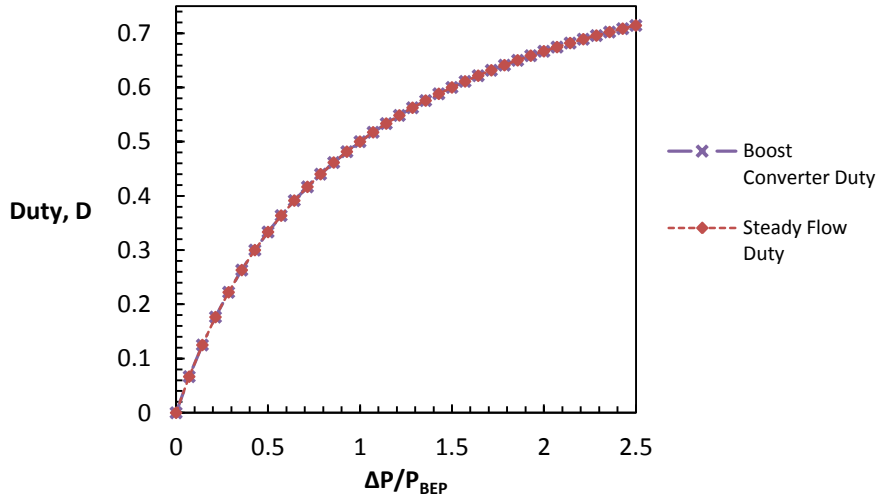

Fig. 5-3. Comparison of Duty evolutions from electronic and steady state theories

5.3 Validation Of The Position Of Average Flow

Consider again **Figure 5-2**, and in particular the theoretical position of the average flow, Q_{BEP} illustrated by the horizontal line which crosses through the flow wave. It is clear to see that the average flow line will cross the fluctuating Q_{L1} flow line between Q_{MAX} and Q_{MIN} marks at some point on the y-axis defined by the equation:

$$Q_{L1\,(Av)} \equiv Q_{BEP} = Q_{L1\,(MIN)} + y \qquad \textbf{Eqn. 5-21}$$

Previously, **Eqns. 5-14** and **5-15** have assumed that this average flow point lies directly half way between the maximum and minimum flows, an assumption that is possible to prove true by considering the total flow as the area beneath the Q_{L1} flow line.

$$Q_{L1\,(Av)} \equiv Q_{BEP} = \frac{1}{T}\left(\frac{1}{2}(\Delta Q_{L1}(t))t_o + \frac{1}{2}(\Delta Q_{L1}(t))t_c\right) + Q_{L1\,(MIN)} \qquad \textbf{Eqn. 5-22}$$

Expanding **Eqn. 5-22**:

$$Q_{L1(Av)} \equiv Q_{BEP} = \frac{1}{T}\left(\frac{1}{2}(Q_{L1(MAX)} - Q_{L1(MIN)})t_o + \frac{1}{2}(Q_{L1(MAX)} - Q_{L1(MIN)})t_c\right) + Q_{L1(MIN)} \qquad \textbf{Eqn. 5-23}$$

Eqn. 5-23 may then be simplified to give an expression for the exact location of the average flow, Q_{BEP}.

$$Q_{BEP} = \frac{1}{2}(Q_{MAX} + Q_{MIN}) \qquad \textbf{Eqn. 5-24}$$

5.4 Theoretical Limit on Pumping Head

As has already been proven, the point at which the average flow lies is given by **Eqn. 5-24**. Now consider that the total average flow across a single time period may be described by **Eqn. 5-25.**

$$\int_0^T Q_{L1(Av)}\, dt = Q_{BEP}.T \qquad \textbf{Eqn. 5-25}$$

In a similar fashion, the total flow across the $Q_{L1}(t)_{OFF}$ period may be described by **Eqn. 5-26**.

$$\int_{TD}^T Q_{L1}(t)_{OFF}\, dt = \frac{1}{2}\,(Q_{MAX} + Q_{MIN}).T(1-D) \qquad \textbf{Eqn. 5-26}$$

Interestingly, this value should also be equal to the total output flow over a single time period as, by definition of the operation of the valve, there is no flow from Q_{L1} to the discharge pipe during the valve ON period. It may also be assumed that any additional flow from the capacitance chamber,Q_K, during the valve ON period will be equal to the loss in flow during the valve OFF period, as the capacitance chamber accumulates 'flow potential'. This gives rise to **Eqn. 5-27**:

$$Q_{D(Av)}.T = \frac{1}{2}\left(Q_{L1(MAX)} + Q_{L1(MIN)}\right).T(1-D) \qquad \textbf{Eqn. 5-27}$$

Hence:

$$Q_{D(Av)} = Q_{BEP}(1-D) \qquad \textbf{Eqn. 5-28}$$

Recalling the definition of duty from the 'Boost Converter' theory presented in **Eqn. 5-19**, **Eqn. 5-28** illustrates how the average output flow will never fall to zero. It can be seen that unless $D = 1$, $Q_{AV(D)}$ can never be zero (and by definition $D < 1$).

5.5 Time Condition 1: ECV (ON)

With the pumping system operating as illustrated in **Figure 5-4,** all flow from the inductance pipe will be diverted through the 'short circuit', created by the ECV being active and thus return to the fluid reservoir.

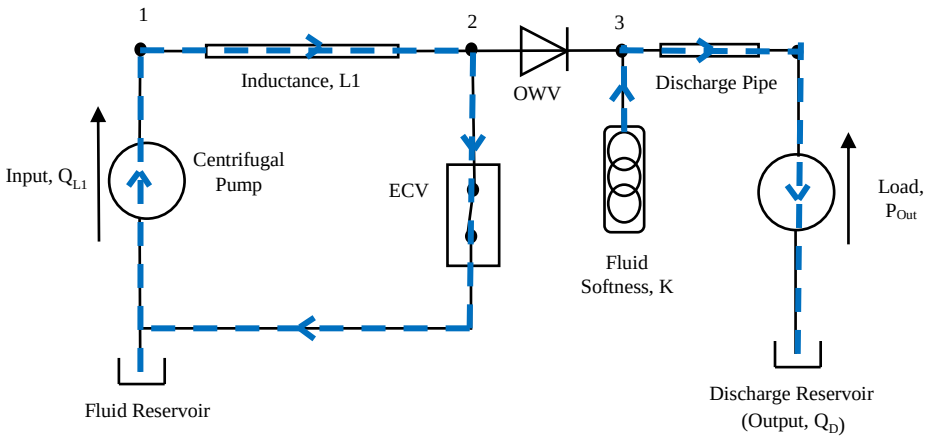

Fig. 5-4. Flow paths during time condition 1: ECV (ON)

Subsequently, the resulting flow through the output pipe over this time condition will be as a result of the discharge from the capacitance chamber, Q_K. It is clear to see that from continuity and **Eqn. 5-2** that with no flow through the OWV:

$$Q_{L1}\,(t)_{ON} = Q_{ECV} \qquad \textbf{Eqn. 5-29}$$

Further, with no flow contribution from the Q_{OWV} term, **Eqn. 5-4** becomes:

$$Q_D\,(t) + Q_K = 0 \qquad \textbf{Eqn. 5-30}$$

Differentiating both of these equations leads to two further equations that will become useful later on in the definition of output flow during the active time condition.

$$\frac{dQ_{L1}\,(t)_{ON}}{dt} = \frac{dQ_{ECV}}{dt} \qquad \textbf{Eqn. 5-31}$$

$$\frac{dQ_D\,(t)}{dt} + \frac{dQ_K}{dt} = 0 \qquad \textbf{Eqn. 5-32}$$

Now that the flow conditions have been set, based on the initial statements of flow through the hydraulic circuit, it is possible to begin substituting in individual flow definitions. Recalling the definition of capacitance from **Chapter 4**:

$$dP = K \int Q.dt \qquad \textbf{Eqn. 5-33}$$

Rearranging:

$$KQ_K = \frac{dP_3}{dt} \qquad \textbf{Eqn. 5-34}$$

Eqn. 5-34 now provides a good substitution for the Q_K term in **Eqn. 5-30**. However, before this is possible, it is necessary to first replace the unknown pressure term from **node 3**. This may be done by considering the pressure difference across the discharge pipe,L_2, between **nodes 3** and **4**. Recalling the definition of inductance from **Chapter 4**:

$$dP = L\frac{dQ}{dt} \qquad \textbf{Eqn. 5-35}$$

Between **nodes 3** and **4**:

$$P_3 - P_4 = \frac{\rho l_D}{A_D}.\frac{dQ_D}{dt} \qquad \textbf{Eqn. 5-36}$$

Differentiating and rearranging to provide a definition to the P_3 term which may be substituted into **Eqn. 5-34**:

$$\frac{dP_3}{dt} = \frac{\rho l_D}{A_D}.\frac{d^2Q_D}{dt^2} + \frac{dP_4}{dt} \qquad \textbf{Eqn. 5-37}$$

As there is no change in standing pressure at the output of the hydraulic system, it can be assumed that $\frac{dP_4}{dt} = 0$ and so combining **Eqn. 5-37** with **Eqn. 5-34** gives:

$$KQ_K = \frac{\rho l_D}{A_D} . \frac{d^2 Q_D}{dt^2} \qquad \textbf{Eqn. 5-38}$$

Rearranging for a complete definition of Q_K :

$$Q_K = \frac{\rho l_D}{K A_D} . \frac{d^2 Q_D}{dt^2} \qquad \textbf{Eqn. 5-39}$$

Now substituting the expanded definition of Q_K into the initial flow equation, **Eqn. 5-30**:

$$\frac{\rho l_D}{K A_D} . \frac{d^2 Q_D}{dt^2} + Q_D\,(t) = 0 \qquad \textbf{Eqn. 5-40}$$

Rearranging:

$$\frac{d^2 Q_D}{dt^2} + \frac{K A_D}{\rho l_D} . Q_D\,(t) = 0 \qquad \textbf{Eqn. 5-41}$$

This equation may be solved as a second order differential equation in the form:

$$y'' + \alpha y = 0 \qquad \textbf{Eqn. 5-42}$$

where:

$$\alpha = \frac{K}{L_D} = \frac{K A_D}{\rho l_D} \qquad \textbf{Eqn. 5-43}$$

Eqn. 5-43 may be manipulated by introducing several additional terms, in order to present a representation of α which is more useful in understanding its effect on the operation of the pumping system. Starting with the basic definition for natural

frequency of the pumping system defined in **Chapter 4** and repeated below for convenience:

$$\omega_n = \sqrt{\frac{K}{L_1}} \qquad \textbf{Eqn. 5-44}$$

Adding a term to describe the ratio of operating frequency to natural frequency of the system, r, gives **Eqn. 5-45.**

$$\frac{\omega}{r} = \sqrt{\frac{K}{L_1}} \qquad \textbf{Eqn. 5-45}$$

where:

$$r = \frac{\omega}{\omega_n} \qquad \textbf{Eqn. 5-46}$$

Then squaring both sides and introducing another new term describing the ratio of output inductance to the input inductance, m, gives **Eqn. 5-47**.

$$\left(\frac{\omega}{r}\right)^2 \frac{1}{m} = \frac{K}{L_1}.\frac{1}{m} \qquad \textbf{Eqn. 5-47}$$

where:

$$m = \frac{L_D}{L_1} \qquad \textbf{Eqn. 5-48}$$

Finally, comparing to the original α it is clear to see that **Eqn. 5-43** is identical to **Eqn. 5-47** such that:

$$\alpha = \left(\frac{\omega}{r}\right)^2 \frac{1}{m} \qquad \textbf{Eqn. 5-49}$$

Solving for the characteristic equation of **Eqn. 5-50:**

$$y^2 + \alpha = 0 \qquad \textbf{Eqn. 5-50}$$

$$y = \pm\sqrt{-\alpha} \qquad \textbf{Eqn. 5-51}$$

and so:

$$y = \pm\sqrt{\alpha}\ i \qquad \textbf{Eqn. 5-52}$$

This gives the general solution to the homogenous equation described by **Eqn. 5-50** as:

$$y_h\ (t) = c_1 \cos\left(\sqrt{\alpha}.t\right) + c_2 \sin\left(\sqrt{\alpha}.t\right) \qquad \textbf{Eqn. 5-53}$$

Here, the $\sqrt{\alpha}$ term has been left in rather than the full expansion for ease of manipulation when the boundary conditions are introduced later in this chapter. The final solution can be seen as the summation of the homogeneous solution and the particular solution as illustrated by **Eqn. 5-54**.

$$y\ (t) = y_h\ (t) + y_P\ (t) \qquad \textbf{Eqn. 5-54}$$

However as there is no particular solution for this time condition, the final solution to the differential equation is (with constants of integration A and B):

$$Q_D\ (t)_{ON} = A \cos\left(\sqrt{\alpha}.t\right) + B \sin\left(\sqrt{\alpha}.t\right) \qquad \textbf{Eqn. 5-55}$$

5.6 Time Condition 2: ECV (OFF)

Following the first time condition, the ECV will become inactive, as illustrated in **Figure 5-5**, resulting in no flow via the ECV back to the water reservoir. With the valve inactive, all available flow is diverted to both the discharge pipe and the capacitance chamber. The exclusion of the short circuit forces the centrifugal pump to work against a greater pumping head and as a result the flow through the inductance pipe, $Q_{L1(OFF)}$, will begin to fall until such a point as either the ECV is again activated or the pump achieves a consistent flow rate. During this time condition it is also assumed that some output flow will be lost as a result of re-priming the capacitance chamber to flow value Q_K.

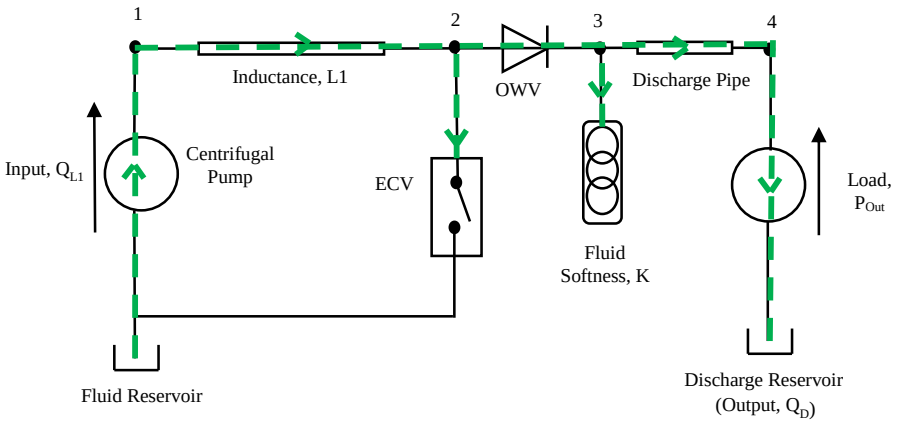

Fig. 5-5. Flow path during time condition 2: ECV (OFF)

Starting from **Eqn. 5-2,** it is possible to see that with no flow through the ECV, $Q_{ECV} = 0$, then for continuity:

$$Q_{L1}\,(t)_{OFF} = Q_{OWV} \qquad \textbf{Eqn. 5-56}$$

Furthermore, by considering the flow through node 3, described by **Eqn. 5-4,** and substituting in **Eqn. 5-56** to remove the Q_{OWV} term it can be stated:

$$Q_{L1}\,(t)_{OFF} = Q_K + Q_D\,(t) \qquad \textbf{Eqn. 5-57}$$

Replacing the capacitance term with the value derived in **Eqn. 5-39** gives the full continuity equation, **Eqn. 5-58**:

$$Q_{L1}\,(t)_{OFF} = \frac{\rho l_2}{KA_2}.\frac{d^2Q_D}{dt^2} + Q_D\,(t) \qquad \textbf{Eqn. 5-58}$$

Rearranging:

$$\frac{d^2Q_D}{dt^2} + \frac{KA_2}{\rho l_2}\,Q_D\,(t) = \frac{KA_2}{\rho l_2}\,Q_{L1}\,(t)_{OFF} \qquad \textbf{Eqn. 5-59}$$

This may be solved as a second order differential equation in the form:

$$y'' + \alpha y = \alpha j(t) \qquad \textbf{Eqn. 5-60}$$

As stated in **Eqn. 5-54,** the solution to this equation is the combination of both the complementary solution to the homogeneous equation, $y_h(t)$, and the particular solution to the full differential equation, $y_P\,(t)$. As the homogeneous equations for both ON and OFF time conditions are the same, as shown in **Eqn. 5-41**, the resulting complimentary solutions must also be the same. As such the complementary solution to **Eqn. 5-59** is given by **Eqn. 5-55**. Moving on to find the particular solution:

$$\alpha j(t) = \alpha Q_{L1}\,(t)_{OFF} \qquad \textbf{Eqn. 5-61}$$

and so:

$$y'' + \alpha y = \alpha Q_{L1}\,(t)_{OFF} \qquad \textbf{Eqn. 5-62}$$

Recalling the definition of $Q_{L1}\,(t)_{OFF}$ and modifying based on the definition for flow ripple yields:

$$Q_{L1}\,(t)_{\,OFF} = \,(1+\mathbb{R})Q_{BEP} - \left(\frac{t-DT}{T-DT}\right)2Q_{BEP}\mathbb{R} \qquad \textbf{Eqn. 5-63}$$

Rearranging:

$$Q_{L1}\,(t)_{\,OFF} = \,Q_{BEP}\left(1+\mathbb{R}\left(\frac{1+D}{1-D}\right)\right) - \,2Q_{BEP}\frac{\mathbb{R}.t}{T-DT} \qquad \textbf{Eqn. 5-64}$$

This gives the full differential equation representing the discharge flow during the valve inactive period as **Eqn. 5-65:**

$$\frac{d^2Q_D}{dt^2} + \,\alpha\,Q_D\,(t) \,=\, \alpha Q_{BEP}\left(1+\mathbb{R}\left(\frac{1+D}{1-D}\right)\right) - \,2\alpha Q_{BEP}\frac{\mathbb{R}.t}{T-DT} \qquad \textbf{Eqn. 5-65}$$

where $j(t)$ is in the form:

$$\alpha j(t) = \,\alpha(A+Bt) \qquad \textbf{Eqn. 5-66}$$

This causes the constant α to be eliminated, giving the particular solution the standard form $(A+Bt)$ and so can be written as shown in **Eqn. 5-67**.

$$y_P(t) = \,Q_{BEP}\left(1+\mathbb{R}\left(\frac{1+D}{1-D}\right)\right) - \,2Q_{BEP}\frac{\mathbb{R}.t}{T-DT} \qquad \textbf{Eqn. 5-67}$$

Combining the solutions presented in **Eqn. 5-55** and **Eqn. 5-67** yields the full solution to the second order differential equation given in **Eqn. 5-59** to be (With constants of integration, C and E):

$$Q_D\,(t)_{OFF} = \,C\cos\left(\sqrt{\alpha}.t\right) + \,E\sin\left(\sqrt{\alpha}.t\right) + \,Q_{BEP}\left(1+\mathbb{R}\left(\frac{1+D}{1-D}\right)\right) - \,2Q_{BEP}\frac{\mathbb{R}.t}{T-DT}$$

Eqn. 5-68

5.7 Constants of Integration

Recalling **Fig. 5-2**, the evolution of flow through the inductance pipe, it is clear to see how the operation of the ECV produces oscillations in flow and also how the flows defined by equations for separate time periods, $Q_{L1}\ (t)_{ON}$ and $Q_{L1}\ (t)_{OFF}$, must agree at transition points. In a similar fashion, it is assumed that the flow from the discharge pipe must be continuous and oscillating, due to the combined actions of the IFS components. Unfortunately, as the flow at any individual time during a single time period, T, is unknown, it is necessary to establish a set of discharge flow boundary conditions. These boundary conditions can then be used to define the constants of integration A, B, C and E.

For the discharge flow to be continuous, the following four boundary conditions are selected:

1. $Q_D\ (0)_{ON} = Q_D\ (T)_{OFF}$
2. $Q_D{}'\ (0)_{ON} = Q_D{}'\ (T)_{OFF}$
3. $Q_D\ (TD)_{ON} = Q_D\ (TD)_{OFF}$
4. $\int_{TD}^{T} Q_{L1}\ (t) = \int_{0}^{TD} Q_D\ (t)_{ON} + \int_{TD}^{T} Q_D\ (t)_{OFF}$

where:

$Q_D\ (t)_{ON}$ is defined from $(t = 0 \rightarrow TD)$;

$Q_D\ (t)_{OFF}$ is defined from $(t = TD \rightarrow T)$

For ease of manipulation in considering the boundary conditions, let:

$\Lambda = Q_{BEP}.\left(1 + \mathbb{R}\ \left(\frac{1+D}{1-D}\right)\right)$;

$$\Psi = \frac{2.Q_{BEP}.\mathbb{R}}{(1-D)}$$

5.7.1 Boundary Condition 1: $[Q_D\,(0)_{ON} = Q_D\,(T)_{OFF}]$

The discharge flow at the start of the time period, T, must be equal to the flow at the end of the time period in order for the equations to define a continuous flow pattern over multiple time periods. Expanding and combining **Eqn. 5-55** and **Eqn. 5-68** to replace the undefined time, t, variables, as outlined in boundary condition 1, provides a definition for the first constant of integration, A:

$$A = C\cos(\sqrt{\alpha}.T) + E\sin(\sqrt{\alpha}.T) + \Lambda - \Psi \qquad \textbf{Eqn. 5-69}$$

5.7.2 Boundary Condition 2: $[Q_D{}'\,(0)_{ON} = Q_D{}'\,(T)_{OFF}]$

Boundary condition 2 uses the same time conditions as boundary condition 1. However, in order to ensure that the transition points between the different discharge flow equations are smooth, the gradients of the points are matched. Differentiating the equations of discharge flow with respect to time:

$$Q_D{}'(t)_{ON} = \sqrt{\alpha}.B\cos(\sqrt{\alpha}.t) - \sqrt{\alpha}.A\sin(\sqrt{\alpha}.t)\,; \qquad \textbf{Eqn. 5-70}$$

$$Q_D{}'(t)_{OFF} = \sqrt{\alpha}.E\cos(\sqrt{\alpha}.t) - \sqrt{\alpha}.C\sin(\sqrt{\alpha}.t) - \Psi \qquad \textbf{Eqn. 5-71}$$

The same process, of expanding and rearranging the differential equations of flow to include boundary condition 2, yields a definition for the second constant of integration, B:

$$B = E\cos(\sqrt{\alpha}.T) - C\sin(\sqrt{\alpha}.T) - \frac{\Psi}{\sqrt{\alpha}.T} \qquad \textbf{Eqn. 5-72}$$

5.7.3 Boundary Condition 3: $\left[Q_D\ (\mathrm{T.D})_{ON} = Q_D\ (T.D)_{OFF}\right]$

The discharge flow, at time $t = TD$, at the end of the valve open period, must be equal for both discharge flow equations. Substituting these time values into **Eqn. 5-55** and **Eqn. 5-68** and rearranging, provides an additional equation to be used in defining the remaining constants of integration C and E.

$$A.\cos\left(\sqrt{\alpha}.T.D\right) + B.\sin\left(\sqrt{\alpha}.T.D\right) = C\cos\left(\sqrt{\alpha}.T.D\right) + E\sin\left(\sqrt{\alpha}.T.D\right) + \Lambda - \Psi.\mathrm{D}$$

Eqn. 5-73

5.7.4 Boundary Condition 4: $\left[\int_{TD}^{T} Q_{L1}\ (t)_{OFF} = \int_{0}^{TD} Q_D\ (t)_{ON} + \int_{TD}^{T} Q_D\ (t)_{OFF}\right]$

As discussed in **Section 5.6,** there is no flow through the ECV during the valve OFF period and thus all flow must be diverted to the discharge pipe. The flow over period $Q_{L1}\ (t)_{OFF}$ will be equal to the discharge flow over both $Q_D\ (t)_{ON}$ and $Q_D\ (t)_{OFF}$ periods as all discharge flow during valve ON period is diverted back to reservoir. Expanding **Eqn. 5-15:**

$$Q_{L1}(t)_{OFF} = (1 + \mathbb{R}).Q_{BEP} - \frac{t.D.P_{BEP}}{L_1.(1-D)} + \frac{T.D^2.P_{BEP}}{L_1.(1-D)} \qquad \textbf{Eqn. 5-74}$$

Now finding the integrals of the above equation and also **Eqn.'s 5-55** and **5-68**:

$$\int Q_{L1}(t)_{OFF} = (1 + \mathbb{R}).Q_{BEP}.t - \frac{t^2.D.P_{BEP}}{2.L_1.(1-D)} + \frac{T.D^2.P_{BEP}.t}{L_1.(1-D)} \quad ; \qquad \textbf{Eqn. 5-75}$$

$$\int Q_D\ (t)_{ON} = \frac{A.\sin\left(\sqrt{\alpha}.t\right)}{\sqrt{\alpha}} - \frac{B.\cos\left(\sqrt{\alpha}.t\right)}{\sqrt{\alpha}} \quad ; \qquad \textbf{Eqn. 5-76}$$

$$\int Q_D\ (t)_{OFF} = \frac{C.\sin\left(\sqrt{\alpha}.t\right)}{\sqrt{\alpha}} + \frac{E.\cos\left(\sqrt{\alpha}.t\right)}{\sqrt{\alpha}} - \frac{\Psi.t^2}{2.T} + \Lambda.t \qquad \textbf{Eqn. 5-77}$$

Boundary condition 4 becomes:

$$\left[(1+\mathbb{R}).Q_{BEP}.t\ -\ \frac{t^2.D.P_{BEP}}{2.L_1.(1-D)}\ +\ \frac{T.D^2.P_{BEP}.t}{L_1.(1-D)}\right]_{TD}^{T} = \left[\frac{A.\sin(\sqrt{\alpha}.t)}{\sqrt{\alpha}} - \frac{B.\cos(\sqrt{\alpha}.t)}{\sqrt{\alpha}}\right]_{0}^{TD} + \left[\frac{C.\sin(\sqrt{\alpha}.t)}{\sqrt{\alpha}} + \frac{E.\cos(\sqrt{\alpha}.t)}{\sqrt{\alpha}} - \frac{\Psi.t^2}{2.T}\ +\ \Lambda.t\right]_{TD}^{T}$$

Eqn. 5-78

where, recalling the definition of average discharge flow from **Section 5.3**, the expansion for total inductance flow may be simplified:

$$Q_{BEP}.(1-D).T = \left[(1+\mathbb{R}).Q_{BEP}.t\ -\ \frac{t^2.D.P_{BEP}}{2.L_1.(1-D)}\ +\ \frac{T.D^2.P_{BEP}.t}{L_1.(1-D)}\right]_{TD}^{T}$$

Eqn. 5-79

This provides the final equation needed in order to define the last two constants of integration.

5.7.5 Solving for Constants of Integration

By manipulating and combining the equations formed from the four boundary conditions described above, it is possible to define the constants of integration in terms of known values. A complete working for these manipulations can be found in **Appendix B**, which concludes that the final two constants, C and E, can be defined as:

$$C = \frac{\Psi}{\xi}.\left(D - cos\left(\sqrt{\alpha}.T.D\right) - \frac{sin\left(\sqrt{\alpha}.T.D\right)}{\sqrt{\alpha}.T}\right) + \frac{\Lambda}{\xi}.\left(cos\left(\sqrt{\alpha}.T.D\right) - 1\right) + E.\frac{\chi}{\xi}$$

Eqn. 5-80

$$E = \frac{\sqrt{\alpha}.\xi.\mathrm{Z} + \chi.\left[\Psi.\left(\frac{sin\left(\sqrt{\alpha}.T.D\right)}{\sqrt{\alpha}.T} + cos\left(\sqrt{\alpha}.T.D\right) - D\right) + \Lambda.\left(1 - cos\left(\sqrt{\alpha}.T.D\right)\right)\right]}{\chi^2 + \xi^2}$$

Eqn. 5-81

where:

$$\chi = \left[\cos\left(\sqrt{\alpha}.T\right).sin\left(\sqrt{\alpha}.T.D\right) + \sin\left(\sqrt{\alpha}.T\right).cos\left(\sqrt{\alpha}.T.D\right) - \sin\left(\sqrt{\alpha}.T.D\right)\right];$$

Eqn. 5-82

$$\xi = \left[\sin\left(\sqrt{\alpha}.T\right).sin\left(\sqrt{\alpha}.T.D\right) + \cos\left(\sqrt{\alpha}.T\right).cos\left(\sqrt{\alpha}.T.D\right) + \cos\left(\sqrt{\alpha}.T.D\right)\right];$$

Eqn. 5-83

and:

$$\mathrm{Z} = \left[Q_{BEP}.(1-D).T + \frac{sin\left(\sqrt{\alpha}.T.D\right)}{\sqrt{\alpha}}.(\Psi - \Lambda) + \frac{\Psi}{\alpha.T}.\left(1 - cos\left(\sqrt{\alpha}.T.D\right)\right) + \frac{\Psi.T}{2}.(1 - D^2) + \Lambda.T.(D-1)\right]$$

Eqn. 5-84

5.5 Summary

The IFS centrifugal pumping system has been analysed and a complete linear analysis of flow through the various components presented, resulting in the formation of two separate equations: one to define flow during the OPEN (ON) phase of the ECV and one for the CLOSED (OFF) phase of the ECV. The operation of the ECV has been evaluated, finding no theoretical limit on operational pressure difference. Combined with the complete equations presented in **Appendix B,** the constants of integration have been found by solving for a series of second order differential equations. These equations will form the basis of the numerical analysis presented in **Chapter 6** and provide a reference for the comparison of later electrical and experimental evaluations.

Chapter 6

Numerical Analysis

Chapter 5 used a lumped parameter analysis to define a series of equations which describe the flow through various sections of the induced-flow centrifugal pumping system. Of these equations, it is those which define the flow patterns through both the inductance and discharge pipes which hold the most interest. This chapter looks at the relationship between the various components of the induced flow subsystem and their effect on pumping performance with regards to pump BEP stability.

6.1 Equations of Flow

Listed below for convenience are the time dependent equations of flow through the discharge pipe for both periods of ECV operation. Also included is the equation for average discharge flow:

$$Q_D\,(t)_{ON} = A\cos\left(\sqrt{\frac{\omega^2}{r^2.m}}.t\right) + B\sin\left(\sqrt{\frac{\omega^2}{r^2.m}}.t\right) \quad ; \qquad \textbf{Eqn. 6-1}$$

$$Q_D\,(t)_{OFF} = C\cos\left(\sqrt{\frac{\omega^2}{r^2.m}}.t\right) + E\sin\left(\sqrt{\frac{\omega^2}{r^2.m}}.t\right) + \Lambda - \frac{\Psi.\mathrm{t}}{T} \quad ; \qquad \textbf{Eqn. 6-2}$$

$$Q_{D(Av)} = \frac{Q_{BEP}.P_{BEP}}{P_{OUT}} \qquad \textbf{Eqn. 6-3}$$

In both **Eqn. 6-1** and **Eqn. 6-2,** the simplified 'α' term used in the manipulations presented in **Chapter 5** has been expanded to show both the ratios of frequency, r, and inductance, m. These will be used in this chapter to model changes to the induced-flow system. Combined with the predicted flow through the inductance pipe, these equations describe the flow through both major sections of the hydraulic circuit. This is of particular interest as it allows for a prediction as to how these flows will change, dependent on the variable factors available to pump operation. These factors range from the operating head of the pump to design parameters such as length of inductance pipe or capacitance chamber 'softness'. Coupled with the theoretical estimation of average discharge flow, **Eqn. 6-3,** and Q_{BEP} as reference points for flow variation, it is possible to ascertain the suitability of the suggested system to off-grid applications and the advantage or disadvantage of changes to any part of the pump.

6.2 Numerical Solutions

Eqns. 6-1 to **6-3** were solved using a numerical software package* for any particular set of input conditions. Firstly, the time period of valve operation was established based on the chosen set of subsystem characteristics and pump specification (giving Q_{BEP} and P_{BEP} values). Next, the ECV operating characteristics were calculated based on the selected frequency ratio of operation (discussed in **Chapters 4** and **5**). By selecting a suitable frequency ratio to give sufficiently fast valve

* The software packages used for the numerical solutions presented in this thesis were MATHCAD 15.0 and Microsoft Excel 2010.

operation, that is also within the criteria set for validity of the lumped parameter model, the open and closed times of the valve are set (based on the resulting time period and duty). Through modification of the frequency ratio, without altering component characteristics, its effect on the flow stability and pump performance could be observed. The limitations on the values of r, which were used in the experimental stage of this research, are covered in detail in **Chapter 8** (being mainly based upon the operational limitations of both the ECV and control system). Its importance in relation to the stability of the centrifugal pumps operating conditions is covered later in this chapter.

Finally, following all of the basic pumping system criteria specifications, the constants of integration, as summarized in **Section B.3,** are solved and used to complete the equations of discharge flow.

6.2.1 Improved Discharge Flow

The first set of data which is of interest is the trend in discharge flow from the pumping system both with and without the engagement of the induced-flow subsystem. The pump and subsystem specification used for the initial numerical solutions match those used in the experimental analysis stage of the research*. These specifications are summarized in **Table 6-1**.

---

* As a note of interest, the IFS test rig was designed and constructed in parallel with the derivation of equations for discharge flow and definition of the system. As such, the limitations of equipment and space available in the lab space were known. Further, the system was seen as a starting point to demonstrate some of the concepts surrounding flow ripple and pump efficiency, as well as system optimization (covered later in this chapter). Additionally it provided data for direct comparison to any results obtained experimentally.

Table 6-1. Experimental test rig specifications

TEST RIG DETAIL	SYMBOL	VALUE	UNIT
Inductance total length	l	3.72	m
Inductance internal diameter	d_{L1}	15×10^{-3}	m
Fluid ' Softness' , K	K	2.31	$GPa.m^{-3}$
Fluid Density	ρ	1000	$kg.m^{-3}$
Inductance pipe area	A_{L1}	1.77×10^{-4}	m^2
Pump BEP Pressure	P_{BEP}	25000	Pa
Pump BEP Flow	Q_{BEP}	0.275	l/s
Pump Max. Head	H_{MAX}	4.9	m

On activation of the induced-flow subsystem, once the load pressure reaches P_{BEP}, **Figure 6-1** shows the discharge flow to remain fairly consistent with the existing pump curve; whilst the duty of the ECV remains low, the IFS effect is minimal. However, as the ECV duty begins to increase and the pressure load begins to exceed the rated head of the pump, there begins to be a divergence between two flows. This result is concurrent with that expected from the theory; from the definition of equations in **Chapter 5**, for the hydraulic power output of the pump to remain at its BEP (i.e. constant maximum hydraulic power) there has to exist a discharge flow proportional to the pressure load on the system. **Figure 6-2** illustrates how the hydraulic power, P_H, of the pumping system indeed remains constant at any pressure load as a result of the discharge flow being modified through increased duty. Being able to deliver an increased hydraulic power output while maintaining the centrifugal pumps BEP operation shows the ability of the tuned IFS pumping system to make greater use of available power, where otherwise the pump would not function.

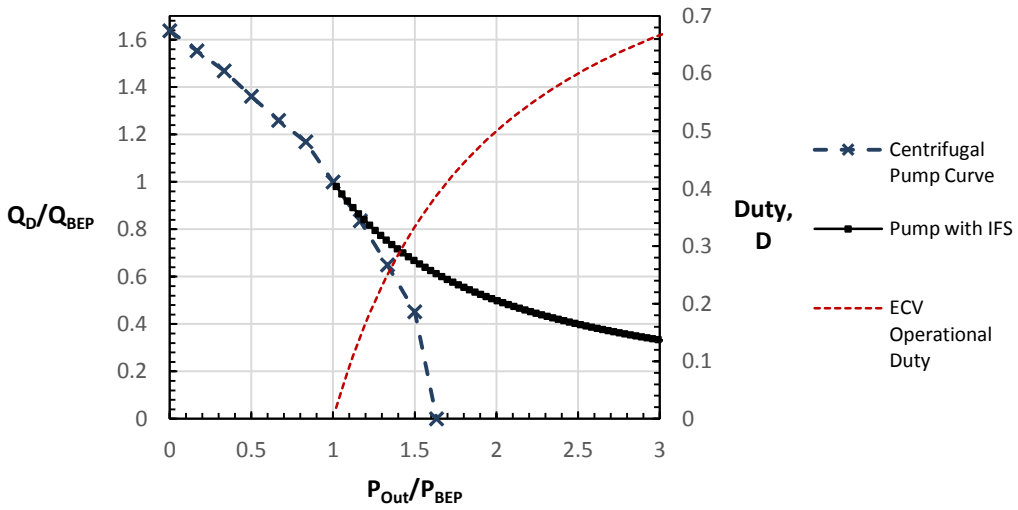

Fig. 6-1. IFS effect on discharge flow, with evolving Duty

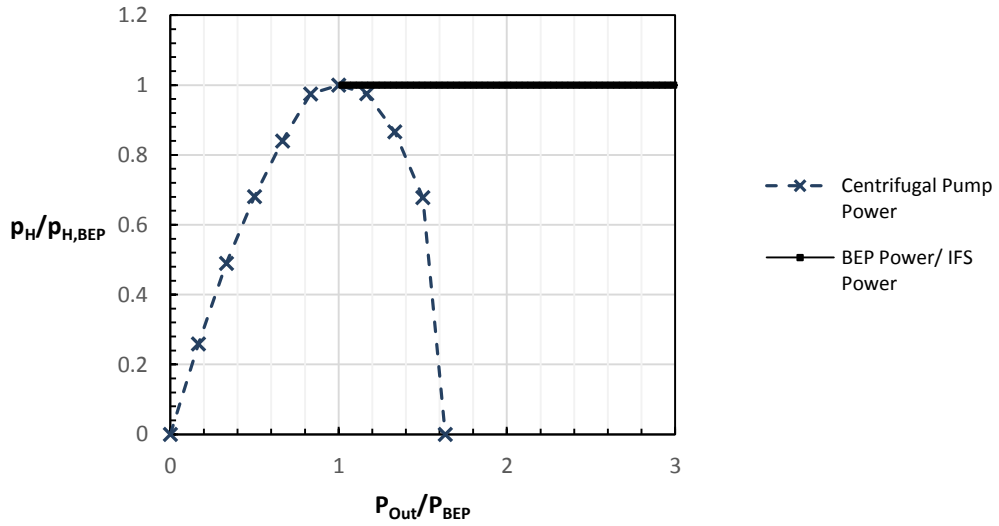

Fig. 6-2 - Pump BEP hydraulic power correction with IFS

6.2.3 Inductance and Discharge Flow Trends

Although being able to deliver a greater hydraulic power across a wider range of operating heads is of great benefit to centrifugal pumps being used in off-grid applications, the primary focus of the IFS is to maintain a BEP operating condition at the centrifugal pump itself. This allows the pump to utilize the maximum amount of energy available to it and promotes a one-size-fits-all application. Furthermore, it is of interest to assess the impact which modification of the ECV duty and operating head has on the flow traces (and more importantly the fluctuations) of both the inductance and discharge flows. **Figures 6-3, 4, 5** and **6** show the inductance and discharge flow transients in relation to the pumps BEP line and theoretical discharge across a range of increasing pumping heads. These are from just above BEP to twice the maximum rated head of the pump without the IFS. Simulations were completed at a frequency ratio of $r = 2$. This range is sufficient to illustrate several interesting characteristics about the flow through the pumping system:

- The higher the pumping head, and thus the load pressure, the greater the duty of the ECV. Subsequently, the open time, t_o, of the valve will be longer. As a result of this there is an increased fluctuation in flow through the inductance pipe at higher pumping heads (i.e. an increase in ripple, $\mathbb{R}$).

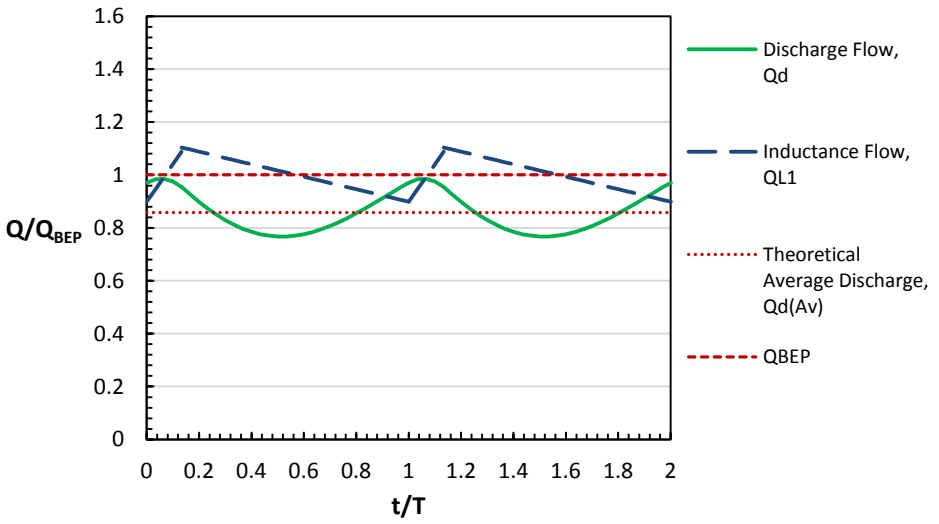

Fig. 6-3 - Pump BEP hydraulic power correction with IFS, 3m

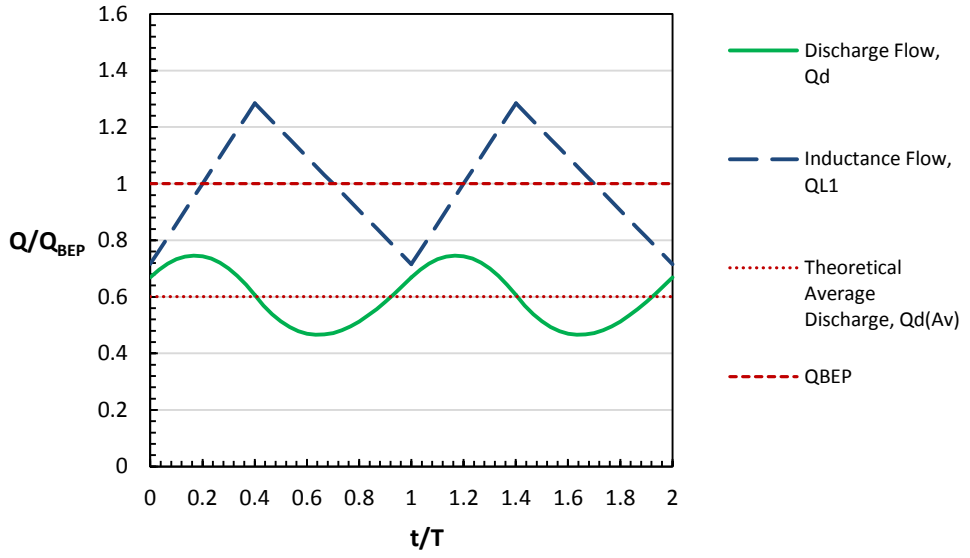

Fig. 6-4 - Pump BEP hydraulic power correction with IFS, 4m

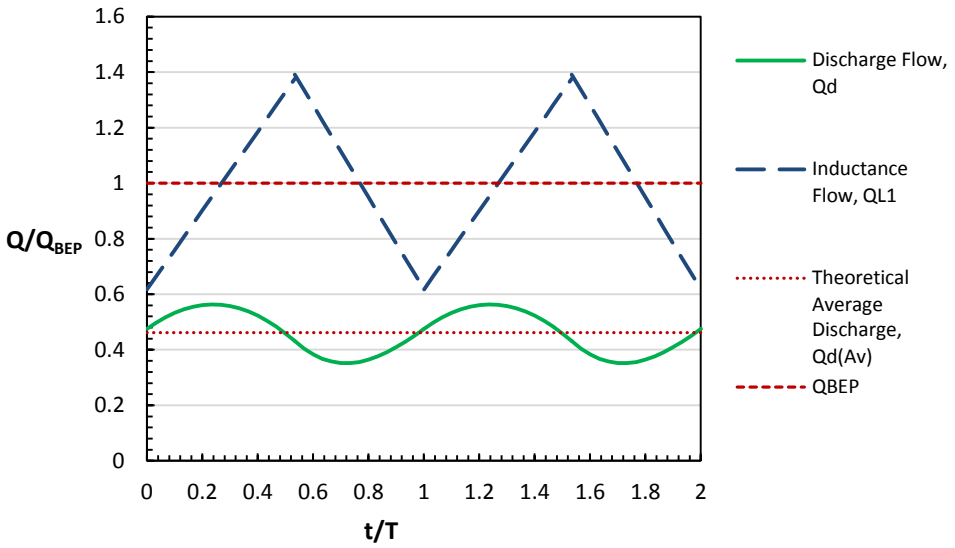

Fig. 6-5 - Pump BEP hydraulic power correction with IFS, 5m

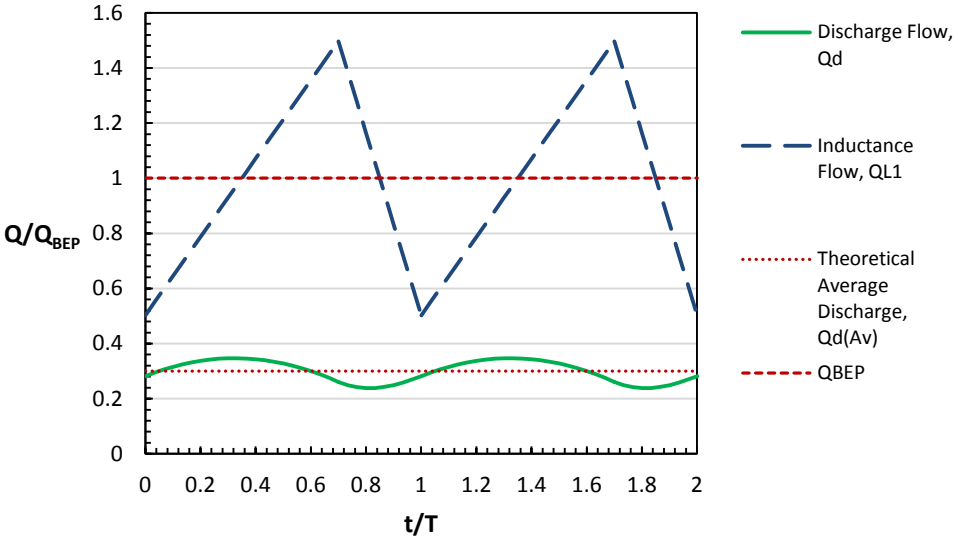

Fig. 6-6 - Pump BEP hydraulic power correction with IFS, 10m

- The fluctuations in discharge flow are reduced with the evolution of pumping head, converse to that of the inductance flow ripple. This would lead to the assumption that, given an infinite pumping head, the discharge flow ripple would be almost negligible, i.e. $Q_D(t)_{ON} = Q_D(t)_{OFF} = Q_{D\,(Av)}$. This is illustrated in **Figure 6-7** (*NB the calculations for* $H = \infty$ *actually used* $= 100m$*; 20 times that of the pumps rated maximum head*). Although it would seem to make sense that if there is less discharge flow on average available then there is a smaller discharge flow ripple, it would also be unlikely that the capacitance chamber would smooth the flow across the time period to provide such a consistent flow.

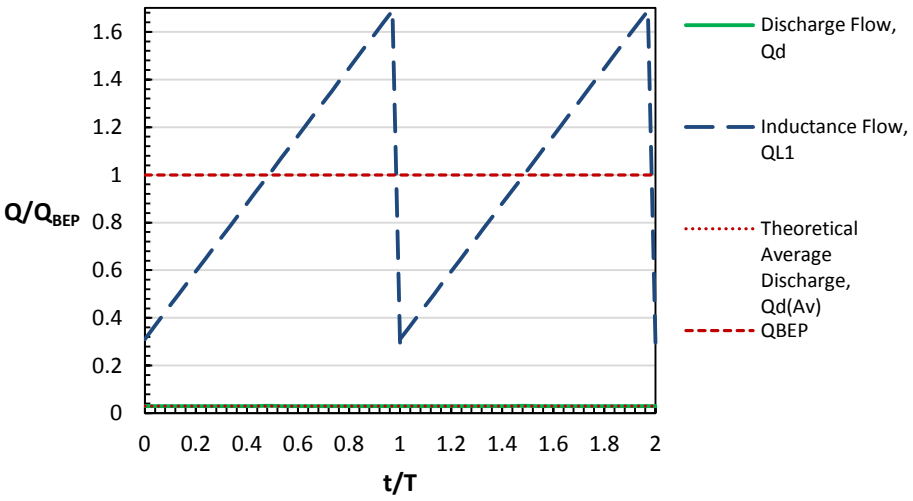

Fig. 6-7 - Pump BEP hydraulic power correction with IFS, infinite head

- There is a clear delay between the drop in inductance flow and subsequent rise in discharge flow when the ECV enters its OFF period and flow is diverted to the discharge pipe. This delay is reduced as the valve duty increases.
- The operation of the ECV produces oscillations in the inductance as expected from boost-converter theory. The development of flow during both periods of valve operation is linear, showing that the defining equations are functioning as intended and holding Q_{L1} at an average BEP.

The main concern here is the flow ripple through the inductance pipe, which should ideally be designed to minimise flow ripple so as to limit the potentially negative effects on the centrifugal pump of rapidly switching pump speeds. As the model assumes the hydraulic circuit to be operating in continuous mode, it can be seen that the inductance flow will always rise and fall consistently to compensate for an average Q_{L1} flow. One way to reduce the maximum inductance flow at any given height (and hence reduce the ripple) could be to run the ECV at a higher frequency ratio; thereby limiting the time in which the flow has to develop.

6.3 Pump Stability

The pumping system may be modified so as to reduce the effects of the flow ripple increase in the inductance pipe, according to the definition of flow presented in **Chapter 5** (shown here as **Eqn. 6-4**).

$$\Delta Q_{L1}\,(t)_{\,ON} = \frac{DTP_{BEP}}{L_1} \qquad \textbf{Eqn. 6-4}$$

From inspection of the equation, it is apparent that by reducing the time period or increasing the inductance of the system, the ripple may be reduced. **Figure 6-8** shows the results of calculating flow ripple across an increasing pumping head for various values of frequency ratio, r. Frequency ratio is used here in place of modifying the time period as it shows how the ripple in the inductance pipe is affected solely by the operation of the ECV and not by the other components in the IFS (such as the capacitance or inductance). This may also have an effect on the time period and natural frequencies of the system by their definitions. For the purposes of the calculations shown in **Figure 6-8** the natural frequency remained constant at $10.475\ rad/s$.

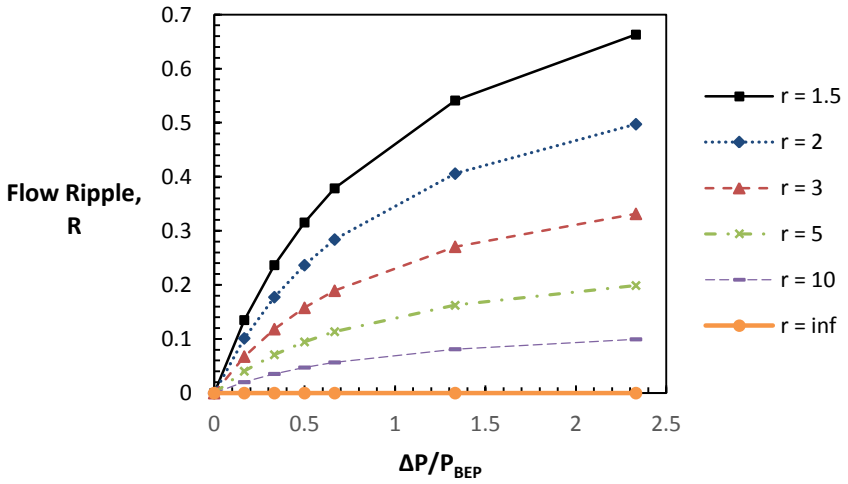

Fig. 6-8 – Evolution of flow stability at various operating frequencies

As already noted in **Section 6.2.3**, the flow ripple is characterized by an increase of diminishing increments as the pumping head increases. **Figure 6-8** additionally reveals that increasing the operating frequency of the ECV lessens the effect which pumping head has on the flow ripple. It is further seen that, as r tends towards

infinity*, the ripple effect in the inductance pipe becomes negligible. A similar inverse trend is noticed when the ripple is calculated for various values of inductance ratio, m, (as defined by modifying the inductance pipe, L_1) shown in **Figure 6-9**. It is also seen that as the inductance ratio is reduced the flow ripple is also reduced.

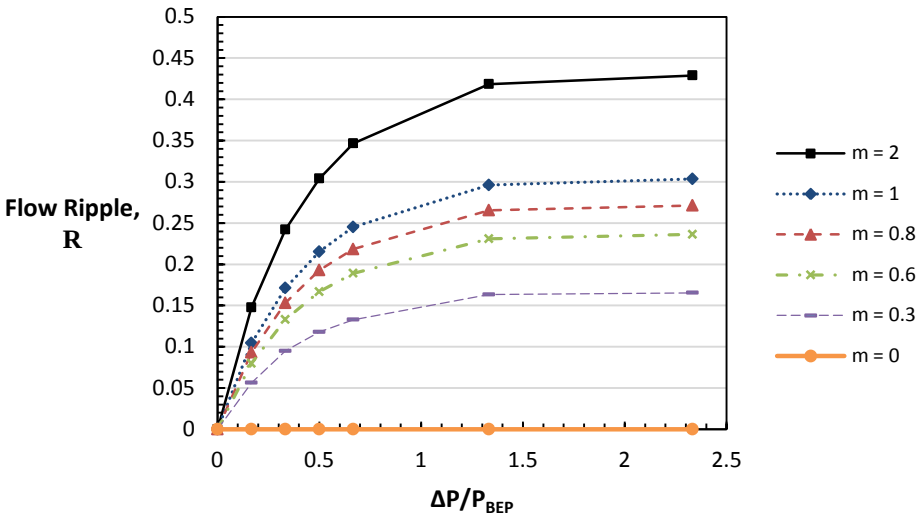

Fig. 6-9 – Evolution of flow stability at various inductance lengths

This data was calculated by modification of inductance, L_1, by increasing the length of the inductance pipe until $m = 0$. Thus, in a pumping system designed around the use of a high operating frequency or large inductance, the centrifugal pump will remain not only at its BEP, but remain stable regardless of changes to pumping head. More practically, the similarity in trends of flow ripple for varying r and m suggest that, for a pumping system with at least a reasonably large inductance (either through increasing pipe length or reducing area) and a frequency ratio greater than 2 (ideally 5 from **Figure 6-8**), the pump will operate independently of head.

* For calculations, values of $r = \infty$ and $m = 0$ actually used $r = 10000$ and $m = 0.000001$. respectively.

6.3.1 Output Inductance

As discussed in **Chapter 3** regarding the induced flow reciprocating pump and its component order for over-resonant pumps, the capacitance is located after the fluid hydraulic inductance in order to decouple it from the discharge pipe inductance. With the IFS system described in **Chapters 4** and **5** and analysed numerically here, the components use this same order as a result of the ECV placement. By design, for a centrifugal pump, the discharge pipe must be separated from the inductance pipe to allow the flow to develop during the periods where the ECV is ON. By running a series of tests at a single pumping head and varying the output inductance, L_2, it was possible to show that the flow through the inductance pipe is indeed completely decoupled from the discharge line. **Figures 6-10** to **6-12** show the flow transients for an operating head of 4m with natural frequency $10.475\ rad/s$. The discharge pipe inductance was separated from the head within the software spreadsheet so as to vary the L_2 without affecting the duty or ECV operation.

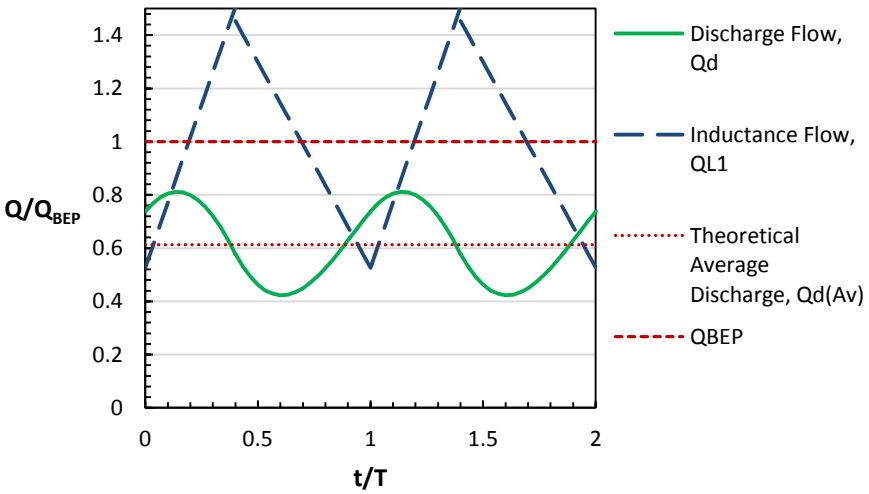

Fig. 6-10 – Flow transients with IFS, unmodified discharge pipe (4m)

It can be seen that, regardless of the variation in discharge pipe length, the inductance flow remains unchanged. Furthermore, it is also seen that an increase in discharge inductance results in a much more stable discharge flow. This agrees with the findings from the initial tests of varying pumping head; which show an increase in inductance pipe ripple but a decrease in discharge flow ripple at higher heads (**Figures 6-3** to **6-6**). This is an important finding as it demonstrates that in a practical installation of such a system, the IFS components ability to maintain BEP operation will be unaffected by any modifications to the discharge line, such as above-ground pipe extensions or distribution networks. This is a key feature of the IFS.

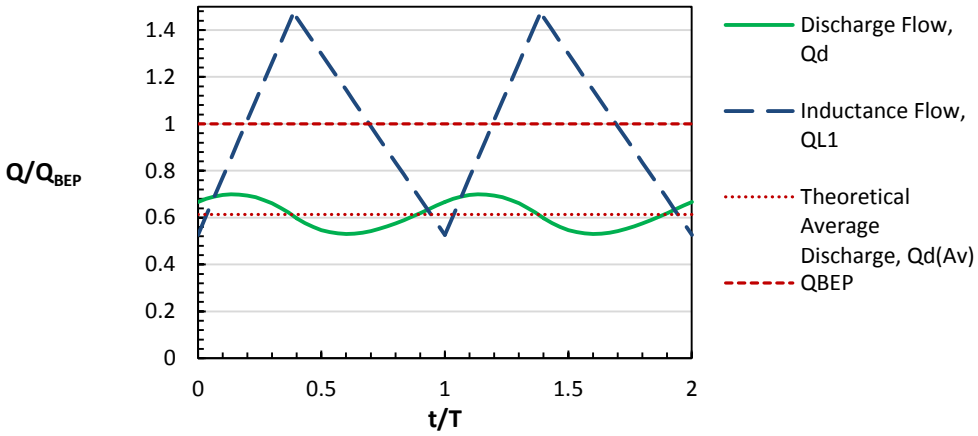

Fig. 6-11 – Flow transients with IFS, modified discharge pipe (8m)

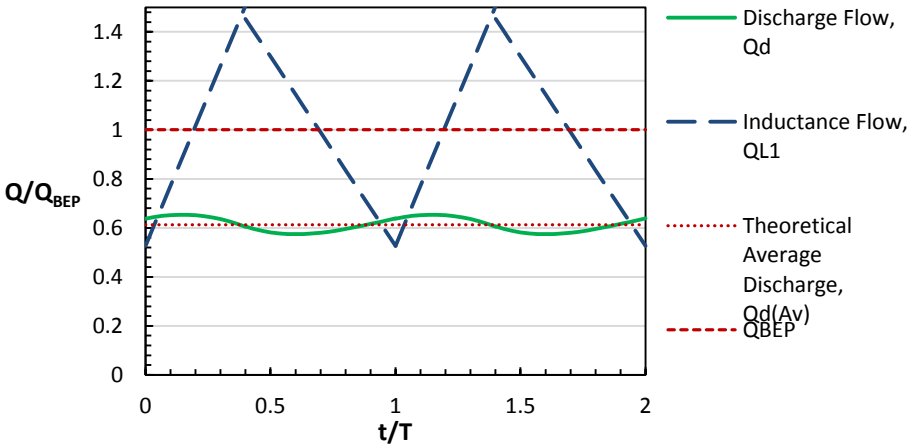

Fig. 6-12 – Flow transients with IFS, modified discharge pipe (16m)

6.4 Computational Testing

In addition to using the linear equations defined in **Chapter 5** to examine the tuned hydraulic system, a computational model of the system was designed and constructed using commercially available software. These tests were completed near to the project offset and so were conducted without the same level of experimental rig knowledge as with the numerical analysis*. As a result, the data obtained is not directly comparable with the experimental, electrical or numerical data and not all is useful or relevant within the context of this thesis. Some, however, such as the basic discharge flow trace for a single case, is included as it does demonstrate some similarities in the effect of the ECV and IFS on discharge flow.

Flowmaster™ is a 1D fluid flow analysis tool which, at the start of this project, was available on a free academic license. By making use of a drag and drop construction process, various fluidic and mechanical components can be chained together to represent an engineering system or series of subsystems which may be linked. The simplicity of the program was useful in the construction of a 1D fluid system to represent the actions of the induced flow components in conjunction with a centrifugal pump and provide another angle of evaluation for comparison with the numerical model. The full induced flow pumping circuit used in the computational tests is illustrated in **Figure 6-13**.

* The first series of computational tests modeled the effects of the induced flow subsystems on a CLARKE SPP-6 Garden pond pump, a pump which was available for experimental testing in the University of Liverpool fluids labs at the time of the computational tests. This pump was unfortunately not fit for the test rig at the time of detailed design and construction. Further, no additional computational tests could be performed due to expiry of the academic license for Flowmaster™.

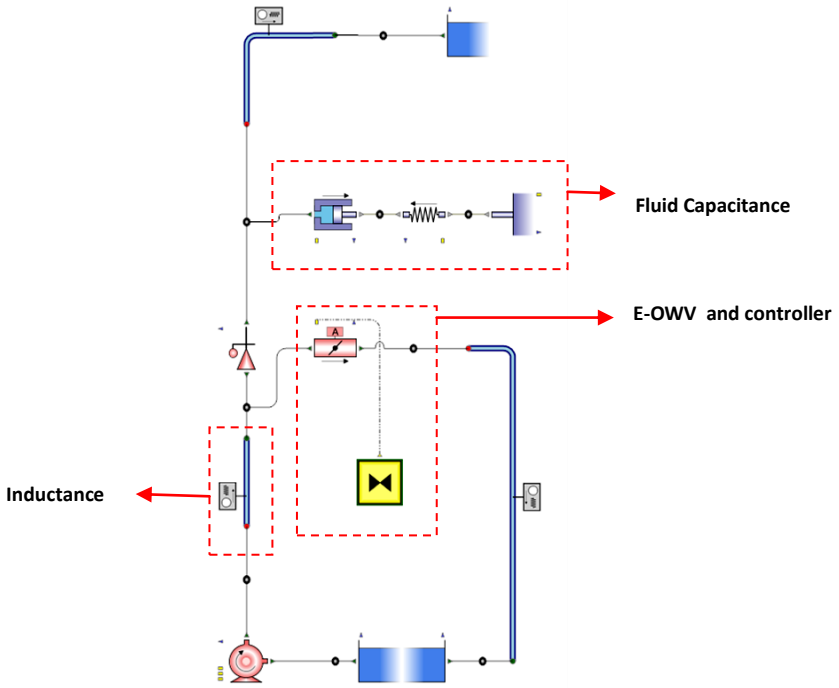

Fig. 6-13 – IFS Centrifugal pumping system as constructed in Flowmaster^{TM}

One of the main issues in constructing the circuit was in defining the capacitance chamber. Whereas all the other components required for the induced flow subsystem could be defined through simple pipe additions or user defined valve controllers, there was no component operator for hydraulic capacitance. As such, the best way of representing the capacitance was to construct a simple mechanical subsystem that could mimic the compression of the capacitance material within the chamber by using a spring in tandem with a piston. This can be seen by the combination of components highlighted as 'Fluid Capacitance' in **Figure 6-13**. As such, the hydraulic 'softness', K, had to be translated into a mechanical spring stiffness value. The mechanical representation of the capacitance chamber may be described by **Figure 6-14**.

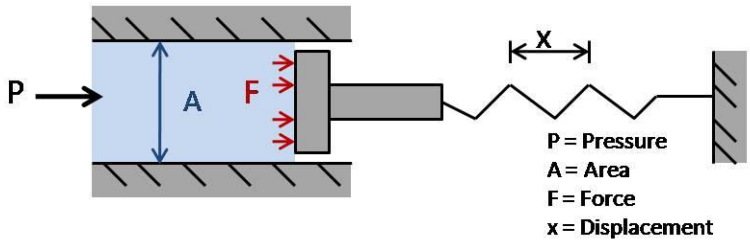

Fig. 6-14 - Basic illustration of the mechanical representation of the capacitance chamber in the complete Flowmaster™ fluid circuit

Using the equations for force, F, spring stiffness, k, and pressure acting on the piston, the hydraulic softness may be described as being:

$$K = \frac{P}{\Delta V} = \frac{P}{Ax} = \frac{F}{\mathrm{AAx}} \qquad \textbf{Eqn. 6-5}$$

This leads to the relationship between hydraulic softness and mechanical spring stiffness being:

$$K = kA^2 \qquad \textbf{Eqn. 6-6}$$

6.4.1 Test Parameters

Computational tests were performed using the pump data from the CLARKE SPP-6 centrifugal pump. BEP data was obtained from trend lines produced from manufacturers data, giving $Q_{BEP} = 0.925\ l/s$ and $P_{BEP} = 39.44\ KPa$ (from BEP head of $4.02m$). The natural frequency of the system, ω_n, was $29.24\ rad/s$, based on inductance length, $l = 2m$, and fluid softness, $K = 6\ \times 10^9 Pa/m$ (equivalent to spring stiffness, $k = 487.35\ N/m$). ECV operation was based on a system operational frequency of $27.6Hz$, resulting in a frequency ratio of $r = 6$ and time period of, $T = 0.0362$. As the simulations performed (especially while ECV was active) were at

high frequencies, it was essential that the correct resolution was used to sufficiently capture the action of the valve. This resolution was based on the opening time, t_o, value of the ECV at the lowest possible duty value for the circuit. With a time period of $0.0362s$, the lowest possible duty based on the inductance value of the circuit equated to an opening time $t_o < 0.003s$. The resolution of the simulation was based on a figure allowing for the opening time to be captured over several points and therefore had to be less than the opening time itself. A resolution of 0.0005s was to be used, ensuring a sample rate of 66 data points per time step and also allowing 6 data points for the smallest possible opening time in the simulation.

For each set of results, the flow rate at the outlet pipe of the fluid circuit was plotted against the control curve created for the CLARKE pump operating with the ECV inactive. In displaying the results in this way, it was possible to see the effect which the additional components of the induced flow subsystems had on the overall flow performance of the system (a format which is maintained during the presentation of the experimental data in **Chapter 8**). **Figure 6-15** shows the evolution of discharge flow from both modified and unmodified pumping systems across an increasing range of static heads. For the purposes of these tests, the duty was based on solely the static head, as the inductance pipe is set at a horizontal level prior to the ECV. As with the theoretical evolution of discharge flow presented in **Figure 6-1**, the operation of the ECV can be seen to extend the range of heads to which the pump can deliver flow. Unexpectedly, in the computational tests, there is a reduction in discharge flow during the period between BEP and maximum head. One possible reason for this could be due to an incorrect calibration of the ECV duty curve, resulting in an insufficient open time of the valve. Another possibility could be due to the way the pre-set components are

defined within the software, or inappropriate selection during the circuit construction. What the results do show, however, is an increase in hydraulic power at heads beyond BEP operation (even, it would seem, under non-ideal operational conditions), shown in **Figure 6-16**.

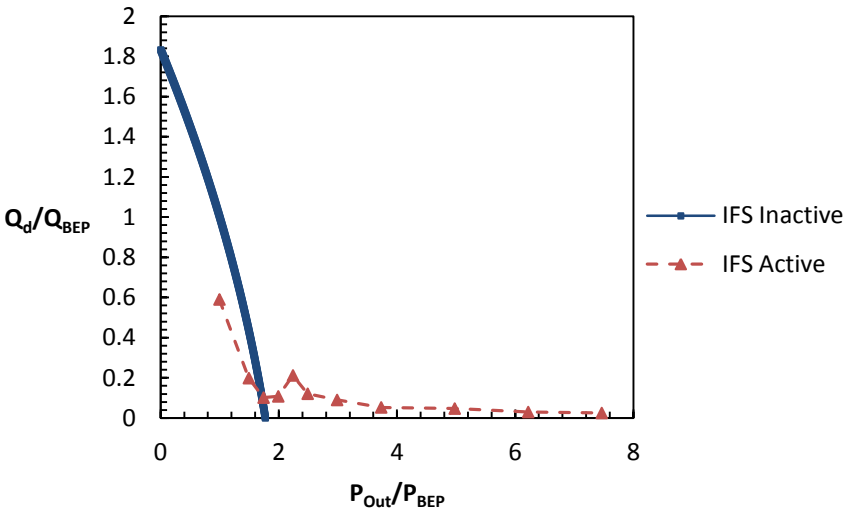

Fig. 6-15 – Computational evolution of discharge flow

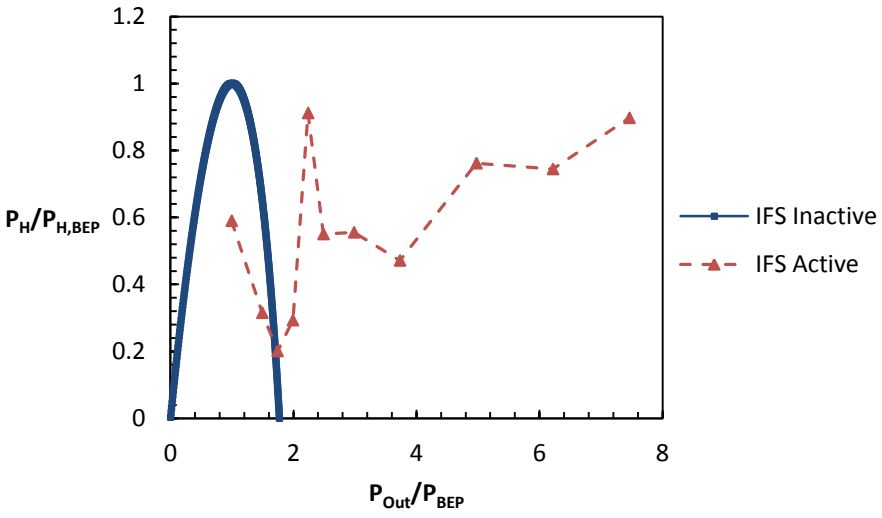

Fig. 6-16 – Computational evolution of hydraulic power

6.5 Conclusions

A numerical analysis of the IFS centrifugal pumping system has been produced using the linear equations defined in **Chapter 5**. Of particular interest from these results is the ability of the IFS centrifugal pump to maintain its BEP under an increasing output head. Further, from investigations into the effect of manipulating the output inductance for no increase in head, the numerical results have shown only the discharge flow trace to be affected. With regards to the flow stability through the inductance pipe, it is an important finding that the ECV must be operating at a sufficiently high frequency to ensure a reasonable flow ripple. Practically speaking, any oscillations in flow through the pump which are above 10% of the operating BEP would be considered damaging to the pump. It is noted that this may also be avoided through modification of the inductance pipe, however, it would remain more acceptable to ensure higher frequency ratios if the pumping system were to be of useful size. Overall, the numerical analysis has provided initial grounds for comparison with both electrical and experimental systems later in this thesis.

Chapter 7

Electrical Analysis

Chapter 3 introduced the electric-hydraulic analogy and discussed the electrical boost-converter circuit and its hydraulic equivalent, demonstrating its similarities to the hydraulic ram and induced flow reciprocating pump. Following from the numerical analysis of the hydraulic circuit, using the equations defined in **Chapter 5**, the electrical DC – DC boost-converter circuit is now briefly considered. From evaluation of the circuit with identical system parameters to those used in **Chapter 6,** a comparison is drawn which demonstrates the similarities and differences between both systems.

7.1 The Electrical Circuit

Figure 7-1 shows the 'hydraulic boost converter' circuit which has been used to define the equations of flow through the IFS centrifugal pumping system in **Chapter 5**. A comparable electrical circuit was constructed using commercially available electrical analysis software. MicroCap™ v. 11 is an analogue/digital circuit simulator based on the popular and more widely used SPICE format, providing an intuitive sketch and component editing platform for electrical analysis. It presents several easy construction and evaluation tools, most useful of which was its transient analysis function. This allowed for the investigation of discharge and inductance 'flows' over time so as to

provide a direct comparison to those results discussed in **Chapter 6**. The equivalent electrical circuit created using the MicroCap™ software is shown in **Figure 7-2**.

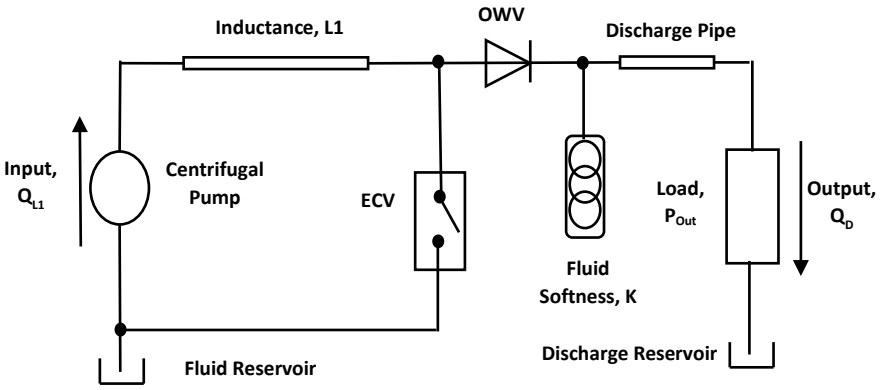

Fig. 7-1 – Hydraulic circuit of centrifugal pumping system with IFS

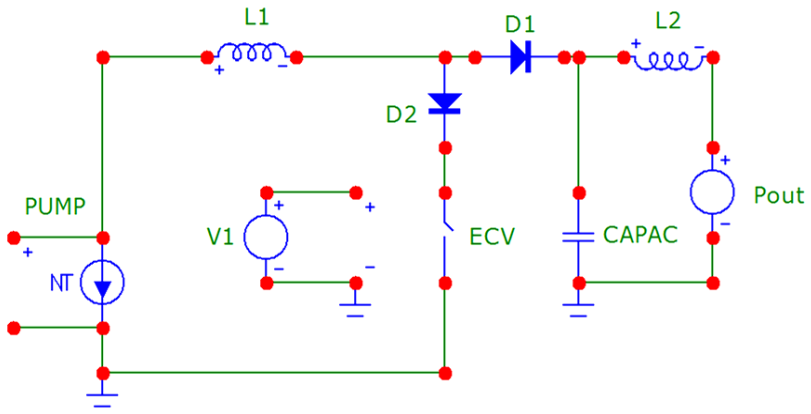

Fig. 7-2 – Microcap electrical equivalent circuit

The circuit was designed so as the individual components and their operation were as closely matched to the theoretical definitions in the hydraulic circuit. All components were modeled as 'perfect'; this is to say that they were defined only by their assigned values and any other characteristics in the software were removed where possible (i.e. there is no parallel capacitance or additional series resistance through components). Furthermore, the software's thermal evaluation mechanic was disabled to remove any effects due to fluctuations in component temperature.

For the electric-hydraulic analogy to be valid, the describing equations in both electrical and hydraulic domains had to be identical (substituting the relevant nomenclature). **Table 7-1** shows a modified version of the numerical analysis system parameters table presented in **Chapter 6**, with additional data illustrating the correct fluid and hydraulic units. The same centrifugal pump curve data used in the numerical analysis was also used in defining the electrical circuit so as to ensure a basis for comparison with the theoretical equations. The objective of doing so was to demonstrate similar, if not identical, operating characteristics in the electrical circuit as a means of validating the theoretical model (which is used extensively in **Chapter 8** as a reference for 'ideal' BEP pump operation).

Table 7-1 – Electric-hydraulic circuit test data

TEST RIG DETAIL	HYDRAULIC SYMBOL	ELECTRICAL SYMBOL	VALUE	HYDRAULIC UNIT	ELECTRICAL UNIT
Capacitance	C	C	4.329×10^{-10}	m^6/J	$Coul^2/J$
Inductance	L	L_E	2.105×10^{7}	Js^2/m^6	$Js^2/Coul^2$
Pump BEP Pressure	P_{BEP}	V_{BEP}	25000	J/m^3	J/Coul
Pump BEP Flow	Q_{BEP}	I_{BEP}	2.75×10^{-4}	m^3/s	Coul/s

It is seen that the equivalent unit of 'fluid' in the electrical domain is the Coulomb. Just as a single volumetric unit of fluid is a cubic metre, the Coulomb is a measurement of a unit of charge, whereby $1\ Coul = 1\ J/s$. It is also noted that by using the electric-hydraulic analogy, the pressure and flow data in the hydraulic circuit correspond to the voltage and current data in the electrical circuit respectively. Just as when dealing with fluids, the flow is defined by the number of units across a single measure of time. The same is true of an electrical current; the measure of time remains

constant in both domains and the Coulomb replacing the cubic metre as discussed above. Thus it is easily understood that for flow and current, the unit relationship is $m^3/s = Coul/s$. For pressure and voltage, the relationship between units is derived as $Pa = N/m^2 = N.m/m^3 = J/m^3$ equivalent to $J/Coul$. Using these analogies, the equations defining flow and pressure through the inductance and capacitance components may be described by **Eqns. 7-1** and **7-2**.

$$V = L_E \frac{dI}{dt} \qquad \textbf{Eqn. 7-1}$$

$$V = \frac{1}{C} \int I \, dt \qquad \textbf{Eqn. 7-2}$$

These are equivalent to **Eqns. 7-3** and **7-4** (repeated form **Chapter 4**):

$$\Delta P = L \frac{dQ}{dt} \qquad \textbf{Eqn. 7-3}$$

$$P = K \int Q \, dt = \frac{1}{C} \int Q \, dt \qquad \textbf{Eqn. 7-4}$$

where, for the above pairs of equations, the units described by **Table 7-1** are manipulated thusly: For capacitance, the units $m^3/Pa = m^6/N.m$ equivalent to m^6/J; and for the inductance, the units $kg/m^4 = J.s^2/m^6$ equivalent to $J.s^2/m^6$ (from $L = \rho.l/A$, **Chapter 4**) as $1\ kg = 1\ J.s^2/m^2$ from pressure and force equations (where $P = m.a/A$, giving $kg/s^2.m = N/m^2$).

7.1.1 Component Definitions

The first component to be discussed is the current source: the electrical equivalent of the centrifugal pump in the hydraulic circuit. After trialing several circuit variations and current source configurations, the closest numerical match to the

theoretical pump definition was to use a variable non-linear 'transfer function source' relating the current to the voltage across the component (NTIofV). This style of component in MicroCap™ enabled the relationship between source current and voltage to be defined by a non-linear transfer function; using ordered pairs of data inputted in a tabular format. The variable used for the NTIofV source is the voltage between the positive input lead and negative input lead to the component. By completing the defining table using the manufacturers pump curve data in corresponding electric-hydraulic units, the current source was programmed to act as the theoretical centrifugal pump; that is, with a defined BEP voltage (pressure) and current (flow). The load pressure,P_{Out}, from the hydraulic circuit was modeled using an independent DC voltage source feeding against the NTIofV current source. This was altered based on the specific test criteria, where a head of $1m$ is equivalent to $9810\ J/Coul$.

The inductance pipe equivalent electrical inductor, L1, was assigned a value based on the hydraulic circuit (length, $3.72m$ at $d = 15 \times 10^{-3}m$) and the second electrical inductor, L2, was varied based on the corresponding test head from the hydraulic circuit; this represents the discharge pipe inductance. As mentioned previously, both inductors were defined with no series resistance or parallel capacitance, making them as simple, or 'perfect', as possible. The capacitor itself was defined based on a hydraulic 'softness' of $2.31\ GPa/m^3$, with no series resistance. Diodes D1 and D2 ensured no current flow through the circuit back towards the current source and were adjusted to have infinitely high resistances in the reverse direction and no complex characteristics (such as thermal noise or flicker noise due to diode current). The diode, D2, represents the hydraulic OWV preventing negative flow during the ECV ON periods and enabling the pressure boost in the hydraulic circuit.

In the case of the ECV, a voltage controlled switch (V-Switch) was selected. This was the simplest way of ensuring the valve behaved as described theoretically, with perfect switching as defined by the theoretical equations in **Chapter 5**. In the V-Switch component definition, the resistance during the ON and OFF periods was adjusted to provide infinite resistance during the OFF period and zero resistance when the switch was closed (the ECV ON period). This ensured that all possible flow diverted to the OWV, D2 (diode), during the OFF periods. A pulsed voltage source was used as the control system for the ECV as it allowed for greater flexibility in defining the time period and duty of operation. **Figure 7-3** is an example of the current across the V-Switch, illustrating the ideal switching produced by the pulsed voltage source and resistance across the switch. The 'peaked' current rises during the ECV ON period are as a result of the increase in flow across the switch, identical to that in the inductor, and seen in the test results later in this chapter.

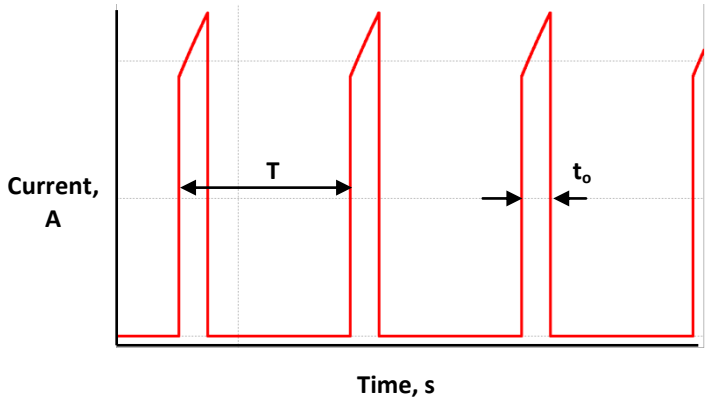

Fig. 7-3 – ECV, V-Switch transient current general example

7.2 MicroCap Simulations

The MicroCap™ simulation was performed using the test conditions defined in **Table 7-1**, with the voltage load on the system varied in accordance with the test heads from **Chapter 6**. This was from just above V_{BEP} to twice the maximum rated head of the hydraulic system. To perform each test, the spreadsheet used in calculating ECV duty from **Chapter 6** was used and pulse data modified accordingly, so as to give the V-Switch correct operation. Simulations were run across a period of 10 seconds, ensuring that the transient simulations had fully stabilized. A sample rate of 1000 data points per second was used to ensure a suitable flow resolution, even at the maximum frequency ratio of $r = 10$. After completing a simulation, the transient data was exported as a .TNO file and analysed using Microsoft Excel 2010. Average flow data was then found through the use of a simple spreadsheet. This section presents the results of these tests.

7.2.1 Inductance and Discharge Flows

The first characteristic of the electrical circuit to be assessed was the evolution in average output and inductance currents. For these tests, the frequency ratio was held constant at $r = 2$, giving a system operating frequency of $3.33Hz$, and the constant voltage load was varied according to those head values used in the numerical analysis. **Figures 7-4** and **7-5** show the results of these simulations, presented in dimensionless terms so as to provide a direct comparison with the theoretical results using the electric-hydraulic analogy. (*NB- the dimensionless terms used will be those of the hydraulic analysis;* $\Delta P/P_{BEP}$ *equivalent to* $\Delta V/V_{BEP}$ *and* Q/Q_{BEP} *equivalent to* $\Delta I/I_{BEP}$ *).*

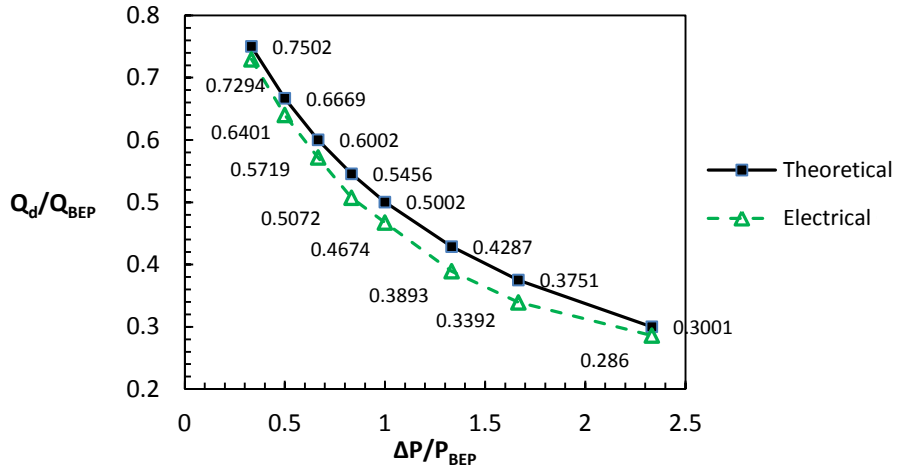

Fig. 7-4 – Comparison of average discharge 'flows'

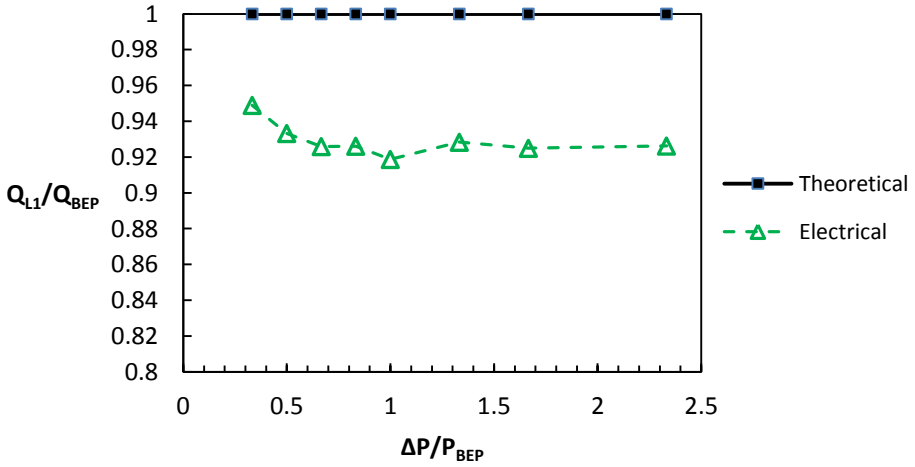

Fig. 7-5 – Comparison of average Inductance 'flows'

The electrical results show good matching to the theoretical averages, with no more than a 4% difference in the worst case of the discharge averages. As with the theoretical results, the average flow at the output of the system drops as the load is increased. The inductance flows are seen to display a greater variation with the majority being below the theoretical by around 8%. Unlike the discharge flow, the action of the V-Switch is seen to hold a relatively consistent inductance flow. This is in agreement with what is expected from a boost converter circuit and the flow definitions from **Chapter 5**.

In order to investigate the differences in flows across the output and inductor further, the flow transients were plotted directly using MicroCap™, the results of which are shown in **Figures 7-6** to **7-10**.

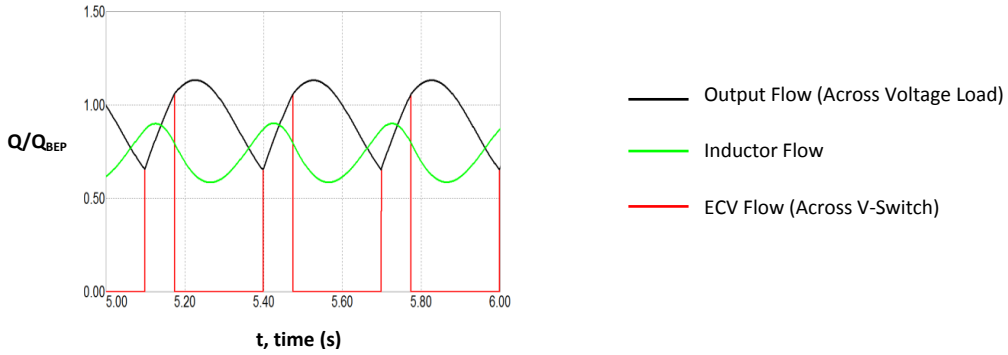

Fig. 7-6 – Electrical transients, 4m equivalent

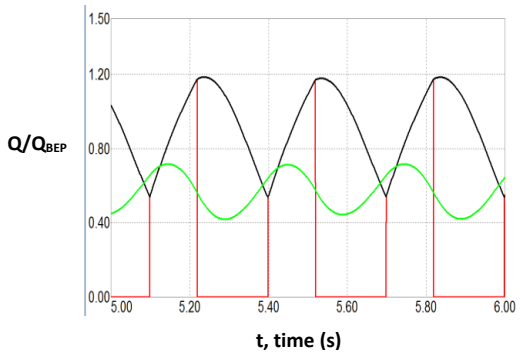

Fig. 7-7 – Electrical transients, 5m equivalent

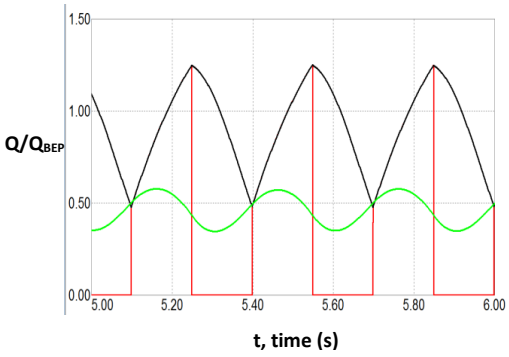

Fig. 7-8 – Electrical transients, 6m equivalent

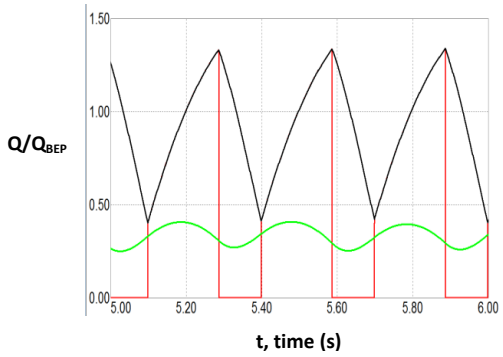

Fig. 7-9 – Electrical transients, 8m equivalent

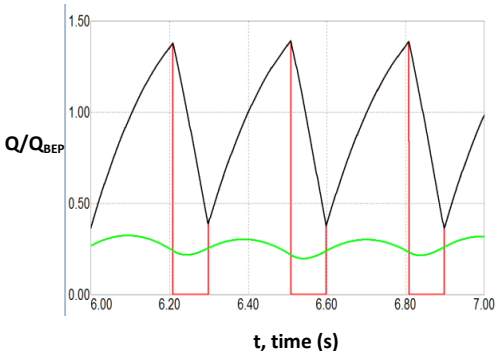

Fig. 7-10 – Electrical transients, 10m equivalent

The figures show a good match to the flow characteristics displayed in **Figures 6-3** to **6-6** from the numerical analysis (which illustrate the theoretical flow traces as described by the equations from **Chapter 5**). It is seen that the action of the V-Switch and inductor-capacitance produces oscillations in current across the inductor. Further, as expected from the definition of duty used in defining the operating characteristics of the switch, the oscillations suggest the circuit is operating in continuous mode. The current does not ever reach a steady maximum or deplete entirely. Current flow across the inductor is also seen to oscillate about a value close to that of the BEP (as shown by **Figure 7-5**) for all variations in system load, with an increase in flow ripple, $\mathbb{R}$, at greater system loads. With regards to the pattern of flow through the inductor, however, it can be clearly seen in **Figures 7-6** and **7-7** that the behavior of the inductor differs from the theoretical model by its non-linear response to variation in current across it. During circuit loads equivalent of up to 6m head in the hydraulic system, the current across the inductor is seen to continue to increase, even after the V-Switch becomes inactive. This is more noticeable in **Figure 7-6**.

The discharge flow shows a sinusoidal pattern very similar to that found in **Chapter 6** for the theoretical hydraulic discharge flows. As shown already in **Figure 7-5**, the average flow also behaves as expected from these previous results. The ripple characteristics are seen to be converse to those displayed across the inductor in that the flow stabilizes as the effective output inductance and load increase. This is again in agreement with the results from **Chapter 6**.

7.2.2 Flow Stability

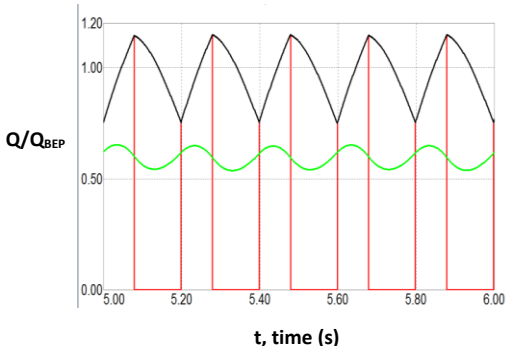

Fig. 7-11 – Electrical transients, r=3

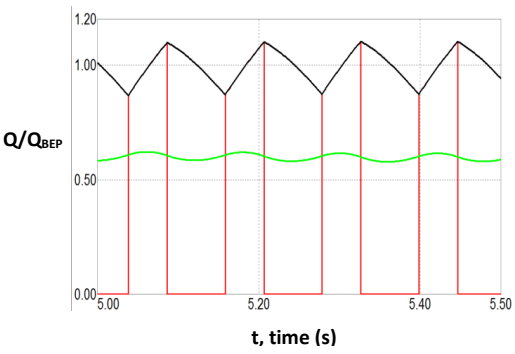

Fig. 7-12 – Electrical transients, r=5

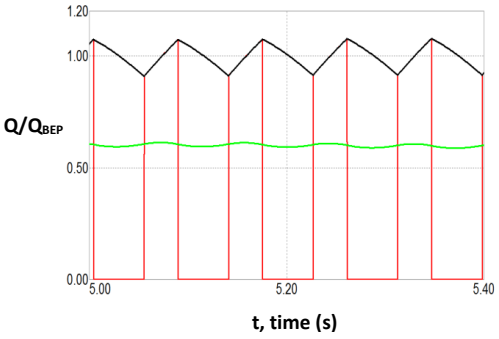

Fig. 7-13 – Electrical transients, r=7

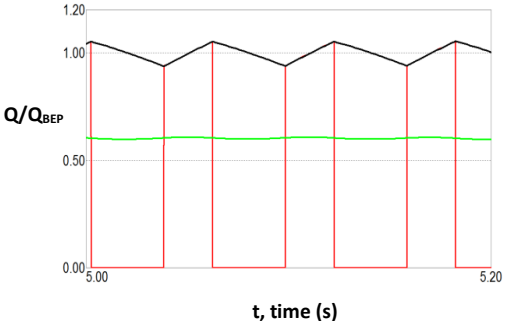

Fig. 7-14 – Electrical transients, r=10

As previously mentioned, the ripple across the inductor was shown to increase in proportion to the load on the system. This agrees with the characteristics observed in the numerical analysis. The ripple in the electrical circuit is, however, found to be greater than that when using the **Chapter 5** equations. As the tests at frequency ratio $r = 2$ were shown to have flow trends which varied from the linear assumptions made in the numerical analysis, simulations were run for a range of frequency ratios. The ratios tested were the same as those used in the numerical analysis, giving a useful range of operating frequencies far beyond those expected of typical practical application, for which the results would be comparable (as any results over $r = 5$ been shown to have strong matching). All simulations were conducted at a load equivalent to 5m head in the hydraulic circuit (equal to $49035\,J/Coul$) and with the same

components parameters described by **Table 7-1**. The transient results are displayed in **Figures 7-11** to **7-14** (the legends for which are the same as for the discharge and inductance flow figures shown previously). From initial observation of the results it is apparent that by increasing the frequency of operation, the ripple across both inductor and voltage load decreases. Further, the flow across the inductor shows a much more linear response as the time period is reduced by increasing frequency ratio. The result of this is a much closer matching to the theoretical model of the hydraulic circuit and the response of the fluid inductance to the fluctuations in operating load to the pump due to the ECV. This matching can be seen in **Figure 7-15,** which shows the comparison in inductance flow ripples across all frequency ratios tested for both electrical and hydraulic circuits.

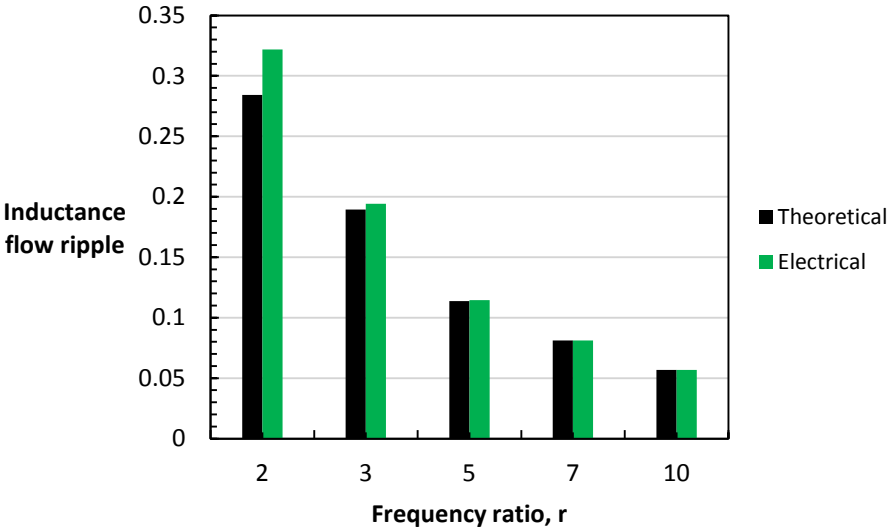

Fig. 7-15 – Comparison of theoretical and electrical inductance flow ripples

Further investigation into the effects of altering frequency ratio show that, in addition to producing flow oscillations far more similar to those displayed in **Chapter 6**, there is an increase in average flow. This increase brings the simulated results up to

those results predicted numerically, which were at fixed average values across all variations in frequency ratio. The evolution in these average flows is shown in **Figure 7-16**.

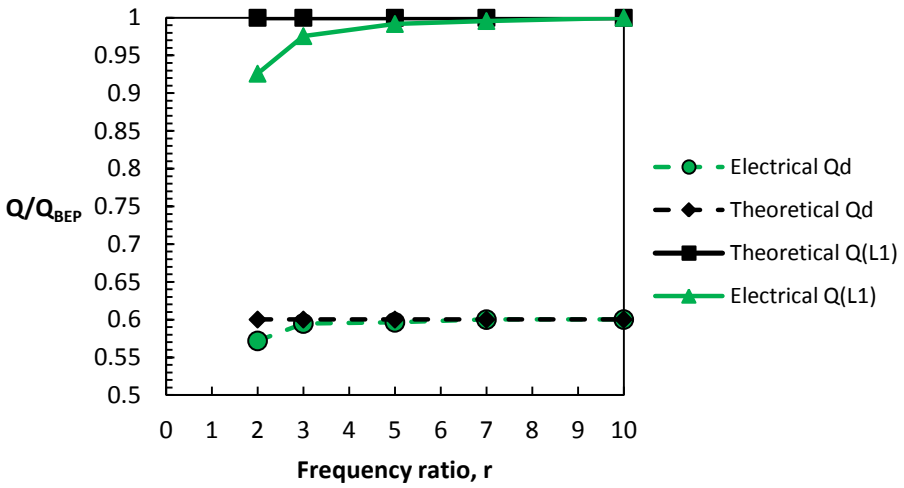

Fig. 7-16 – Comparison of average inductance and output flows

7.2.3 Decoupling of Current Source

In the same way that the numerical analysis was able to alter the discharge pipe parameters (and hence output inductance) without affecting the system load, MicroCap™ enabled the modification of inductance L2 in the same fashion. In order to explore the pump-load decoupling displayed in **Chapter 6,** a similar set of tests were performed using the electrical system. The circuit parameters from **Table 7-1** remained constant, as did the operating load of $49035\,J/Coul$ and frequency ratio of 2. The equivalent hydraulics length of the discharge pipe was varied. **Figures 7-17** and **7-18** show the circuit operating with double and quadruple length discharge pipes for no additional system load as a means of observing the effect on flow across the inductor (*NB -legends remain the same as those used previously*).

From these figures it can be seen that the inductor flow trace is unaffected by the increase in inductance past the diode, D1, (OWV from hydraulic circuit). The increase in inductance, L2, instead is shown to affect only the flow stability across the output voltage source in the same way as an increase in operating load does (that is, to say, a reduction in ripple). The average flow, however, remains constant with the value found initially for tests at the same operating load. These results demonstrate that the operation of the electrical centrifugal pump equivalent (the NTIofV source) is completely decoupled from the load on the system. This further agrees with the findings from the numerical analysis.

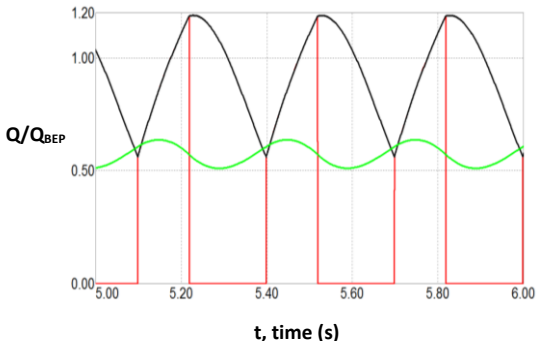

Fig. 7-17 – Flow transients at double equivalent discharge pipe length

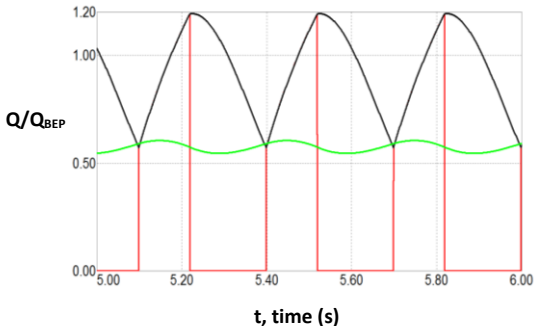

Fig. 7-18 – Flow transients at quadruple equivalent discharge pipe length

7.3 Discussion and Conclusions

In general, the MicroCap™ simulation results are shown to be in good agreement with the theoretical results presented by the numerical analysis in **Chapter 6**. There are, however, some characteristics which are not quite as were expected before completing the simulations. The equations presented in **Chapter 5** are based on the use of a duty equation taken from boost-converter theory, specifically a boost-converter operating in continuous mode. The theory suggests that the oscillations in flow produced by the action of the electronically controlled V-Switch (or ECV) would be linear, resulting in the equations defining inductance flow across the two operating periods, **Eqns. 5-12** and **5-13**. This also led to the theory for defining the average flow through the inductance pipe in **Chapter 5,** using the ripple characteristics. Interestingly, it is seen from the electrical simulations that the flow across the inductor was not linear until the frequency of operation was increased and hence the time period decreased to a sufficiently low degree. This could be explained by the way in which MicroCap™ models the inductors in the circuit. From transient inductor theory, it is seen that the rate at which an inductor resists change (i.e. the degree of impedance to the buildup of current) is proportional to the rate of change of current. As the current begins to reach a maximum and stabilize, this resistance to change will diminish until there is no impedance. Therefore it can be expected that, in the electrical circuit, for lower frequencies of operation, the current (or flow) across the inductor, L1, will exhibit a non-linear 'curved' response. This is why, at higher frequency ratios, the flow oscillations are observed to be more linear as they are at the point where the rate of change in current is greatest. Perhaps this explanation also justifies the closer average

flow matching at higher frequency ratios where the electrical model is operating much more closely to the way in which the hydraulic model predicts behavior.

As the results from **Section 7.2.3** display, the operation of the pump, or pump equivalent in the electrical circuit, is decoupled from the operating conditions beyond the OWV equivalent in the circuit. This is in agreement with the numerical findings in **Chapter 6**. Within the context of centrifugal pumps using IFS components, however, it demonstrates the ability to hold a pump at its BEP (MPP) irrespective of operating head. Further, the electrical system also shows an output current during operating conditions where the hydraulic equivalent pump would otherwise be unable to perform.

Overall the electrical results hold promise for the use of simple electrical software, such as MicroCap™ or SPICE, in making quick adjustments to a hydraulic equivalent system by making use of the electric-hydraulic analogy. Such tools would be useful in predicting performance across a wide range of operating conditions, where complex fluid analysis tools or CFD software would prove otherwise expensive, time consuming or demanding on resources. They also go some way to validating the theoretical model as a good initial means of estimating the performance of the hydraulic system and ensure that the results from the numerical analysis in **Chapter 6** can be used to present an 'ideal system' for comparison with the experimental results presented in **Chapter 8**.

Chapter 8

Experimental Analysis

This chapter covers, in detail, the experimental setup and procedure used to determine the effects of adding the previously defined IFS to a standard centrifugal pump. Based on the induced-flow, centrifugal water pumping system outlined in **Chapter 4**, an experimental rig was developed and constructed at the University of Liverpool's (UoL) hydraulics lab. The reasoning behind choices made in the rigs design, as well as a summary of the results obtained from the testing phase, can be found here. For the full sets of discharge flow, valve operation and flow trace data, please refer to **Appendix C.**

8.1 Experimental Limitations

8.1.1 ECV Operation Time

In designing the IFS test rig, there were several key considerations to be made. The first of these considerations involved an appropriate range of ECV operating times and duties for complete testing of the pumping system. The aim of the rig was to monitor the IFS's effect on flow at various points of the system (namely the inductance pipe and the discharge pipe) to determine such a systems suitability as a 'one-size fits-all' off-grid solution. Further, the validity of the theory presented in **Chapter 4** could be

tested by monitoring any oscillations in flow through the inductance pipe and pump BEP stability.

For testing at over-resonant conditions, the operating frequency of the ECV had to be sufficiently high to allow for r values of 2 or higher. This required that the primary inductance, L_1, of the system be maximized in order to minimize the systems natural frequency, hence allowing for higher frequency ratios to be implemented based on the restrictions of the ECV. These restrictions were rooted mainly in the acquisition of a programmable electronic valve, capable of not only high operating frequencies, but also exceptionally fast opening and closing times in order to minimize delay in the duty cycles. The selected valve is discussed in **Section 8.2.2**.

8.1.2 Laboratory Space

The allocated space available in the UoL's hydraulics lab for this research was restricted not only in terms of running length, but also height*. This limited not only the maximum achievable inductance (and hence maximum time period) but also the range of pumping heads the system could be tested for at a given power input. Controlling the maximum operating head of the centrifugal pump by restricting its power input was one way of increasing the amount of data obtainable.

* The height of the testing space had not been considered an issue originally, as the pressures applied to the pumping system to simulate increasing head were assumed to be created using an adjustable gate valve to restrict flow. However, following several issues with this original set-up, the valves were replaced with the adjustable height sub-assembly discussed in **Section 8.2.4.**

8.1.3 The Pump

Given limitations on lab space, versus the amount of data which it would be necessary to collect in order to validate or contest the theory presented in **Chapters 4, 5** and **6,** it wasn't possible to perform any experimental tests using a commercially available centrifugal pump of any significant size. As such it was decided that a smaller centrifugal pump be used and the experimental test rig scaled down in order to test the principles of the IFS operation and any effects on the discharge flow and flow through the inductance pipe/centrifugal pump. The pump selected was a 'Totton DC30/5' 12V magnetically coupled centrifugal pump.

Experimental testing of the pump rated it to maximum head of 4.2m with a BEP of 2.88m. The range of test duties was maximized by running the centrifugal pump at voltages as low as 6V at which maximum head was only 1.7m. In this way, the output flow of the IFS rig could be monitored over a variety of operating conditions. The pump was operated and adjusted manually using a variable DC power supply. Full details for the pump can be found in **Table 8-1** and characteristic curves for each test voltage found in **Appendix C**.

8.2 Induced Flow Subsystem Setup

The novel IFS test rig was completed as illustrated in **Figure 8-1** and further demonstrated by the photograph in **Figure 8-2**. The main construction was simple, primarily comprising the DC centrifugal pump, a rigid stainless steel inductance pipe, electronically controllable high speed ON/OFF valve (ECV), one-way check valve, capacitance chamber and an adjustable head output pipe. A summary of the full test rig specifications are presented in **Table 8-2**. For the purpose of testing, a mains

variable power source was used to produce a range of possible testing scenarios. Although the rig was a fraction of the size of a practical 'off-grid' borehole pumping system, it was designed to be representative of a larger pumping system, and all components are able to scale according to their theoretical definitions.

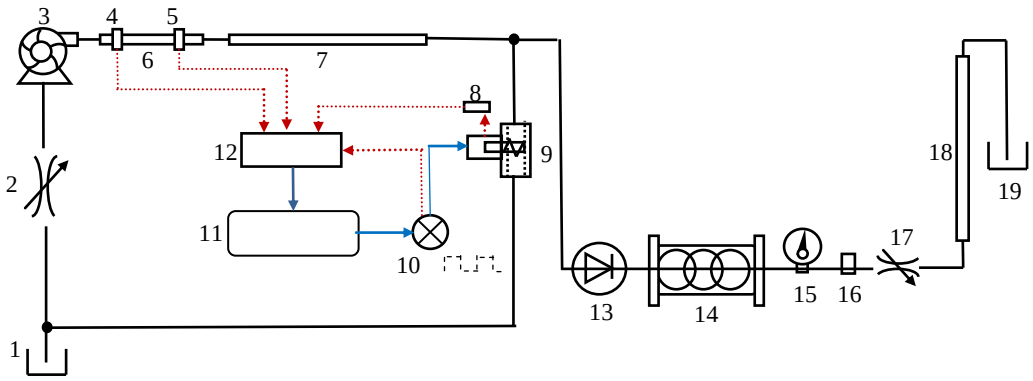

Fig. 8-1 - Schematic of experimental test rig. 1- Fluid reservoir, 2- Throttle valve, 3- Centrifugal pump, 4- Pump-side pressure transducer, 5- Valve-side pressure transducer, 6- 0.15m inductance pipe length, 7- Additional 3.55m inductance pipe length, 8- Piezo-electric transducer for measuring physical valve timing, 9- High-speed ON/OFF solenoid valve and coil, 10- Arduino chip valve controller, 11- Computer, 12- Data acquisition unit, 13- One-way check valve, 14- Capacitance chamber 15- Pressure gauge, 16- 5-bar safety pressure release valve, 17- Throttle valve, 18- Adjustable discharge pipe, 19- Output fluid reservoir

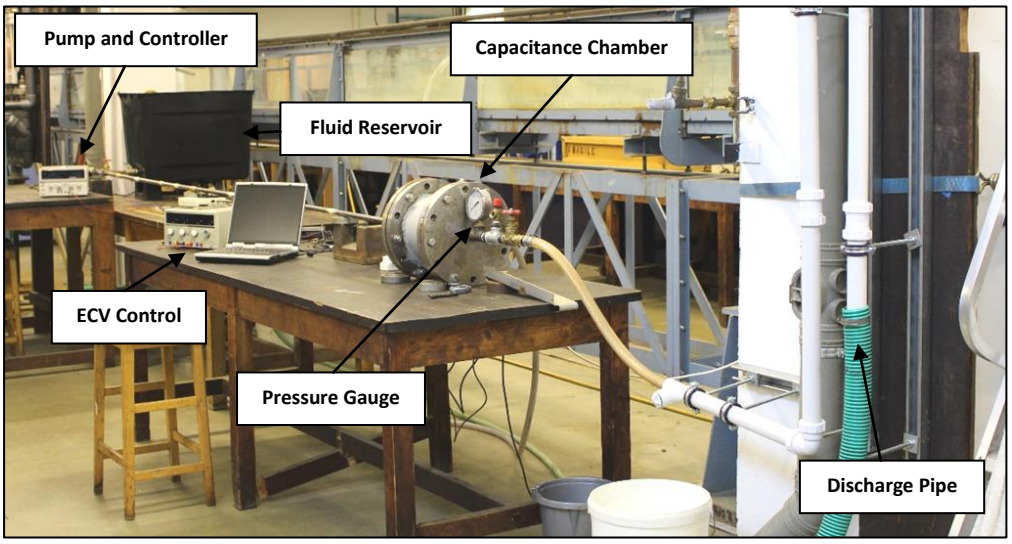

Fig. 8-2 – Experimental test rig with IFS at the University Of Liverpool

Table 8-2. Experimental test rig specifications

TEST RIG DETAIL	SYMBOL	VALUE	UNIT
Inductance total length	l	3.7	m
Inductance internal diameter	d_i	15×10^{-3}	m
Fluid ' Softness' , K	K	2.31	$GPa.m^{-3}$
Fluid Density	ρ	1000	$kg.m^{-3}$
Inductance pipe area	A	1.77×10^{-4}	m^2
ECV open time response	-	30	ms
ECV closing time response	-	20	ms
Steel pipe wave celerity	a	1360	$m.s^{-1}$
Data acquisition sample rate	-	1	ms
Data acquisition sample period	-	2	s

8.2.1 The Inductance Pipe

The inductance pipe was split into two equal diameter sections, the first of which contained the pair of pressure transducers at 0.15m spacing used to measure instantaneous flow through the inductance pipe. The second section supplied the additional length to make up the complete inductance pipe*. An inductance length of 3.72m using 15mm diameter stainless steel pipe was selected to ensure correct valve operation over a complete range of heads. This was based on the definition of time period in relation to the natural frequency of the IFS and also on the space restrictions which would allow the greatest time period for the ECV operation:

$$T = \frac{2\pi}{r\omega_n} \qquad \textbf{Eqn. 8-1}$$

*The full additional length was actually made up of several detachable sections of pipe which were designed to reduce the total length and alter the pumping systems natural frequency for a series of additional tests. Unfortunately, due to time constraints, it was only possible to test using a single inductance and the time period was instead modified using varying frequency ratios.

where:

$$\omega_n = \sqrt{\frac{KA}{\rho l}} \qquad \textbf{Eqn. 8-2}$$

Using **Eqn. 8-1** with frequency ratio, $r > 1$, set for over-resonant pumping conditions the time period of ECV was set at $T = 0.3s$, for $r = 2$. Although substantially longer than would be anticipated for practical use, the inductance pipe allowed the high speed ON/OFF valve to operate at lower frequencies and so test across a complete range of duties (*NB - While it is envisaged that a higher performance valve would be required to improve the overall performance of the test rig and scale down its size for practical applications, the valve selected for lab testing was sufficient to provide a good 'Proof Of Concept' to assess feasibility*).

8.2.2 Electronic Control Valve (ECV)

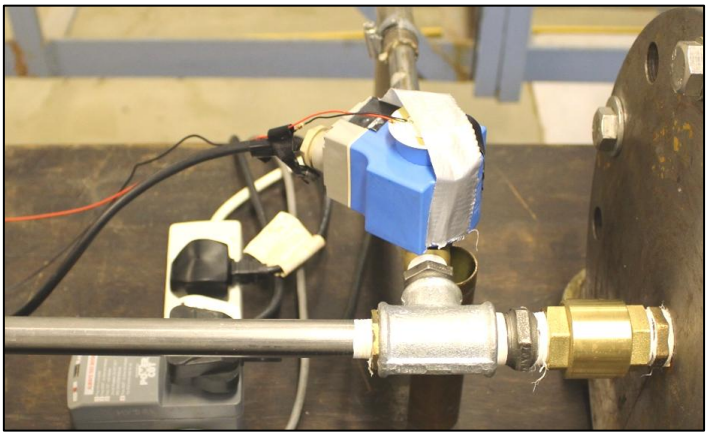

Fig. 8-3 – ECV installation and monitoring equipment on IFS test rig

After considering several other possible solutions to a high-speed, variable operation, controllable valve, a commercially available Danfoss™ series EV210-10B NC

(normally closed) solenoid valve was selected. This valve had a minimum cycling time of 50ms, comfortably enabling the basic operating frequency of the pumping system, at $r = 2$, of $3.3\ Hz$. The opening and closing delay times of 30ms and 20ms respectively also allowed for the possibility of testing for a full range of duties up to the allowable test head of 5m for the lowest pump input voltage of 6V.

The valve was connected to the main pumping system assembly by means of a 15mm internal diameter stainless steel pipe T-junction and appropriately threaded connecting sections as illustrated in **Figure 8-3**. The waste water created by the short circuit when the ECV was open during time t_o was diverted to the lab drains. **Figure 8-3** also shows the non-return valve immediately to the right of the T-junction. This valve was spring operated with an internal plastic plate to resist the return flow from the capacitance chamber (NB This type of non-return valve was found to be a significant improvement over the swing valve originally installed in the pumping system as it allowed for faster cycling of the ECV and increased pressurization of the capacitance chamber).

The digital timing of the valve was controlled by a simple Arduino chip (Arduino Pro mini 328 – 5V 16MHz) circuit using a software interface which allowed the valve to be timed according to the relevant testing duty. The Arduino chip used a basic 'blink' program which was designed to control an LED bulb. The circuit itself also contained a bulb so as the user could physically see the inputted operation of the ECV and ensure the correct signal would be sent to the solenoid and identify any programming issues. A variable DC power unit was attached to the circuit so as the available power to the ECV could be manually controlled between programming. During the tests, and due to the

delayed response time of the ECV, the open and closed times were modified based on the digital readings of valve position (from the piezo electric sensor installed immediately in contact with the solenoid coil housing above the valve mechanism). The full process is discussed further in **Section 8.5**. Valve duties were selected and programmed based on a variable output head in relation to each pump input powers BEP data. A full record of these programmed valve timings can be found in **Appendix C**, **Section C-1**.

8.2.3 Capacitance Chamber

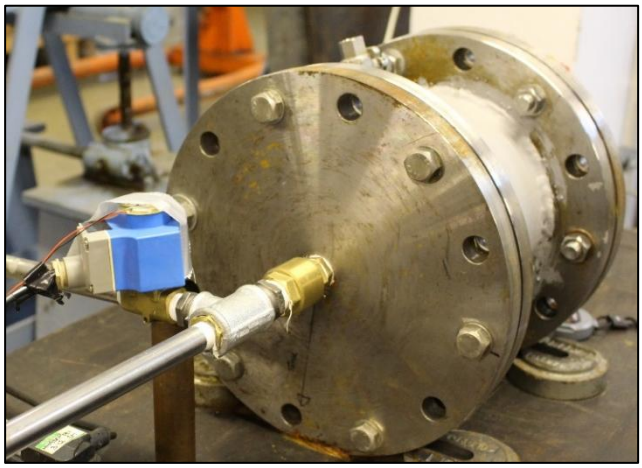

Fig. 8-4 – Capacitance chamber installation on IFS test rig

The capacitance chamber comprised of a steel tube chamber simply sealed at both ends with plates and bolts, see **Figure 8-4**. In the upright position the chamber had a ball valve 'vent' on the top side of the chamber so as to ensure the capacitance chamber could be fully flooded with water during testing. This removed any additional capacitance due to air pockets in the chamber. The capacitance within the chamber was provided by a series of firm rubber balls, sourced from various locations and

previous pumping rigs within the University. These balls were tested for compressibility and found to have a total hydraulic stiffness of $K = 2.31 \times 10^9\ Pa/m^3$. This rated the capacitance chamber as having a hydraulic capacitance of $C = 4.329 \times 10^{-10}\ m^3/Pa$ (equal to m^6/J and equivalent to $coul^2/J$ from the electrical analogy). Combined with an inductance length of $3.72m$, this produced a natural frequency in the system of $10.46\ rad/s$ and hence the operating frequency of $3.3\ Hz$ as defined in **Section 8.2.1**.

8.2.4 Adjustable Head Assembly

Fig. 8-5 – Adjustable head assembly and mounting on IFS test rig

Originally the pumping system test rig was constructed using a gate valve downstream of the capacitance chamber as a means of providing a variable load pressure. However, after an initial series of subsystem tests, it was discovered that

there was a definite maximum pressure the system could be loaded to before all flow was shut off entirely. Furthermore, as the IFS is designed to act as a pressure boost system, this resulted in an increase in capacitance chamber pressure for no additional discharge flow. This prevented any accurate comparison between the performances of the system in terms of flow delivery past BEP of the pump. It was decided that an alternate means of delivering a load pressure was to be devised.

The photograph in **Figure 8-5** illustrates the adjustable head assembly as it was in the lab space at the UoL. The discharge pipe was designed in a modular fashion so as the active testing head could be increased from 0.5m to 5m (given lab height restrictions as discussed). The entire assembly was constructed of 1 1/2 inch BSP diameter PVC piping (approximately 42mm internal diameter) cut to length by hand and sanded to ensure a smooth finish and flush fit, with minimum discrepancies between lengths. The sections could be fitted using 'quick-release' torsion lock PVC connecters. The assembly was designed as two parallel pipe sections to allow for the collection of discharge flow at the base of the assembly. Both sections of pipe were fastened to a stainless steel mounting rail. These sections of mounting rail were in turn securely fixed to an upright length of timber attached to a pillar in the lab space. A water release cap was also installed at the base of the assembly on the connecting pipe to the capacitance chamber. This cap could be used to drain the vertical column of water created in the assembly in between each test scenario, as it was decoupled from the IFS section of the rig by a gate valve: allowing the assembly height to be modified.

8.3 Lumped Parameter Analysis

Recalling the pumping system requirement introduced in **Chapter 4** that, for the lumped parameter method to give a valid analysis, as assumed by both the theory and numerical analysis, the more conservative criterion of Wylie and Streeter must be met, whereby:

$\frac{\omega l}{c} \ll \frac{\pi}{12}\ (= 0.2612)$.

Eqn. 8.3 shows the equation for wave celerity, c, [106].

$$c = \frac{\sqrt{\varepsilon/\rho}}{\sqrt{1+\frac{dp.\varepsilon}{e.E}}} \qquad \textbf{Eqn. 8.3}$$

Here, E is the elasticity modulus of the pipe (in the test bed case, steel), ε the bulk elasticity modulus for water, d_P the pipe diameter, e pipe thickness and ρ fluid density. Solving the equation for the experimental system where $E = 2 \times 10^{11} N/m^2$, $\varepsilon = 2.14 \times 10^9 N/m^3$, $d_p = 15 \times 10^{-3} m$, $e = 2 \times 10^{-3} m$ and $\rho = 1000\ Kg/m^3$ a value of $1407.48\ m/s$ is found. This holds well with other approximations for wave celerity in rigid steel pipes as being around $1360 ms^{-1}$ [64, 107]. For calculated celerity and natural frequency, ω_n, of the experimental test rig as $10.46\ rad/s$, then for an operating frequency of $20.92\ rad/s$ (at $r = 2$), this gives $\omega l/c = (20.92 \times 3.72)\ /\ 1407.48 = 0.055 \ll 0.2612$. Even when taking a much lower wave celerity approximation of $850 m/s$ for a more flexible pipe [107] $\omega l/c = 0.092$ - still well within Wylie and Streeter's criterion. Hence, for the test rig specified, the lumped parameter method is well within requirement. Furthermore, it ensures that the system can be

tested for frequency ratios much higher than 2 at constant ω_n, up to a maximum ratio of $r = 9.4$.

8.4 Instrumentation

8.4.1 Average Discharge Flow Measurement

At the outlet from the discharge flow assembly, a rubber hose was used to divert flow into a plastic water storage container. Inside this container was a secondary 'sump' pump used to empty the storage container to the drains. This set-up allowed the pumping system to reach a fully developed flow at the outlet before discharge flow measurements began. Upon reaching a fully developed flow and stable pressure readout from the system, the flow was manually diverted into a secondary water container. Discharge flow was collected for a period of 1 minute, timed manually using a stopwatch. The total mass of water collected was then calculated by weighing the container and the water collectively and subtracting the known weight of the container. The accuracy of the digital scales used was to $0.01Kg$ (or $10ml$). The mass flow rate obtained from this measurement could then be converted into a volumetric flow rate, Q_D , in l/s or m^3/s. This process was repeated several times for each pumping head to obtain an average discharge flow.

8.4.2 Inductance Pipe Flow Measurement

For comparison to be drawn between the practical application and theoretical simulation of the IFS components effect on flow through the inductance pipe (and hence the centrifugal pump), it was necessary to measure not only the average discharge flow rate, but also the instantaneous flow rate though the inductance pipe. The aim was to produce a flow trace over several time periods of ECV operation to

identify any changes or patterns in flow through the inductance pipe, similar to those produced in **Chapter 6** describing oscillations in flow Q_{L1}. This could then be used to validate the theory of maintaining BEP operating conditions of the pump through timing of the ECV.

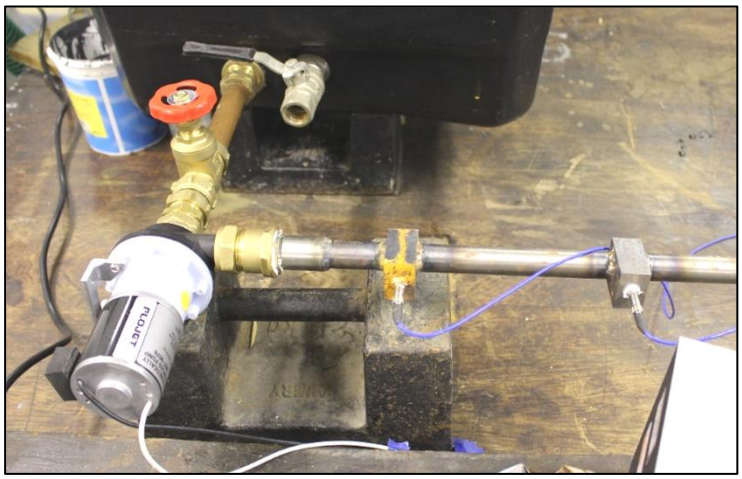

Fig. 8-6 – Pressure sensor arrangement on inductance pipe

The first section of the inductance pipe (approximately 0.2m) was manufactured with two pressure transducer housings 0.15m apart, see **Figure 8-6**. The sensors were flush mounted inside the housings. The output signal from each sensor was then connected to the data acquisition system so as readings could be taken in real time as each test was carried out. The difference in pressure was then used to obtain the instantaneous flow data through integration (see **Appendix C**, **Section C.3** for experimental procedure, or **Section 8.5** for details on data manipulation).

8.4.3 System Pressure

Fig. 8-7 – Pressure gauge, release and gate valve after the capacitance

Figure 8-7 shows the test rig pressure measurement configuration immediately after the capacitance chamber. Pressure readings were taken using a standard 'Bourdon' style pressure gauge. Given the installation of the test rig, the level of each pumping head fell short by a small degree when compared to the level of the centrifugal pump mounting. As such, all head values in meters were simply used as a reference for ease of use during the testing phase. The actual pressure readouts taken for each test scenario were used in the final manipulation and evaluation of flows through the pumping system. The figure also shows the safety pressure release valve and gate valve used to decouple the pumping system from the adjustable head assembly between test configurations. The gate valve was also used during the initial pressurization of the pumping system at the start of each test to ensure the capacitance chamber was fully flooded and had no additional capacitance. The full process is described in **Appendix C**, **Section C-2**.

8.4.4 ECV Position Measurement

Initial instrumentation tests showed the pressure transducers to be operating correctly, however, the flow traces obtained were not matched-up with the programmed operating times of the ECV. Furthermore, it was noted that, without a means of establishing the position of the ECV, there was no means of confirming whether any oscillations in flow through the inductance pipe were as a direct result of the valve and, if so, the exact mechanic of its action. As the instantaneous flow data produced by the pressure sensors in the inductance pipe alone were not sufficient to calibrate the ECV to perform at the correct duty for each test scenario, a physical measurement method was employed.

A piezo-electric transducer was fixed directly to the solenoid housing as a means of physically measuring the valve timing. The transducer was set up so as to send an output to the data acquisition unit and be measured alongside the instantaneous flow data. From the voltage peaks created at the point of ECV valve opening or closing it was possible to establish a rough position of the ECV. Further to this method, a direct output from the Arduino chip and circuit used to control the ECV was fed to the data acquisition unit. This provided another important tool for establishing correct operation of the ECV for each test set, by allowing the ECV to be calibrated based on its physical response time. This is described in more detail in **Appendix C**, **Section C-2**. **Figure 8-8** shows an example readout of physical valve position versus digital control of the ECV from the data collected by the data acquisition unit. The large spikes on the dotted blue line trace represent the points at which the ECV was fully open or closed and are simply created by the impact of the valve. It is

quite apparent that there is a larger delay between the digital signal and the physical response of the valve during the closing period of the valve.

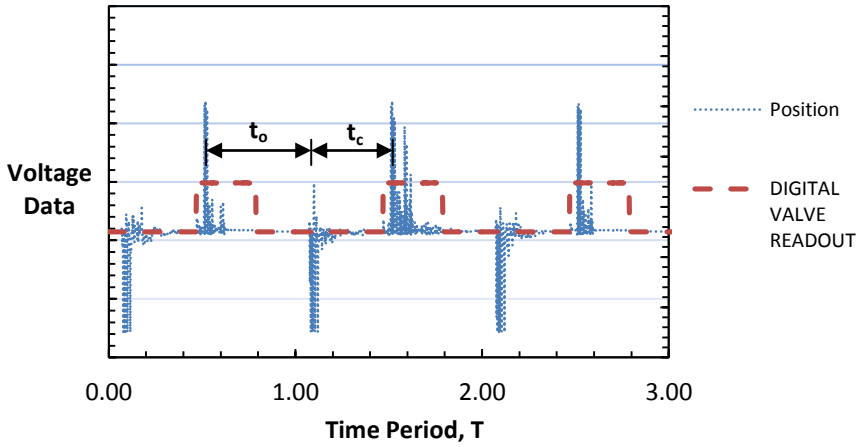

Fig. 8-8 – Example digital and physical valve position readout from transient data samples

8.4.5 Data Acquisition

An OMEGA™ OMB-DAQ-3001 series voltage data acquisition system, see **Figure 8-9**, was used to collect information about the pumping systems performance in real-time during tests. This was used to convert analogue input data into digital data, which could be analyzed and manipulated, in order to monitor the pumping systems performance throughout the experimental testing phase. The A/D (analogue-digital) module had 8 differential analogue input channels which were used to collect data on the following items of interest:

1. I-Motor - The current traces from the centrifugal pump DC power supply.
2. V-Motor - The voltage trace from the centrifugal pump DC power supply.
3. P-Pump – Voltage data from the pressure transducer at the pump end of the inductance pipe test section.

4. P-Sol – Voltage data from the pressure transducer at the solenoid end of the inductance pipe test section.
5. ECV-Position – Voltage data from the piezo-electric transducer coupled to the ECV housing as a means of monitoring valve position.
6. ECV-Digital – Voltage data from the Arduino pro mini chip used to control the ECV valve.

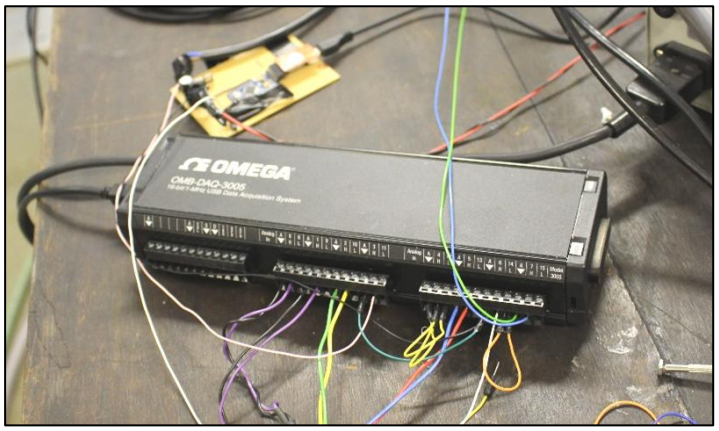

Fig. 8-9 – Data acquisition unit as connected to receive sampling data from test apparatus

The acquisition card used a sample resolution of 16 bits at a range of +/-10V. In order to collect data at this range an amplification unit was required to boost the analogue voltage data from the pressure sensors and I-Motor channel. The amplification ratio used was 10, hence all data had to be converted back during the data manipulation phase. The V-Motor channel was recorded at half voltage for protection of the A/D card.

The digital data collected by the card was monitored and controlled using DaqView™ software (available for use with the OMEGA™ OMB-DAQ-3001 series card)

which enabled the modification of sample rates, times and data-dump location. The software also enabled the data to be written into Microsoft Excel for ease of analysis and post sample review. The card was set up with a sampling speed of 2000 samples per second for a period of 2 seconds for all tests. This gave a comfortably accurate flow trace in all cases, without impacting too much on the processing speed of the test results. The skew rate of the card was $1\mu s$ per channel as each channel was sampled sequencially, giving the total skew rate as $6\mu s$. This was sufficiently small enough to ensure the divergence between multiple data samples would not impact on the final results.

8.5 Data Manipulation

After the data from a single test run had been collected from the 'dump' file created by the acquisition software, it was copied across to a Microsoft Excel spreadsheet where it could be manipulated. This subsequent manipulation and analysis involved a process to convert the voltage data into useable flow data, which is fully described in **Section C.3, Appendix C**. Following this manipulation, the following information could be displayed on a single graph for comparison: the digital position of the ECV, the physical position of the ECV and the Instantaneous flow from the system. **Figures 8-10** and **8-11** provide an example of the raw, unmodified data as it was imported into the analysis spreadsheet for the pump, pressure transducers and control valve, whereas **Figure 8-12** shows the final result of the manipulation. This is the format used to present the transient data throughout the rest of this chapter and also in the full catalogue in **Appendix C**.

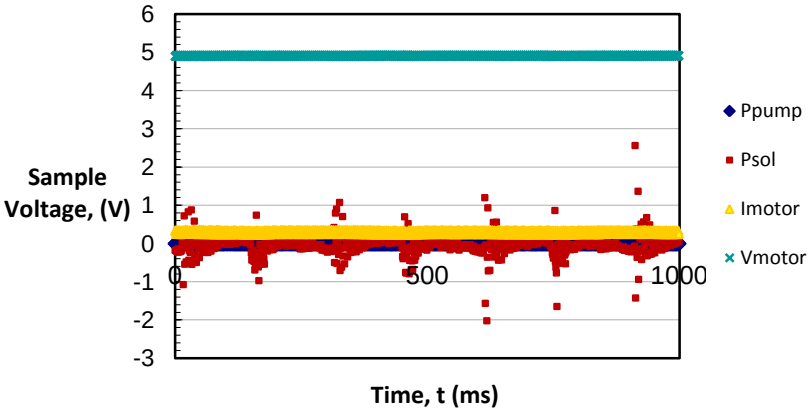

Fig. 8-10 –Example of raw voltage data from the DAQ unit

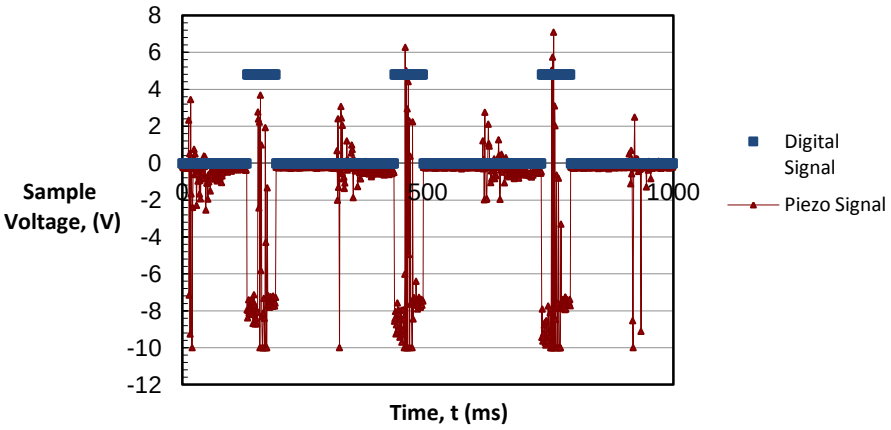

Fig. 8-11 – Example of the raw ECV trace data from the DAQ unit

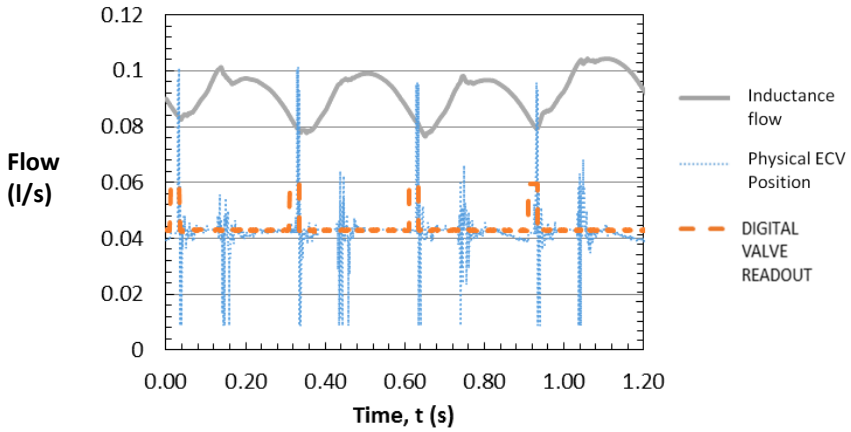

Fig. 8-12 – Example final data plot displaying ECV and flow traces

8.6 Performance Test Results

8.6.1 Discharge Flow

For each set of results, the average discharge flow at the outlet pipe of the fluid system was plotted against the control curve, based on input voltage, with no IFS. A full summary of these curves and the BEP data at each voltage can be found in **Section C.1**. All results are presented non-dimensionally, relative to associated Q_{BEP} and P_{BEP} at each voltage. **Figure 8-13** presents the comparison in discharge flow, both with and without IFS, under increasing output pressure and over a range of input voltages for over resonant condition, $r = 2$. The theoretical discharge flow represents the maximum achievable flow at perfect operation of the IFS, obtained using the numerical model. On activation of the IFS, in all test cases, an increase was observed in average discharge flow above that of the unmodified pumping system. Additionally, the system was able to pump against a greater pressure load with the IFS active. The relationship

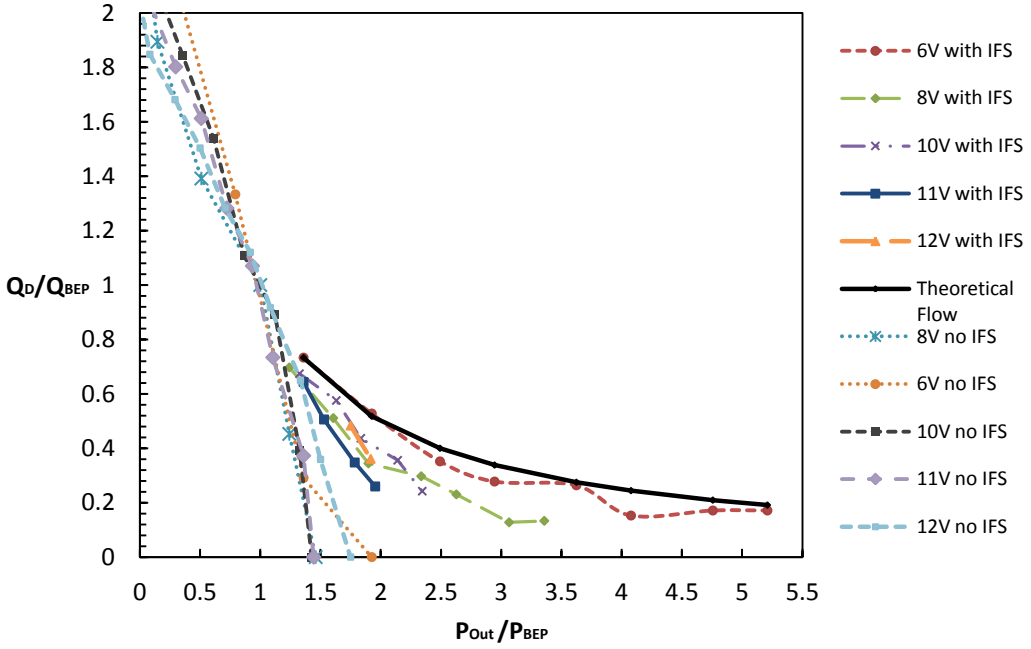

Fig. 8-13 – Comparison of discharge flows at varying input voltage both with and without IFS

between increasing Duty and output pressure was validated as the boost in pressure allowed the test rig to produce an output flow even after the maximum operating head of the pump had been reached, and exceeded, for each operating voltage. In the case of the 6V pump operation, it was noted that the pump was operating at well above twice its maximum rated load, albeit with a significantly reduced flow to the start of the ECV operation. It is also seen from **Figure 8-13** that the flow trends are a good match to the theoretical data, with a closer match being achieved at the lowest of the test voltages.

Discharge flow tests were repeated for varying values of frequency ratio, r. The primary goal of these tests was to monitor the frequency ratios effect on the stability of flow Q_{L1} and draw comparison to the simulations discussed in **Chapter 6**. However, collecting information on the discharge flow performance of the system was additional data which could give extra insight into the effect of the ECV and induced flow subsystems. The degree to which r value could be increased for each test voltage was limited by the speed at which the ECV could operate comfortably versus the duty at which it was required to operate. Recalling the duty equation and the relationship between load pressure and open time of the ECV, a higher r value results in a lower time period and hence a reduced open time, t_o. It was found that under increased flow rates, such as those produced at higher pump operating voltages, the delay time in the ECV operation and control was increased. Thus, for the lower duties and shortened open times at higher voltages, there was no possibility of testing above values of $r = 2$. However, it was possible to test at $r = 1.5$ for all operating voltages and $r = 2.5$ for 10V or lower. A complete set of all recorded discharge flows and pressure loads can be found in **Appendix C, Section C-4**. **Figures 8-14** to **8-18** summarise this data graphically.

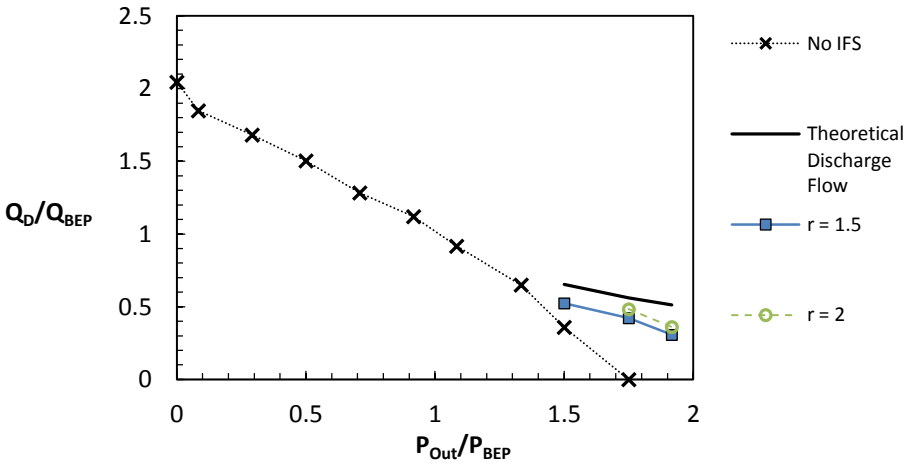

Fig. 8-14 – Discharge flow traces at 12V

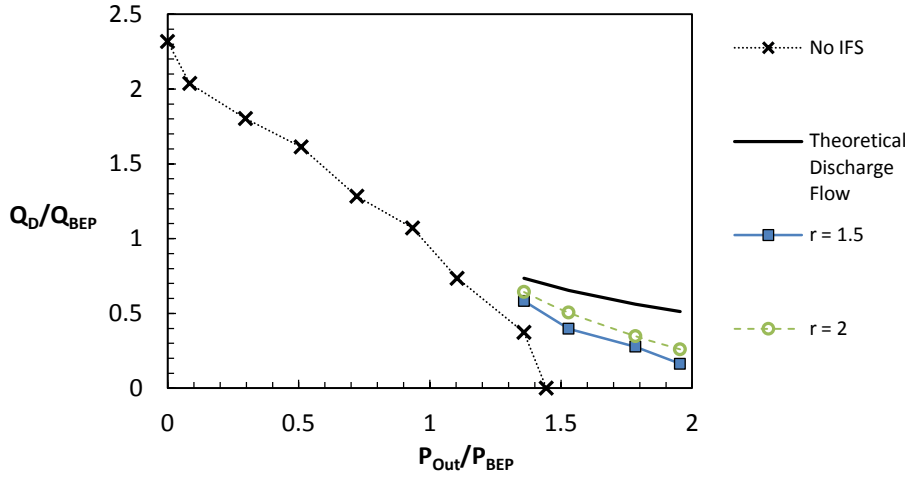

Fig. 8-15 – Discharge flow traces at 11V

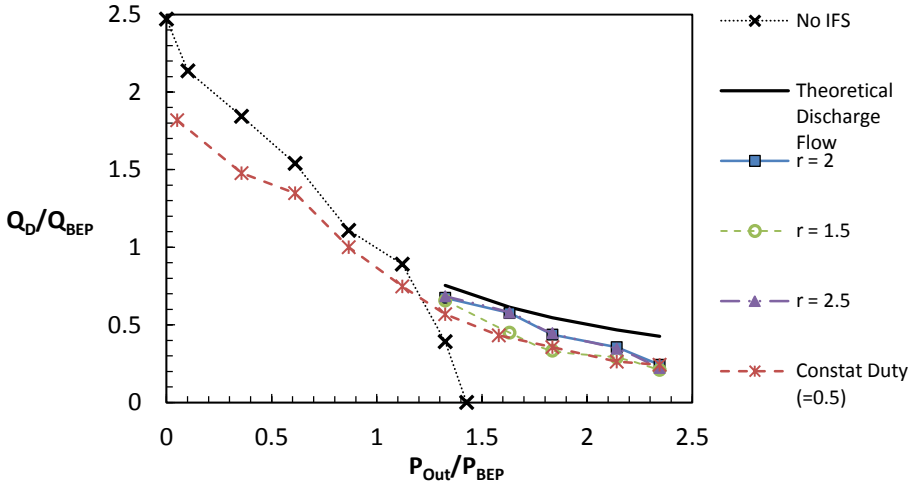

Fig. 8-16 – Discharge flow traces at 10V

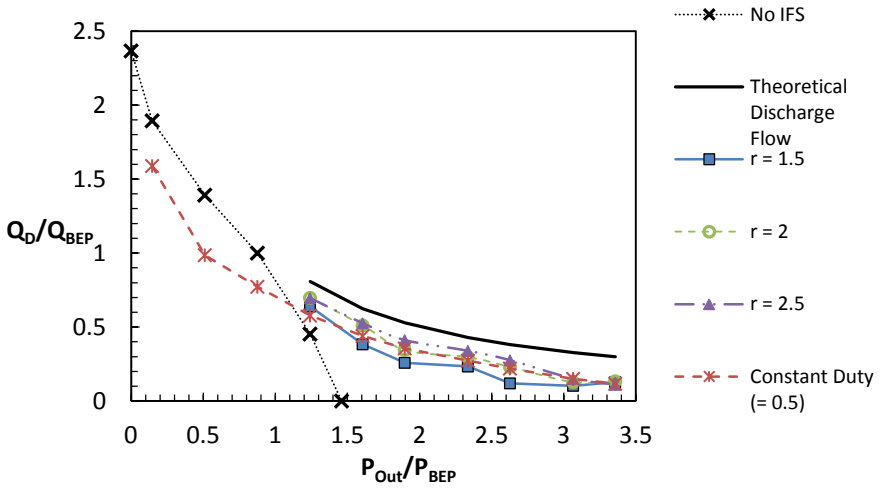

Fig. 8-17 – Discharge flow traces at 8V

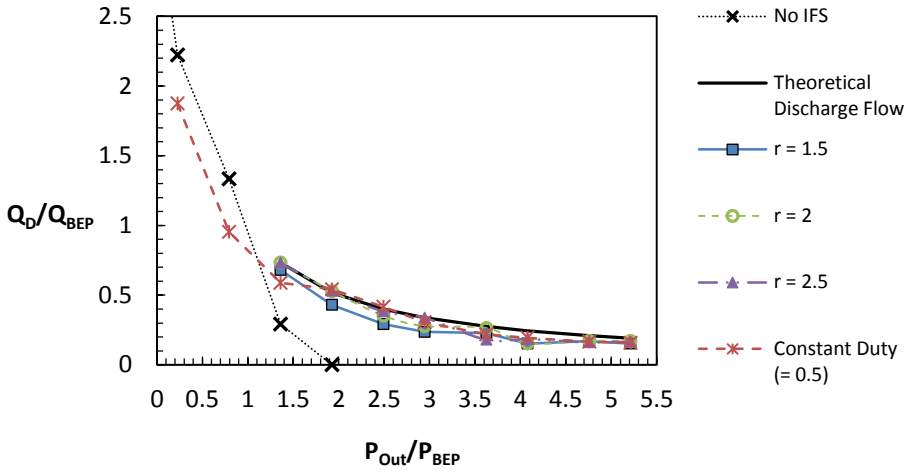

Fig. 8-18 – Discharge flow traces at 6V

8.6.2 Frequency Ratio and Discharge Flow

The trends across all r values of ECV operation are consistent in that they all produce an elevated level of discharge flow above BEP operation of the pump. It can be seen that, with the ECV active in all test cases, the discharge flow was not only increased above that of the pump operating without an IFS installation, but continued to operate until reaching the maximum obtainable load pressure by design of the test

rig. Beyond this point there were no signs during testing that the system was not capable of delivering to even greater loads. This is in line with the pumping theory presented in **Chapters 4** and **5** which predicts no upper limit on pumping head and also an increased discharge flow during ECV operation in order to maintain a BEP hydraulic power output from the system.

One of the more interesting findings from testing at various r values was the definite increase in discharge flow across the majority of test cases with an increase in r, leading to a closer match to those discharge flows predicted in the numerical analysis. As it was expected that the flows obtained from the test rig would not be a match to the theoretical on account of the negation of certain losses in the pumping system, the difference between the observed and predicted flow was not a surprise. However, the numerical analysis presented in **Chapter 6** does not predict that altering the operating frequency of the ECV would affect the average discharge flow, this being held at a theoretically 'ideal' value (BEP), but rather reduce the flow ripple through the inductance pipe and hence stabilize the pump operation. The conclusion may be that the reduced ripple and therefore weaker fluctuations in flow through the inductance pipe allow the pump in the test rig to operate more effectively and closer to the theoretical predictions. The relevance of this in regards to the IFS pump in general is the consideration that the ECV must be operating at a sufficiently high frequency (relative to the natural frequency of the system) in order to produce the desired effects.

As a means of exploring the experimental effect of r value further, an additional series of tests were performed at a set load pressure and pump voltage where that ECV could be operated at frequency ratios higher than 2.5. A voltage and

test head of 10V and 4.5m (equivalent to 41KPa) were chosen, giving the ECV and pumping system a duty of 0.52. This enabled the ECV to cope with a minimum open time of $t_o = 88ms$ (which was reduced to $15ms$ as a result of the ECV delay in operation). Thus, a maximum value of $r = 3.5$ (equivalent to operating frequency of $36.47\ rad/s$ and time period, $T = 170ms$) was achievable. **Figure 8-19** plots the results of these additional tests.

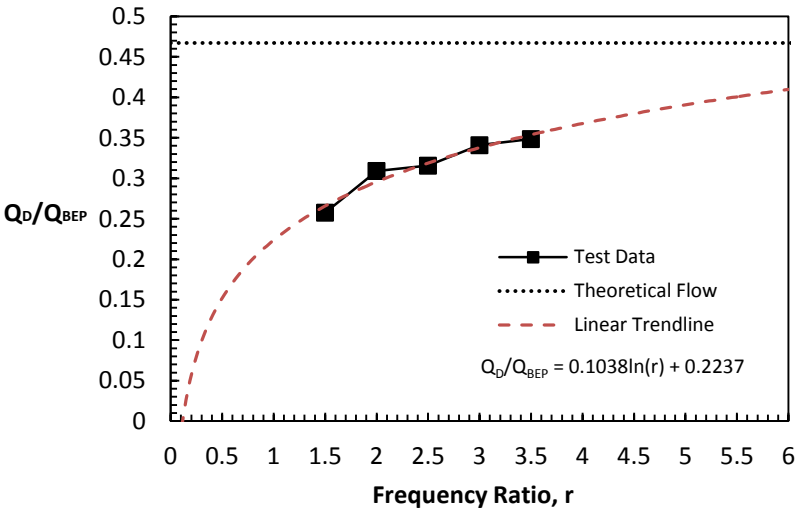

Fig. 8-19 – Varying frequency ratios at duty, D = 0.52, 10V

The data plot points indicate an overall increase in discharge flow as the frequency ratio is increased, for no additional modification of the system. This reinforces the idea that, in practice, a more stable flow through the inductance pipe is desirable not only for increased pump performance but also for system discharge performance. A logarithmic trend line plotted using the data points provides a brief estimate of the frequency at which the ECV would have to operate in order to match the upper bounds of discharge flow. This is indicated by the dashed red line. It holds well with the theoretical prediction of the ideal r value of 5 to give a minimal ripple.

This value would also appear to be consistent with the frequency ratio prediction obtained from the electrical analysis in **Chapter 7**, which found the same convergence with theoretical results around $r = 5$. Although it is still understood that a practical system would most likely not be able to match the theoretical model perfectly, these additional results do go some way to reinforcing the idea that a sufficiently fast operating frequency ensures numerical modeling (and even electrical modeling) can provide a good predictive tool.

8.6.3 ECV Constant Duty

A second set of additional tests were conducted using a constant ECV Duty of 0.5, at $= 2$. The aim of these tests was to examine the effect, on system performance, which any deviation in ECV operation from the theoretical Duty had. These additional tests were performed for pump voltages of 10V, 8V and 6V as these would provide a more suitable number of test points beyond BEP for comparison. The average results of these tests may be seen in **Figures 8-14** to **18** and the full results found in **Section C-4**. Unsurprisingly, the average discharge flow was reduced during periods of ECV operation below BEP pressure; this is as predicted in **Chapter 4**. Here, the benefit of increasing flow through the inductance pipe is forfeit due to the flow loss to submergence pressure from the return arm of the ECV.

At points above BEP, the IFS continued to perform in line with results seen previously for varying r values. Interestingly, the ECV at constant duty operation showed no significant loss in flow and there was good grouping with other discharge flows, especially at higher pressure loads. There was even seen to be a marked improvement over the lower operating frequency results for both 8V and 6V test sets

across the smaller duties. This would suggest that, in a practical system, the ECV would not necessarily have to provide the fastest of valve operation times and could instead revert to a predetermined duty which provides a reasonable substitute. Alternatively, in a pumping system operating at heads far beyond the systems BEP, a maximum duty could be imposed to eliminate the response time constraint (t_c at higher duties) on the valve. Coupled with closer matching to the theoretical model from an increase in r, a system which employs a constant duty cycle may be capable of operation at far higher operating frequencies and hence pump stabilities.

8.6.4 Hydraulic Power Output

Hydraulic power output of the system is calculated as the product of discharge flow and load pressure such that:

$$P_H = \rho g H_{Out} Q_D \qquad \textbf{Eqn. 8-4}$$

It is noted that it is the efficiency of the pump that remains constant and not the discharge flow from the system. From theory, if the pump follows its BEP irrespective of pumping head then, for the same power input to the pump, the hydraulic power output should remain constant as indicated by the dashed red line in **Figures 8-20** to **8-24**. Thus, from **Eqn. 8-4** it is understood that as the pumping head (and hence load pressure) increases so does the discharge flow drop. This drop in discharge flow is shown, however, to be less severe than the equivalent case of pumping without IFS across the range of normal operating pressures.

Figures 8-20 to **8-24** clearly demonstrate the degree to which the test data at lower operational voltages more closely matches the theoretical BEP hydraulic power

line. It is also seen that, for operation with ECV active, the increase in discharge flow discussed in Section **8.6.1 leads** to a significant boost in hydraulic power. This is especially relevant at the lower heads, still above P_{BEP}, before the pump reaches its maximum rated head. At these points there exists a greatly improved discharge flow and hydraulic power above that of the pump without IFS, demonstrating the IFS's ability to optimize system performance.

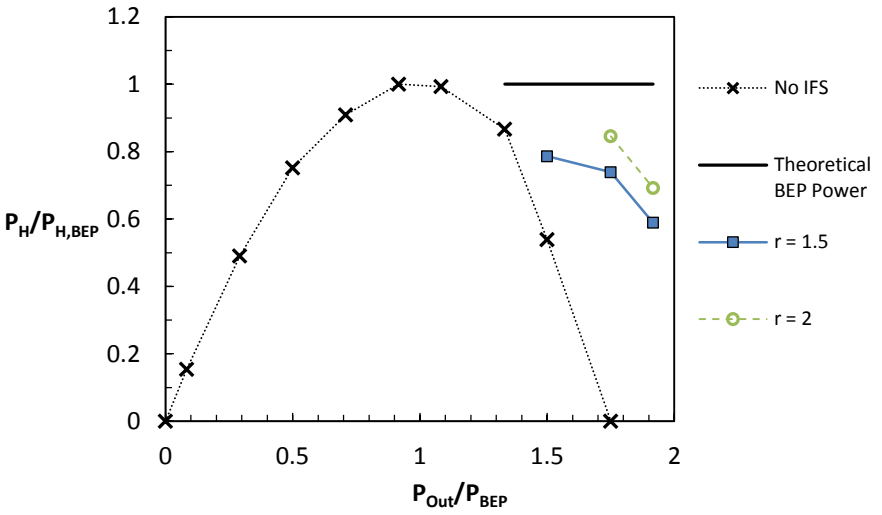

Fig. 8-20 – Hydraulic power output traces at 12V

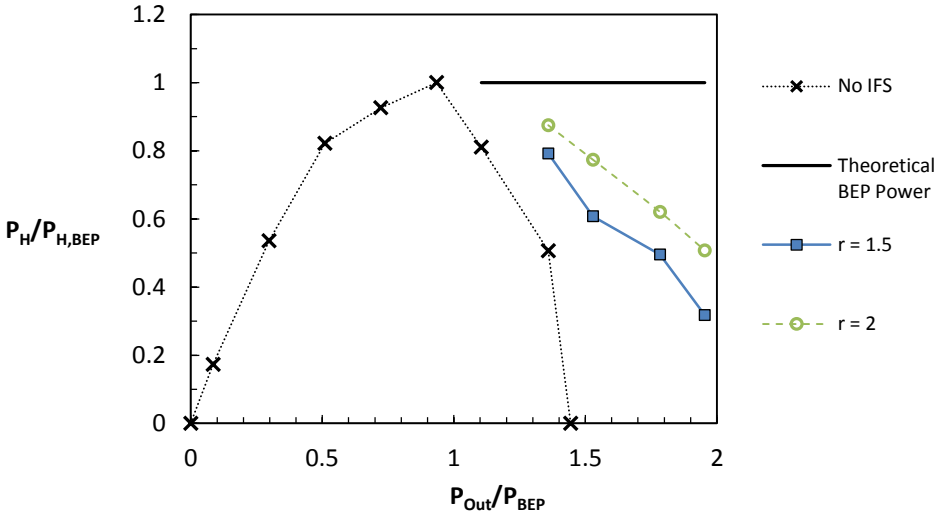

Fig. 8-21 – Hydraulic power output traces at 11V

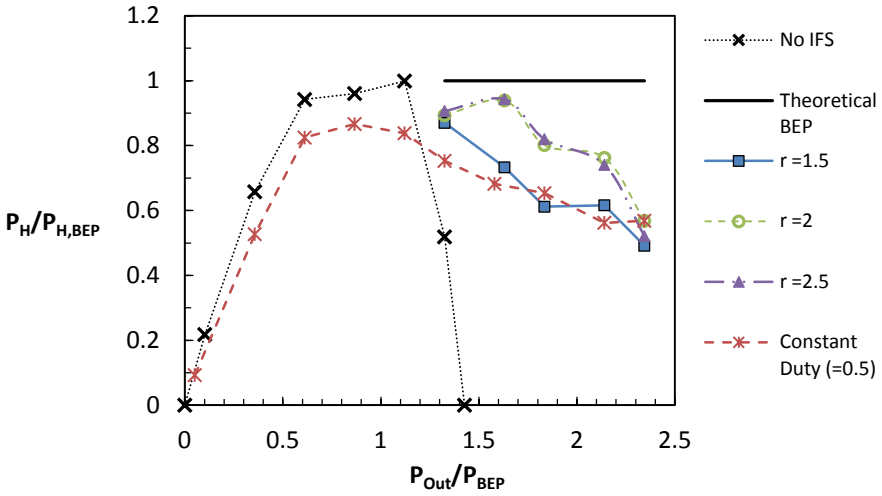

Fig. 8-22 – Hydraulic power output traces at 10V

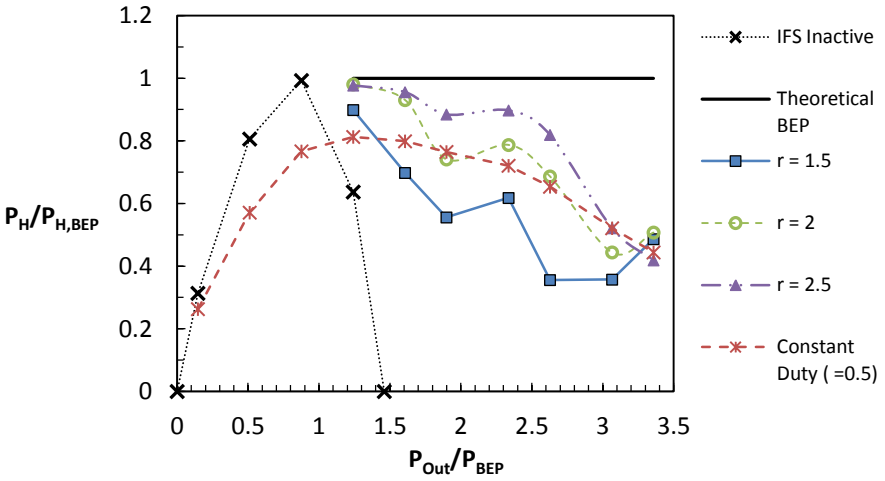

Fig. 8-23 – Hydraulic power output traces at 8V

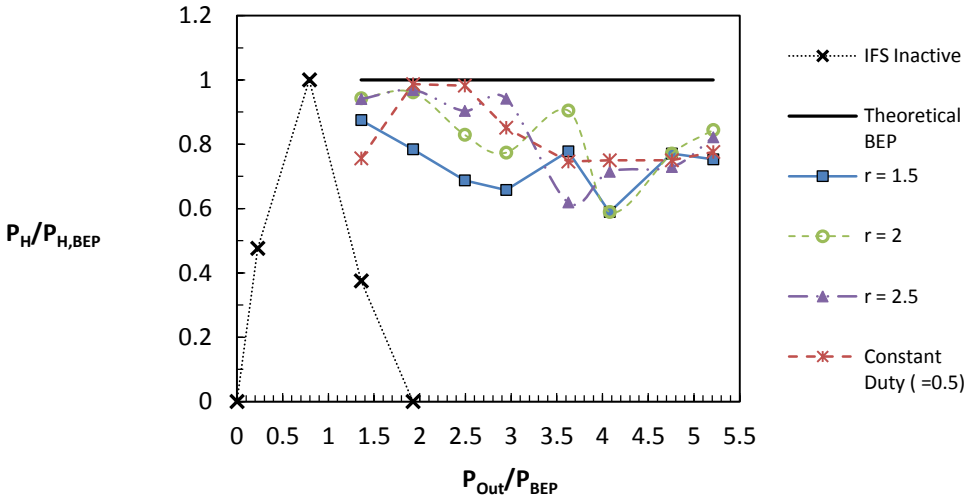

Fig. 8-24 – Hydraulic power output traces at 6V

8.6.5 Pumping System Efficiency

Plotting the relationship between pumping head and operating power (from the product of pump current draw and operating voltage, $P_E = I.V$) it is obsereved that there is a greater energy draw by the pump while the IFS is active. This is illustrated in **Figures 8-25** and **26,** using the pump current draw data obtained at 8V and 10V testing voltages.

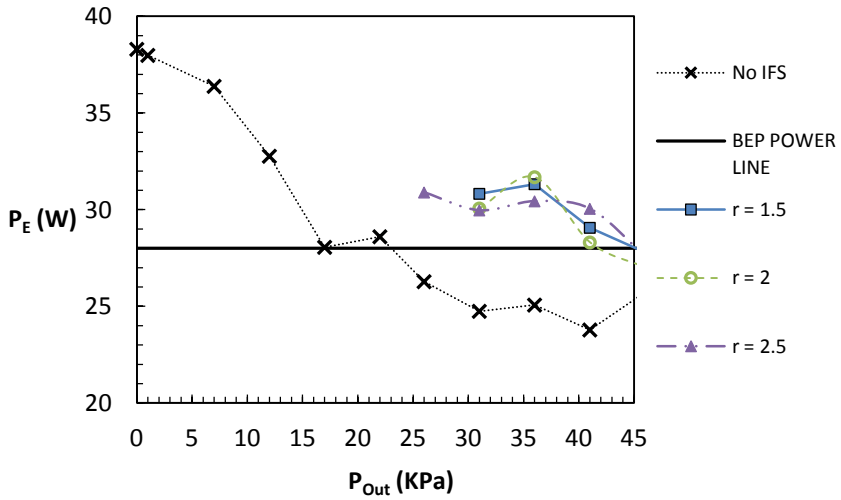

Fig. 8-25 – Centrifugal pump power traces, 10V operation

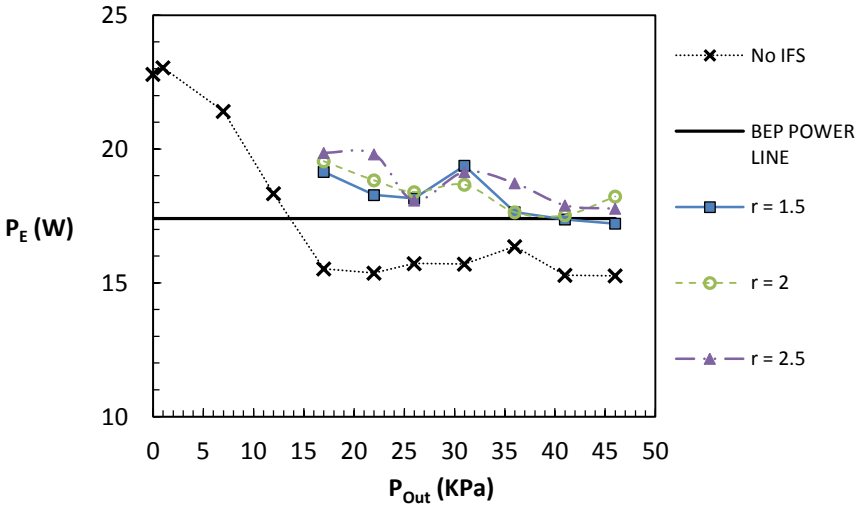

Fig. 8-26 – Centrifugal pump power traces, 8V operation

After the pump reaches its maximum potential head, the hydraulic power of the system without IFS reaches zero (indicated by the characteristic curves on **Figures 8-20** to **24)**. Past this point, the efficiency of the pumping system can be assumed to be zero as pumping efficiency is defined as the ratio of hydraulic power output and electrical power input to the system, $\eta = P_H/P_E$ (where efficiency η, is relative to the systems BEP and a value of $\eta = 1$ is the nominally maximum value achievable). **Figures 8-27** and **28** demonstrate this improved efficiency. As discussed previously regarding the discharge flow data obtained experimentally, the theoretical BEP flow was not achievable using the current test rig. This has obviously led to a lower than optimum boost in efficiency. Despite this, the experimental data identifies a marked improvement in efficiency over the pumping system without an IFS.

While similar to the increased pumping capabilities of reciprocating pumps using an IFS, the results from centrifugal pumps differ by means of efficiency. As has been previously shown by Burton and Short [8] reciprocating pumps, while providing good matching to renewable energy sources through increased output flow and greater energy usage, prove to be less efficient with the IFS. It has been shown that the opposite is the case for the centrifugal pumping system analysed here. There is instead an increase in 'wire-to-water' efficiency. It is seen that, for heads above BEP conditions, the IFS pumping system makes greater use of the energy available to the pump while also providing increased hydraulic power. This further reinforces the themes discussed in **Chapter 2**, such as the potential of such subsystems for use with off-grid (and in particular direct power renewable) power sources.

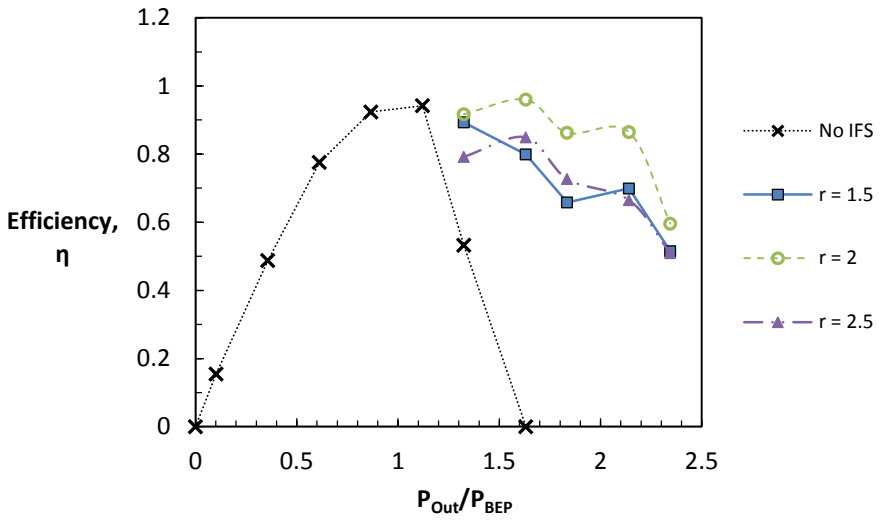

Fig. 8-27 – IFS 'wire-to-water' efficiency, 10V operation

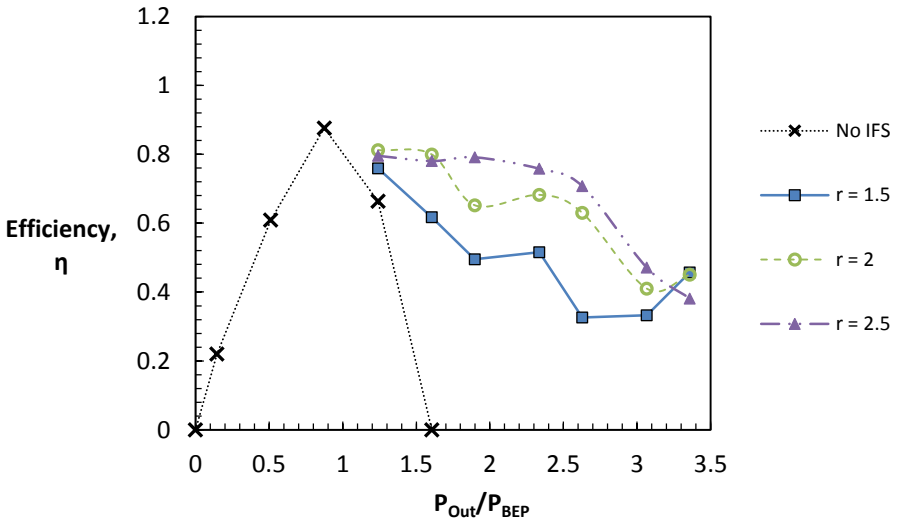

Fig. 8-28 – IFS 'wire-to-water' efficiency, 8V operation

8.6.6 Instantaneous Flow Data

The instantaneous flow traces through the inductance pipe hold great interest as to the effect of the ECV and overall IFS on the operation of the pump. Three key observations are:

1. The comparison between theoretical and recorded flows.
2. The matching of pump flow to BEP flow through use of IFS.
3. The effect of altering ECV operating frequency on flow stability.

The operation of the ECV was observed to produce oscillations in the inductance pipe at the specific operating frequency for each given test scenario. This holds true for all test data, a full selection of which may be found in **Appendix C** and an example of which is illustrated in the $r = 2$ tests at 11V shown in **Figures 8-29** to **31**. The piezo electric position sensor readouts for each test case indicate a repeat cycling time period of 0.3s, which is in line with the required operating frequency for $r = 2$ at a system natural frequency of $10.475\,rad/s$. Furthermore, the flow traces clearly indicate a strong correlation between the fluctuations in flow and action of the valve, as predicted in the theory. This demonstrates the correct interaction between the ECV and inductance flow, whereby an increase in flow is seen during the ECV ON periods and subsequent fall during OFF periods. It is also important to note that the evolution in flow through the inductance pipe is observed to resist the change in flow in the same way as predicted by the electrical analysis in **Chapter 7**. This is to say that the flow trend is non-linear.

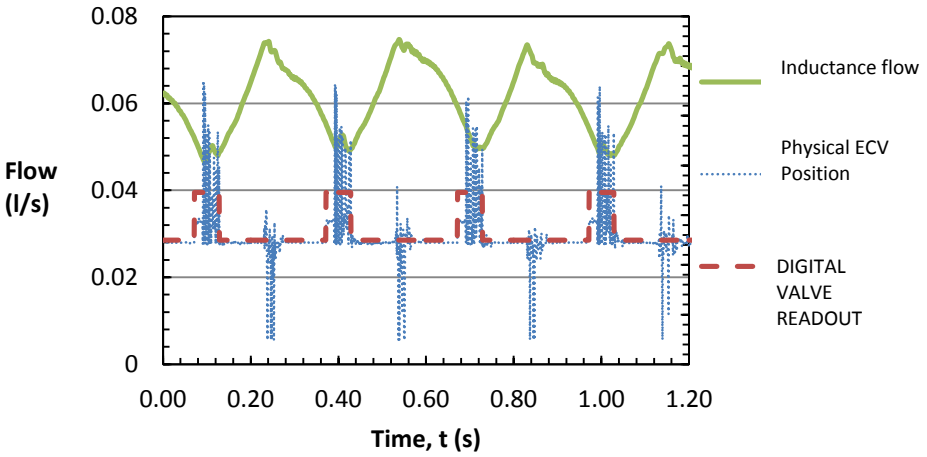

Fig. 8-29 - 11V, r = 2, 5m assembly height

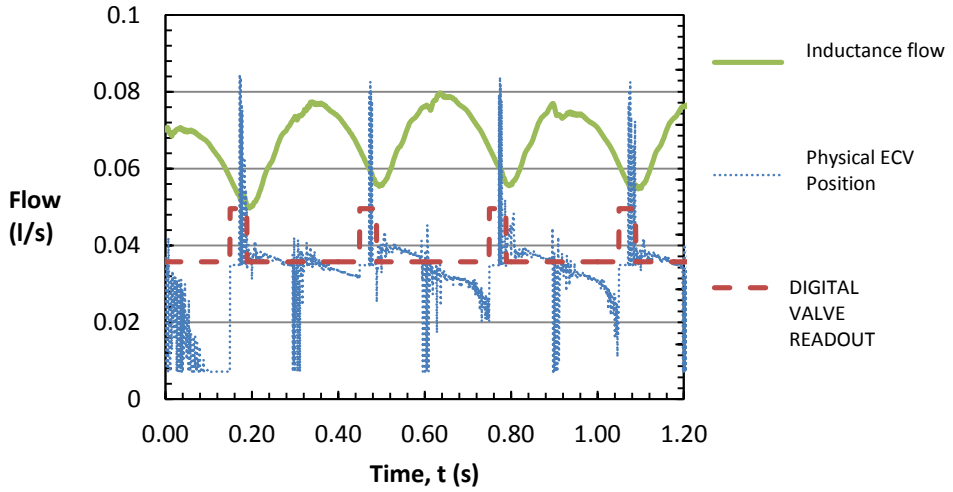

Fig. 8-30 - 11V, r = 2, 4.5m assembly height

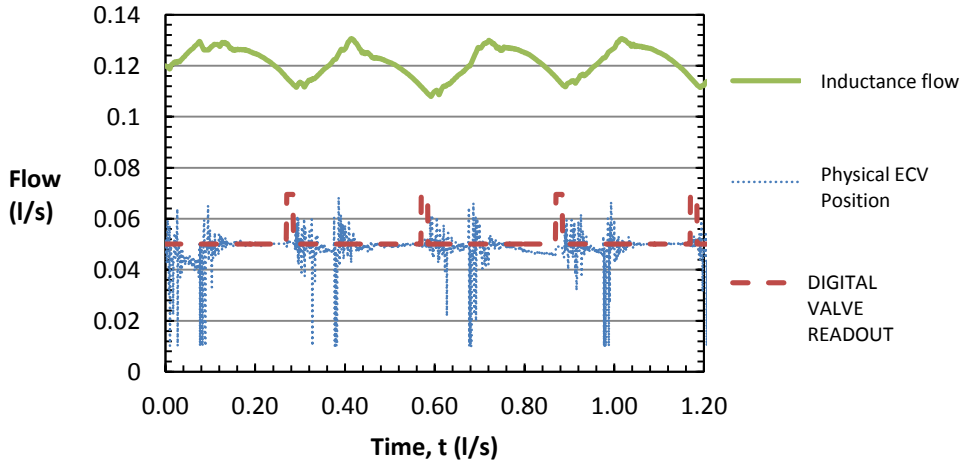

Fig. 8-31 - 11V, r = 2, 3.5m assembly height

A comparison between **Figures 8-29** to **31** shows a reduction in the amplitude of flow ripple with decreasing head. Again, this is in accordance with the predictions made during the numerical and electrical analyses that for BEP to be sustained at an ever decreasing ECV OFF time period, the amplitude of the ripple would increase to compensate for a given frequency ratio. **Figures 8-32** to **34** further reinforce this idea by demonstrating the same ripple characteristics for the 11V tests at $r = 1.5$.

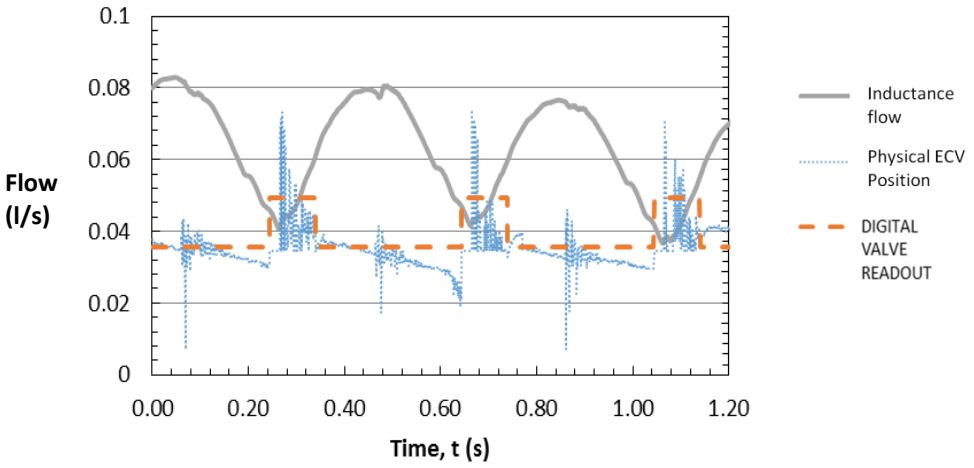

Fig. 8-32 - 11V, r = 1.5, 5m assembly height

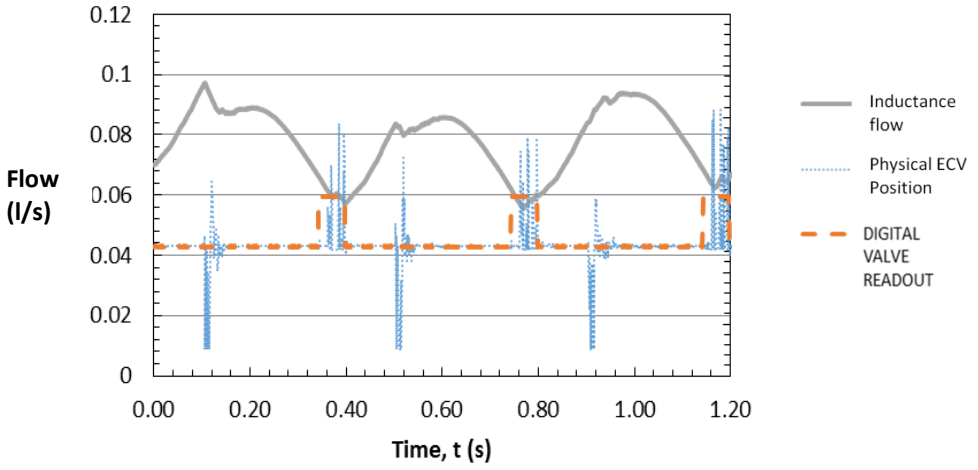

Fig. 8-33 - 11V, r = 1.5, 4m assembly height

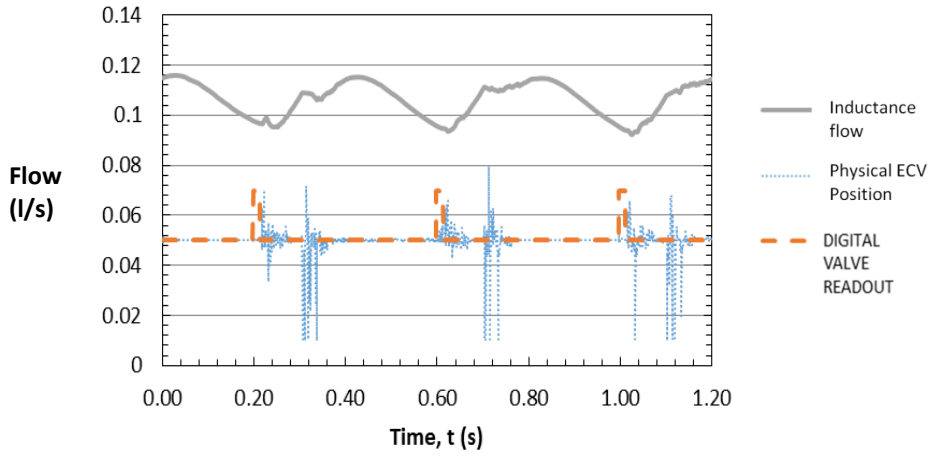

Fig. 8-34 - 11V, r = 1.5, 3.5m assembly

In these tests, it is observed that as the frequency ratio is decreased, the flow stability decreases also. This trend is more apparent in the study of the completed set of flow traces presented in **Appendix C**.

Most importantly, presented by the flow traces and ECV timings, is the centrifugal pumps consistent performance at average flow closer to the pumps BEP. These average flows through the inductance pipe are discussed further in **Section 8.6.8**.

8.6.7 Experimental and Theoretical Comparison

Comparison of experimental and numerical inductance flow reveals that although there is a similar trend in amplitude across varying heads, the experimental ripple is far lower. **Figure 8-35** shows not only a greater fluctuation in inductance flow across a time period but also a greater average flow rate, providing a match to the pumps BEP. In fact, upon analyzing the data from numerous other tests it was found that the BEP matching of the experimental rig was not ideal and in all cases the ripple amplitude was far lower than predicted numerically, even during tests close to BEP where the inductance flow was a close match to Q_{L1}. See **Figure 8-36**.

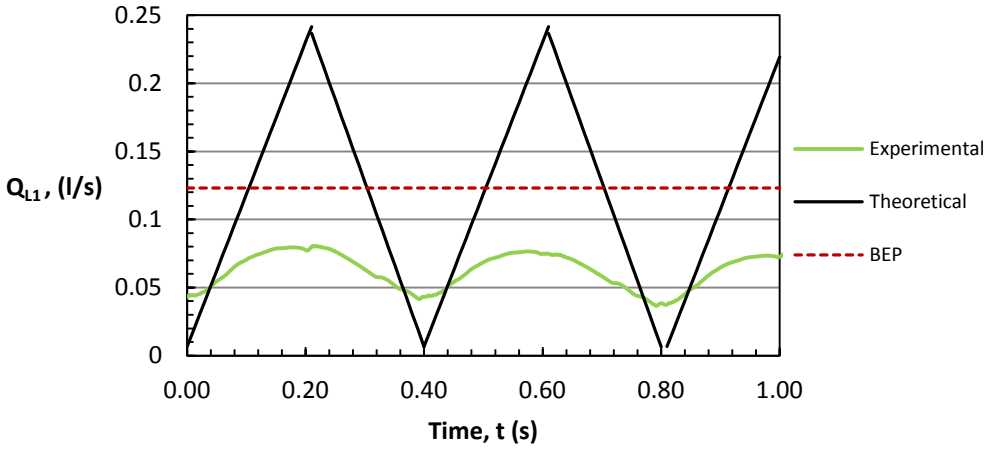

Fig. 8-35 – Flow comparison for 11V, r = 1.5, 5m assembly height

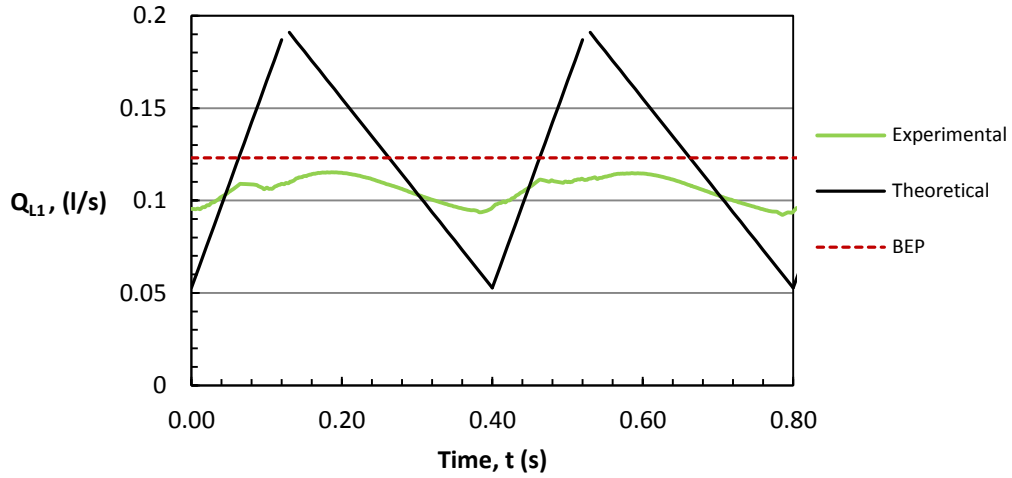

Fig. 8-36 – Flow comparison for 11V, r = 1.5, 3.5m assembly height

It would seem unlikely that the operation and control of the ECV would cause this difference as the flow trends have shown a consistently good match with the time period for each test case. The fault is most likely to lie in the idealised definition of the inductance flow in the characteristic equations. These would need to be refined in order to more closely represent the change in flow through the inductance pipe so as the correct frequency ratio for ECV operation could be selected for practical

application. Irrespective of this difference, the instantaneous flow traces provide two very important pieces of information:

1. The flow through the inductance pipe is smooth in transition lending to the theory that the IFS is acting in a continuous mode (analogous to the continuous mode boost converter which the system duty is based upon in **Chapter 5**). Further, the trace characteristics agree with those from the numerical and electrical analyses. This strengthens the idea that the system may be analysed using the duty definition borrowed from electrical boost converter theory.
2. Although the experimental results do not perfectly fit the BEP matching presented numerically, the overall lower amplitude in ripple could actually be viewed as a positive finding. Lower fluctuations in inductance flow mean less stress on the centrifugal pump and a closer matching to the average power line (However, further investigation would be needed to confirm or refute the idea that the average inductance flow, and indeed discharge flow, could be improved solely through modification of the test rig).

8.6.8 Average Inductance Flow

With regards to lower than theoretical inductance pipe flow rates, the issue is most likely in the speed of ECV operation. After determining the average Q_{L1} flows across all test cases, it was possible to produce **Figures 8-37** to **8-41**. These figures display and compare the performance of the pump both with and without IFS much in the same way the comparison was presented for discharge flow. As with the discharge flow and BEP hydraulic power output matching, the test rig was able to deliver flows at a far closer match to the pumps BEP than without IFS. Furthermore, it was seen that

the closer BEP matching was produced at not only higher frequency ratios but during tests at lower voltages. Considering the voltages, one reason for the increased matching to the numerical predictions could be due to reduced losses in the system at lower flow rates (i.e. lower pump Q_{BEP}), although this would require a detailed individual component analysis (discussed in the future work section of the concluding chapter).

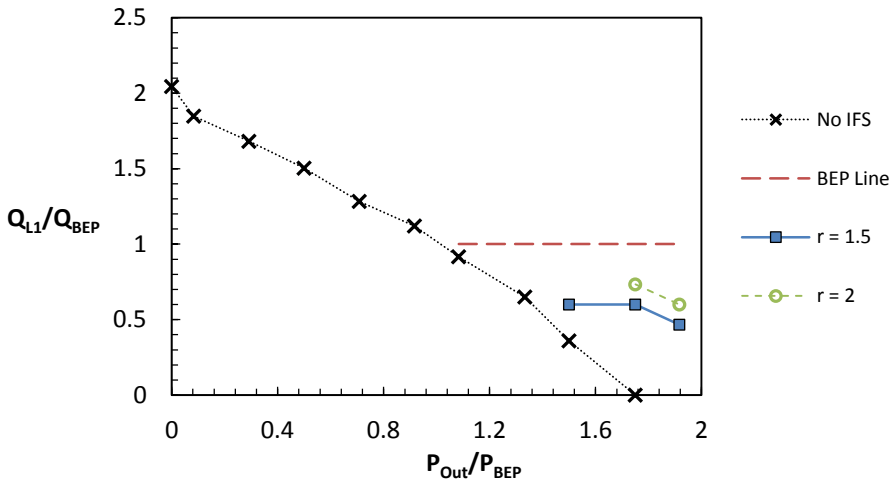

Fig. 8-37 – Average inductance flow comparison for 12V

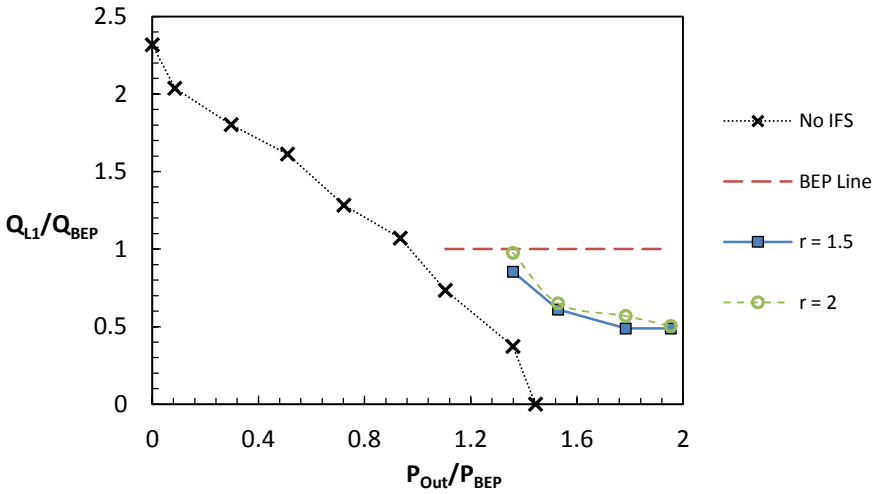

Fig. 8-38 – Average inductance flow comparison for 11V

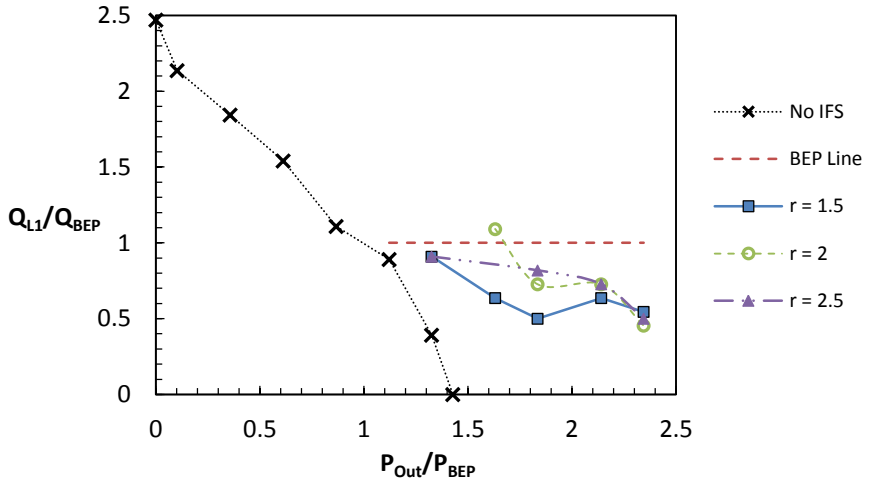

Fig. 8-39 – Average inductance flow comparison for 10V

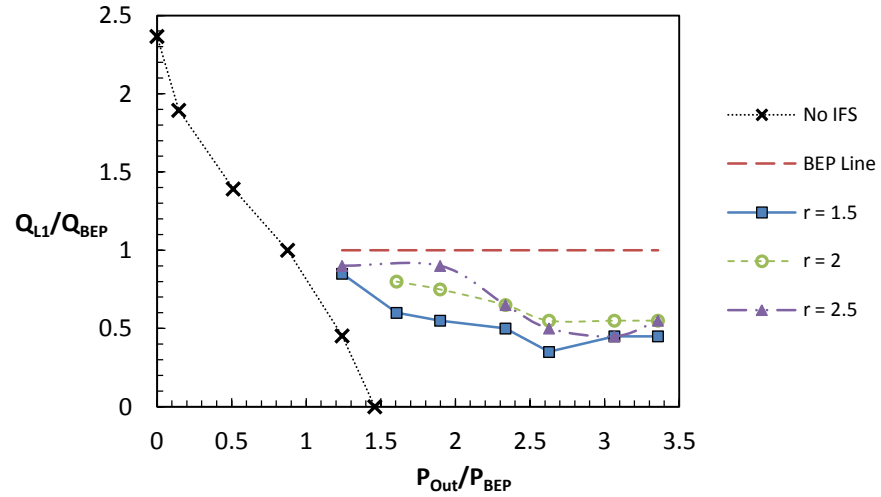

Fig. 8-40 – Average inductance flow comparison for 8V

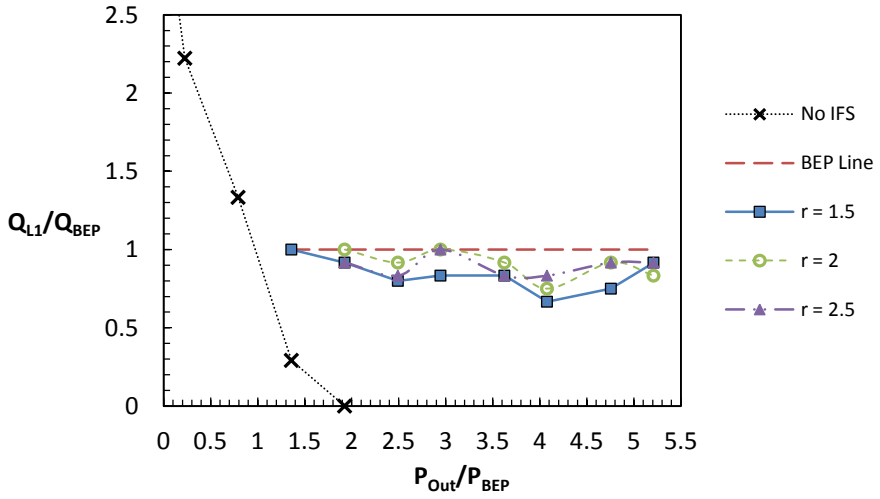

Fig. 8-41 – Average inductance flow comparison for 6V

Recall the comparison in inductance flow stability with varying frequency ratio, from **Chapters 6** and **7**, the numerical and electrical analysis. Inspection of **Figures 8-29** and **8-32** reveal the same increase in flow stability with frequency ratio observed in the theoretical tests. This trend can further be observed for the majority of the flow traces presented in **Appendix C.** These results again suggest that for a pumping system operating a sufficiently high speed, the numerical model could provide a simple means of predicting performance.

8.6.9 Performance Test Summary

As a summary of the findings from experimental analysis of the pumping system test rig with IFS:

- The addition of a tuned hydraulic system to a standard centrifugal pump has been shown to produce increased discharge flow rates than an equivalent system without. This is especially true at pumping heads above that of a pumps maximum rated head, where the tuned system is able to deliver flow where the standard pump cannot.
- The transient characteristics, produced experimentally, agree well with the theory and both numerical and electrical simulations using the characteristic equations defined in **Chapter 5**, particularly the improvement in flow stability on increasing the frequency ratio of the ECV. The only notable difference was in the amplitude of flow ripple, which was more exaggerated in the numerical study.
- Discharge and hydraulic power outputs from the tuned hydraulic system with IFS show a good match to theory in the majority of cases with a strong

argument for a system based on higher operating frequencies being optimum. This is again most likely due to the increased flow stability, creating a stronger match with the theoretical results.

- The addition of the IFS modifies the standard pumping power requirement of a pump allowing it make greater use of available energy. Overall output efficiency is improved above BEP of the pump.
- The IFS enables the centrifugal pump to operate far closer to its MPP, irrespective of operating conditions, effectively decoupling its operation from the discharge section of the pumping system. This is a characteristic which is true of all tested frequency ratios or heads.

8.7 Conclusions

The series of tests performed on a modified system, which include novel induced flow components controlled through the use of a timed ECV, have produced several interesting findings. The addition of IFS to a standard centrifugal pump for the purpose of sustainable, off-grid water pumping systems has been shown to maximize the use of available energy by enabling the pump to maintain a close to maximum hydraulic power point based on BEP. This is in-line with the theory presented in **Chapters 4** and **5** and suggests that the presence of this subsystem results in no upper limit on the head to which the pump can deliver a hydraulic output. Further, it suggests an improved output flow at conditions beyond those expected of the pump, increasing its effective operating range and reliability. Also displayed, is the IFS's potential to negate some of the issues presented in **Chapter 2** regarding fluctuation of pump operating conditions and losses due to improper installation.

The increase in direct power efficiency, which was observed above BEP operation, allowed the test pump to utilize more energy available to it than without IFS. This is a characteristic which would allow centrifugal pumps, particularly those utilizing renewable energy sources, to benefit. It additionally demonstrates that such a system may lend itself to an auto-setup capability, reducing costs and widening accessibility to sustainable, off-grid pumping: in essence a one-size-fits-all-pump.

Chapter 9

Conclusions and Outlook

The research presented by this thesis had discussed the effect of introducing a novel, induced flow subsystem to a centrifugal pump which is based on DC-DC boost converter theory from power electronics and other induced flow systems. This concluding chapter summarises the key findings of each stage of the project, highlighting their relevance in relation to the original hypothesis and broader theme of the research. As part of this summary, a series of general conclusions about the operation and applications of the tuned centrifugal pumping system will be discussed. Furthermore, suggestions for future research in this area are made, along with possible improvements and issues.

9.1 General Summary

Chapter 1 introduced the need for a one-size-fits-all pumping system as a means of addressing some of the issues surrounding water supply/demand in rural areas. The aim of the project, along with all relevant objectives, was discussed in addition to the definition of the research hypothesis:

''*The use of an IFS can ensure that a centrifugal pump is itself operating at its MPP (BEP), thereby decoupling its operation from the conditions around it.*''

Chapter 2 presented a broad literature review, providing a background to many of the key issues surrounding the justification of research, including: the requirement for clean water in rural areas and developing communities, dangers of poor water supply and current potential barriers in place which prevent the availability of pumping technology for rural areas. From a more technical aspect the literature also discussed the various pump and motor types, along with rural power sources and the benefits/drawbacks of each. The general conclusions drawn from this chapter were the need for a pumping system which is able to deliver a sufficient and reliable water supply across a wide range of conditions, while reducing implementation costs and eliminating some of the issues associated with electronic control systems or batteries (such as reliability, sustainability and increase in unit cost). Ideally, the system would also make use of, and be well suited to work in symbioses with, renewable energy systems such as wind, solar or a hybrid of both.

Chapter 3 briefly introduced the electric-hydraulic analogy and the DC-DC boost converter circuit. Throughout this chapter, comparisons were made between the subsystem components of the boost-converter and both hydraulic ram and reciprocating pump subsystems (both of which make use of the induced flow principle). It was discussed that the use of a boost-converter style hydraulic circuit, incorporating a centrifugal pump, would provide a means of controlling the operation point of the pump through a tuned hydraulic valve (similar to a controllable version of the waste valve from the hydraulic ram).

The principles introduced in **Chapter 3** allowed for the development and design of a simple hydraulic boost-converter system in **Chapter 4**. This system would, instead of boosting output voltage, boost the operating pressure of the pumping system whilst simultaneously providing a means to stabilise the average flow from the pump itself. The operation and definitions of the various components were discussed and analysed, providing the building blocks for the development of the later model in **Chapter 5,** which describes flow through the system. Of particular relevance was the discussion of operation and principles behind the ECV. This included the identification of equations defining the duty and timing of the valve to enable continuous MPP operation of the pump.

Using the basic system design from **Chapter 4**, **Chapter 5** worked to describe fluid flow at the system oulet using a lumped parameter method to define a set of two linear, second order differential equations. The full expansion of these equations was subsequently solved in **Appendix B**. It was shown that, by neglecting friction and using idealized versions of the subsystem components, a simple equation could be used for each period of operation of the valve to define discharge flow. These two equations made up the flow definition for a single time period, enabling the creation of a model to predict the theoretical ideal operation of the pumping system. It was further shown, through various manipulations, that the flow through the hydraulic inductance (and therefore the centrifugal pump) would remain at a constant BEP on activation of the ECV.

Taking the equations of flow defined in **Chapter 5**, **Chapter 6** presented an analysis of the pumping system using a simple numerical spreadsheet. The theoretical

results suggested the development of oscillations in flow through the pumping system (due to the ECV) and provided average flow predictions for a pump operating above its BEP and even maximum rated head. Flow stability through the inductance pipe was shown to improve at shorter time periods of operation (due to increasing the frequency ratio) suggesting that the systems performance could be optimized through faster ECV response and operating time. Of particular importance from these results was the behavior of inductance flow upon modification of both system output pressure and discharge inductance. It was established that, irrespective of pressure load to the system, the average centrifugal pump discharge (through the inductance pipe) remained constant and followed its MPP value. Furthermore, upon modification of the discharge pipe length (and hence output inductance), there was seen to be no change in the flow through the inductance pipe. This established that the combined action of the ECV and OWV was enough to completely decouple the pump from its operating conditions whilst enabling pump BEP operation: A very important finding in relation to the hypothesis set in **Chapter 1**. An additional series of simple computational tests using commercially available fluid analysis software reinforced the systems ability to deliver discharge flows above those expected under 'normal' operating conditions and even extend the operating range of the pump.

In **Chapter 7** the electric-hydraulic analogy was further discussed and an electrical equivalent of the IFS centrifugal pumping system was developed using commercially available software. Simulations using this software demonstrated system characteristics that were consistent with those produced in **Chapter 6**. Most importantly, the relationship between the circuit 'flow' source and system load was shown to be decoupled, allowing the current source to perform near to its BEP. From

the oscillations set up in the inductor and at the system output, along with average flow data, the assumptions made in the theoretical model were, to a large extent, validated. Although the results obtained from the electrical tests did not match the theoretical ones completely, at least not until higher frequencies of operation, the reasons for this were discussed. Furthermore, the simulations provide an interesting insight into the potential for using electrical software as a simple means of predicting hydraulic system behavior.

Finally, **Chapter 8** covered the design and construction of a full hydraulic IFS pumping system at the UoL. The reasoning behind certain component parameter and design choices was discussed and a detailed explanation of the test procedures and data collection techniques was provided. From the test results, it was possible to draw a strong correlation between the flow characteristics given by the experimental rig and those found in **Chapters 6** and **7**. When comparing the hydraulic power output, it was found to provide better matching to the pumps MPP than without the IFS components and provided a discharge flow well above the supposed operating limits of the pump. This was in agreement with the theory provided in **Chapter 4**. Most importantly, the experimental results show the development of oscillations in flow through the inductance pipe due to the operation of the ECV and that the oscillations may be altered directly by changing the duty and time period of the valve. The actions of the ECV were observed to allow the pump to operate much closer to its BEP across the entire range of heads tested. Various reasons, including the operational frequency limits of the mechanical valve and subsequent modifications of subsystems to compensate have been suggested as part of the reason for not completely realising the theoretical results from **Chapter 6**. Further, the idealized nature of the theoretical

predictions could not provide an entirely accurate model for the performance of a 'real' pumping system, an issue discussed in more detail later in this chapter. Despite this, the trend of increasing the operating frequency of the ECV was shown to improve the correlation to theoretical results and improved the stability of the transient results.

Overall, the results of the numerical, electrical and experimental testing showed system characteristics and traits which were consistent, if not entirely matched, across all cases. Furthermore, these results all identify the ability of the IFS centrifugal pumping system to operate at its MPP independent of operating load.

9.2 Project Aim and Objectives

Addressing the project aim laid out in **Chapter 1** which states, (referring to the centrifugal pump):

''*……to assess the feasibility of using a tuned hydraulic subsystem…… as a means of optimizing power utilization and discharge performance over a greater range of operating conditions……*''

The various numerical, electrical and experimental tests have indeed demonstrated an induced flow system to operate far closer to a pumps MPP across all operating heads above BEP conditions. Further to this, improvements in discharge flow have been observed experimentally at heads beyond the pumps BEP. This would suggest that the project aim has been fulfilled by concluding that the use of such a system is indeed feasible.

Regarding the project objectives set in the introduction, they have been addressed as follows:

- *''Develop an analytical theory, considering in detail the validity of the assumptions made in the project proposal.''* – The theory from a DC-DC boost-converter was taken and translated into a hydraulic theory to define an equivalent system based around the use of a centrifugal pump. As a result, the equations defining flow through various components and eventually the system outlet were defined using a simple linear analysis technique.
- *''Use the analytical theory to produce a numerical study into the pumping systems operation under varying hydraulic conditions.''* – The Equations were used to create a simple numerical spreadsheet. This spreadsheet was then used to simulate a range of operating conditions based on a pump which would later be used in the experimental analysis of the hydraulic circuit.
- *''Compare any analytical theory to existing electrical theory on the use of boost-converters in order to validate the electric-hydraulic analogy for this research.''* – The electrical analysis software, MicroCap™ was used to develop an equivalent electrical circuit to the one defined by the equations used in the numerical analysis. The results from the subsequent electrical analysis were found to be in good agreement with the numerical analysis and demonstrated the validity of the electric-hydraulic analogy.
- *''Design and manufacture a centrifugal pump test bed as a means of assessing the accuracy of the computational model and hence analytical theory.''* – A test rig based on the hydraulic system design used in the numerical analysis was constructed.
- *''Use the centrifugal pump test bed with the addition of the tuned hydraulic system to obtain performance data for the modified system.''* - A range of tests,

assessing the test rigs performance under varying heads, frequencies and duties were performed. Furthermore, the transient response of the system to the action of the induced flow subsystems and ECV was collected and analysed.

- *''Compare all set of data from analytical to experimental as a means of providing evidence of any performance improvements with the tuned hydraulic system.''* – The data from the electrical tests was used to validate the theory used in the numerical analysis. This data was then used as the basis of comparison for the experimental results. Both sets show similar trends and improvements in MPP tracking across a range of heads.

9.3 General Conclusions

9.3.1 Pump BEP Operation

From the idealized theoretical system predictions, it has been demonstrated that the performance of a centrifugal pump may be decoupled from its operating conditions through the use of a timed ECV and IFS. These theoretical predictions have been reasonably validated through both electrical and experimental findings, all of which show the system to be operating as a boost-converter in continuous mode. The implications of these, in relation to the original hypothesis and literature review, are that such pumping systems would certainly be capable of self-regulation and auto set-up (in essence a one-size-fits-all system). Additionally, such a system would be able to make optimum use of any energy available to it, particularly in the case of renewable energy systems where there is a continuous supply of 'free' energy. This would enable the system to forgo the use of complex energy storage systems or MPP trackers in favour of a more simple water reservoir storage method. Within the context of

pumping in rural areas this of great benefit as means of making centrifugal automated pumping technology more widely available and accessible.

9.3.2 IFS Pump Output

As suggested by the theoretical equations and the way in which the system was defined in **Chapter 4,** the IFS centrifugal pumping system has been shown to produce discharge flows above those expected within the pumps standard operating range. Additionally, the discharge flow results have shown that a centrifugal pumping system, making use of an IFS circuit, is capable of delivering discharge flow even outside the operating range of the pump on its own. These results suggest that implementing such a system could potentially increase the net water delivery capabilities above current centrifugal pumping systems without an IFS. Furthermore, it would allow a pump to operate under fluctuating environmental conditions or negate poor installation. As mentioned previously regarding the pump BEP operation, self-regulation of MPP would ensure the maximum utilisation of available power from any rural energy source (most notably renewable). These results holds great importance within the context of water provision in developing communities, where the availability of water through potentially fluctuating conditions is more important than the storage of energy through battery sources.

9.3.3 ECV Operation

The duty equation used to define the operation of the ECV in all analyses was shown to operate correctly in continuous mode, as suggested in **Chapter 4**. Although the timing and speed of valve operation proved to be one of the more difficult tasks in this project, the experimental results and transient data show a strong consistency in

operational characteristics across all forms of analysis. It is of particular note that as long as the inductance and capacitance characteristics of the IFS's are defined to allow maximum inductance (given space constrains) and therefore lowest natural frequency possible, the ECV frequency ratio has a substantial impact on the systems stability and performance. By increasing the frequency ratio, it can be ensured that the pump does not fluctuate outside of reasonable ripple limitations, so as not to incur undue wear or damage to the centrifugal pump. Furthermore, the higher the achievable frequency of operation, the better the matching to the theoretical results and MPP of the pump can be.

9.3.4 Power Utilisation

In **Chapter 2** it was noted that, if a pumping system were to run solely on a renewable energy source and that said source was abundant in nature, it would make sense to attempt to utilise as much as possible within a given timeframe. It was further identified that by far the most simple and reliable means of storing energy was not to employ a battery system, but rather ensure a water supply through a sufficiently sized reservoir. It has been identified that an IFS centrifugal pumping system is able to deliver enhanced levels of discharge flow at the pumps continual MPP. Within the context of a rural water supply, it can therefore be suggested that such a system would provide an innovative means of trading energy for water more effectively. This is to say that an IFS centrifugal pump would not only be capable of greater power utilisation, but that the additional power consumption would yield a greater water return than an equivalently sized pump.

9.3.5 Potential Applications

It is possible to suggest that a pump which is capable not only of maintaining its MPP, but also of self-regulating could be considered a one-size-fits-all pump. This is especially true given the discharge flow performance of the IFS pump, revealing the pumps operating range to be expanded with no theoretical limit on head. Assuming then that the novel subsystem studied in this thesis is feasible, it provides genuine progress for the future and a key step towards a universal pumping system for rural water supply (for the system to be truly self-reliant, however, there would need to be further development into a reliable control system for the ECV).

A ''one-size–fits-all'' pumping system would hold many benefits for water pumping in rural areas. Firstly, the use of a centrifugal pump as a means of water delivery would ultimately prove to be a cheap and efficient solution, holding benefits over the use of other pump types, as discussed in **Chapter 2**. The main benefit would be the delivery capability of high quantities of water at low to medium heads, expanded by the use of the IFS. Installation costs of such units would also be reduced, as a single pump could be specified for a much larger range of operating conditions. This could hopefully improve the availability and reliability of automated water pumps.

Aside from standard pumping applications in rural areas, such as domestic or agricultural water supplies, this thesis also holds relevance for centrifugal pumping technology in a broader sense. Nearly any pumping application or system which is subject to fluctuations in operating conditions could benefit from the physical MPP (BEP) tracking of the IFS. This would be especially true if such a system were easily retro-fitted to existing centrifugal pumping systems. There also exists the potential for

improved power generation/ energy storage. As the additional IFS components allow for a greater level of energy to be harnessed as improved discharge flow, greater amounts of wind or solar energy could be utilised at peak production hours. This energy could then be stored as potential energy for use with a hydro-electric system to subsidise periods of higher energy demand.

9.4 Future Work/Considerations

The results of the experimental work, and comparison to theoretical and electrical systems, demonstrate that there is still some great way to go before a practical version of the system can be designed. Several key issues with the operation and construction of the experimental rig have been identified in **Chapter 8**, which hopefully can be investigated further in future work.

Firstly, although the numerical and electrical results demonstrated the decoupling of the centrifugal pump operation from output load through modification of the 'horizontal' output inductance, this was not possible in the experimental tests. The experimental results have demonstrated that the pump is able to operate independently of increase in output head through modification of the vertical discharge pipe sections. It would be beneficial, for comparison with theoretical results, to replicate the modification to output inductance, independent of operating head, in order to determine if the flow through the inductance pipe is truly decoupled from the output inductance. This could involve re-designing the existing style of test rig (described in **Chapter 8**) or through the creation of a system specifically aimed at testing this single characteristic.

The operation of the ECV has been mentioned as one of the more difficult aspects of the test rig design. This was due to the high frequencies expected from its operation. In fact, the majority of the test rig specifications, including inductance length, were determined solely on the limits presented by the ECV. Should the IFS ever be considered for practical use, one of the first areas of design improvement would be this valve. This also stands true for any additional future tests wishing to expand the known characteristic range of the pumping system or to improve the operation of the system in general. The reasoning here is that it has been shown across all system analyses that increasing the frequency ratio, of the ECV and system, not only improves the stability of flow through the centrifugal pump, but also enables a closer match to 'ideal' operation of the system. Furthermore, through improving the operating frequency range of the valve, the limitations on the inductance and capacitance parameters of the system would be relieved, enabling the IFS circuit to be reduced in size. This is of exceptional importance should this form of system ever wish to progress to practical application. **Chapter 8** additionally identified the ECV's capability to deliver improved MPP matching and hydraulic power output whilst using a more manageable constant duty. A further line of research would be to test the extent to which the IFS can still provide an improved performance whilst minimizing the demand of the ECV.

Having previously discussed future investigations into reducing the size of the IFS, another interesting avenue of research includes the potential of the complete system to be retro-fitted onto existing centrifugal pumps. This would be heavily reliant on research into the miniaturisation of the inductance pipe and increased frequency range of the ECV. Retro-fitting could offer a cost effective way of improving the stability of operation to many centrifugal pumping systems in addition to providing greater

power utilisation. Such a system could be designed to work with existing centrifugal borehole pumps as a means of improving rural pumping technology without the need to 're-invest' in newer centrifugal pumps or entirely new systems. Future study into this area would assess whether it was possible to provide a universal IFS extension to existing systems, or if it would be more practical to retro-fit on a bespoke basis, based on the size and performance range adjustable with the IFS.

Finally, one area which has not been addressed fully in this thesis is the energy trade required for the use of an IFS circuit. It was discussed in **Chapter 8** that the pumping efficiency did indeed improve based on the power requirements of the pump and discharge flow, but further research would be required into the power consumption of the entire system in operation. This would also include individual and detailed component testing, to model the specific losses and increases in power consumption from their addition to a pumping system. Further, by modelling the individual effect of each IFS component it could be possible to re-develop and improve the current linear model of flow presented in **Chapter 5**, so as to provide a more accurate estimate of performance. Such a model would also be useful in the optimisation of an IFS unit for practical use, by allowing the quick modification and trialing of designs before a complex experimental rig was designed and constructed.

9.5 Concluding remarks

This thesis has presented the theory and design of a pumping system based upon the use of a centrifugal pump, which is able to operate at its MPP irrespective of variation in operating conditions. The resulting hydraulic circuit utilises a subsystem analogous to a DC-DC boost-converter from power electronics and similar to the

hydraulic ram and reciprocating induced flow pumps. The theory presented offers the potential for this pumping system to be developed as a one-size-fits-all pump for use in rural areas, lessening some of the disadvantages of current pumping systems such as cost, maintainability and accessibility. In conclusion, the system has been tested and found to have feasibility within the context of rural water pumping technology and will hopefully go some way to granting more people access to automated pumping technology and, ultimately: clean water.

References

1. Short T. D & Oldach R, *Solar powered water pumps - The past, the present and the future?* Journal of Solar Energy Engineering, 2003. **125**(1): p. 76-82.
2. Barlow R, McNelis B & Derrick A, *Solar pumping: an introduction and update on the technology, performance, costs and economics.* World Bank Technical Paper, intrmdt. tech. pub. ltd., 1993. **168**.
3. Derrick A, *20 years of PV water pumping - successes and problems.* International workshop on PV water supply issues, Marrakech, 1998.
4. Kaunmuang P *et al*, *Assessment of photovoltaic pumping systems in Thailand - one decade experience.* Solar energy materials and solar cells, 2001. **67**(1-4): p. 529-532.
5. IT Power Ltd., *Concerted Action On the Testing and Cost Reduction of PV Water Pumping Systems: Final Report.* IT Power Ltd., Chineham, Hants, UK, ITP/95501, 1997.
6. Short T. D & Burton J. D, *The benefits of induced flow solar powered water pumps.* Solar Energy, 2003. **74**(1): p. 77-84.
7. Burton J. D & Short T. D, *Induced Flow Reciprocating Pumps: Part 1.* Proc. Instn. Mech. Engrs., 1999. **213**: p. 363-373.
8. Burton J. D & Short T. D, *Induced Flow Reciprocating Pumps: Part 2.* Proc. Instn. Mech. Engrs., 1999. **213**: p. 375-389.
9. Burton J. D & Loboguer J, *Induced Flow Reciprocating Pump Theory Supported by New Performance Data.* Journal of Basic Engineering, 1972. **94**(4): p. 706-714.
10. Creedon R. L, Lobo-Guerrero J, Selwood P. R & Burton J. D, *High speed induced flow reciprocating pumps.* Proc. Instn. Mech. Engrs., 1972. **186**: p. 785-791.
11. Short T. D & Burton J. D, *The benefits of induced flow solar powered water pumps.* Journal of Solar Energy 2003. **74**: p. 77-84.
12. Short T. D & Mueller M. A, *Solar powered water pumps: Problems, pitfalls and potential*, in *International Conference on Power Electronics, Machines and Drives. Inst. Elec. Engrs.,* 2002: Edison. p. 280-285.

13. Short, T. D. & Oldach, R., *Solar powered water pumps: The past, the present-and the future?* Journal of Solar Energy Engineering-Transactions of the Asme, 2003. **125**(1): p. 76-82.
14. Short T. D & Thompson P, *Breaking the mould: solar water pumping - the challenges and the reality.* Solar Energy, 2003. **75**(1): p. 1-9.
15. Wade N. S & Short T. D, *The performance of a new positive displacement pump targeted to improve rural water supplies.* Proceedings of the Institution of Mechanical Engineers Part a-Journal of Power and Energy, 2007. **221**(A8): p. 1163-1171.
16. Tessema A. A, *Hydraulic Ram Pump System Design and Application*, in *ESME 5th Annual Conference on Manufacturing and Process Industry,* 2000.
17. Atlam O & Kolhe M, *Performance evaluation of directly photovoltaic powered DC PM (direct current permanent magnet) motor - propeller thrust system.* Energy, 2013. **57**: p. 692-698.
18. Kolhe M, Joshi J. C & Kothari D. P, *Performance analysis of a directly coupled photovoltaic water-pumping system.* IEEE Transactions on Energy Conversion, 2004. **19**(Article): p. 613-618.
19. Oldach R, Derrick A & Whitfield G R, *Concerted action on the testing and cost reduction of PV water pumping systems under the EC AVICENNE programme.* 14th European Photovoltaic Solar Energy Conference, 1997.
20. World Bank Group, *Addressing the Electricity Access Gap - Background Paper for the World Bank Group Energy Sector Strategy*, 2010: worldbank.org.
21. Soubbotina T. P & Sheram K. A. *Beyond Economic Growth, Meeting The Challenges of Global Development*. 2000. International Bank for Reconstruction and Development.
22. Noble N*, Solar Photovoltaic Water Pumping*. 2012.
23. United Nations General Assembly, *The human right to water and sanitation.* A/RES, 2010. **64**.
24. Gleick P. H, *Dirty Water: Esitmated deaths from water related diseases 2000-2020.* Pacific Institute Research Report, 2002.
25. World Health Organisation, *Minimum water quantity needed for domestic use in emergencies.* Technical note, World Health Organisation (WHO), 2005.

26. United Nations, *The Millenium Goals.* United Nations Millenium Declaration, 2000. **A/RES/55**(2).
27. United Nations, *Millenium Development Goals and Beyond 2015*, 2015.
28. Nogier A, *Setting up an organisational PV pumping scheme in Nigeria.* International workshop on PV water supply issues, Marrakech, 1998.
29. Kaboré F, *Le programme régional solaire: L'hydraulique villageoise et pompage solaire au service du développement duarble dans les pays du Sahel. Lecons et impacts sur le terrain.* International Workshop on PV Water Supply Issues, Marrakech, 1998.
30. Posorski R, *Photovoltaic water pumps, an attractive tool for rural drinking water supply.* Solar Energy, 1996. **58**: p. 155-163.
31. Posorski R, H. K., *The economics of photovoltaic pumping systems.* Deutsch Gesellschaft Fur Technische Zassamenabeit (GTZ), GmbH, 1997.
32. Fahlenboch B, *Project Schlussbericht, PVP- Phillipinen.* Internal GTZ report, GTZ, 1995.
33. Hahn A. *Technical Maturity and Reliability of Photovoltaic Pumping Systems*. in *13th European PV Solar Conference*. 1995. Nice.
34. Hahn A, *Lessons Learned from the International Photovoltaic Pumping Program.* International workshop on PV water supply issues, Marrakech, 1998.
35. Barlow R & Derrick A. *Solar Pumping for Rural Development: Current Status and Future Directions*. in *BWEA/RAL Workshop*. 1995.
36. Metwally H. M. B & Anis W. R, *Performance Analysis of PV Pumping Systems Using Swiched Reluctance Motor Drives.* Solar Energy 1996. **56**(2): p. 161-168.
37. Anderson G. O, *The role, reliability and limitations of solar photo-voltaic systems in Botswana*, in *Ninth International Conference on Harmonics and Quality of Power Proceedings, Vols I - Iii*, A. Domijan, Editor 2000. p. 973-982.
38. Odeh I, Yohanis Y. G & Norton B, *Influence of pumping head, insolation and PV array size on PV water pumping system performance.* Solar Energy, 2006. **80**(1): p. 51-64.
39. Zaki A & Eskander M, *Matching of Photovoltaic Motor-pump Systsems for Maximum Efficiency Operation.* Renewable Energy, 1996. **7**(3): p. 279-288.

40. Metwally H. M. B & Anis W. R, *Performance analysis of photovoltaic pumping systems using switched reluctance motor drives.* Progress in Photovoltaics: Research and Applications, 1995. **3**(4): p. 253-264.
41. Akbaba M, Qamber I & Kamal A, *Matching of separately excited dc motors to photovoltaic generators for maximum power output.* Solar Energy, 1998. **63**(6): p. 375-385.
42. Olorunfemi O, *Analyses of current source induction motor drive fed from photovoltaic energy source.* IEEE Transaction on Energy Conservation, 1991. **6**(1): p. 99-106.
43. Bekta A & Moussi A, *Performance optimization of a photovoltaic induction motor pumping system.* Renewable Energy, 2004. **29**.
44. Kamel K & Dahl C, *The economics of hybrid power systems for sustainable desert agriculture in Egypt.* Energy, 2005. **30**(1271-1281).
45. Odeh I, Yohanis Y. G & Norton B, *Economic viability of photovoltaic water pumping systems.* Solar Energy, 2006. **80**(7): p. 850-860.
46. Vick B. D & Neal B. A, *Analysis of off-grid hybrid wind turbine/solar PV water pumping systems.* Solar Energy, 2012. **86**(5): p. 1197-1207.
47. Hahn A. *Lessons Learned from the International Photovoltaic Pumping Program*. in *International Workshop on PV Water Supply Issues*. 1998. Marrakech.
48. Jafar M, *A model for small-scale photovoltaic solar water pumping.* Renewable Energy, 2000. **19**(1-2): p. 85-90.
49. Ramos J. S & Ramos H. M, *Solar powered pumps to supply water for rural or isolated zones: A case study.* Energy for Sustainable Development, 2009. **13**(3): p. 151-158.
50. McNelis B & Derrick A, *Solar Water Pumping: clean water for rural areas.* Proc. 2nd ASEAN Science and Technology Week, 1989: p. 19.
51. Elgendy M. A, Zahawi B & Atkinson D. J, *Comparison of directly connected and constant voltage controlled photovoltaic pumping systems.* IEEE Transactions on Sustainable Energy, 2010. **1**(3): p. 184-192.
52. Elgendy M. A, Zahawi B & Atkinson D. J. *Analysis of the performance of DC photovoltaic pumping systems with maximum power point tracking*. in *IET Institute Conference of Power Electronics, Machines and Drives*. 2008. York, U.K.

53. Akbaba M, *Optimum matching parameters of an MPPT unit based for a PVG-Powered water pumping system for maximum power transfer.* Energy Research, 2006. **30**: p. 395 - 409.

54. Hadi H, Tokudu S & Rahardjo S, *Evaluation of performance of photovoltaic systems with maximum power point tracker (MPPT).* Solar Energy Materials. Solar Cells, 2003. **75**: p. 673 - 678.

55. Caton P, *Design of rural photovoltaic water pumping systems and the potential of manual array tracking for a West-African village.* Solar Energy, 2014. **103**: p. 288-302.

56. Abete A, Brossa G & Cane F. *Operation and characteristics of direct current motors directly powered by photovoltaic generators*. in *4th European Conference on Power Electronics and Application*. 1991. Firenze.

57. Anis W. R & Metwally H. M. B, *Dynamic performance of a directly coupled PV pumping system.* Solar Energy, 1994. **53**(4): p. 369-377.

58. Singer S & Appelbaum J, *Starting characteristics of direct current motors powered by solar cells.* NASA Technical Memorandum 101981, 1989.

59. Kolhe M & Joshi J. C, *Performance analysis of directly coupled photovoltaic electro-mechanical systems.* Power and Energy, 2002: p. 453 - 464.

60. Chandratilleke T.T & Ho J.C, *A Study of a Photovoltaic Array for Water Pumping.* Solar Wind Technology, 1986. **3**: p. 59-71.

61. Boutelhig A., B. Y., Hadj Mahammed I. and Hadj Arab A, *Performaces study of different PV powered DC pump configurations for an optimum energy rating at different heads under the outdoor conditions of a desert area.* Energy 2012. **39**(1): p. 33-39.

62. Roger J, *Theory of the direct coupling between DC motors and photovoltaic solar arrays.* Solar Energy, 1979. **23**: p. 193 - 198.

63. Firatoglu Z. A & Yesilata B, *New approaches on the optimization of directly coupled PV pumping systems.* Solar Energy, 2004. **77**(1): p. 81-93.

64. Short, T. D, *Induced flow water pumping for stand alone renewable energy systems*, University of Reading, 1999.

65. Solar Electric Light Fund (SELF), *A cost and reliability comparison between solar and diesel powered pumps.* Solar electric light fund publication, 2008. **Sourced; http://self.org/solarvsdiesel (Jan 2012)**.

66. Anis W. R & Nour M. A, *Switching mode photovoltaic pumping system.* Energy Conversion Management, 1994. **35**(9): p. 765 - 773.

67. Navarte L, Lorenzo E & E, C., *PV pumping analystical design and characteristics of boreholes*, Instituto de Energia Solar, ETSI Telecommunicacion, Ciudad Universitaria Madrid, Spain.

68. Wagner E. G & Lanoix J. N, *Water supply for rural areas and small communities*, in *Monograph Series, No. 42*1959, World Health Organization.

69. Machinery Spaces. *Marine Displacement Pumps Principles and Working Procedure*. [cited 2012; Available from: http://www.machineryspaces.com/displacement-pumps.html.

70. Barlow R, McNelis B & Derrick A, *Solar Pumping- An introduction and update on the technology, performance, costs and economics.* Natural Resources Forum, 1993. **18**(1): p. 72-73.

71. Valge Pumps. [cited 2012; Available from: http://www.metalvalley.com.br/en/empresas/valge/produtos-e-servicos/helical-pump-sanitary-line-vgs.

72. Mokeddem A, Midoun A, Kadri D, Hiadsi S & Raja I. A, *Performance of a directly-coupled PV water pumping system.* Energy Conversion and Management, 2011. **52**(10): p. 3089-3095.

73. Argaw N, *PV Pumps Field Experience in Ethiopia*, in *13th European Photovoltaic Solar Enegy Conference,* 1995: Nice.

74. Dunn P. D, *Appropriate Technology.* The Macmillan Press ltd., 1978.

75. Whitfield G. R, W, B. R. & Mogotsi B, *Improving the cost effectiveness of small solar photovoltaic water pumping systems.* Renewable Energy Sources, 1991: p. 51 - 56.

76. Whitfield G. R & Bentley R. W, *The efficiency of small solar photovoltaic water pumping systems*, in *Ninth EC Photovoltaic Solar Energy Conference,* 1989: Freiburg, Germany. p. 1123 - 1127.

77. Norton B, *Solar Energy Thermal Technology,* 1992, London, UK: Springer-Verlag.

78. Twidell J. W, *Wind energy R&D Discussion Network.* 1999.
79. Twidell J. W & Weir A. D, *Renewable Energy Sources*. Second Edition ed2006, New York: Taylor and Francis.
80. EC, *Concerted action for the testing and cost reduction of PV water pumping systems*, 1997, Contract AVI-CT 94-0004, IT Power: Chineham, Hants, U.K.
81. Ewbank T, *A Descriptive and Historical Account of Hydraulic and Other Machines for Raising Water, Ancient and Modern,* 1842: D. Appleton and Company.
82. Lobo-Guerro J, *Analisis de Flujo Hidraulico en Una Bomba Reciprocante con Elementos Inductivos y Capacitivos*, 1969, La Universidad de Los Andes: Bogota.
83. Burton J D & Lobo-Guerrero J, *Bomba Reciproca Analisis con Flujo Inducido*, 1971: Bogota, Columbia.
84. Burton J. D & Lobo-Guerrero U. J, *Induced Flow Reciprocating Pump Theory Supported by New Performance Data.* Journal of Basic Engineering, 1972. **94**(4): p. 706-714.
85. Food and Agriculture Organisation of the United States (FAO). *Reciprocating Inertia (Joggle) Pumps*. Water Lifting Devices - Natural Resources Management and Environment Department [cited 2013; Available from: http://www.fao.org/docrep/010/ah810e/ah810e07.htm.
86. Burton J. D & Beltran R, *Stability Problems in High Speed Induced Flow Reciprocating Pumps*, in *5th Conference on Fluid Machinery*1975: Budapest. p. 171 - 180.
87. Cefis G, *Pat.*, 1993: Italy.
88. Mohammed S. N, *Design and Construction of a Hydraulic Ram Pump.* Leonardo Electrical Journal of Practices and Technologies, 2007: p. 59 - 70.
89. Whitehurst J, *Account of a Machine for Raising Water, Executed at Oulton, Cheshire in 1772 (A letter from Mr J Whitehurst to Dr Franklin).* Philisophical transactions of The Royal Society, 1775. **65**: p. 277 - 279.
90. Montgolfier J. M. d, *Note on the Hydraulic Ram and on the Method of Calculating its Effects.* Journal de Mines, 1803. **13**: p. 42 - 51.
91. Krol J, *Automatic Hydraulic Pump.* Proc. I. Mech. Eng., 1951. **164**: p. 103.
92. Calvert N. G, *Hydraulic Ram.* The Engineer, 1967.

93. Wilson D. R, *All About Hydraulic Ram Pumps: How and where they work*1995: Atlas Publications.

94. Thomas T. H, *Algebraic Modelling of the Behaviour of Hydraulic Ram Pumps*, in *Working Paper No. 41*1994, Development Technology Unit, University of Warwick.

95. Sheikh S, Handu C. C & Ninawe A. P, *Design Methodology for Hydraulic Ram Pump (Hydram).* International Journal of Mechanical Engineering and Robotics Research, 2013. **2**(4).

96. Hyper Physics. *DC Water Circuit Analogy*. [cited 2013; Available from: http://hyperphysics.phy-astr.gsu.edu/hbase/electric/watcir.html.

97. Wang F, Gu L. Y & Chen Y, *A Hydraulic Pressure-Boost System Based on High-Speed ON-OFF Valves.* Ieee-Asme Transactions on Mechatronics, 2013. **18**(2): p. 733-743.

98. Scheidl R, Steiner B, Winkler B & Mikota G, *Basic problems in fast hydraulic switching valve technology*. Proceedings of the Sixth International Conference on Fluid Power Transmission and Control, ed. Lu Y. X, Wang Q. F, and Wei L, 2005, Hong Kong: International Academic Publishers Ltd. 53-57.

99. Pan M, Johnston N, Plummer A, Kudzma S & Hillis A, *Theoretical and experimental studies of a switched inertance hydraulic system.* Proceedings of the Institution of Mechanical Engineers Part I-Journal of Systems and Control Engineering, 2014. **228**(1): p. 12-25.

100. Guglielmino E, Semini C, Kogler H, Scheidl R & Caldwell D. G, *Power Hydraulics - Switched Mode Control of Hydraulic Actuation*, in *2010 International Conference on Intelligent Robots and Systems*2010, Ieee: New York. p. 3031-3036.

101. Kypuros J. A & Longoria R. G, *Model synthesis for design of switched systems using a variable structure system formulation.* Journal of Dynamic Systems Measurement and Control-Transactions of the Asme, 2003. **125**(4): p. 618-629.

102. White F. M, *Fluid Mechanics, 7th Ed.* 2011.

103. Chaudry M. H, *Applied Hydraulic Transients*. 2nd ed. 1987: Van Nostrand Reinhold Company Inc.

104. Wylie E. B & Streeter B. E, *Fluid Transients*1978: McGraw - Hill.

105. Streeter V. L, Wylie E. B & Bedford K. W, *Fluid Mechanics.* 1998.

106. Mambretti S, *Water Hammer Simulations*, 2014, Southampton, Boston: WIT Press.

107. Stephenson D, *Pipeline Design for Water Engineers*. 1st ed. Developments in Water Science, ed. C. V.T, 1976: Elesevier.

Appendix A

The Timed ECV

Presented in this section of the thesis are the additional manipulations of equations presented in **Chapter 4**. Primarily, the aim of this appendix is to provide a more comprehensive presentation of the process in constructing the equations used to define the pumping system.

A.1 Defining the Duty Cycle

In order for the centrifugal pump to operate at its BEP, independent of operating conditions, the duty cycle of the E-OWV may be modified according to the operational pressure head. This section of the appendix describes the derivation of the quadratic formula defining the duty cycle at varying heads. Firstly, the time period, T, may be defined as the sum of the times of the cycle when the E-OWV is either open or closed. This may be seen in **Eqn. A-1**:

$$T = t_o + t_c \qquad \textbf{Eqn. A-1}$$

Additionally, the duty cycle of the system may be defined as:

$$D = \frac{t_o}{T} \qquad \textbf{Eqn. A-2}$$

Following assumptions 1 and 2, made in **Section 4.3**, the combined flow rates from the inductance pipe to the ECV or OWV must be equal to the flow rate at the output of the inductance section, giving the simple relationship:

$$Q_{L1} = Q_{ECV} + Q_{OWV}$$ **Eqn. A-3**

As the flow may be through only one component at a time due to perfect switching, the duty cycle may be used to define each flow rate in terms of a single flow rate, hence:

$$Q_{L1} = (1 - D)Q_{L1} + DQ_{L1}$$ **Eqn. A-4**

where:

$$Q_{OWV} = (1 - D)Q_{L1}$$ **Eqn. A-5**

and,

$$Q_{ECV} = DQ_{L1}$$ **Eqn. A-6**

Moving on from the basic flow rate, the energy stored in the system may be defined using the steady-state fluid equation [102]:

$$\Delta E = \sum \dot{m}\left(U + \frac{P}{\rho} + \frac{u^2}{2} + gz\right) = 0$$ **Eqn. A-7**

where:

$$\dot{m} = \rho Q$$ **Eqn. A-8**

Combining to give:

$$\sum \rho Q\left(U + \frac{P}{\rho} + \frac{u^2}{2} + gz\right) = 0$$ **Eqn. A-9**

When considering the pumping system defined in **Chapter 4** in terms of **Eqn. A-9**, and for the sake of simplicity, only the inertial terms are required and the gravitational term may be ignored due to the negligible distance, z, between the

inductance pipe exit and the next components*. Expanding the energy equation now yields:

$$\rho Q_{L1}\left(\frac{P_{L1}}{\rho}+\frac{{u_{L1}}^2}{2}\right)-\rho Q_{ECV}\left(\frac{P_{ECV}}{\rho}+\frac{{u_{ECV}}^2}{2}\right)-\rho Q_{OWV}\left(\frac{P_{OWV}}{\rho}+\frac{{u_{OWV}}^2}{2}\right)=0$$

Eqn. A-10

This may be rearranged to give:

$$\rho Q_{L1}\left(\frac{P_{L1}}{\rho}+\frac{{u_{L1}}^2}{2}\right)=\rho Q_{ECV}\left(\frac{P_{ECV}}{\rho}+\frac{{u_{ECV}}^2}{2}\right)+\rho Q_{OWV}\left(\frac{P_{OWV}}{\rho}+\frac{{u_{OWV}}^2}{2}\right)$$

Eqn. A-11

Replacing the fluid velocity terms in this equation and noting that for each section of the system, all pipe cross sectional area values are equal due to the same diameter pipe being used throughout, **Eqn. A-11** becomes:

$$\rho Q_{L1}\left(\frac{P_{L1}}{\rho}+\frac{{Q_{L1}}^2}{2A^2}\right)=\rho Q_{ECV}\left(\frac{P_{ECV}}{\rho}+\frac{{Q_{ECV}}^2}{2A^2}\right)+\rho Q_{OWV}\left(\frac{P_{OWV}}{\rho}+\frac{{Q_{OWV}}^2}{2A^2}\right)$$

Eqn. A-12

using:

$$u=\frac{Q}{A}$$ **Eqn. A-13**

Through expanding and re-introducing **Eqns. A-5** and **A-6**, **Eqn. A-12** may be expressed in terms of a single flow rate:

*Further, in the experimental testing section covered by **Chapter 8,** the *z* term is neglected due to the horizontal set-up of the IFS and ECV apparatus.

$$\rho Q_{L1}\left(\frac{P_{L1}}{\rho}+\frac{{Q_{L1}}^2}{2A^2}\right)=(1-D)\rho Q_{L1}\left(\frac{P_{OWV}}{\rho}+\frac{(1-D)^2{Q_{L1}}^2}{2A^2}\right)+D\rho Q_{ECV}\left(\frac{P_{ECV}}{\rho}+\frac{D^2{Q_{L1}}^2}{2A^2}\right)$$

Eqn. A-14

Continuing on to simplify by dividing through by ρQ_{L1}:

$$\frac{P_{L1}}{\rho}+\frac{{Q_{L1}}^2}{2A^2}=(1-D)\left(\frac{P_{OWV}}{\rho}+\frac{(1-D)^2{Q_{L1}}^2}{2A^2}\right)+D\left(\frac{P_{ECV}}{\rho}+\frac{D^2{Q_{L1}}^2}{2A^2}\right)$$ **Eqn. A-15**

Then through a series of rearrangements and working through, **Eqn. A-15** may be described by **Eqn. A-21**. The steps are as follows:

$$\frac{P_{L1}}{\rho}+\frac{{Q_{L1}}^2}{2A^2}-\frac{DP_{ECV}}{\rho}-\frac{D^3{Q_{L1}}^2}{2A^2}=(1-D)\left(\frac{P_{OWV}}{\rho}+\frac{(1-D)^2{Q_{L1}}^2}{2A^2}\right)$$ **Eqn. A-16**

$$\frac{1}{(1-D)}\left(\frac{P_{L1}-DP_{ECV}}{\rho}+\frac{{Q_{L1}}^2}{2A^2}(1-D)\right)=\frac{P_{OWV}}{\rho}+\frac{(1-D)^2{Q_{L1}}^2}{2A^2}$$ **Eqn. A-17**

$$\frac{P_{L1}-DP_{ECV}}{\rho(1-D)}+\frac{{Q_{L1}}^2}{2A^2}\frac{(1-D^3)}{(1-D)}-\frac{(1-D)^2{Q_{L1}}^2}{2A^2}=\frac{P_{OWV}}{\rho}$$ **Eqn. A-18**

$$\frac{P_{L1}-DP_{ECV}}{\rho(1-D)}+\frac{{Q_{L1}}^2}{2A^2}\left[\frac{(1-D^3)}{(1-D)}-(1-D)\right]=\frac{P_{OWV}}{\rho}$$ **Eqn. A-19**

$$\frac{P_{OWV}}{\rho}=\frac{P_{L1}-DP_{ECV}}{\rho(1-D)}+\frac{3D{Q_{L1}}^2}{2A^2}$$ **Eqn. A-20**

$$P_{OWV}=\frac{P_{L1}-DP_{ECV}}{(1-D)}+\frac{3\rho D{Q_{L1}}^2}{2A^2}$$ **Eqn. A-21**

At this point it is noted that some of the terms may be replaced to make the equation more relevant to the describing the system. These terms include $Q_{L1}=Q_{BEP}$ (as flow through the inductance pipe is to be held at pump BEP point), $P_{ECV}=P_{sub}$ (return from the ECV back to borehole submergence pressure) and $P_1=P_{BEP}-P_{sub}$ (from BEP operation of the pump, minus borehole submergence pressure). Also, the pressure

downstream of the OWV will be subjected to the total pressure load on the system, hence $P_{OWV} = P_{Out}$. As such, **Eqn. A-21** becomes:

$$P_{Out} = \frac{(P_{BEP} - P_{sub}) - DP_{sub}}{(1-D)} + \frac{3\rho DQ_{BEP}{}^2}{2A^2} \qquad \textbf{Eqn. A-22}$$

Here, the pressure at end of the inductance pipe is equal to that of the pressure at the outlet of the centrifugal pump operating at its BEP; taking into account the submergence pressure of the pump. Rearranging gives:

$$P_{Out} = \frac{P_{BEP}}{(1-D)} + P_{sub}\left(\frac{1-D}{1-D}\right) + \frac{3\rho DQ_{BEP}{}^2}{2A^2} \qquad \textbf{Eqn. A-23}$$

Simplifying:

$$P_{Out} = \frac{P_{BEP}}{(1-D)} + P_{sub} + \frac{3\rho DQ_{BEP}{}^2}{2A^2} \qquad \textbf{Eqn. A-24}$$

Eliminating submergence pressure as the difference between pump outlet and ECV (which is considered to be negligible as z term in Steady State Energy equation is removed), then:

$$P_{Out} = \frac{P_{BEP}}{(1-D)} + \frac{3\rho DQ_{BEP}{}^2}{2A^2} \qquad \textbf{Eqn. A-25}$$

Ultimately, the equation being derived must be useful for calculating the variation of duty cycle over a range of given pumping heads, therefore it is necessary to continue to manipulate **Eqn. A-25** to include the pressure difference between BEP pressure and operating head, where:

$$\Delta P = P_{Out} - P_{BEP} \qquad \textbf{Eqn. A-26}$$

This results in **Eqn. A-27**:

$$P_{Out} - P_{BEP} = \frac{P_{BEP}}{(1-D)} + \frac{3\rho D {Q_{BEP}}^2}{2A^2} - P_{BEP}$$ **Eqn. A-27**

or, by working through:

$$\Delta P = P_{BEP}\left(\frac{1}{1-D} - 1\right) + \frac{3\rho D {Q_{BEP}}^2}{2A^2} \quad ;$$ **Eqn. A-28**

and so;

$$\Delta P = \frac{Dp_{BEP}}{1-D} + \frac{3\rho D {Q_{BEP}}^2}{2A^2}$$ **Eqn. A-29**

This equation may then be arranged and solved using the quadratic formula in order to find an solution for ECV duty cycle, D. The series of steps leading to this point are demonstrated below:

$$P_{Out} - P_{BEP} = \frac{DP_{BEP}}{(1-D)} + \frac{3\rho D {Q_{BEP}}^2}{2A^2} - P_{BEP} \quad ;$$ **Eqn. A-30**

$$(1-D)\left(P_{Out} - p_{BEP} - \frac{3\rho D {Q_{BEP}}^2}{2A^2}\right) = Dp_{BEP} \ ;$$ **Eqn. A-31**

$$P_{Out} - P_{BEP} - DP_{Out} + DP_{BEP} - \frac{3\rho D {Q_{BEP}}^2}{2A^2} + \frac{3\rho D^2 {Q_{BEP}}^2}{2A^2} = Dp_{BEP}$$

Eqn. A-32

Simplifying:

$$P_{Out} - DP_{Out} - P_{BEP} - \frac{3\rho D {Q_{BEP}}^2}{2A^2} + \frac{3\rho D^2 {Q_{BEP}}^2}{2A^2} = 0$$ **Eqn. A-33**

This may then be rearranged into quadratic form:

$$\left(\frac{3\rho {Q_{BEP}}^2}{2A^2}\right)D^2 - \left(P_{Out} + \frac{3\rho {Q_{BEP}}^2}{2A^2}\right)D + \Delta P = 0$$ **Eqn. A-34**

Following through using the quadratic formula:

$$D = \frac{P_{Out} + \frac{3\rho {Q_{BEP}}^2}{2A^2} \pm \sqrt{\left(P_{Out} + \frac{3\rho {Q_{BEP}}^2}{2A^2}\right)^2 - \frac{12\rho {Q_{BEP}}^2}{2A^2}\Delta P}}{\frac{6\rho {Q_{BEP}}^2}{2A^2}} \qquad \textbf{Eqn. A-35}$$

Finally, replacing the repeated terms to simplify the equation:

$$D = \frac{P_{Out} + \varphi \pm \sqrt{(P_{Out} + \varphi)^2 - 4\varphi\Delta P}}{2\varphi} \qquad \textbf{Eqn. A-36}$$

where:

$$\varphi = \frac{3\rho {Q_{BEP}}^2}{2A^2}$$

Appendix B

Discharge Flow Boundary Conditions

This appendix contains the full manipulations used in defining the constants of integration, A, B, C and D, needed to complete the equations of discharge flow presented in **Chapter 5**.

B.1 Introduction to Boundary Conditions

Starting with the boundary conditions defined in **Section 5.4:**

1. $Q_D\,(0)_{ON} = Q_D\,(T)_{OFF}$
2. $Q_D{}'\,(0)_{ON} = Q_D{}'\,(T)_{OFF}$
3. $Q_D\,(TD)_{ON} = Q_D\,(TD)_{OFF}$
4. $\int_{TD}^{T} Q_{L1}\,(t) = \int_{0}^{TD} Q_D\,(t)_{ON} + \int_{TD}^{T} Q_D\,(t)_{OFF}$

These boundary conditions are used to define the time, t, in the equations of discharge flow so as each constant may be eliminated sequentially until a definition for only one constant remains. This final constant can then be used as a definition for each other constant previously eliminated. The equations of discharge flow, including differential versions, are stated below for ease of reference in this appendix:

$$Q_D\,(t)_{ON} = A\cos\left(\sqrt{\alpha}.t\right) + B\sin\left(\sqrt{\alpha}.t\right) \quad ; \qquad \textbf{Eqn. B-1}$$

$$Q_D\,(t)_{OFF} = C\cos\left(\sqrt{\alpha}.t\right) + E\sin\left(\sqrt{\alpha}.t\right) + \Lambda - \frac{\Psi.t}{T} \quad ; \qquad \textbf{Eqn. B-2}$$

$$Q_D{}'(t)_{ON} = \sqrt{\alpha}.B\cos(\sqrt{\alpha}.t) - \sqrt{\alpha}.A\sin(\sqrt{\alpha}.t) \quad ; \qquad \textbf{Eqn. B-3}$$

$$Q_D{}'(t)_{OFF} = \sqrt{\alpha}.E\cos(\sqrt{\alpha}.t) - \sqrt{\alpha}.C\sin(\sqrt{\alpha}.t) - \frac{\Psi}{T} \qquad \textbf{Eqn. B-4}$$

where:

$$\Lambda = Q_{BEP}.\left(1 + \mathbb{R}\left(\frac{1+D}{1-D}\right)\right);$$

$$\Psi = \frac{2.Q_{BEP}.\mathbb{R}}{(1-D)}$$

B.2 Defining the Constants of Integration

Following the boundary conditions and replacing the time variables with fixed time values, the constants of integration may be defined. Using the first three boundary conditions:

$$A = C\cos(\sqrt{\alpha}.T) + E\sin(\sqrt{\alpha}.T) + \Lambda - \Psi \quad ; \qquad \textbf{Eqn. B-5}$$

$$B = E\cos(\sqrt{\alpha}.T) - C\sin(\sqrt{\alpha}.T) - \frac{\Psi}{\sqrt{\alpha}.T} \quad ; \qquad \textbf{Eqn. B-6}$$

$$A.\cos(\sqrt{\alpha}.T.D) + B.\sin(\sqrt{\alpha}.T.D) = C\cos(\sqrt{\alpha}.T.D) + E\sin(\sqrt{\alpha}.T.D) + \Lambda - \Psi.\mathrm{D}$$

Eqn. B-7

Here, **Eqn. B-7** can be used to eliminate the first two constants, A and B, by substituting in their individual definitions such that:

$$\left(C\cos(\sqrt{\alpha}.T) + E\sin(\sqrt{\alpha}.T) + \Lambda - \Psi\right).\cos(\sqrt{\alpha}.T.D) + \left(E\cos(\sqrt{\alpha}.T) - C\sin(\sqrt{\alpha}.T) - \frac{\Psi}{\sqrt{\alpha}.T}\right).\sin(\sqrt{\alpha}.T.D) = C.\cos(\sqrt{\alpha}.T.D) + E.\sin(\sqrt{\alpha}.T.D) + \Lambda - \Psi.D$$

Eqn. B-8

Expanding and rearranging:

$$C.\left(\cos\left(\sqrt{\alpha}.T\right).cos\left(\sqrt{\alpha}.T.D\right)-\sin\left(\sqrt{\alpha}.T\right).sin\left(\sqrt{\alpha}.T.D\right)-\cos\left(\sqrt{\alpha}.T.D\right)\right)=$$

$$E.\left(\sin\left(\sqrt{\alpha}.T.D\right)-\sin\left(\sqrt{\alpha}.T\right).cos\left(\sqrt{\alpha}.T.D\right)-\cos\left(\sqrt{\alpha}.T\right).sin\left(\sqrt{\alpha}.T.D\right)\right)+\Lambda-$$

$$\Psi.D-\Lambda.cos\left(\sqrt{\alpha}.T.D\right)+\Psi.cos\left(\sqrt{\alpha}.T.D\right)+\frac{\Psi}{\sqrt{\alpha}.T}.\sin\left(\sqrt{\alpha}.T.D\right)$$

Eqn. B-9

Through inspection it is clear that **Eqn. B-9** may be arranged to represent the constant C and also simplified through the addition of new terms, χ and ξ.

$$C=\frac{\Psi}{\xi}.\left(D-cos\left(\sqrt{\alpha}.T.D\right)-\frac{sin\left(\sqrt{\alpha}.T.D\right)}{\sqrt{\alpha}.T}\right)+\frac{\Lambda}{\xi}.\left(cos\left(\sqrt{\alpha}.T.D\right)-1\right)+E.\frac{\chi}{\xi}$$

Eqn. B-10

where:

$$\chi=\left[\cos\left(\sqrt{\alpha}.T\right).sin\left(\sqrt{\alpha}.T.D\right)+\sin\left(\sqrt{\alpha}.T\right).cos\left(\sqrt{\alpha}.T.D\right)-\sin\left(\sqrt{\alpha}.T.D\right)\right];$$

$$\xi=\left[\sin\left(\sqrt{\alpha}.T\right).sin\left(\sqrt{\alpha}.T.D\right)+\cos\left(\sqrt{\alpha}.T\right).cos\left(\sqrt{\alpha}.T.D\right)+\cos\left(\sqrt{\alpha}.T.D\right)\right]$$

This gives the first equation needed in defining C as a constant. In order to eliminate C completely and provide a full definition for the constant E, a final set of boundary conditions must be introduced.

B.2.1 Finding the Final Constant

The fourth boundary condition is defined by assuming flow over period Q_{L1} must be equal to the discharge flow over both Q_D on and Q_D off periods, as all discharge flow during ECV off period is diverted back to reservoir. This boundary condition takes into consideration the discharge flow contribution from the capacitance

chamber during periods where all flow is diverted to reservoir as during the valve of periods it is also assumed that some of the flow to the discharge pipe will be absorbed into re-pressurising the chamber.

Firstly, the equation of flow through the inductance pipe during the valve OFF period is expanded:

$$Q_{L1}(t)_{OFF} = (1 + \mathbb{R}).Q_{BEP} - \frac{t.D.P_{BEP}}{L_1.(1-D)} + \frac{T.D^2.P_{BEP}}{L_1.(1-D)} \qquad \textbf{Eqn. B-11}$$

Next, all of the integral equations needed in solving the boundary condition are defined:

$$\int Q_{L1}(t)_{OFF}\, dt = (1 + \mathbb{R}).Q_{BEP}.t - \frac{t^2.D.P_{BEP}}{2.L_1.(1-D)} + \frac{T.D^2.P_{BEP}.t}{L_1.(1-D)} \; ; \qquad \textbf{Eqn. B-12}$$

$$\int Q_D\,(t)_{ON}\, dt = \frac{A.\sin(\sqrt{\alpha}.t)}{\sqrt{\alpha}} - \frac{B.\cos(\sqrt{\alpha}.t)}{\sqrt{\alpha}} \; ; \qquad \textbf{Eqn. B-13}$$

$$\int Q_D\,(t)_{OFF}\, dt = \frac{C.\sin(\sqrt{\alpha}.t)}{\sqrt{\alpha}} + \frac{E.\cos(\sqrt{\alpha}.t)}{\sqrt{\alpha}} - \frac{\Psi.t^2}{2.T} + \Lambda.t \qquad \textbf{Eqn. B-14}$$

So in full, boundary condition 4 becomes:

$$\left[(1 + \mathbb{R}).Q_{BEP}.t - \frac{t^2.D.P_{BEP}}{2.L_1.(1-D)} + \frac{T.D^2.P_{BEP}.t}{L_1.(1-D)}\right]_{TD}^{T} = \left[\frac{A.\sin(\sqrt{\alpha}.t)}{\sqrt{\alpha}} - \frac{B.\cos(\sqrt{\alpha}.t)}{\sqrt{\alpha}}\right]_0^{TD} + \left[\frac{C.\sin(\sqrt{\alpha}.t)}{\sqrt{\alpha}} + \frac{E.\cos(\sqrt{\alpha}.t)}{\sqrt{\alpha}} - \frac{\Psi.t^2}{2.T} + \Lambda.t\right]_{TD}^{T} \qquad \textbf{Eqn. B-15}$$

Expanding:

$$(1 + \mathbb{R}).Q_{BEP}.T + \frac{T^2.D^2.P_{BEP}}{L_1.(1-D)} - \frac{T^2.D.P_{BEP}}{2.L_1.(1-D)} - (1 + \mathbb{R}).Q_{BEP}.T.D - \frac{T^2.D^3.P_{BEP}}{L_1.(1-D)} + \frac{T^2.D^3.P_{BEP}}{2.L_1.(1-D)} = \frac{A.\sin(\sqrt{\alpha}.T.D)}{\sqrt{\alpha}} - \frac{B.\cos(\sqrt{\alpha}.T.D)}{\sqrt{\alpha}} + \frac{B}{\sqrt{\alpha}} + \frac{C.\sin(\sqrt{\alpha}.T)}{\sqrt{\alpha}} - \frac{E.\cos(\sqrt{\alpha}.T)}{\sqrt{\alpha}} - \frac{\Psi.T}{2} + \Lambda.T - \frac{C.\sin(\sqrt{\alpha}.T.D)}{\sqrt{\alpha}} + \frac{E.\cos(\sqrt{\alpha}.T.D)}{\sqrt{\alpha}} + \frac{\Psi.T.D^2}{2} - \Lambda.T.D \qquad \textbf{Eqn. B-16}$$

As with **Eqn. B-8** the individual constant definitions for A and B are substituted into **Eqn. B-16**:

$$(1+\mathbb{R}).Q_{BEP}.T(1-D) + \frac{D.T^2.P_{BEP}}{L_1.(1-D)}.\left(D - \frac{1}{2} - D^2 + \frac{D^2}{2}\right) = \left(C.cos\left(\sqrt{\alpha}.T\right) + E.sin\left(\sqrt{\alpha}.T\right) + \Lambda - \Psi\right).\frac{sin\left(\sqrt{\alpha}.T.D\right)}{\sqrt{\alpha}} - \left(E.cos\left(\sqrt{\alpha}.T\right) - C.sin\left(\sqrt{\alpha}.T\right) - \frac{\Psi}{\sqrt{\alpha}.T}\right).\frac{cos\left(\sqrt{\alpha}.T.D\right)}{\sqrt{\alpha}} + \left(E.cos\left(\sqrt{\alpha}.T\right) - C.sin\left(\sqrt{\alpha}.T\right) - \frac{\Psi}{\sqrt{\alpha}.T}\right).\frac{1}{\sqrt{\alpha}} + \frac{C.sin\left(\sqrt{\alpha}.T\right)}{\sqrt{\alpha}} - \frac{E.cos\left(\sqrt{\alpha}.T\right)}{\sqrt{\alpha}} - \frac{\Psi.T}{2} + \Lambda.T - \frac{C.sin\left(\sqrt{\alpha}.T.D\right)}{\sqrt{\alpha}} + \frac{E.cos\left(\sqrt{\alpha}.T.D\right)}{\sqrt{\alpha}} + \frac{\Psi.T.D^2}{2} - \Lambda.T.D$$

Eqn. B-17

Expanding and simplifying:

$$(1+\mathbb{R}).Q_{BEP}.T(1-D) + \frac{D.T^2.P_{BEP}}{L_1.(1-D)}.\left(D - \frac{1}{2} - D^2 + \frac{D^2}{2}\right) = \frac{C.\cos\left(\sqrt{\alpha}.T\right).sin\left(\sqrt{\alpha}.T.D\right)}{\sqrt{\alpha}} + \frac{E.\sin\left(\sqrt{\alpha}.T\right).cos\left(\sqrt{\alpha}.T.D\right)}{\sqrt{\alpha}} + \frac{\Lambda.sin\left(\sqrt{\alpha}.T.D\right)}{\sqrt{\alpha}} - \frac{\Psi.sin\left(\sqrt{\alpha}.T.D\right)}{\sqrt{\alpha}} - \frac{E.\cos\left(\sqrt{\alpha}.T\right).cos\left(\sqrt{\alpha}.T.D\right)}{\sqrt{\alpha}} + \frac{C.\sin\left(\sqrt{\alpha}.T\right).cos\left(\sqrt{\alpha}.T.D\right)}{\sqrt{\alpha}} + \frac{\Psi.cos\left(\sqrt{\alpha}.T.D\right)}{\alpha.T} - \frac{\Psi}{\alpha.T} - \frac{\Psi.T}{2} + \Lambda.T - \frac{C.\sin\left(\sqrt{\alpha}.T.D\right)}{\sqrt{\alpha}} + \frac{E.\cos\left(\sqrt{\alpha}.T.D\right)}{\sqrt{\alpha}} + \frac{\Psi.T.D^2}{2} \Lambda.T.D$$

Eqn. B-18

Finally Giving:

$$(1+\mathbb{R}).Q_{BEP}.T(1-D) + \frac{D.T^2.P_{BEP}}{L_1.(1-D)}.\left(D - \frac{1}{2} - D^2 + \frac{D^2}{2}\right) = C.\left[\frac{\cos\left(\sqrt{\alpha}.T\right).sin\left(\sqrt{\alpha}.T.D\right)}{\sqrt{\alpha}} + \frac{\sin\left(\sqrt{\alpha}.T\right).cos\left(\sqrt{\alpha}.T.D\right)}{\sqrt{\alpha}} - \frac{\sin\left(\sqrt{\alpha}.T.D\right)}{\sqrt{\alpha}}\right] + E.\left[\frac{\sin\left(\sqrt{\alpha}.T\right).sin\left(\sqrt{\alpha}.T.D\right)}{\sqrt{\alpha}} + \frac{\cos\left(\sqrt{\alpha}.T\right).cos\left(\sqrt{\alpha}.T.D\right)}{\sqrt{\alpha}} - \frac{\cos\left(\sqrt{\alpha}.T.D\right)}{\sqrt{\alpha}}\right] + \frac{sin\left(\sqrt{\alpha}.T.D\right)}{\sqrt{\alpha}}.(\Lambda - \Psi) + \frac{\Psi}{\alpha.T}.\left(cos\left(\sqrt{\alpha}.T.D\right) - 1\right) + \frac{\Psi.T}{2}.(D^2 - 1) + \Lambda.T.(1-D)$$

Eqn. B-19

Again the equation may be simplified by introducing the χ and ξ terms and rearranging to find a second definition for the constant C:

$$C = \left[(1+\mathbb{R}).Q_{BEP}.T(1-D) + \frac{D.T^2.P_{BEP}}{L_1.(1-D)}.\left(D - \frac{1}{2} - D^2 + \frac{D^2}{2}\right) - \frac{E.\xi}{\sqrt{\alpha}} + \frac{sin(\sqrt{\alpha}.T.D)}{\sqrt{\alpha}}.(\Psi - \Lambda) + \frac{\Psi}{\alpha.T}.\left(1 - cos(\sqrt{\alpha}.T.D)\right) + \frac{\Psi.T}{2}.(1-D^2) + \Lambda.T.(D-1)\right].\frac{\sqrt{\alpha}}{\chi}$$

Eqn. B-20

Combining both **Eqn. B-10** and **Eqn. B-20** to eliminate$C$**:**

$$\frac{\Psi}{\xi}.\left(D - cos(\sqrt{\alpha}.T.D) - \frac{sin(\sqrt{\alpha}.T.D)}{\sqrt{\alpha}.T}\right) + \frac{\Lambda}{\xi}.\left(cos(\sqrt{\alpha}.T.D) - 1\right) + E.\frac{\chi}{\xi} = \left[(1+\mathbb{R}).Q_{BEP}.T(1-D) + \frac{D.T^2.P_{BEP}}{L_1.(1-D)}.\left(D - \frac{1}{2} - D^2 + \frac{D^2}{2}\right) - \frac{E.\xi}{\sqrt{\alpha}} + \frac{sin(\sqrt{\alpha}.T.D)}{\sqrt{\alpha}}.(\Psi - \Lambda) + \frac{\Psi}{\alpha.T}.\left(1 - cos(\sqrt{\alpha}.T.D)\right) + \frac{\Psi.T}{2}.(1-D^2) + \Lambda.T.(D-1)\right].\frac{\sqrt{\alpha}}{\chi}$$

Eqn. B-21

Then rearranging:

$$E.\left(\frac{\chi}{\xi} + \frac{\xi}{\chi}\right) = \frac{\sqrt{\alpha}}{\chi}.\left[(1+\mathbb{R}).Q_{BEP}.T(1-D) + \frac{D.T^2.P_{BEP}}{L_1.(1-D)}.\left(D - \frac{1}{2} - D^2 + \frac{D^2}{2}\right) + \frac{sin(\sqrt{\alpha}.T.D)}{\sqrt{\alpha}}.(\Psi - \Lambda) + \frac{\Psi}{\alpha.T}.\left(1 - cos(\sqrt{\alpha}.T.D)\right) + \frac{\Psi.T}{2}.(1-D^2) + \Lambda.T.(D-1)\right] + \frac{1}{\xi}.\left[\Psi.\left(\frac{sin(\sqrt{\alpha}.T.D)}{\sqrt{\alpha}.T} + cos(\sqrt{\alpha}.T.D) - D\right) + \Lambda.\left(1 - cos(\sqrt{\alpha}.T.D)\right)\right]$$

Eqn. B-22

Finally, through simplification and manipulation, a definition for the final constant of integration if found:

$$E = \frac{\sqrt{\alpha}.\xi.\mathrm{Z} + \chi.\left[\Psi.\left(\frac{sin(\sqrt{\alpha}.T.D)}{\sqrt{\alpha}.T} + cos(\sqrt{\alpha}.T.D) - D\right) + \Lambda.\left(1 - cos(\sqrt{\alpha}.T.D)\right)\right]}{\chi^2 + \xi^2}$$

Eqn. B-23

where:

$$\mathrm{Z} = \left[Q_{BEP}.(1-D).T + \frac{sin(\sqrt{\alpha}.T.D)}{\sqrt{\alpha}}.(\Psi-\Lambda) + \frac{\Psi}{\alpha.T}.\left(1 - cos\left(\sqrt{\alpha}.T.D\right)\right) + \frac{\Psi.T}{2}.(1-D^2) + \Lambda.T.(D-1)\right]$$

Eqn. B-24

Here, the additional term used for simplification, Z, replaces the longer integral expansion of flow through the inductance pipe with the definition for total average flow through the discharge pipe, defined in **Chapter 5** where:

$$Q_{BEP}.(1-D).T = (1+\mathbb{R}).Q_{BEP}.T(1-D) + \frac{D.T^2.P_{BEP}}{L_1.(1-D)}.\left(D - \frac{1}{2} - D^2 + \frac{D^2}{2}\right)$$

Eqn. B-25

This now enables the equations of discharge flow to be solved and all constants of integration are defined using known terms.

B.3 Summary

The constants of integration produced in defining the discharge flow equations were found through producing a series of boundary conditions for discharge flow. These boundary conditions were selected so as to smooth the discharge flow and also enable matching of specific points when flow in the system transitions into valve ON and OFF periods. Furthermore, these boundary conditions were selected so as the equations of discharge flow could be repeated to produce a constant flow pattern. After eliminating the unknown variables in the discharge flow equations through using the boundary conditions, the final equations were found to be as follows:

$$A = C\cos\left(\sqrt{\alpha}.T\right) + E\sin\left(\sqrt{\alpha}.T\right) + \Lambda - \Psi \ ;$$

$$B = E\cos\left(\sqrt{\alpha}.T\right) - C\sin\left(\sqrt{\alpha}.T\right) - \frac{\Psi}{\sqrt{\alpha}.T} \ ;$$

$$C = \frac{\Psi}{\xi}.\left(D - cos\left(\sqrt{\alpha}.T.D\right) - \frac{sin\left(\sqrt{\alpha}.T.D\right)}{\sqrt{\alpha}.T}\right) + \frac{\Lambda}{\xi}.\left(cos\left(\sqrt{\alpha}.T.D\right) - 1\right) + E.\frac{\chi}{\xi} \ ;$$

$$E = \frac{\sqrt{\alpha}.\xi.\mathrm{Z} + \chi.\left[\Psi.\left(\frac{sin\left(\sqrt{\alpha}.T.D\right)}{\sqrt{\alpha}.T} + cos\left(\sqrt{\alpha}.T.D\right) - D\right) + \Lambda.\left(1 - cos\left(\sqrt{\alpha}.T.D\right)\right)\right]}{\chi^2 + \xi^2}$$

where:

$$\chi = \left[\cos\left(\sqrt{\alpha}.T\right).sin\left(\sqrt{\alpha}.T.D\right) + \sin\left(\sqrt{\alpha}.T\right).cos\left(\sqrt{\alpha}.T.D\right) - \sin\left(\sqrt{\alpha}.T.D\right)\right] \ ;$$

$$\xi = \left[\sin\left(\sqrt{\alpha}.T\right).sin\left(\sqrt{\alpha}.T.D\right) + \cos\left(\sqrt{\alpha}.T\right).cos\left(\sqrt{\alpha}.T.D\right) + \cos\left(\sqrt{\alpha}.T.D\right)\right] \ ;$$

$$\mathrm{Z} = \left[Q_{BEP}.(1 - D).T + \frac{sin\left(\sqrt{\alpha}.T.D\right)}{\sqrt{\alpha}}.(\Psi - \Lambda) + \frac{\Psi}{\alpha.T}.\left(1 - cos\left(\sqrt{\alpha}.T.D\right)\right) + \frac{\Psi.T}{2}.(1 - D^2) + \Lambda.T.(D - 1)\right]$$

Appendix C

Flow Data and Experimental Analysis

C.1 Pump Characteristics and ECV Operation

Before Tests using the active IFS could begin, the BEP data for each pump operating power had to be established. A full summary of the BEP data obtained from initial testing of the centrifugal pump is presented in **Table C-1**. **Figure C-1** then shows the variation in characteristic pumping curve for each applied voltage to the Totton DC centrifugal pump and compares these curves to the manufacturer's data. It is immediately apparent that the experimental rig produces a different characteristic curve at an equal voltage to the manufacturer's data, however this was not deemed to be of any concern as the experimental curves provide a more accurate comparison for the discharge values with the IFS active.

Table C-1 – Pump BEP data for varying power input

Pump Voltage (V)	Q_{BEP} (l/s)	P_{BEP} (KPa)	P_{MAX} (KPa)
12	0.140	24.05	42
11	0.123	23.54	32
10	0.110	19.62	28
8	0.088	13.73	20
6	0.060	8.80	17

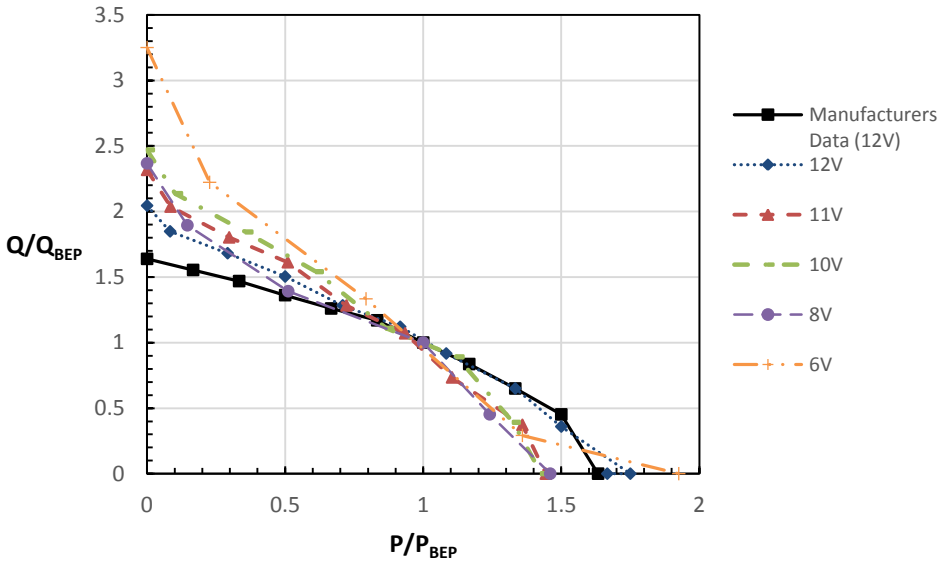

Fig. C-1 – Pump curve comparison for varying pump input voltage

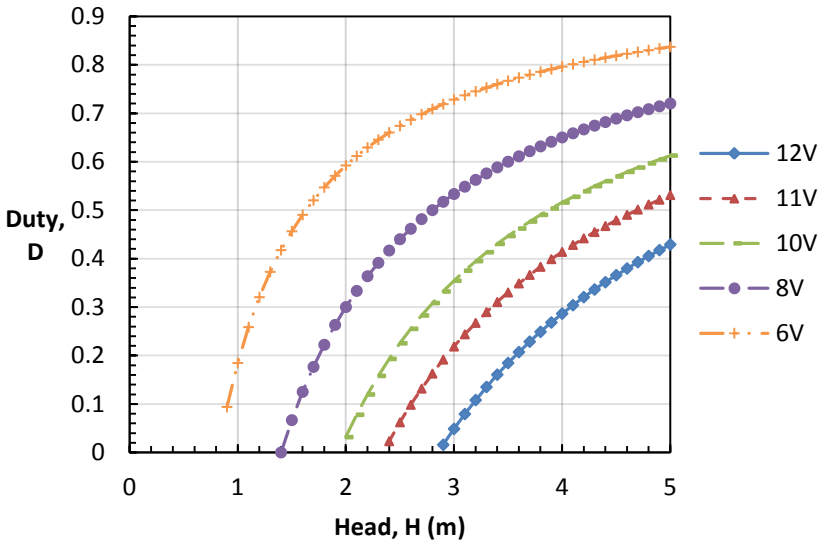

Fig. C-2 – Duty curve comparison for varying pump input voltage

From the BEP data it was possible to establish a duty curve for each pumping power and from these curves calculate the open and closed times for control of the ECV. The duty curves are shown in **Figure C-2**. As discussed in **Chapter 8** the times used in controlling the ECV, using the Arduino chip and program, had to be modified to compensate for delays in the opening and closing times of the valve. For each test duty

the IFS was run using the theoretical open time and then manually modified so as the piezo-electric reading for valve position matched the correct open and closed times. A full list of these times compared to their theoretical counterparts for all tests is shown in **Table C-2** (*NB for constant duty tests at 10V, 8V and 6V the theoretical operational times at 0.5 duty of 150ms both ways were modified to 52ms and 248ms open and closed times respectively at frequency ratio* $r = 2$).

Table C-2 – ECV operating times for all tests

Pump Voltage (V)	Frequency Ratio, r	Load Pressure (KPa)	Duty	Theoretical ECV Times (ms)		Actual ECV Times (ms)	
				t_o	t_c	t_o	t_c
12	1.5	36	0.21	84	316	15	385
		41	0.31	124	276	34	366
		46	0.38	152	248	62	338
	2	41	0.31	93	207	15	285
		46	0.38	114	186	24	276
11	1.5	32	0.24	96	304	15	385
		36	0.35	140	260	55	345
		41	0.43	172	228	72	328
		46	0.49	196	204	97	303
	2	36	0.24	105	195	20	280
		41	0.35	129	171	39	261
		46	0.43	147	153	57	243
10	1.5	26	0.25	98	302	20	380
		31	0.37	148	252	52	348
		36	0.46	182	218	82	318
		42	0.53	212	188	112	288
		46	0.57	228	172	128	272
	2	26	0.25	74	226	13	287
		32	0.37	111	189	18	282
		36	0.46	137	163	44	256
		42	0.53	159	141	59	241
		46	0.57	171	129	62	238
	2.5	26	0.25	59	181	12	228
		32	0.37	89	151	13	227
		36	0.46	109	131	31	209
		42	0.53	125	115	25	215
		46	0.57	137	103	47	193
	3	42	0.52	104	96	15	185
	3.5	42	0.52	88	82	15	165
8	1.5	17	0.19	76	324	12	388
		22	0.37	148	252	54	346
		26	0.47	189	211	89	311
		31	0.56	224	176	130	270
		36	0.62	248	152	148	252
		42	0.67	268	132	168	232

Pump Voltage (V)	Frequency Ratio, r	Load Pressure (KPa)	Duty	Theoretical ECV Times (ms)		Actual ECV Times (ms)	
				t_o	t_c	t_o	t_c
8	1.5	46	0.70	280	120	180	220
	2	17	0.19	57	243	12	288
		22	0.37	113	187	20	280
		26	0.47	142	158	40	260
		31	0.56	168	132	72	228
		36	0.62	186	114	86	214
		42	0.67	201	99	101	199
		46	0.70	210	90	110	190
	2.5	17	0.19	46	194	12	228
		22	0.37	91	149	13	227
		26	0.47	114	126	19	221
		31	0.56	134	106	37	203
		36	0.62	149	151	40	251
		42	0.67	160	80	60	180
		46	0.70	168	72	68	172
6	1.5	12	0.27	108	292	15	285
		17	0.48	192	208	92	308
		22	0.6	240	160	140	260
		26	0.66	264	136	158	242
		31	0.72	288	112	188	212
		36	0.76	304	96	202	198
		42	0.79	316	84	216	184
		46	0.81	324	76	224	176
	2	12	0.27	81	219	13	287
		17	0.48	144	156	40	260
		22	0.6	180	120	80	220
		26	0.66	198	102	98	202
		31	0.72	216	84	116	184
		36	0.76	228	72	128	172
		42	0.79	237	63	147	153
		46	0.81	243	57	143	157
	2.5	12	0.27	65	175	13	227
		17	0.48	115	125	19	221
		22	0.6	144	96	30	210
		26	0.66	158	82	58	182
		31	0.72	173	67	73	167
		36	0.76	182	58	82	158
		42	0.79	190	50	90	150
		46	0.81	194	46	94	146

C.2 Experimental Procedure

The following is a summary of the experimental procedure observed during the acquisition of the final test data presented in this chapter. The procedure assumes a starting point directly after the previous test and so begins with the pumping system fully primed.

C.2.1 Setting the Test Head

- Gate valve between the capacitance chamber and adjustable head assembly fully closed, decoupling head from pumping system.
- Water column drained from the vertical discharge pipe assembly by unscrewing the release cap at the base of the assembly.
- Water cap is replaced.
- Adjustable head assembly is modified to the appropriate testing height by addition or subtraction of pipe work.
- Pipe work is added by loosening quick release locks on both parallel sections of the assembly in addition to the rail clamps located behind the pipe work for any sections above those being modified. The entire piping section is then elevated by an increment of 0.5m to accommodate the additional pipe work and the rail clamps re-tightened. Additional pipe work is then fitted securely in place by tightening torsion locks.
- Pipe work is subtracted in a similar fashion to the addition of pipe work; however instead of elevating the entire pipe work section, the section is lowered after the removal of both parallel 0.5m sections of pipe.

C.2.2 Priming the Pumping System

- Gate valve between the capacitance chamber and adjustable head assembly is set to fully open position to release the pressure in the capacitance chamber.
- ECV control system is checked to be in OFF state, hence ECV closed.
- Variable DC power supply is set to required testing voltage.
- Power supply is turned ON, enabling action of the centrifugal pump.
- Pressure gauge is monitored until it either reaches a stable pressure, or discharge flow is obtained at the output of the system (in the cases of lower testing heads).
- Centrifugal pump is turned OFF.
- Test rig is checked for leaks and pressure gauge is monitored for any drops in system pressure.
- Leaks are dealt with by tightening, and if necessary replacing or re-fitting, joints between subsystems and pipe work.
- If system appears to be stable the capacitance chamber is checked for any trapped air which could cause unwanted changes in capacitance.
- To check the capacitance chamber, the ball valve on the top of the chamber is opened gradually to bleed any air from within. If only water is forced out then the chamber is fully primed.

C.2.3 Programming the ECV and system Duty

- The theoretical duty tables are consulted based on the relevant testing pressure readout from the pressure gauge after system priming.
- Times t_o and t_c are calculated based on the system time period and duty.

- Operation times are adjusted accordingly on the ECV control program and uploaded to the Arduino control chip from the laboratory computer.
- The LED monitoring light is monitored during the upload to ensure the data transfer is complete.
- The centrifugal pump and ECV are powered ON simultaneously.
- The flows through the return pipe after the ECV and the discharge pipe are monitored along with the pressure gauge until the system is operating stably.
- The data acquisition software is run to collect data for a single session (2s at 1KHz = 2000 data points).
- Both centrifugal pump and ECV are turned OFF.
- Data from the test period is analyzed and the physical readout from the piezo-electric transducer is checked for a match with the operating times of the ECV (also plotted as the digital signal sent from the Arduino control chip to the valve.
- If the actual performance of the valve does not match the programmed performance a not is made on the differences between both open and closed times.
- The Arduino control chip is re-programmed with adjusted operating times.
- The ECV operation test process is repeated until the physical valve timing matches the theoretical duty timings for the current testing system pressure.

C.2.4 Collecting Flow Data

- Before starting the flow analysis for a test condition it is ensured the system is stable, leak free and has the correct ECV operation and system pressure.

- The centrifugal pump and ECV are turned ON.
- First, the instantaneous flow data is collected. The data acquisition software is run for a single period.
- Data collected is then transferred to a Microsoft™ Excel spreadsheet and checked to ensure there are no issues with the data collection or signals from each input. This includes loss of signal strength due to failing batteries in the amplifier.
- Assuming there are no issues, the data acquisition software is run three times, each time saving the data file into an Excel spreadsheet and filing in the appropriate destination for later analysis.
- With the system at stable operation the discharge flow is manually diverted into a water storage container whilst simultaneously starting a stopwatch.
- The discharge flow is collected for a period of 1 minute at which point the flow is diverted back into the secondary container which is continuously emptied into the lab drains.
- The container is weighed using a set of digital scales (accurate to $0.05Kg$ equivalent to $0.05\ l/s$) and water mass found by subtracting the mass of the container.
- The total value is noted for analysis.
- This process is repeated until three steady results have been obtained.
- The centrifugal pump and ECV are turned OFF.
- End single testing phase.

C.3 Data Manipulation

As discussed briefly in **Chapter 8**, the data collected from the pressure transducers during the experimental tests allowed for the analysis of transient flow data. The process for manipulating and analysing this data is described in this section. Firstly, **Figure C-3** shows the raw pressure transducer data as it was exported into the analysis spreadsheet.

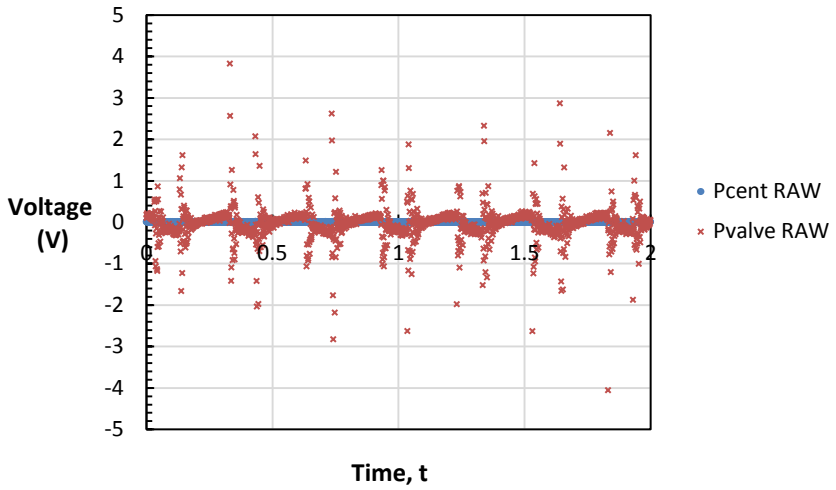

Fig. C-3 – Raw voltage data from the pump and valve transducers in the inductance pipe

In addition to the voltage data from the pressure transducers, there was also the data from the ECV, including both operating signal and transducer output. These were matched with the inductance pipe transducer traces immediately upon exporting to the spreadsheet. However, as the inductance flow transducers required more manipulation it is more beneficial to describe their process separately. Once the raw data was obtained, it was multiplied to eliminate any of the amplification used during the acquisition process. Further, the individual transducers were then calibrated for low pressure applications according to the manufacturer's guidelines. This translated the voltage data into useable pressure data. Before the pump and valve pressures

could be used to create a pressure difference,ΔP, needed to calculate the output flow, the data was filtered to eliminate any excessively high spikes. This was only necessary for valve sensor, which experienced some values which were uncharacteristically high when compared with the rest of the data. The calibrated and filtered data is shown by **Figure C-4** (filtered data is represented by the green line).

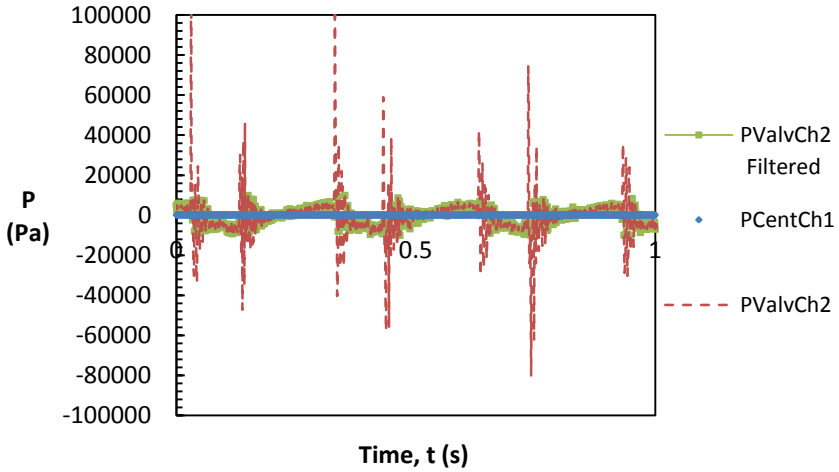

Fig. C-4 – Duty curve comparison for varying pump input voltage

The filtered data was then used to produce a value for ΔP, needed for the final flow data. After discovering that the final flow output had a drift, a shift function was imposed on the ΔP value as a means of negation. **Figures C-5** and **C-6** demonstrate the ΔP and final flow traces before and after the shift to demonstrate its effect on the final data output. Although the effect of the pressure difference shift is seen to be minimal, its effect on the final flow trace is immediately apparent.

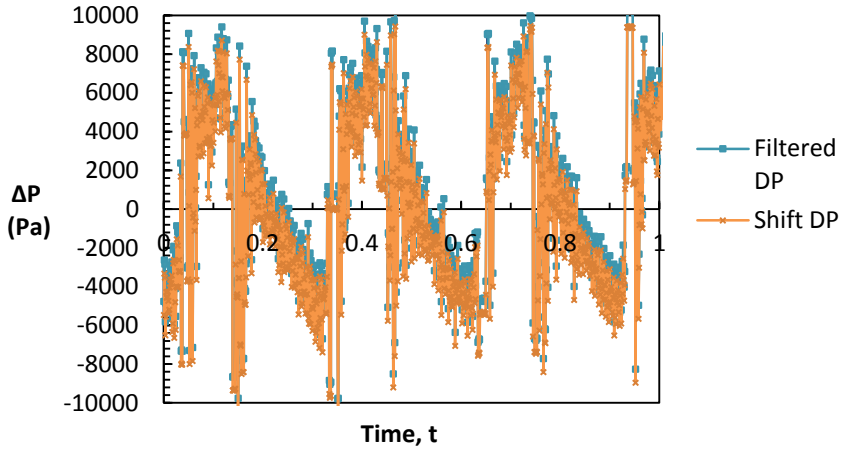

Fig. C-5 – Comparison of modified and unmodified pressure difference traces

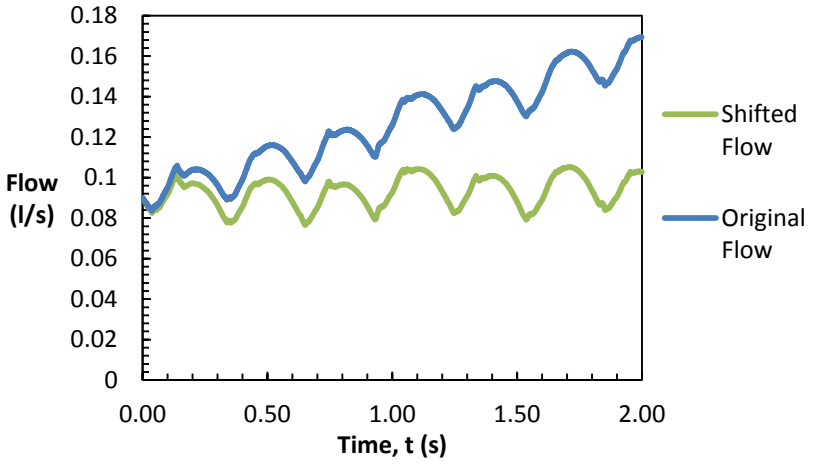

Fig. C-6 – Effect of pressure difference shift on flow trace

Using the filtered and shifted data it was possible to calculate the overall flow traces using **Eqn. C-1**:

$$Q = \int -\frac{\Delta P}{L}\, dt \qquad \textbf{Eqn. C-1}$$

This was derived from the use of Euler's equation, **Eqn. C-2**, given that the inductance pipe may be considered to be a short, rigid pipe with uniform cross section and no change in height across the inductance pipe length. This manipulation finds **Eqn. C-3**:

$$\frac{1}{\rho}\frac{dP}{ds} + \frac{du}{dt} + g\frac{dz}{ds} = 0 \qquad \textbf{Eqn. C-2}$$

$$\frac{1}{\rho}\frac{dP}{ds} + \frac{\partial u}{\partial t} = 0 \qquad \textbf{Eqn. C-3}$$

Further, as discussed in the definition of inductance in **Chapter 4** the change in length ds is replaced with Δs and the velocity converted to flow via $Q = u.A$, thus (recalling the definition of inductance across a unit length) **Eqn. C-4** is found from **Eqn. C-1.**

$$\frac{\Delta P}{\Delta s} = -\frac{\rho}{A}\frac{\partial Q}{\partial t} \qquad \textbf{Eqn. C-4}$$

The integral of ΔP was found using the trapezium rule between successive points from the data spreadsheet, such that:

$$\Delta Q = -\frac{t\times 0.5\times(\Delta P_n + \Delta P_{n+1})}{L} = \frac{-1}{2L}\int_n^{n+1} \Delta P \; dt \qquad \textbf{Eqn. C-5}$$

This gave the average flow difference between two successive points, with the initial point selected based on the physical discharge flow values found manually using the 'bucket and scale' technique described in **Chapter 8**, which would give the desired average flow. The time step used in all calculations was equal to the sampling rate between each data point in the spreadsheet. In the case of the tests performed, this was set at $2ms$. An example of the final flow trace is illustrated by **Figure C-7.**

As the positional data provided by the ECV piezoelectric transducer and Arduino control output was used only as a reference for the transient flows, its actual value was inconsequential. Therefore, applying a simple multiplier and data shift to the raw data in the analysis spreadsheet was sufficient to bring the ECV position traces onto the

same graphical display as the flow data. This made it far easier to analyse the flow-ECV relationship and spot any inconsistencies in the valve operation.

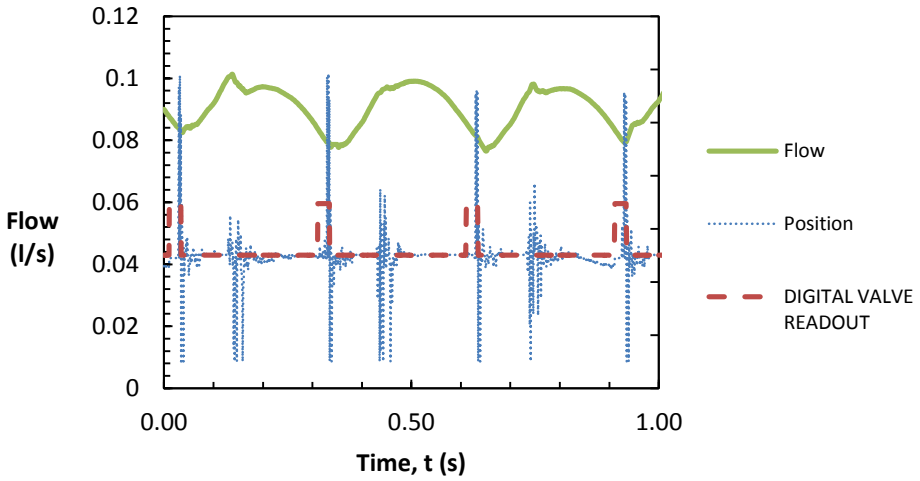

Fig. C-7 – Example of final ECV and flow traces

C.4 Experimental Discharge Flow Data

Discharge flow data was obtained as described in **Chapter 8** by taking measurements using digital scales and then converting the averages into flow rates in l/s. The digital scales were accurate to 2 decimal places in increments of $5g$ (giving accuracy in the measurements of flow to within $0.05\ l/s$). Corrected mass data in the tables was obtained by eliminating the mass of the measuring container. The tables in this section summarise the results from all of the experimental tests performed using the IFS rig and are included as a reference for the graphs presented in **Chapter 8**.

Table C-3. Discharge flow data without IFS at 12V

Pressure Reading (KPa)	Total Mass (kg)			Av Mass (kg)	Corrected Mass (kg)	Flow rate (l/s)
	Test 1	Test 2	Test 3			
0	9.95	9.95	9.95	9.95	9.20	0.3067
2	9.10	9.05	9.05	9.01	8.32	0.2772
7	8.35	8.30	8.30	8.31	7.57	0.2522
12	14.30	14.25	14.30	14.28	13.53	0.2256
17	12.35	12.25	12.30	12.30	11.55	0.1925
22	10.90	10.80	10.80	10.83	10.08	0.1681
26	9.00	9.00	9.00	9.00	8.25	0.1375
32	6.65	6.55	6.6	6.60	5.85	0.0975
36	3.95	4.00	4.00	3.98	3.23	0.0539
38	0	0	0	0	0	0.0000

Table C-4. Discharge flow data with IFS at 12V, r=2

Pressure Reading (bar)	Total Mass (kg)			Av. Mass (kg)	Corrected Mass (Kg)	Flow rate (l/s)
	Test 1	Test 2	Test 3			
42	5.10	5.10	5.10	5.10	4.35	0.0725
46	3.95	4.00	4.05	4.00	3.25	0.0542

Table C-5. Discharge flow data with IFS at 12V, r=1.5

Pressure Reading (KPa)	Total Mass (kg)			Av. Mass (kg)	Corrected Mass (kg)	Flow rate (l/s)
	Test 1	Test 2	Test 3			
36	5.45	5.50	5.45	5.47	4.72	0.0786
42	4.65	4.50	4.50	4.55	3.80	0.0633
46	3.45	3.55	3.55	3.52	2.77	0.0461

Table C-6. Discharge flow data without IFS at 11V

Pressure Reading (bar)	Total Mass (kg)			Av. Mass (kg)	Corrected Mass (kg)	Flow rate (l/s)
	Test 1	Test 2	Test 3			
0	9.60	9.40	9.50	9.50	8.75	0.2917
2	8.45	8.50	8.45	8.47	7.72	0.2572
7	7.60	7.60	7.60	7.60	6.85	0.2283
12	12.90	12.85	12.80	12.85	12.10	0.2017
17	10.50	10.35	10.40	10.42	9.67	0.1611
22	8.85	8.85	8.85	8.85	8.10	0.1350
26	6.25	6.50	6.35	6.37	5.62	0.0936
32	3.65	3.70	3.75	3.70	2.95	0.0492
34	0.00	0.00	0.00	0.00	0.00	0.0000

Table C-7. Discharge flow data with IFS at 11V, r=2

Pressure Reading (bar)	Total Mass (kg)			Av. Mass (kg)	Corrected Mass (kg)	Flow rate (l/s)
	Test 1	Test 2	Test 3			
32	5.50	5.50	5.50	5.50	4.75	0.0792
36	4.55	4.50	4.40	4.48	3.73	0.0622
42	3.50	3.20	3.25	3.32	2.57	0.0428
46	2.40	3.20	2.40	2.67	1.92	0.0319

Table C-8. Discharge flow data with IFS at 11V, r=1.5

Pressure Reading (bar)	Total Mass (kg)			Av. Mass (kg)	Corrected Mass (kg)	Flow rate (l/s)
	Test 1	Test 2	Test 3			
31	5.25	5.25	5.25	5.25	4.50	0.0750
36	3.90	3.90	3.85	3.88	3.13	0.0522
42	3.00	3.00	3.00	3.00	2.25	0.0375
46	2.15	2.15	2.15	2.15	1.40	0.0233

Table C-9. Discharge flow data without IFS at 10V

Pressure Reading (bar)	Total Mass (kg)			Av. Mass (kg)	Corrected Mass (kg)	Flow rate (l/s)
	Test 1	Test 2	Test 3			
0	8.90	8.90	8.90	8.90	8.15	0.2717
2	7.80	7.80	7.80	7.80	7.05	0.2350
7	6.80	6.85	6.85	6.83	6.08	0.2028
12	10.95	10.90	10.90	10.92	10.17	0.1694
17	8.15	7.75	8.30	8.07	7.32	0.1219
22	6.75	6.70	6.70	6.72	5.97	0.0994
26	3.00	3.50	3.50	3.33	2.58	0.0431
28	0.00	0.00	0.00	0.00	0.00	0.0000

Table C-10. Discharge flow data with IFS at 10V, r=2

Pressure Reading (bar)	Total Mass (kg)			Av. Mass (kg)	Corrected Mass (kg)	Flow rate (l/s)
	Test 1	Test 2	Test 3			
0.26	5.25	5.15	5.20	5.20	4.45	0.0742
0.31	4.55	4.50	4.60	4.55	3.80	0.0633
0.37	3.60	3.65	3.65	3.63	2.88	0.0481
0.42	3.10	3.10	3.10	3.10	2.35	0.0392
0.46	2.30	2.35	2.40	2.35	1.60	0.0267

Table C-11. Discharge flow data with IFS at 10V, r=1.5

Pressure Reading (bar)	Total Mass (kg)			Av. Mass (kg)	Corrected Mass (kg)	Flow rate (l/s)
	Test 1	Test 2	Test 3			
0.28	5.15	5.00	5.10	5.08	4.33	0.0722
0.32	3.80	3.70	3.65	3.72	2.97	0.0494
0.37	3.00	3.00	2.85	2.95	2.20	0.0367
0.44	2.70	2.60	2.65	2.65	1.90	0.0317
0.49	2.15	2.15	2.10	2.13	1.38	0.0231

Table C-12. Discharge flow data with IFS at 10V, r=2.5

Pressure Reading (bar)	Total Mass (kg)			Av. Mass (kg)	Corrected Mass (kg)	Flow rate (l/s)
	Test 1	Test 2	Test 3			
0.26	5.30	5.25	5.25	5.27	4.52	0.0753
0.31	4.50	4.60	4.60	4.57	3.82	0.0636
0.36	3.70	3.70	3.70	3.70	2.95	0.0492
0.42	3.00	3.00	3.10	3.03	2.28	0.0381
0.46	2.25	2.20	2.20	2.22	1.47	0.0244

Table C-13. Discharge flow data with IFS (Constant Duty, D = 0.5) at 10V, r=2

Pressure Reading (bar)	Total Mass (kg)			Av. Mass (kg)	Corrected Mass (kg)	Flow rate (l/s)
	Test 1	Test 2	Test 3			
0.01	12.75	12.75	12.75	12.75	12.00	0.2000
0.07	10.50	10.50	10.50	10.50	9.75	0.1625
0.12	9.65	9.60	9.70	9.65	8.90	0.1483
0.17	7.40	7.30	7.35	7.35	6.60	0.1100
0.22	5.55	5.55	5.95	5.68	4.93	0.0822
0.26	4.50	4.55	4.45	4.50	3.75	0.0625
0.31	3.90	3.50	3.40	3.60	2.85	0.0475
0.36	3.10	3.10	3.10	3.10	2.35	0.0392
0.42	2.40	2.45	2.60	2.48	1.73	0.0289
0.46	2.35	2.35	2.35	2.35	1.60	0.0267

Table C-14. Discharge flow data without IFS at 8V

Pressure Reading (bar)	Total Mass (kg)			Av. Mass (kg)	Corrected Mass (kg)	Flow rate (l/s)
	Test 1	Test 2	Test 3			
0.00	7.85	7.85	7.85	7.85	7.10	0.2367
0.02	6.40	6.45	6.45	6.43	5.68	0.1894
0.07	9.15	9.05	9.10	9.10	8.35	0.1392
0.12	6.65	6.85	6.75	6.75	6.00	0.1000
0.17	3.40	3.60	3.40	3.47	2.72	0.0453
0.18	0.00	0.00	0.00	0.00	0.00	0.0000

Table C-15. Discharge flow data with IFS at 8V, r=2

Pressure Reading (bar)	Total Mass (kg)			Av. Mass (kg)	Corrected Mass (kg)	Flow rate (l/s)
	Test 1	Test 2	Test 3			
0.17	4.95	4.95	4.90	4.93	4.18	0.0697
0.22	3.80	3.85	3.80	3.82	3.07	0.0511
0.26	2.90	2.75	2.80	2.82	2.07	0.0344
0.31	2.50	2.50	2.60	2.53	1.78	0.0297
0.36	2.10	2.20	2.10	2.13	1.38	0.0231
0.42	1.60	1.50	1.45	1.52	0.77	0.0128
0.46	1.50	1.55	1.60	1.55	0.80	0.0133

Table C-16. Discharge flow data with IFS at 8V, r=1.5

Pressure Reading (bar)	Total Mass (kg)			Av. Mass (kg)	Corrected Mass (kg)	Flow rate (l/s)
	Test 1	Test 2	Test 3			
0.17	4.60	4.60	4.55	4.58	3.83	0.0639
0.22	3.05	3.05	3.05	3.05	2.30	0.0383
0.26	2.30	2.30	2.30	2.30	1.55	0.0258
0.31	2.15	2.15	2.15	2.15	1.40	0.0233
0.36	1.40	1.50	1.50	1.47	0.72	0.0119
0.42	1.45	1.35	1.30	1.37	0.62	0.0103
0.46	1.50	1.55	1.50	1.52	0.77	0.0128

Table C-17. Discharge flow data with IFS at 8V, r=2.5

Pressure Reading (bar)	Total Mass (kg)			Av. Mass (kg)	Corrected Mass (kg)	Flow rate (l/s)
	Test 1	Test 2	Test 3			
0.17	4.90	4.90	4.95	4.92	4.17	0.06944
0.22	4.10	3.80	3.80	3.90	3.15	0.05250
0.26	3.25	3.20	3.20	3.22	2.47	0.04111
0.31	2.80	2.80	2.75	2.78	2.03	0.03389
0.36	2.40	2.40	2.40	2.40	1.65	0.02750
0.42	1.70	1.60	1.60	1.63	0.88	0.01472
0.46	1.30	1.30	1.35	1.32	0.57	0.00944

Table C-18. Discharge flow data with IFS (Constant Duty, D = 0.5) at 8V, r=2

Pressure Reading (bar)	Total Mass (kg)			Av. Mass (kg)	Corrected Mass (kg)	Flow rate (l/s)
	Test 1	Test 2	Test 3			
0.00	7.85	7.85	7.85	7.85	7.10	0.2367
0.02	10.15	10.35	10.35	10.28	9.53	0.1589
0.07	6.50	6.75	6.75	6.67	5.92	0.0986
0.12	5.35	5.40	5.40	5.38	4.63	0.0772
0.17	4.20	4.25	4.20	4.22	3.47	0.0578
0.22	3.40	3.35	3.40	3.38	2.63	0.0439
0.26	2.85	2.90	2.90	2.88	2.13	0.0356
0.31	2.35	2.40	2.40	2.38	1.63	0.0272
0.36	2.10	2.10	2.00	2.07	1.32	0.0219
0.42	1.85	1.80	1.80	1.82	1.07	0.0178
0.46	1.35	1.50	1.50	1.45	0.70	0.0117

Table C-19. Discharge flow data without IFS at 6V

Pressure Reading (bar)	Total Mass (kg)			Av. Mass (kg)	Corrected Mass (kg)	Flow rate (l/s)
	Test 1	Test 2	Test 3			
0.00	6.60	6.60	6.60	6.60	5.85	0.1950
0.02	8.75	8.75	8.75	8.75	8.00	0.1333
0.07	5.55	5.55	5.55	5.55	4.80	0.0800
0.10	1.80	1.80	1.80	1.80	1.05	0.0175
0.10	0.00	0.00	0.00	0.00	0.00	0.0000

Table C-20. Discharge flow data with IFS at 6V, r=2

Pressure Reading (bar)	Total Mass (kg)			Av. Mass (kg)	Corrected Mass (kg)	Flow rate (l/s)
	Test 1	Test 2	Test 3			
0.12	3.50	3.50	3.50	3.50	2.75	0.04583
0.17	2.65	2.65	2.65	2.65	1.90	0.03167
0.22	2.00	2.05	2.00	2.02	1.27	0.02111
0.26	1.75	1.75	1.75	1.75	1.00	0.01667
0.31	1.70	1.70	1.70	1.70	0.95	0.01583
0.36	1.30	1.30	1.30	1.30	0.55	0.00917
0.42	1.35	1.35	1.40	1.37	0.62	0.01028
0.46	1.35	1.35	1.40	1.37	0.62	0.01028

Table C-21. Discharge flow data with IFS at 6V, r=1.5

Pressure Reading (bar)	Total Mass (kg)			Av. Mass (kg)	Corrected Mass (kg)	Flow rate (l/s)
	Test 1	Test 2	Test 3			
0.12	3.20	3.20	3.20	3.20	2.45	0.0408
0.17	2.30	2.30	2.30	2.30	1.55	0.0258
0.22	1.85	1.80	1.75	1.80	1.05	0.0175
0.26	1.60	1.60	1.60	1.60	0.85	0.0142
0.31	1.60	1.55	1.55	1.57	0.82	0.0136
0.36	1.40	1.25	1.25	1.30	0.55	0.0092
0.42	1.35	1.35	1.40	1.37	0.62	0.0103
0.46	1.30	1.30	1.30	1.30	0.55	0.0092

Table C-22. Discharge flow data with IFS at 6V, r=2.5

Pressure Reading (bar)	Total Mass (kg)			Av. Mass (kg)	Corrected Mass (kg)	Flow rate (l/s)
	Test 1	Test 2	Test 3			
0.12	3.35	3.40	3.40	3.38	2.63	0.0439
0.17	2.85	2.75	2.75	2.78	2.03	0.0339
0.22	2.35	2.35	2.35	2.35	1.60	0.0267
0.26	1.95	2.00	1.95	1.97	1.22	0.0203
0.31	1.40	1.40	1.40	1.40	0.65	0.0108
0.36	1.45	1.40	1.40	1.42	0.67	0.0111
0.42	1.30	1.40	1.30	1.33	0.58	0.0097
0.46	1.40	1.30	1.35	1.35	0.60	0.0100

Table C-23. Discharge flow data with IFS (Constant Duty, D = 0.5) at 6V, r=2

Pressure Reading (bar)	Total Mass (kg)			Av. Mass (kg)	Corrected Mass (kg)	Flow rate (l/s)
	Test 1	Test 2	Test 3			
0.00	6.60	6.60	6.60	6.60	5.85	0.1950
0.02	7.40	7.55	7.55	7.50	6.75	0.1125
0.07	4.15	4.20	4.20	4.18	3.43	0.0572
0.12	2.85	2.90	2.85	2.87	2.12	0.0353
0.17	2.70	2.70	2.70	2.70	1.95	0.0325
0.22	2.25	2.25	2.25	2.25	1.50	0.0250
0.26	1.85	1.85	1.85	1.85	1.10	0.0183
0.31	1.60	1.50	1.50	1.53	0.78	0.0131
0.36	1.45	1.45	1.45	1.45	0.70	0.0117
0.42	1.35	1.35	1.35	1.35	0.60	0.0100
0.46	1.30	1.35	1.30	1.32	0.57	0.0094

C.5 Instantaneous Flow Data

After manipulating the experimental data as described in **Section C.3** a value could be calculated for the inductance pipe flow rate, Q_{L1}. A summary of these values for each test condition can be found in **Table C-24**. (*NB – as discussed in* **Chapter 8** *it was not possible to test at* $r = 2.5$ *for voltages above 10V due to the restricted operating speeds of the ECV. These values are blanked out in the summary table*).

Table C-24. Average inductance pipe flow from instantaneous flow data

Test Voltage (V)	Assembly Height (m)	Recorded Pressure (Kpa)	Flow rate (l/s)		
			r=1.5	r=2	r=2.5
12	4.00	36.0	0.090	-	-
	4.50	42.0	0.090	0.110	-
	5.00	46.0	0.070	0.090	-
11	3.50	32.0	0.105	0.120	-
	4.00	36.0	0.075	0.080	-
	4.50	42.0	0.060	0.070	-
	5.00	46.0	0.060	0.062	-
10	3.00	26.0	0.100	-	-
	3.50	32.0	0.070	0.120	0.110
	4.00	36.0	0.055	0.080	0.090
	4.50	42.0	0.070	0.080	0.080
	5.00	46.0	0.060	0.050	0.055
8	2.00	17.0	0.085	-	-
	2.50	22.0	0.060	0.080	0.900
	3.00	26.0	0.055	0.075	0.090
	3.50	32.0	0.050	0.065	0.065
	4.00	36.0	0.035	0.055	0.050
	4.50	42.0	0.045	0.055	0.045
	5.00	46.0	0.045	0.055	0.055
6	1.50	12.0	0.060	-	-
	2.00	17.0	0.055	0.060	0.055
	2.50	22.0	0.048	0.055	0.050

Test Voltage (V)	Assembly Height (m)	Recorded Pressure (Kpa)	Flow rate (l/s)		
			r=1.5	r=2	r=2.5
6	3.00	26.0	0.050	0.060	0.060
	3.50	32.0	0.050	0.055	0.050
	4.00	36.0	0.040	0.045	0.050
	4.50	42.0	0.045	0.055	0.055
	5.00	46.0	0.055	0.050	0.055

The full flow traces are divided into subsections, with each subsection presenting a series of data from a specific frequency ratio. Although the data was sampled for a period of 2s in all test cases, the flow traces have been adjusted to show a stable flow pattern for a period of 1.2s in the majority of cases and 1s for the tests at $r = 1.5$. This is adequate enough to show the evolution of flow for each test. Flow traces begin upon initiation of the data acquisition unit apart from in a minority of special cases. These cases present data from the first point of flow stabilization, but still display an equal number of time periods as all other tests (*NB – see **Figure C-70**, r=2.5, 6V, 4m assembly height, which begins at* $t = 1s$ *due to unforeseen fluctuations in the data during the first second of sampling*).

The same plot formatting is used in all figures, with the flow traces used represented by the following legend:

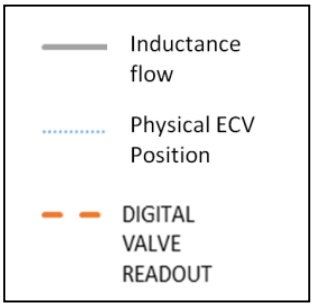

C.5.1 Frequency Ratio, r = 2

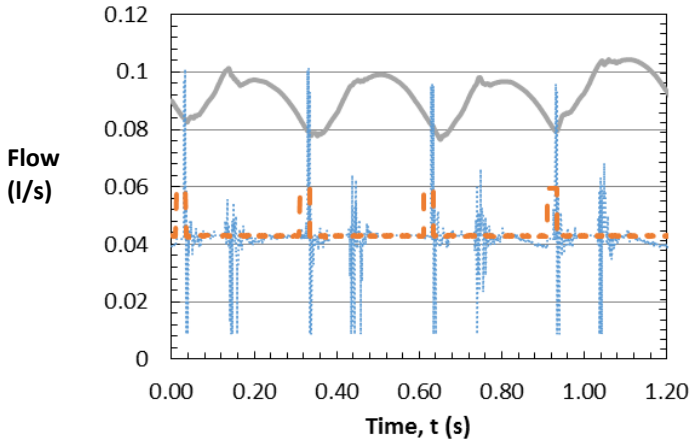

Fig. C-8 - 12V, r = 2, 5m assembly height

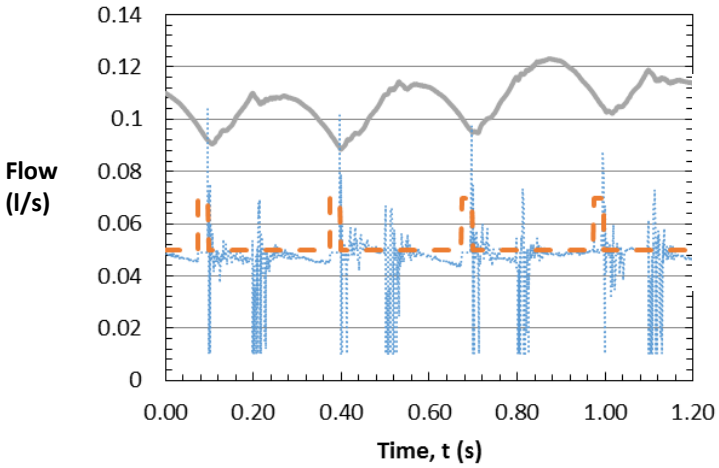

Fig. C-9 - 12V, r = 2, 4.5m assembly height

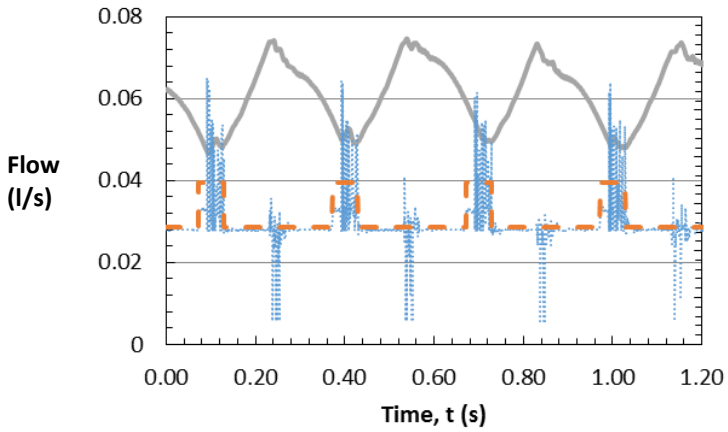

Fig. C-10 - 11V, r = 2, 5m assembly height

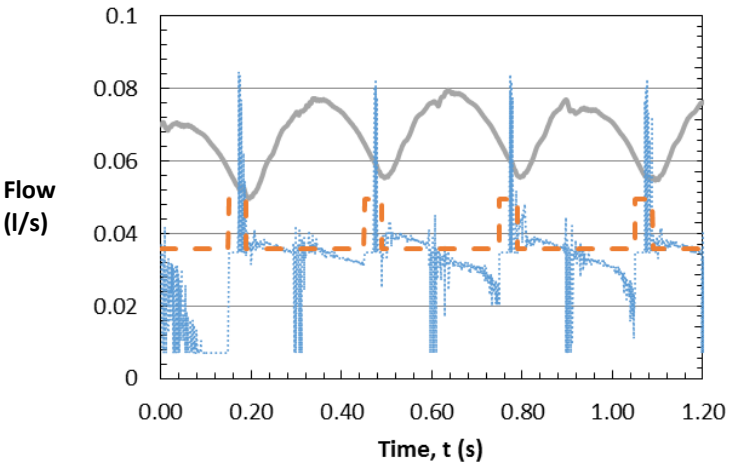

Fig. C-11 - 11V, r = 2, 4.5m assembly height

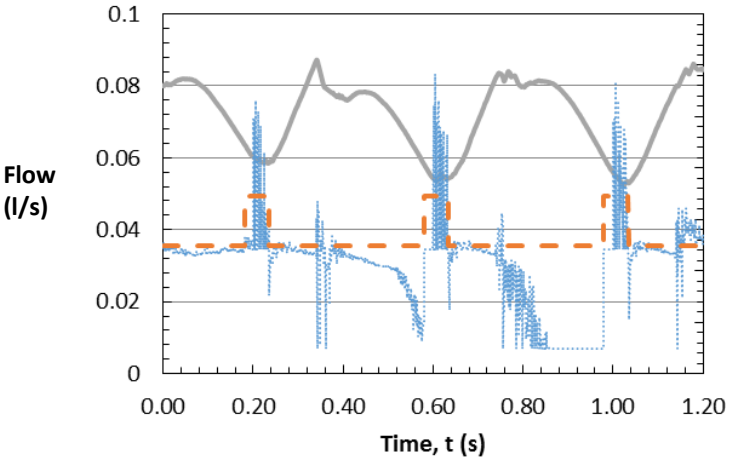

Fig. C-12 - 11V, r = 2, 4m assembly height

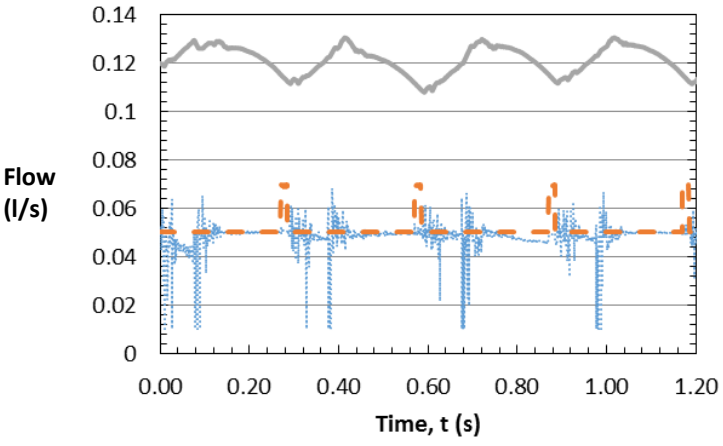

Fig. C-13 - 11V, r = 2, 3.5m assembly height

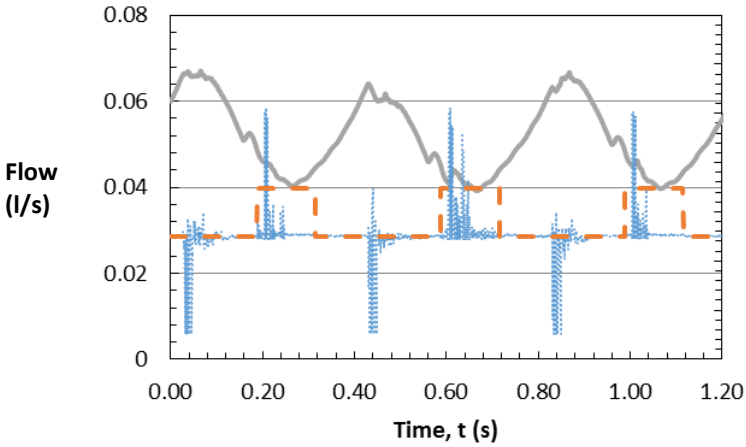

Fig. C-14 - 10V, r = 2, 5m assembly height

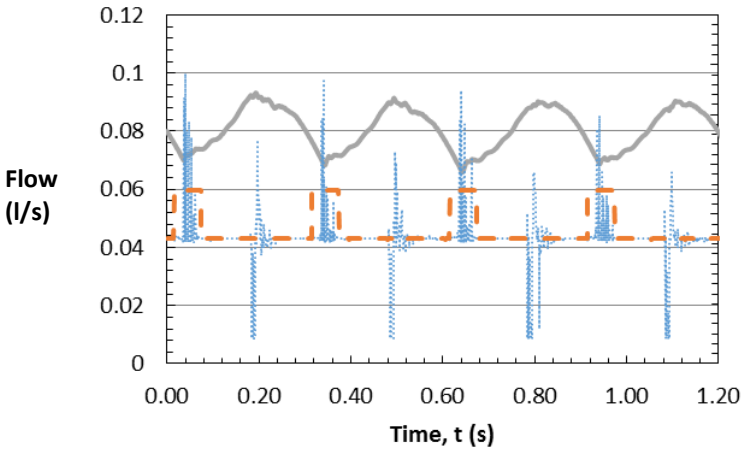

Fig. C-15 - 10V, r = 2, 4.5m assembly height

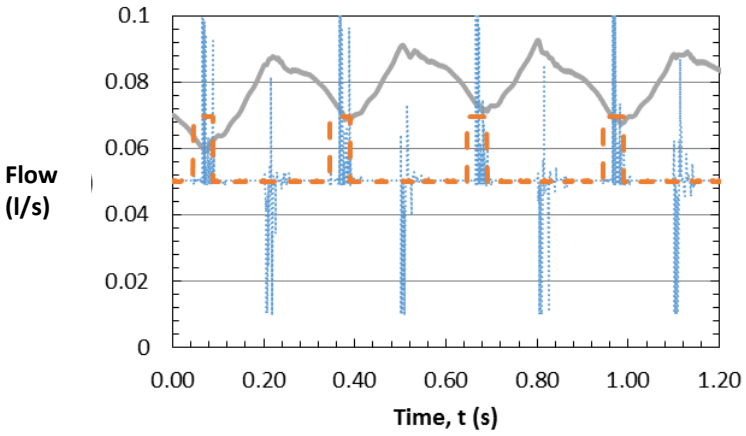

Fig. C-16 - 10V, r = 2, 4m assembly height

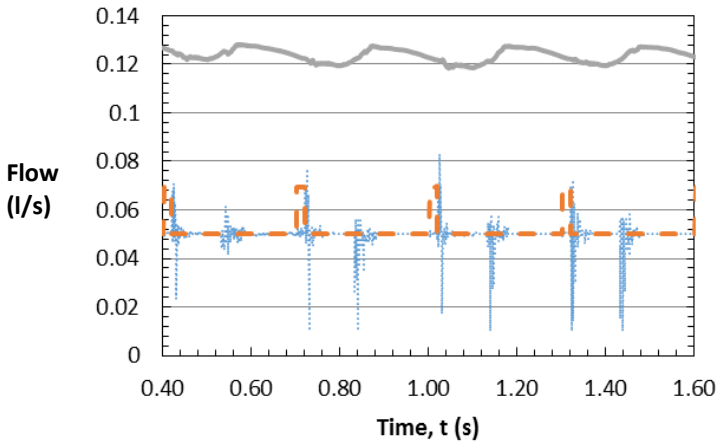

Fig. C-17 - 10V, r = 2, 3.5m assembly height

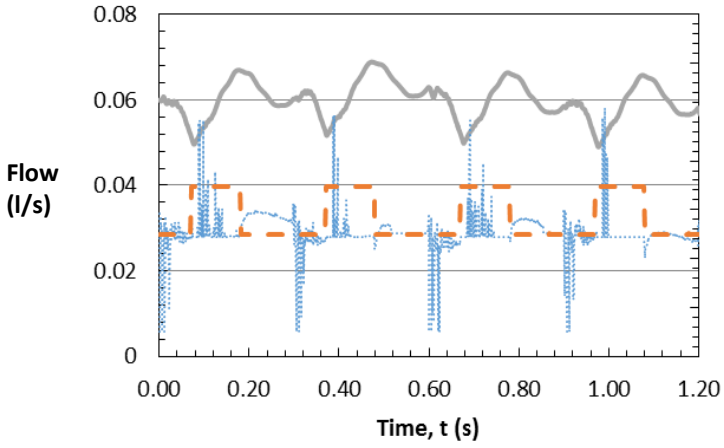

Fig. C-18 - 8V, r = 2, 5m assembly height

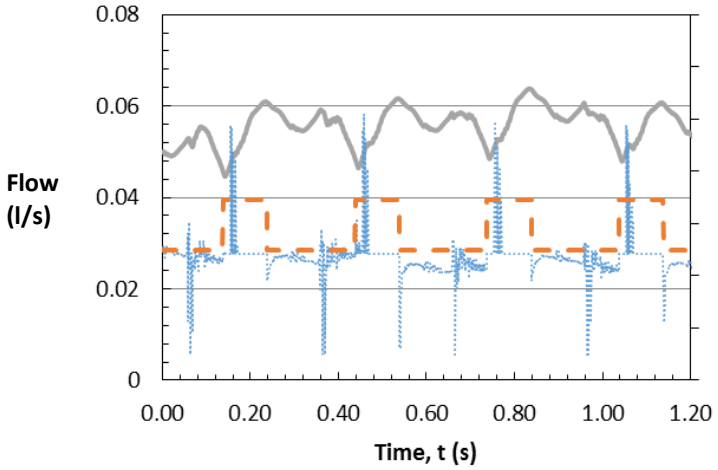

Fig. C-19 - 8V, r = 2, 4.5m assembly height

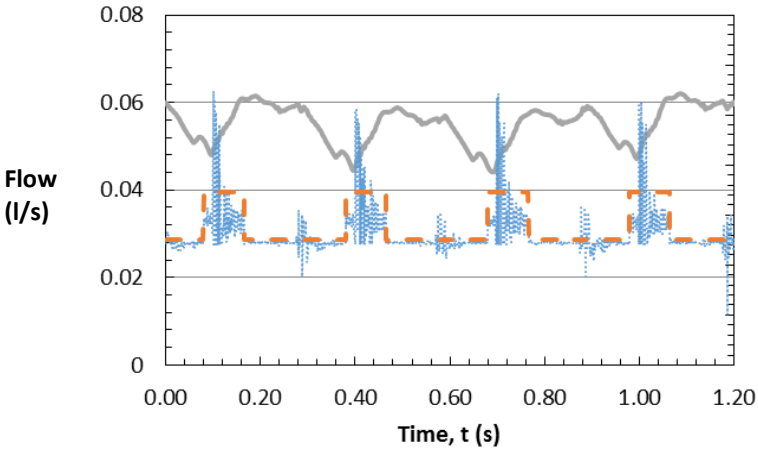

Fig. C-20 - 8V, r = 2, 4m assembly height

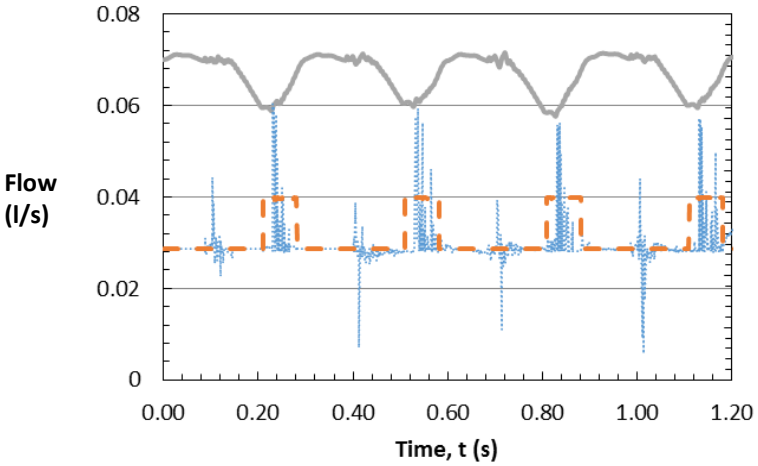

Fig. C-21 - 8V, r = 2, 3.5m assembly height

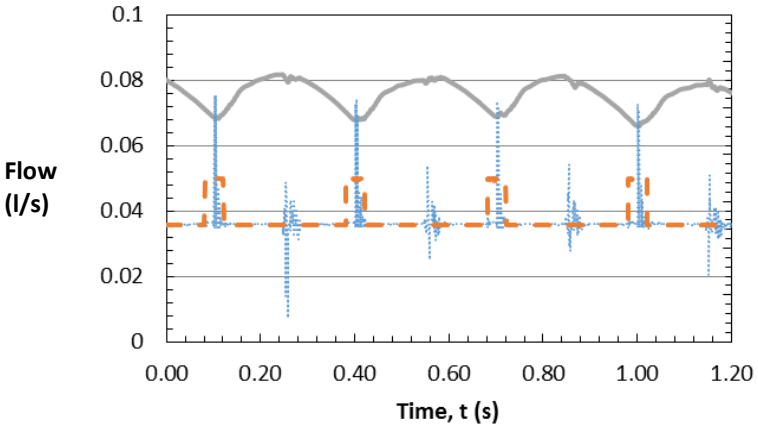

Fig. C-22 - 8V, r = 2, 3m assembly height

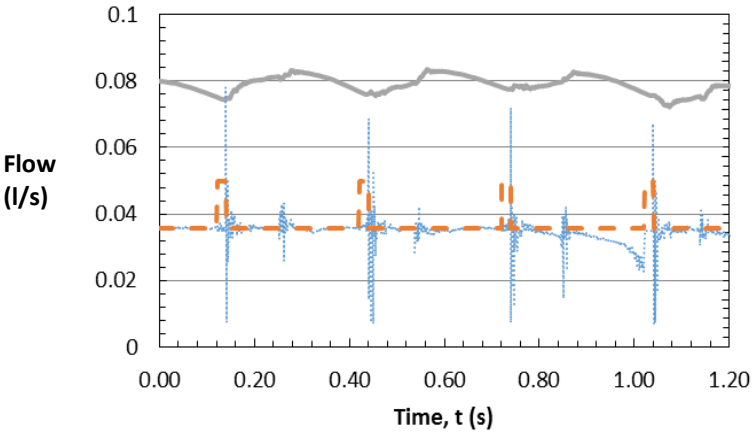

Fig. C-23 - 8V, r = 2, 2.5m assembly height

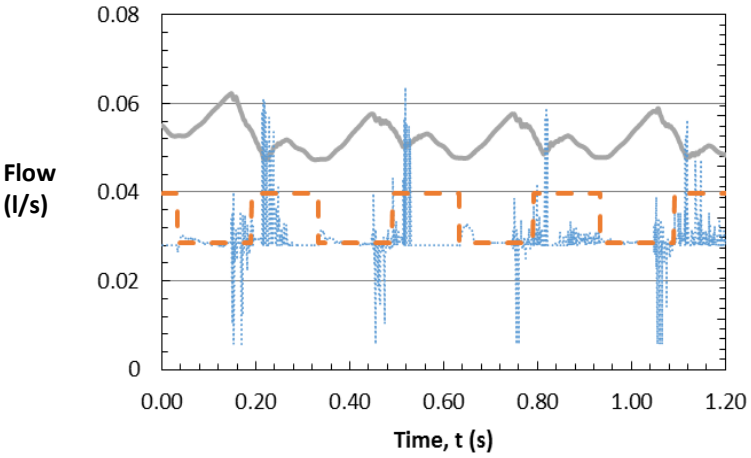

Fig. C-24 - 6V, r = 2, 5m assembly height

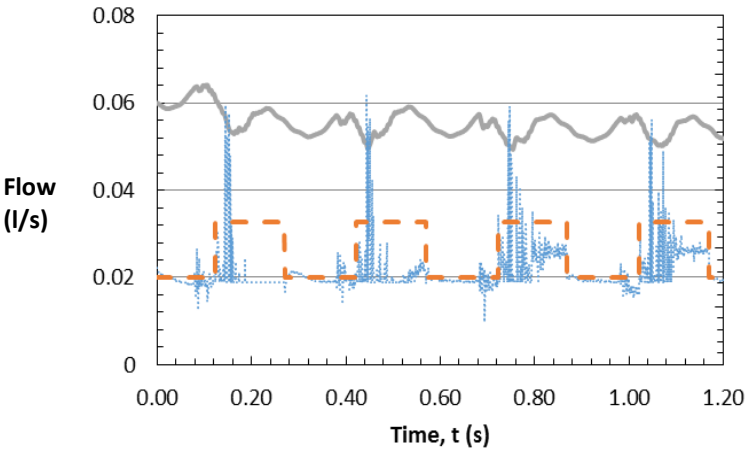

Fig. C-25 - 6V, r = 2, 4.5m assembly height

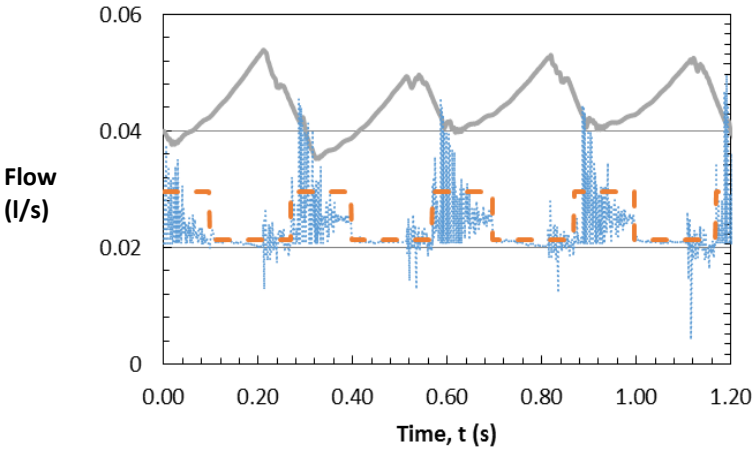

Fig. C-26 - 6V, r = 2, 4m assembly height

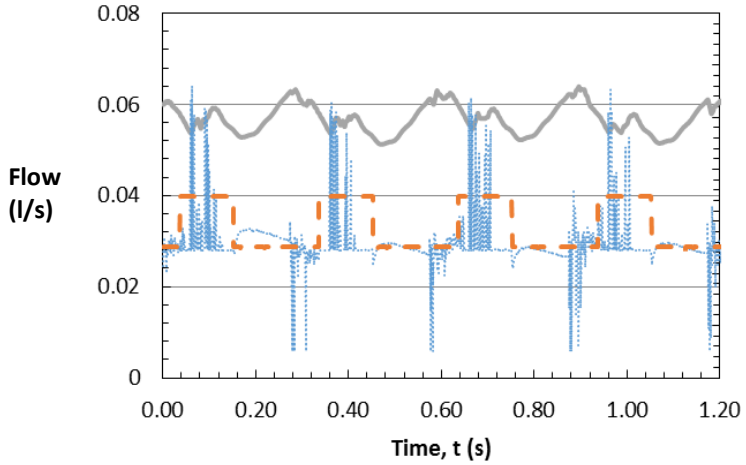

Fig. C-27 - 6V, r = 2, 3.5m assembly height

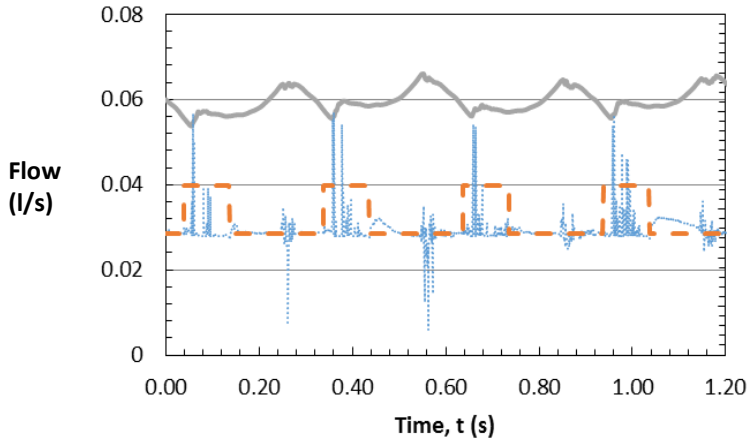

Fig. C-28 - 6V, r = 2, 3m assembly height

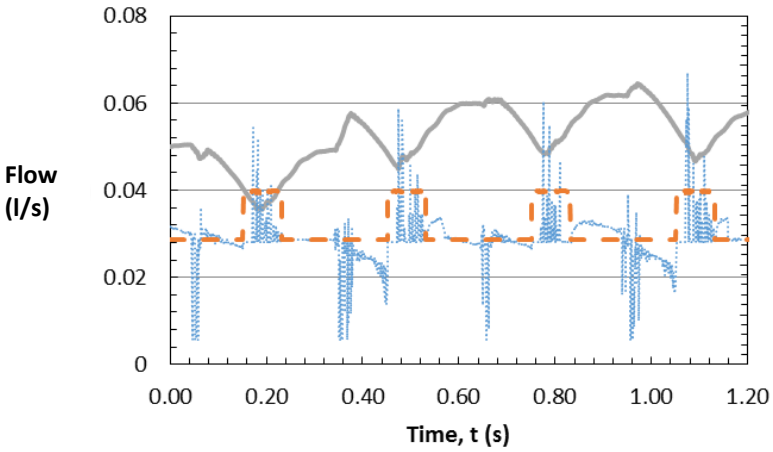

Fig. C-29 - 6V, r = 2, 2.5m assembly height

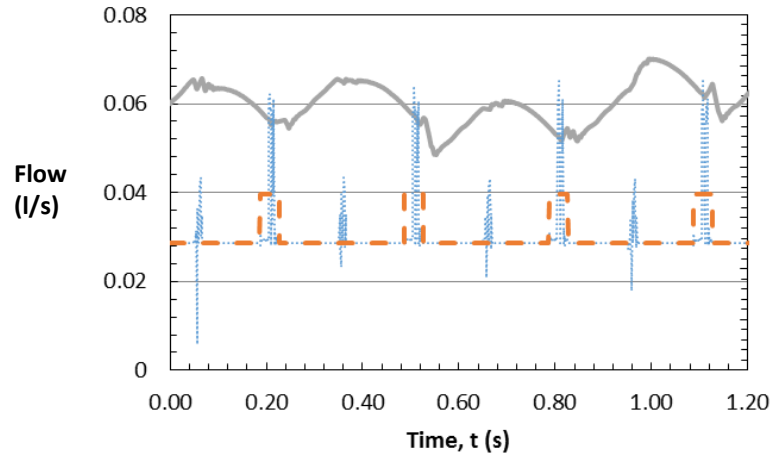

Fig. C-30 - 6V, r = 2, 2m assembly height

C.5.2 Frequency Ratio, r = 1.5

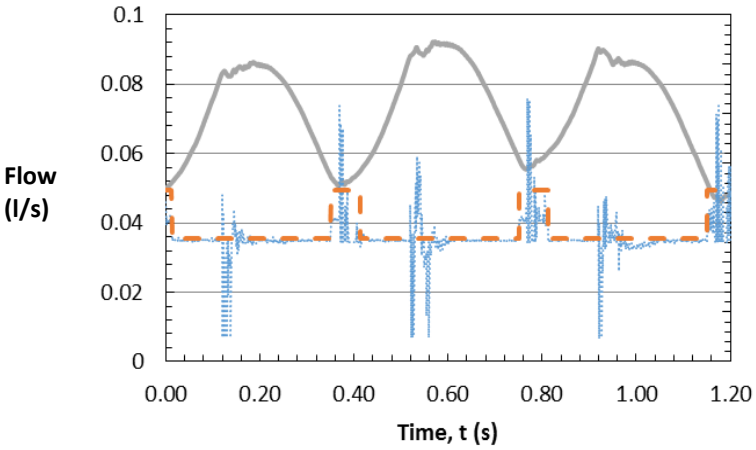

Fig. C-31 - 12V, r = 1.5, 5m assembly height

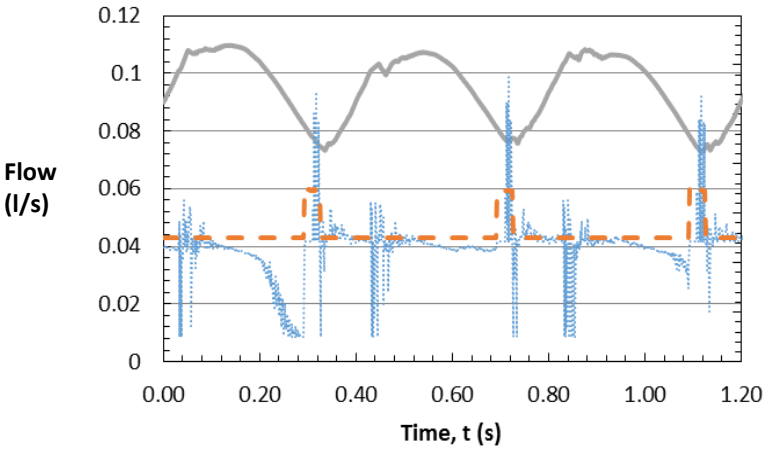

Fig. C-32 - 12V, r = 1.5, 4.5m assembly height

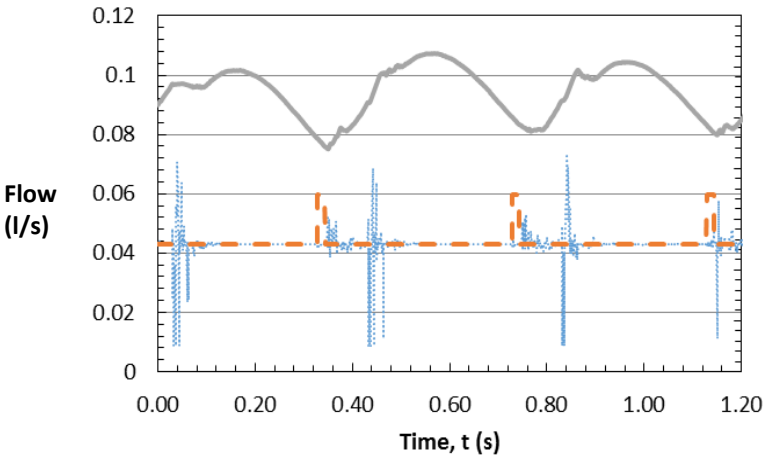

Fig. C-33 - 12V, r = 1.5, 4m assembly height

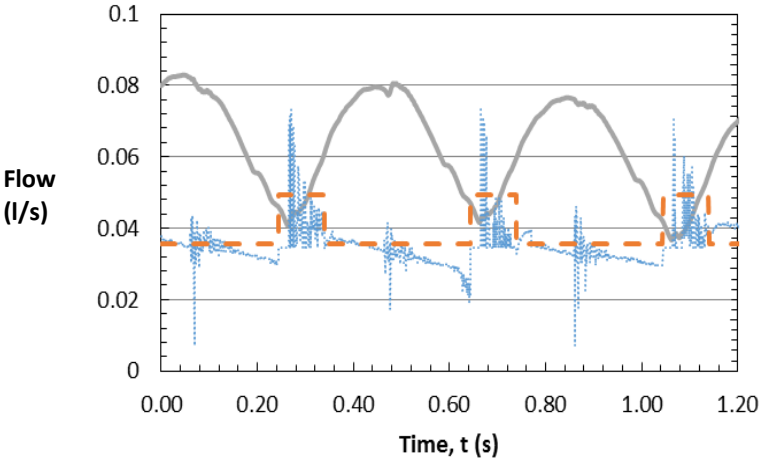

Fig. C-34 - 11V, r = 1.5, 5m assembly height

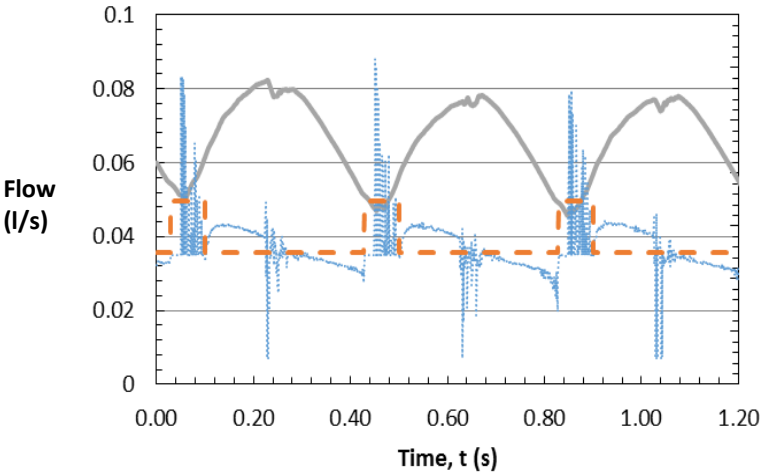

Fig. C-35 - 11V, r = 1.5, 4.5m assembly height

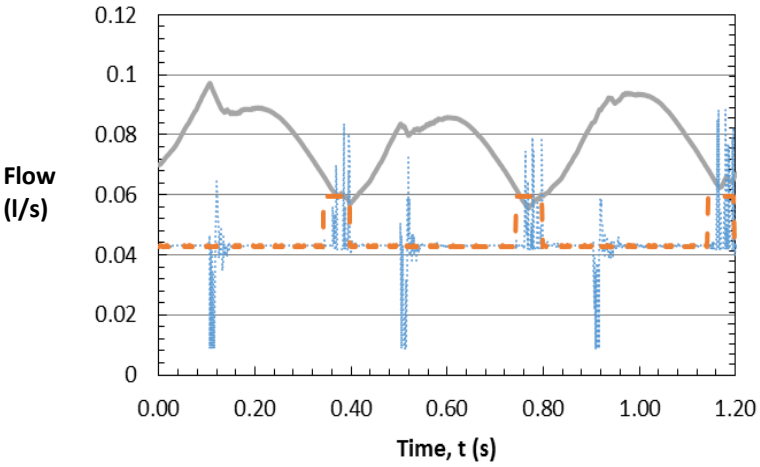

Fig. C-36 - 11V, r = 1.5, 4m assembly height

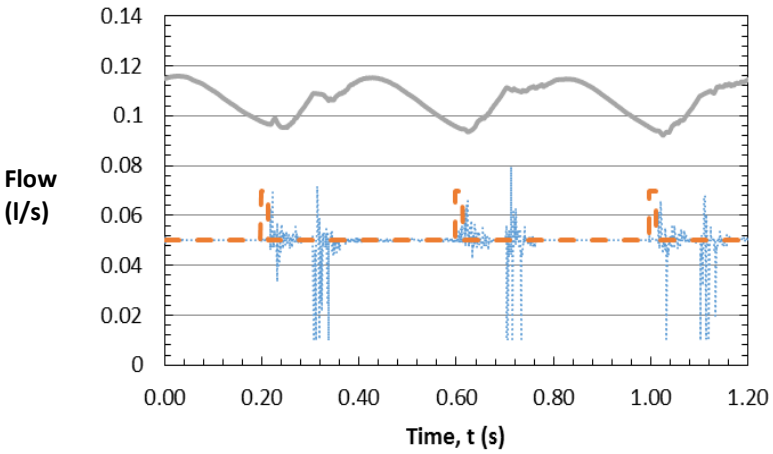

Fig. C-37 - 11V, r = 1.5, 3.5m assembly height

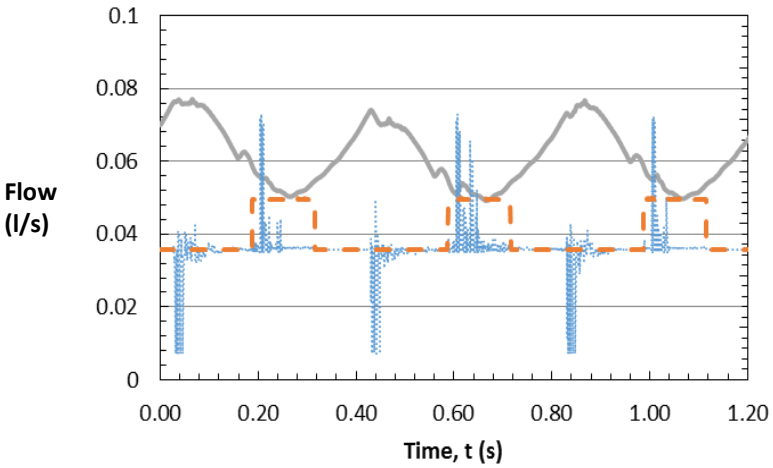

Fig. C-38 - 10V, r = 1.5, 5m assembly height

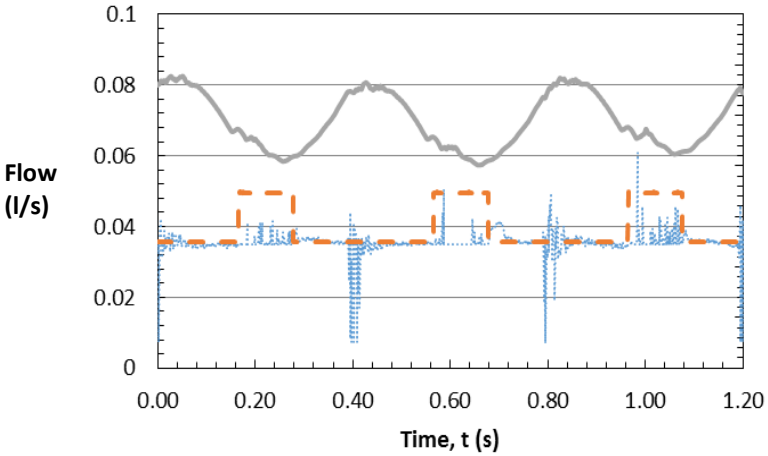

Fig. C-39- 10V, r = 1.5, 4.5m assembly height

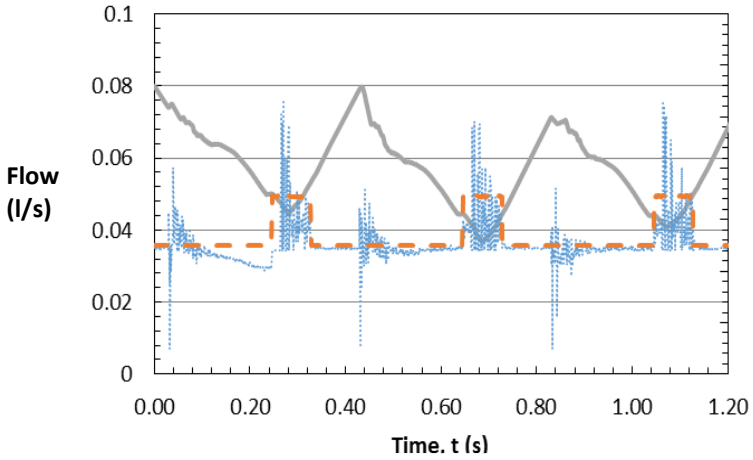

Fig. C-40 - 10V, r = 1.5, 4m assembly height

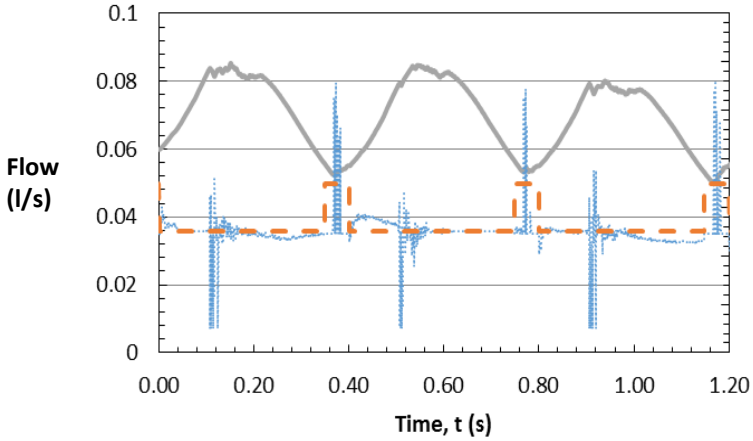

Fig. C-41 - 10V, r = 1.5, 3.5m assembly height

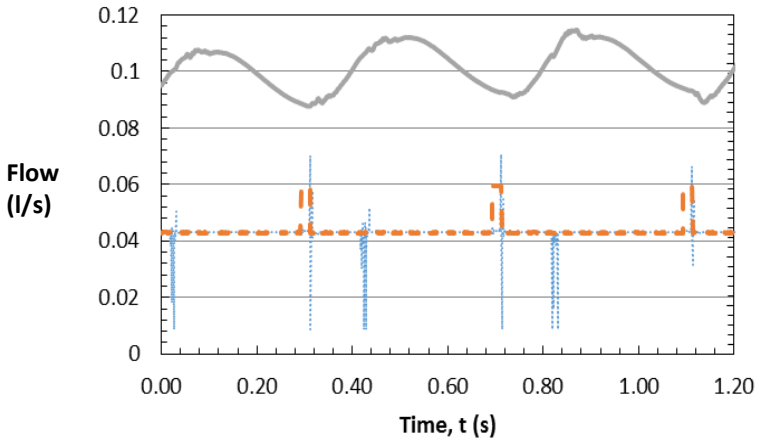

Fig. C-42 - 10V, r = 1.5, 3m assembly height

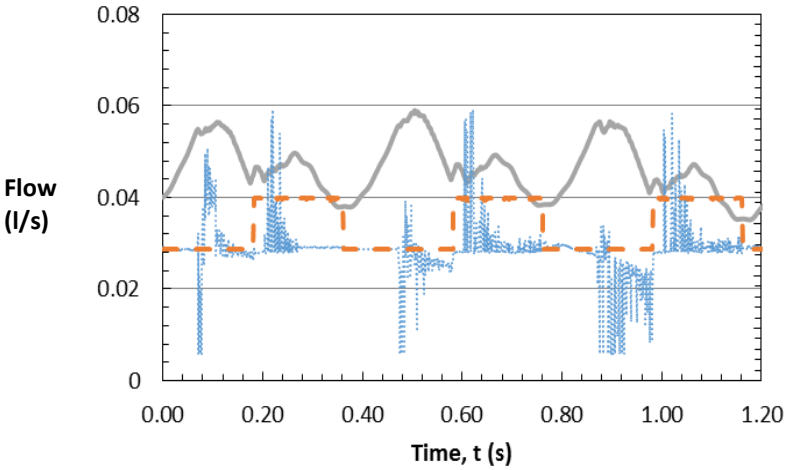

Fig. C-43 - 8V, r = 1.5, 5m assembly height

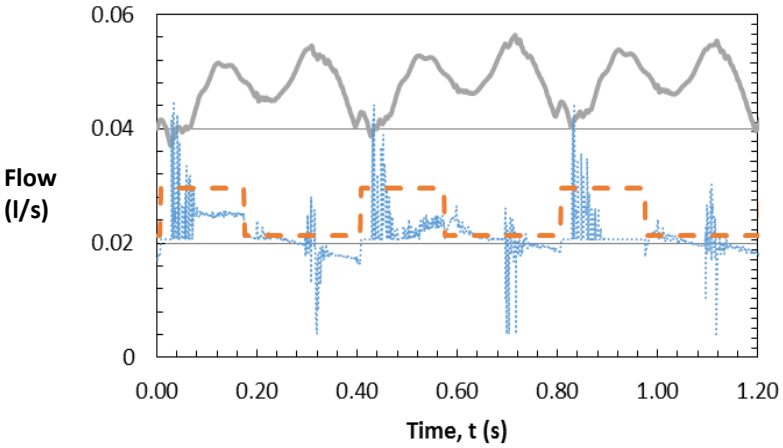

Fig. C-44 - 8V, r = 1.5, 4.5m assembly height

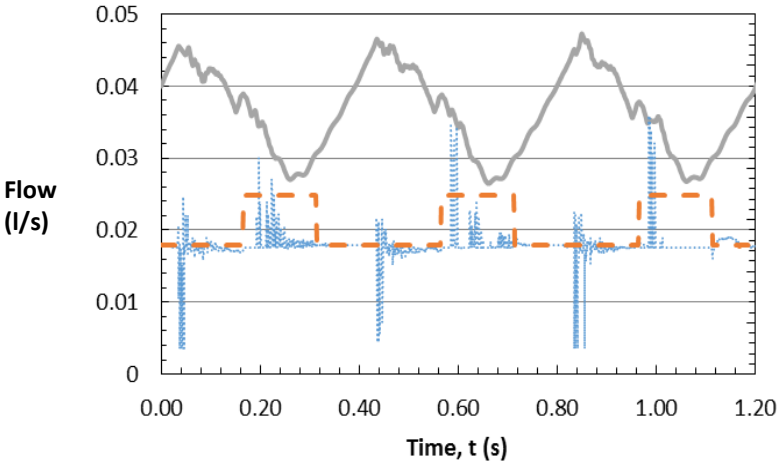

Fig. C-45 - 8V, r = 1.5, 4m assembly height

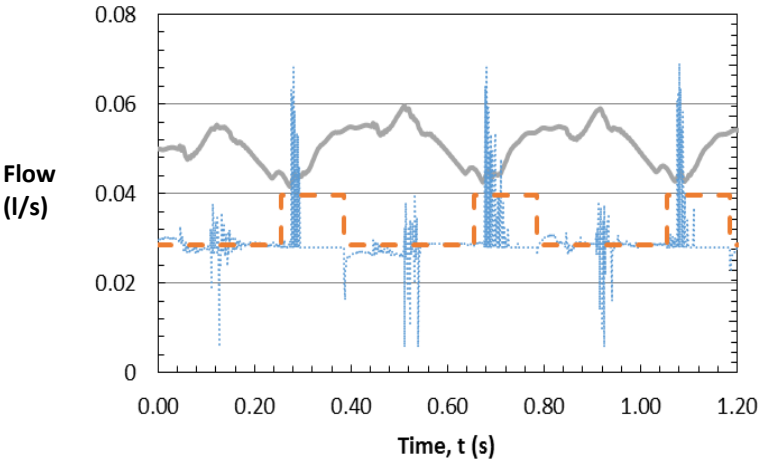

Fig. C-46 - 8V, r = 1.5, 3.5m assembly height

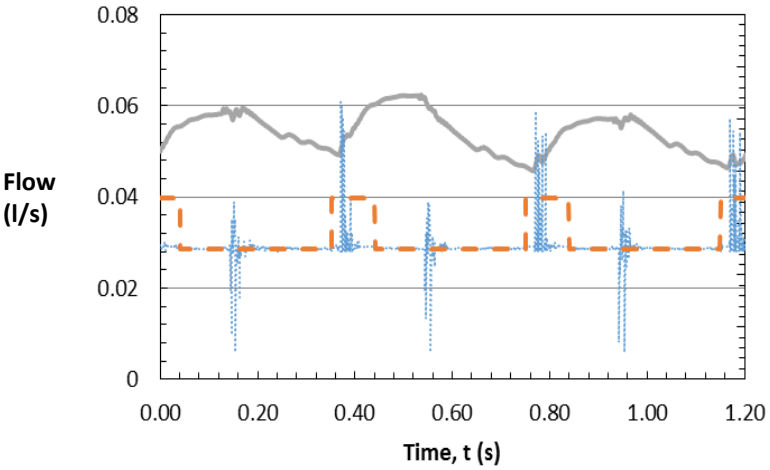

Fig. C-47 - 8V, r = 1.5, 3m assembly height

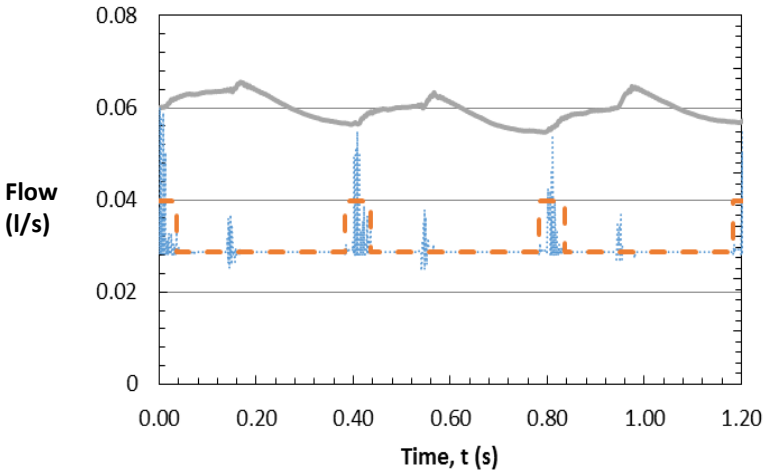

Fig. C-48 - 8V, r = 1.5, 2.5m assembly height

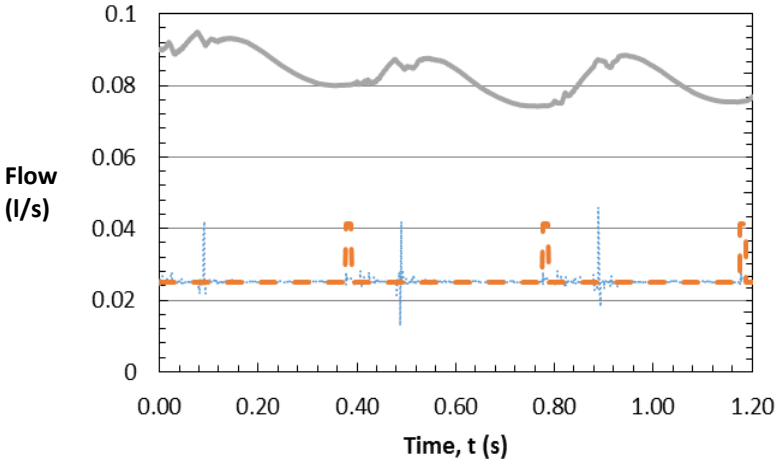

Fig. C-49 - 8V, r = 1.5, 2m assembly height

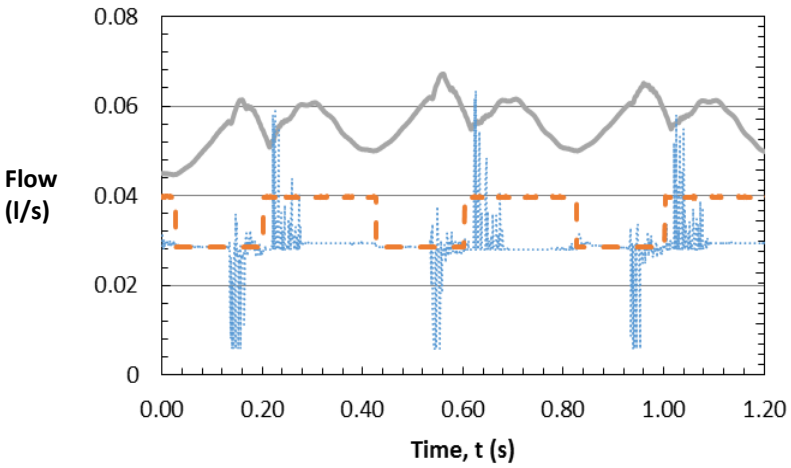

Fig. C-50 - 6V, r = 1.5, 5m assembly height

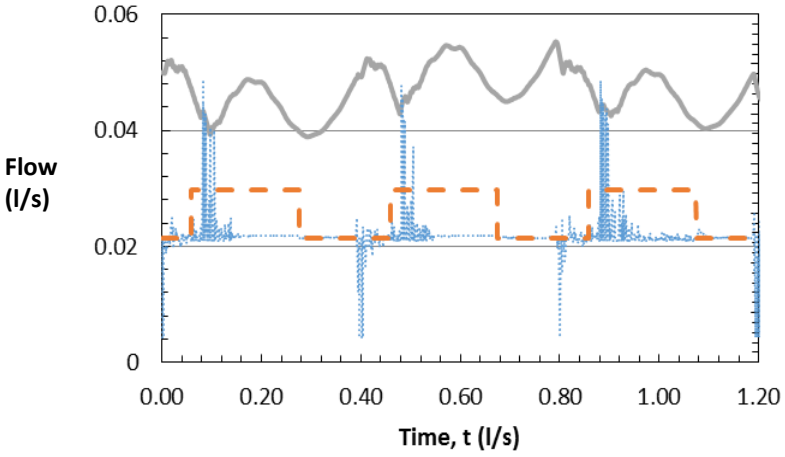

Fig. C-51 - 6V, r = 1.5, 4.5m assembly height

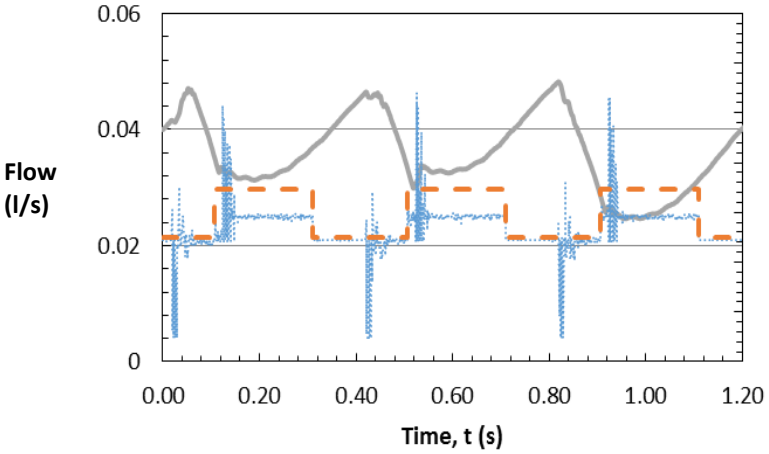

Fig. C-52 - 6V, r = 1.5, 4m assembly height

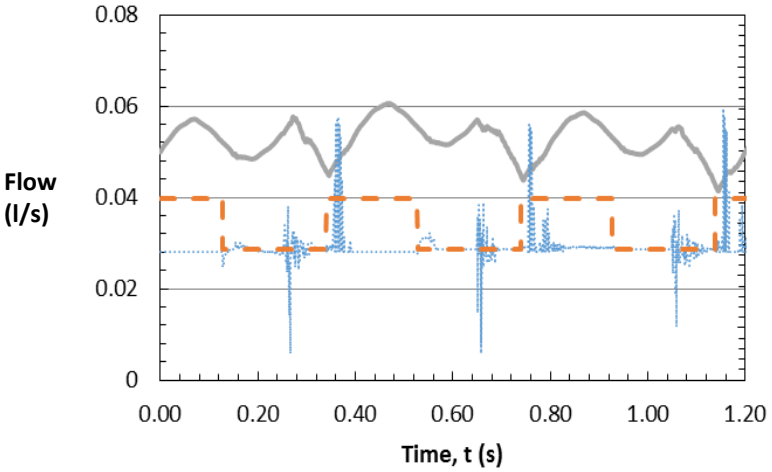

Fig. C-53 - 6V, r = 1.5, 3.5m assembly height

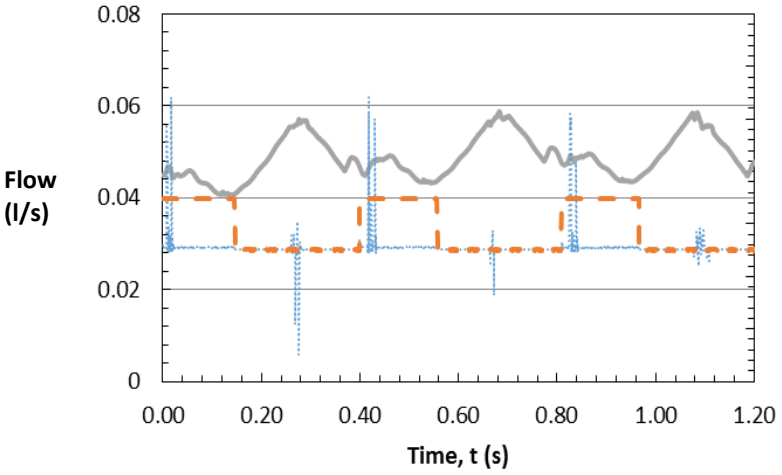

Fig. C-54 - 6V, r = 1.5, 3m assembly height

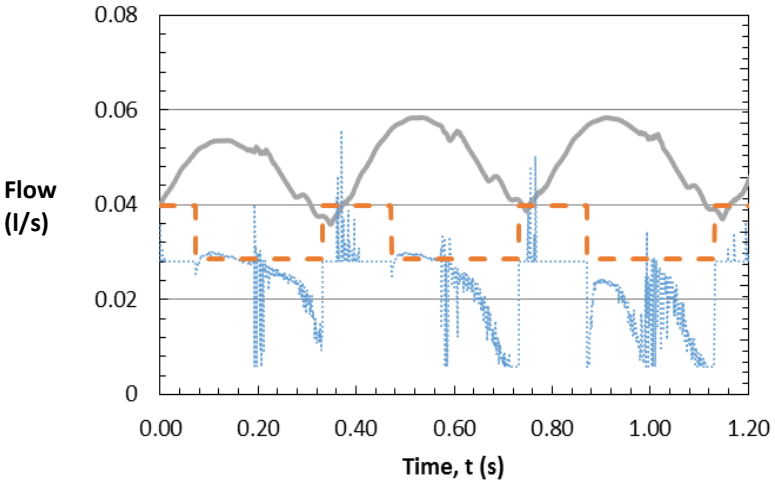

Fig. C-55 - 6V, r = 1.5, 2.5m assembly height

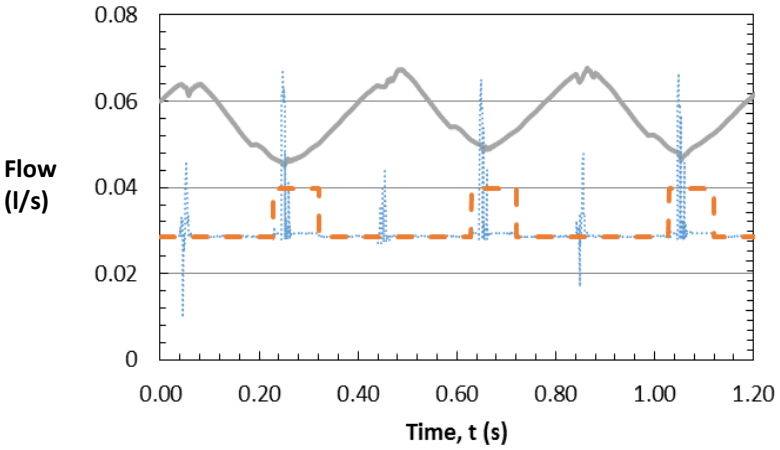

Fig. C-56 - 6V, r = 1.5, 2m assembly height

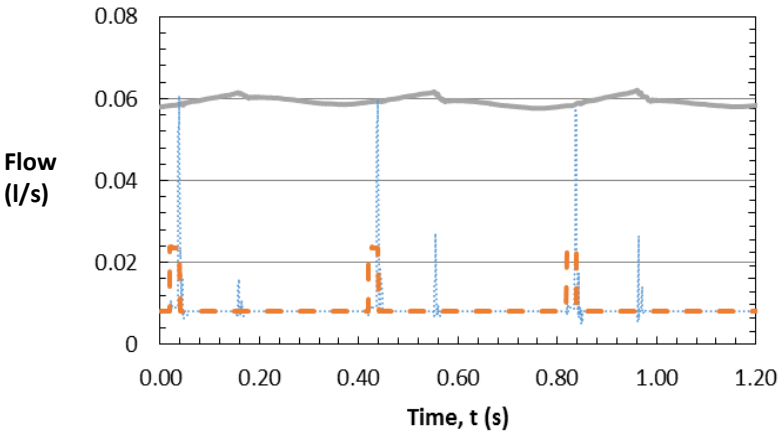

Fig. C-57 - 6V, r = 1.5, 1.5m assembly height

C.5.3 Operating Frequency, r = 2.5

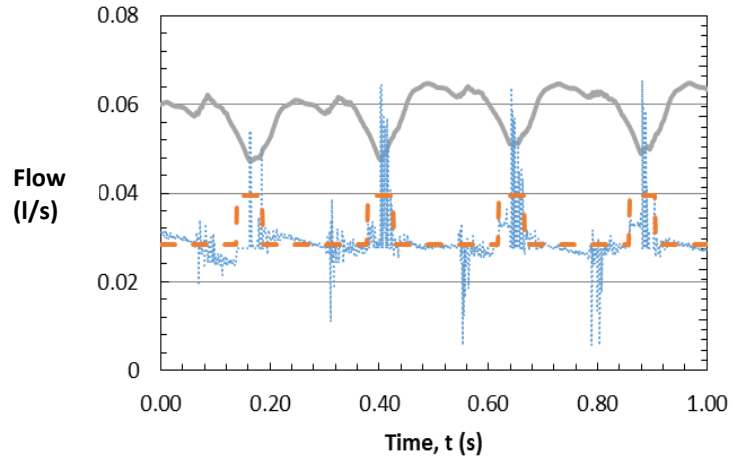

Fig. C-58 - 10V, r = 2.5, 5m assembly height

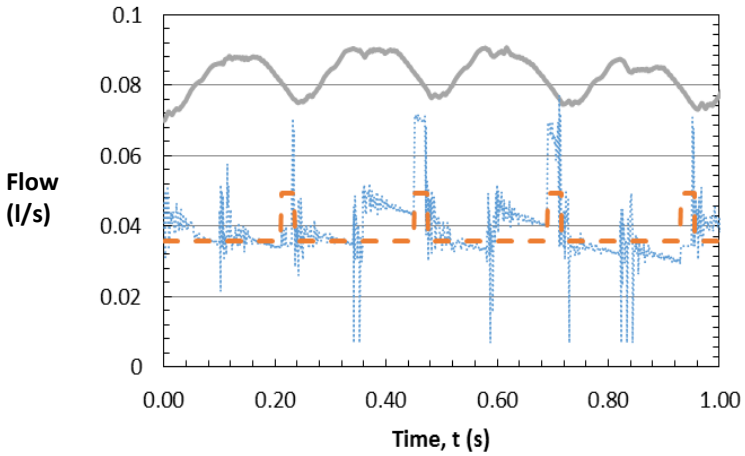

Fig. C-59 - 10V, r = 2.5, 4.5m assembly height

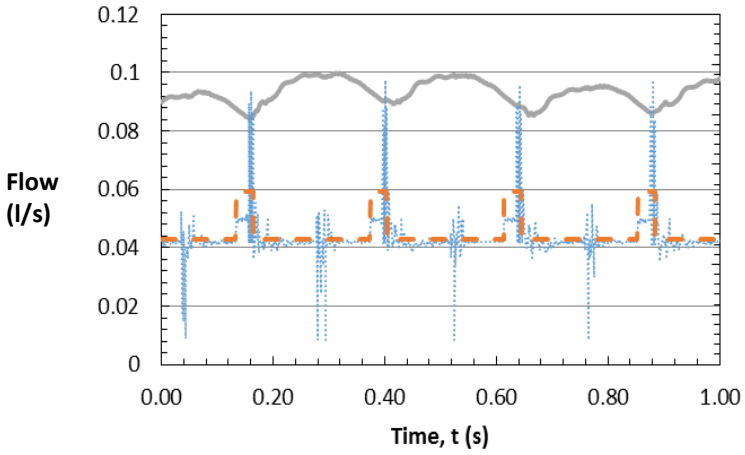

Fig. C-60 - 10V, r = 2.5, 4m assembly height

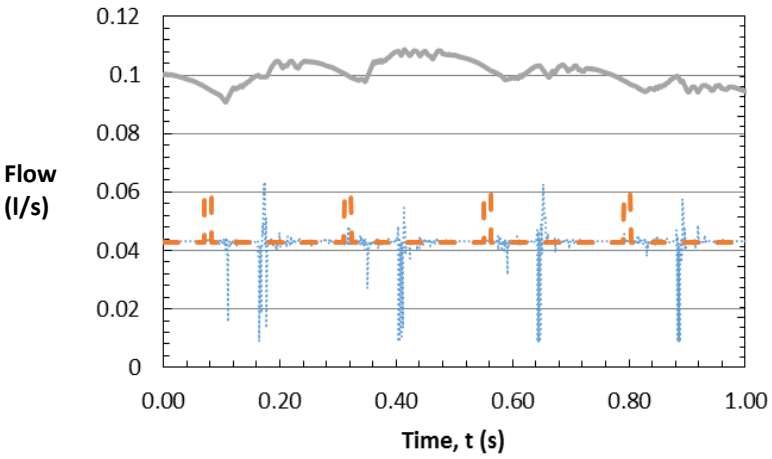

Fig. C-61 - 10V, r = 2.5, 3.5m assembly height

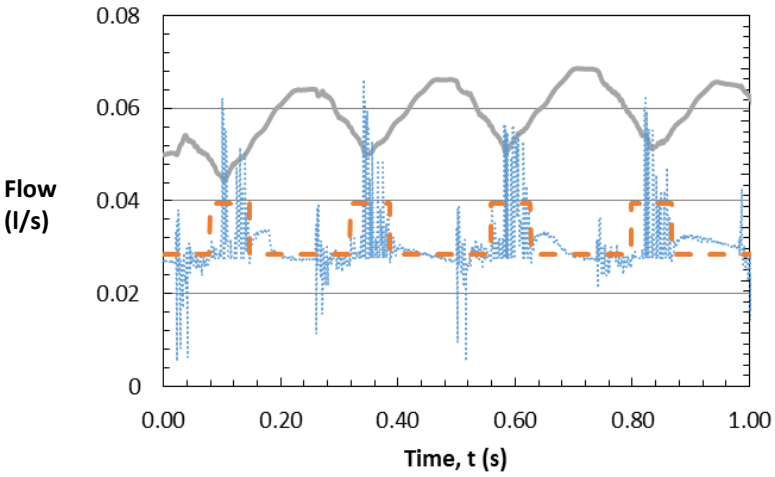

Fig. C-62 - 8V, r = 2.5, 5m assembly height

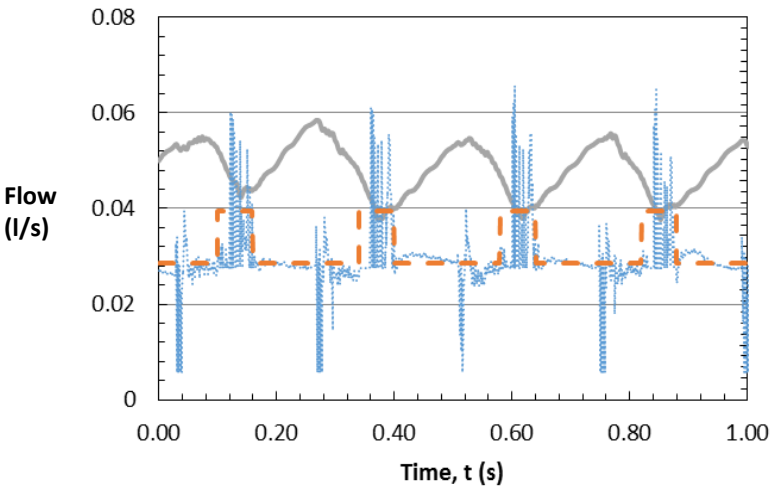

Fig. C-63 - 8V, r = 2.5, 4.5m assembly height

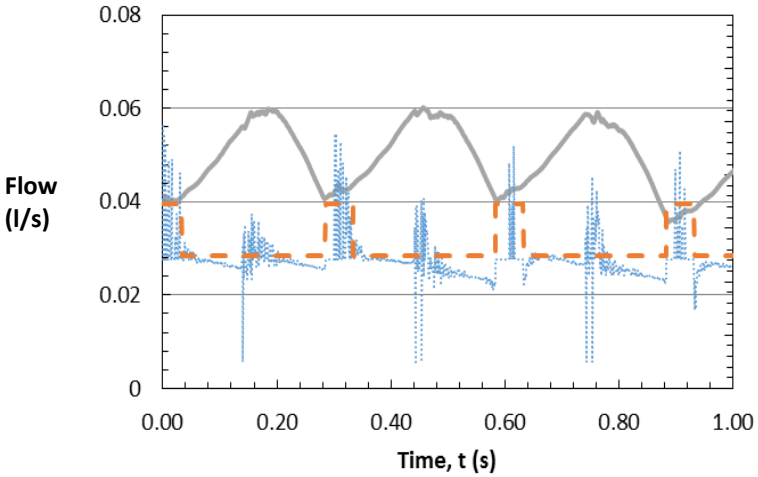

Fig. C-64 - 8V, r = 2.5, 4m assembly height

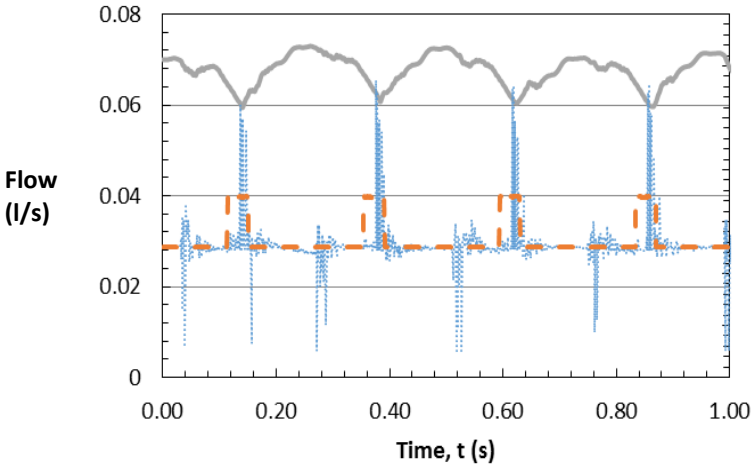

Fig. C-65 - 8V, r = 2.5, 3.5m assembly height

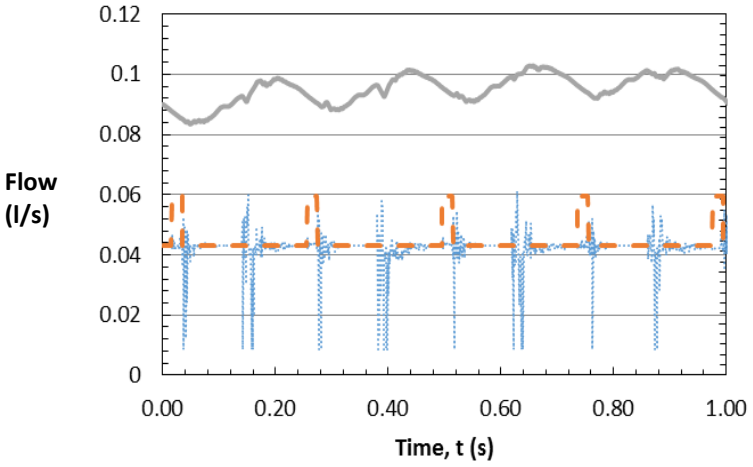

Fig. C-66 - 8V, r = 2.5, 3m assembly height

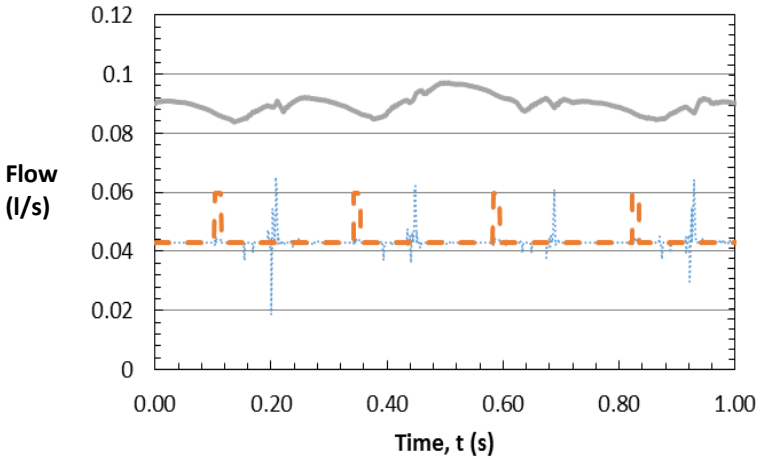

Fig. C-67 - 8V, r = 2.5, 2m assembly height

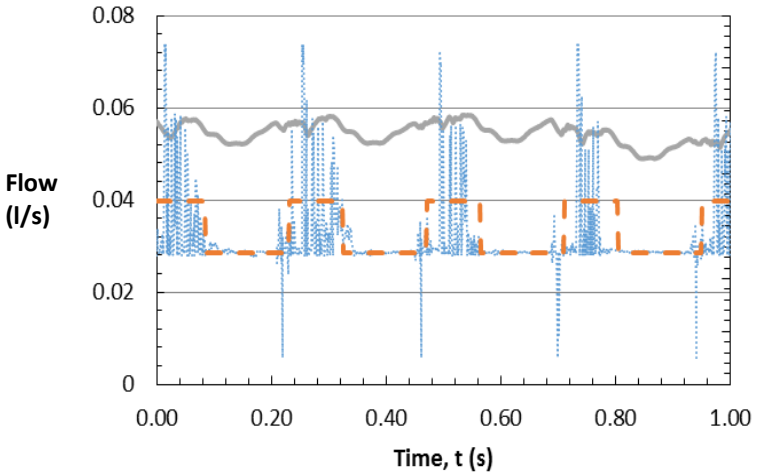

Fig. C-68 - 6V, r = 2.5, 5m assembly height

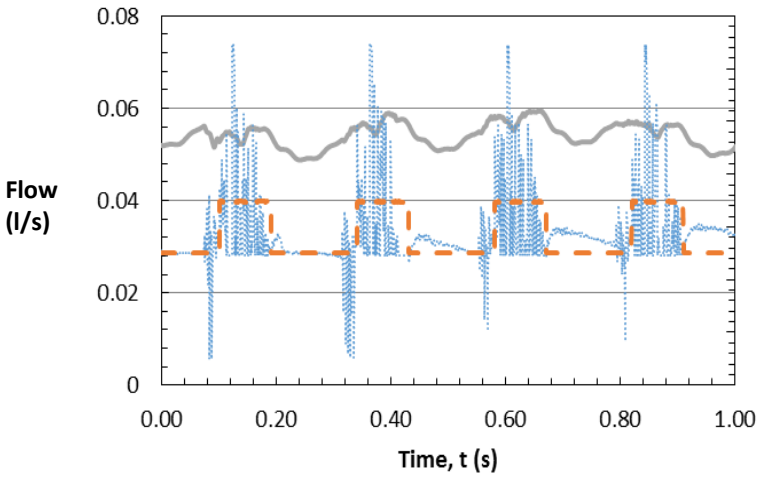

Fig. C-69 - 6V, r = 2.5, 4.5m assembly height

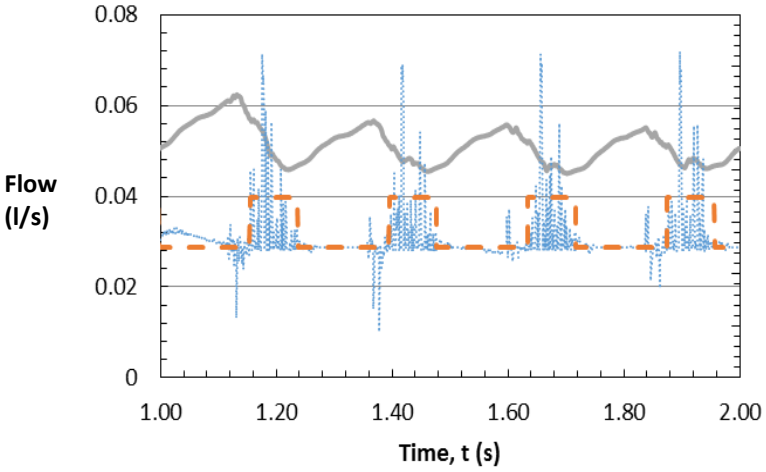

Fig. C-70 - 6V, r = 2.5, 4m assembly height

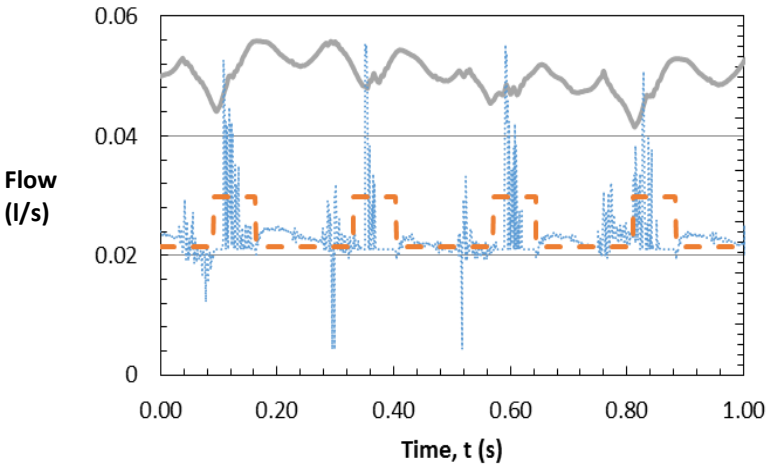

Fig. C-71 - 6V, r = 2.5, 3.5m assembly height

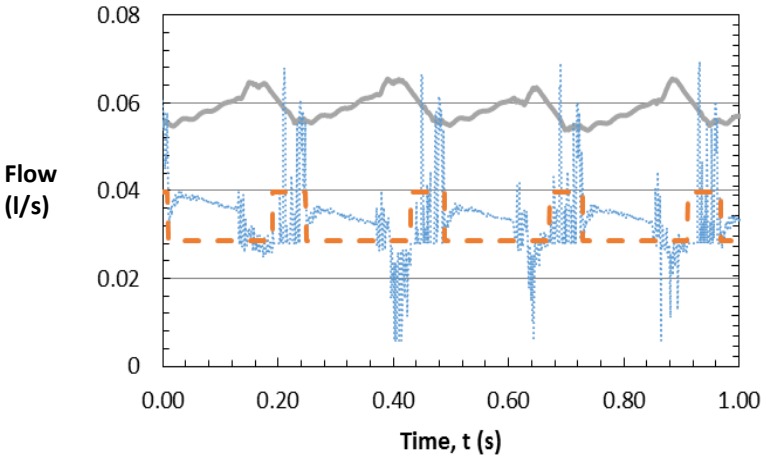

Fig. C-72 - 6V, r = 2.5, 3m assembly height

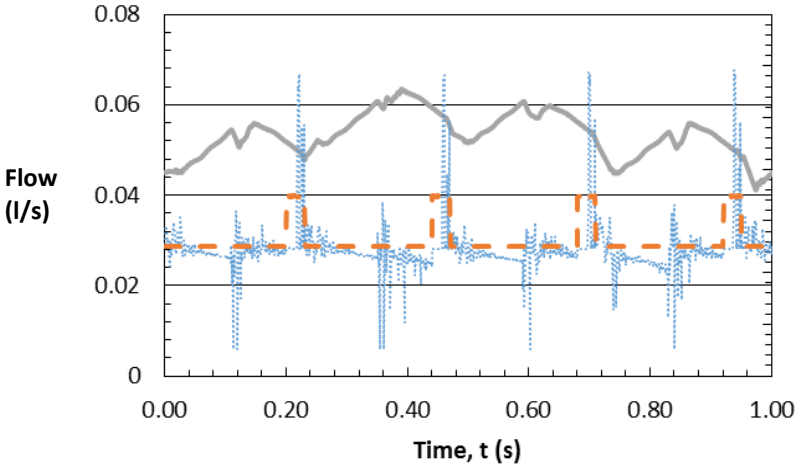

Fig. C-73 - 6V, r = 2.5, 2.5m assembly height

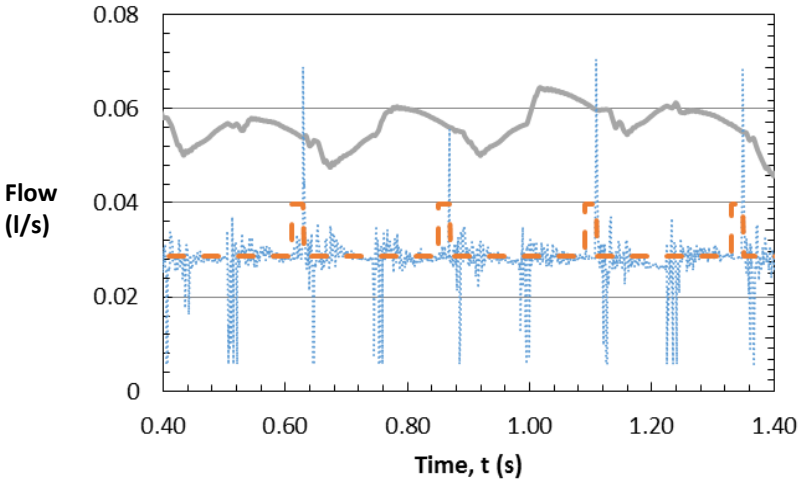

Fig. C-74 - 6V, r = 2.5, 2m assembly height